Shear connection of a prefabricated lightweight steel-concrete composite flooring system

by

Inas Mahmood Ahmed

Submitted in accordance with the requirements for the degree of Doctor of Philosophy

The University of Leeds
School of Civil Engineering

September, 2019

The candidate confirms that the work submitted is her own, except where work which has formed part of jointly-authored publications has been included. The contribution of the candidate and the other authors to this work has been explicitly indicated below. The candidate confirms that appropriate credit has been given within the thesis where reference has been made to the work of others.

The work in Chapter 2 of the thesis has appeared in the following publication:

Ahmed, IM and Tsavdaridis, KD (2019) The Evolution of Composite Flooring Systems: and Applications, Testing, Modelling and Eurocode Design Approaches. Journal of Constructional Steel Research, 155.pp. 286-300.

The work in Chapter 4 of the thesis has appeared in the following publications:

Ahmed, I. and Tsavdaridis, K.D., 2017, March. A New Breed of Sustainable Ultra-lightweight and Ultra-Shallow Steel-Concrete Composite Flooring System: LCA. In University of Leeds Proceedings.

Ahmed, I., Tsavdaridis, K.D. and Neysari, F., 2017, May. A new breed of sustainable ultra-lightweight and ultra-shallow steel-concrete composite flooring system: life cycle assessment (LCA) of materials. In CESARE'17 Proceedings. Jordan University of Science and Technology.

Ahmed, I.M. and Tsavdaridis, K.D., 2018. Life cycle assessment (LCA) and cost (LCC) studies of lightweight composite flooring systems. Journal of Building Engineering, 20, pp.624-633.

The work in Chapter 5 of the thesis has appeared in the following publication:

Ahmed, I., Tsavdaridis, K., Neysari, F. and Forth, J., 2018, June. Push-Out Tests for a Novel Prefabricated Steel-Concrete Composite Shallow Flooring System. In Proceedings of the 12th International Conference on Advances in Steel-Concrete Composite Structures. ASCCS 2018 (pp. 101-106). Editorial Universitat Politècnica de València.

All aspects of the publications above were undertaken by the candidate. However, the candidate benefited from the guidance and suggestions from the named co-authors who played the usual role of supervisor.

Dedication

To my husband for his endless love, support and encouragement

To my dear children ''Abdulazeez'' and ''Abdulrahman'' for all the moments I took away from them to fulfil my dream

Acknowledgements

Table of Contents

List of Tables

List of Figures

List of Abbreviations

AASHTO	American Association of State Highway and Transportation Officials
ACI	American Concrete Institute
AHP	Analytical Hierarchy Process
AISC	American Institute of Steel Construction
ASB	Asymmetric Slimflor beam
BMCC	Building Material and Component Combination
BS	British Standards
CA	Coarse Aggregate
CO_2	Carbon Dioxide
CoSFB	Composite Slimflor Beam
COV	Coefficient of Variation
DOF	Degrees of Freedom
EC	Expanded Clay
EC	Embodied Carbon
EE	Embodied Energy
EPS	Expanded Polystyrene
Eq.	Equation
Eqs.	Equations
FA	Fine Aggregate
FEA	Finite Element Analysis
GWP	Global Warming Potential
ISO	International Organization for Standardization
LCA	Life Cycle Assessment
LCC	Life Cycle Cost
LCI	Life Cycle Inventory
LCIA	Life Cycle Impact Assessment
le	Bending length of the shear connector

LWA	Lightweight Aggregate
LWC	Lightweight Concrete
NS	Natural Sand
NWC	Normal Weight Concrete
P.N.A	Plastic Neutral Axis
PFC	Parallel Flange Channel
RA	Recycled Aggregate
RC	Reinforced Concrete
RCRs	Reinforced Concrete Ribs
RCS	Reinforced Concrete Slab
SI	Sustainability Index
T1	Test Group 1
T2	Test Group 2
TBL	Triple Bottom-Line
U.S.	United States
UC	Universal Column
ULWC	Ultra Lightweight Concrete
USFB	Ultra Shallow Floor Beam
W/C	Water to Cement ratio
WWSS	Web-Welded Shear Studs

List of Notations

f_u	ultimate strength of the stud
P_{Rd}	design shear resistance of headed studs shear connectors
d	diameter of the stud
γ_v	partial factor
f_{ck}	concrete cylinder compressive strength according to Eurocode 4 specifications
E_{cm}	secant modulus of concrete
h_s	overall height of the stud
A_{sc}	stud cross-section area
$f_c`$	concrete cylinder compressive strength according to AISC specifications
F_u	specified tensile strength of the stud
$a_r`$	effective edge distance
k_v	Factor according to the stud position
h	overall height of the headed stud
a	horizontal spacing of studs
s	spacing of stirrups
$\varnothing_s$	diameter of the stirrups
$\varnothing_\ell$	diameter of the longitudinal reinforcement
C_v	vertical concrete cover
$a_{r,o'}$	relevant effective edge distance
d_s	stud's diameter
Q_p	shear capacity due to concrete pull-out failure
A_c	area of concrete pull-out failure surface
λ	factor that depends on the type of concrete used
f_{cu}	cube strength of the concrete

A_p	concrete pull-out failure surface area
K_c	reduction factor for the cylinder strength of the concrete
Q	load (kip)
Δ	slip
f_{ctm}	mean tensile strength of the concrete
K_R	resistance facto
$A_{\varnothing w}$	area of the web hole
P_{us}	design shear resistance of the shear connector
f_{ct}	tensile splitting strength of concrete
D	diameter of the web opening
t	thickness of the web
R_{add}	additional resistance of the tie-bar or studs
h_d	concrete dowel height
t_w	web thickness
i	raw material constituting the flooring system
n	number of raw materials added for each flooring system production
Wi	unit weight
EE_{i_LCI}	embodied energy inventory of raw material
EC_{i_LCI}	embodied carbon inventory of raw material
EE_{i-CE}	embodied energy inventory of the operation of construction equipment
EC_{i-CE}	embodied carbon inventory of the operation of construction equipment t operation time for the equipment.

Di	transportation distance of each flooring system constituent material $EE_{(i)-LCI(TR)}$ embodied energy inventory related to the heavy haulage vehicle
$EC_{(i)-LCI(TR)}$	embodied carbon inventory related to the heavy haulage vehicle
$EE_{(i)-LCI(RC)}$	embodied energy inventory form the recycling process
$EC_{(i)-LCI(EOL)}$	embodied carbon inventory form the recycling process
$EE_{(i)-LCI(R)}$	embodied energy inventory for the demolition of concrete
$EC_{(i)-LCI(EOL)}$	embodied carbon inventory ($kgCO_2e/kg$) for the demolition of concrete.
Cc	construction costs
Cu	usage costs
C_{EOL}	end of life costs
FC	future cost
PV	present value
DPV	discounted present value
f	inflation rate
d	discount rate
n	number of years.
$C_{CM\&T}$	costs of extraction, production, and transport of construction materials $C_{L\&OH}$ labour and overhead costs
C_{MF}	fuel costs for the machinery used in the construction of the flooring systems
δ_{uk}	Characteristic slip capacity of the shear connector
δ_u	slip capacity of the shear connector
K	stiffness of the shear connector
σ_c	compressive stress of the normal concrete,

f_{cm}	characteristic compressive cylinder strength of normal concrete
ε_{c1}	compressive strain of the normal concrete at the peak stress f_c
w	crack opening displacement
w_c	crack opening displacement at which stress can no longer be transferred
c_1	material constant
c_2	material constant
K	initial slope of the curve
K_p	final slope of the curve
f_o	reference stress
n	curve-shape parameter
P_D	spatial stress status of fracture initiation
Ø	the resistance factor for shear connectors
P_{sd}	shear resistance of shear stud or dowel
δ	slip
M_{Rd}	design moment resistance of the composite
$M_{pl,a,Rd}$	plastic moment resistance
η	degree of shear connection
$M_{pl,Rd}$	design moment resistance of the composite section
$\sigma_{c,Rd}$	concrete compressive stress
$R_{t/f}$	resistance of the top flange
$R_{t/w}$	resistance of the top flange
$R_{b/w}$	resistance of the web post of the bottom tee
$R_{b/f}$	resistance of the bottom flange
Ms	plastic moment resistance of the steel section

$D_{t/f}$ distance between the $R_{t/f}$ and P.N.A,

$D_{t/w}$ distance between the $R_{t/w}$ and P.N.A,

$D_{b/w}$ distance between the $R_{b/w}$ and P.N.A,

$D_{b/f}$ distance between the $R_{b/f}$ and P.N.A.

B_e effective width of the concrete slab;

D depth of the P.N.A

P_y steel stress

R_q longitudinal shear resistance of the connectors

List of Publications

Part of the outcome of the research presented in this thesis has been published in an international conferences and journals.

- Ahmed, Inas, and Konstantinos Daniel Tsavdaridis. "A New Breed of Sustainable Ultra-lightweight and Ultra-Shallow Steel-Concrete Composite Flooring System: LCA." In *University of Leeds Proceedings*. 2017.
- Ahmed, I., Tsavdaridis, K.D. and Neysari, F., 2017, May. A new breed of sustainable ultra-lightweight and ultra-shallow steel-concrete composite flooring system: life cycle assessment (LCA) of materials. In *CESARE'17 Proceedings*. Jordan University of Science and Technology.
- Ahmed, I., Tsavdaridis, K., Neysari, F. and Forth, J., 2018, June. Push-Out Tests for a Novel Prefabricated Steel-Concrete Composite Shallow Flooring System. In *Proceedings of the 12th International Conference on Advances in Steel-Concrete Composite Structures. ASCCS 2018* (pp. 101-106). Editorial Universitat Politècnica de València.
- Ahmed, I.M. and Tsavdaridis, K.D., 2018. Life cycle assessment (LCA) and cost (LCC) studies of lightweight composite flooring systems. *Journal of Building Engineering*, *20*, pp.624-633.
- Ahmed, I.M. and Tsavdaridis, K.D., 2019. The evolution of composite flooring systems: applications, testing, modelling and eurocode design approaches. *Journal of Constructional Steel Research*, *155*, pp.286-300.

List of Presentations

Findings form the present research has been presented at

- Ahmed, Inas, and Konstantinos Daniel Tsavdaridis. *Enhancing the performance of shallow flooring systems with the use of lightweight materials.* [Poster]. The PGR Students' Conference. 2016, 27-28 September, School of Civil Engineering. University of Leeds.
- Ahmed, Inas, and Konstantinos Daniel Tsavdaridis. Optimising the performance of shallow flooring systems with the use of ultra-lightweight materials. [Poster]. The Royal Academy Conference. 2016, 12th of September, School of Electrical Engineering. University of Leeds.

Abstract

This research PhD thesis investigates the shear connection behaviours and failure modes of two new connection systems used in a newly proposed fully prefabricated lightweight ultra shallow flooring system. The shear connection systems are different to anything presented up to date in the literature and they serve the purpose of the novel prefabricated slab. Experimental, computational and analytical studies were carried out with the aim of improving and optimising the design details, as well as advancing the method of shear connection systems in the prefabricated ultra shallow slabs.

A comprehensive Life Cycle Assessment (LCA) was initially performed, followed by an extensive literature review in order to understand the characteristics of shallow and lightweight steel-concrete composite flooring systems. The LCA study resulted in selecting the materials of the prefabricated ultra shallow flooring system (lightweight concrete and steel), before designing the flooring system. Moreover, analytical LCA and LCC studies were also carried out to examine the ecological impact of the new flooring systems, which were then compared with existing prefabricated shallow flooring systems, such as the hollow core precast slab and Cofradal slab.

The prefabricated ultra shallow flooring system proposed in this research was developed by this PhD research programme. It is made of a T-ribbed lightweight concrete floor and C-channel steel edge beams, connected with the use of web-welded shear studs (herein called WWSS), and in some cases, horizontally lying dowels too. Their unique configuration minimises its structural depth and results in ultra-shallow floors (structural depths). Thus, two types of shear connection systems were studied: (a) web-welded shear studs only (WWSS), and (b) web-welded shear studs with dowels (WWSS with dowels).

In total, eight (8) full scale push-out tests were conducted in the Heavy Structures Laboratory at the University of Leeds, to examine the load-slip behaviour and longitudinal shear resistance of the two shear connection systems under direct shear force. The failure mechanisms of the two forms of shear connection systems were extensively studied, which led to the development of a design method for calculating the shear capacity.

Finite Element Analyses (FEA) of the shear connection systems were then performed, supported by eighty four (84) parametric models to further verify the design method that was previously established.

Finally, an accurate and reliable moment resistance design method of the prefabricated ultra shallow flooring system was proposed as a practical outcome of this PhD thesis in accordance with the Eurocode 4 and BS5950 standards.

Chapter 1 Introduction

1.1 Background and Motivation

In recent years, there has been increasing demand for buildings that are quick to construct, with large uninterrupted floor areas (free of columns), which are flexible in their intended final use. Modern design and construction techniques enable steel-concrete composite construction to satisfy such demands by producing structures that are competitive in terms of resistance and overall cost. The present trend is towards the use of longer spans and lightweight floor systems, which has resulted in the development of various slimflor systems, as shown in Figure 1-1, such as Slimflor, Slimdek, asymmetric Slimflor beams, ultra-shallow floor beams and composite slimflor beams, which are most likely being used in commercial and residential buildings, hospitals, schools, etc.
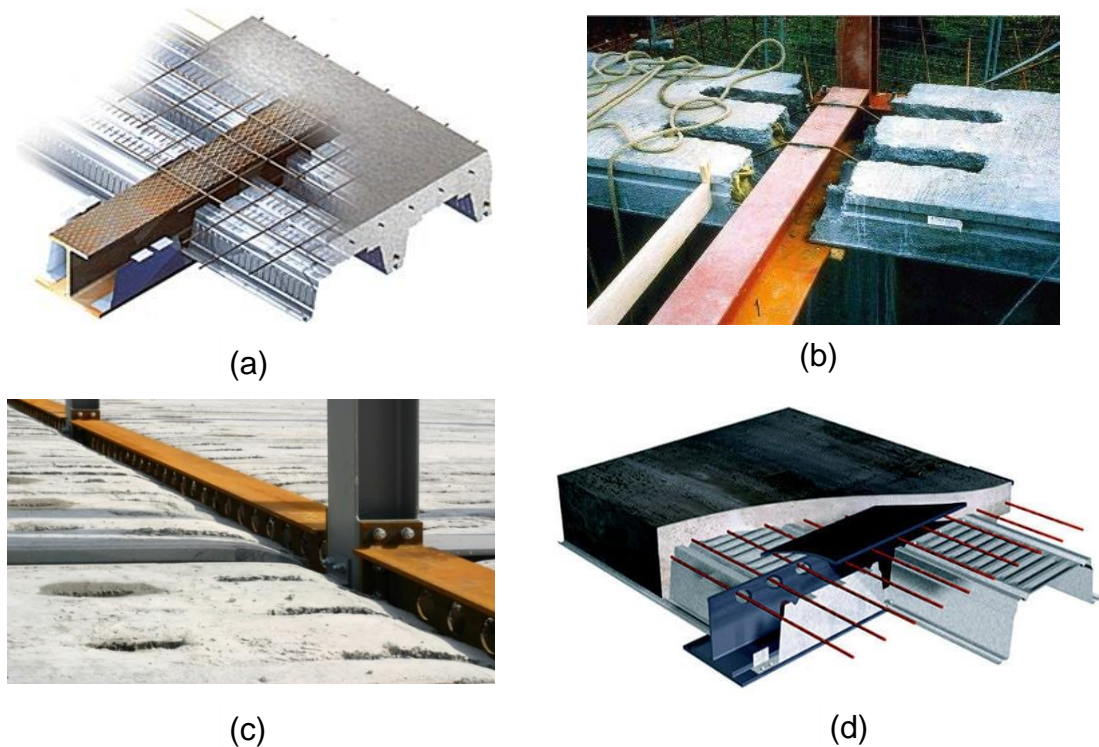
Figure 1-1: (a) Slimflor construction with deep composite decking, (b) Slimflor construction with precast concrete slab (Lawson et al., 2015), (c) Ultra Shallow Floor Beam (Tsavdaridis et al., 2013), (d) Composite Slimflor Beam (Hechler et al., 2013)

Slimflor systems have become widespread all over Europe. Because the concrete slabs are within the structural depth of the steel beam, as a result, this will reduce the depth of the floor structure (Hicks, 2003). Constructions of high-rise residential buildings profit from shallow flooring systems, since the floor-to-

floor height is a substantial factor (Mullett, 1992). These slimflor systems, which are widely used in the construction of buildings, allow for fast erection, reduced weight, and incorporates lightweight elements (Frangi et al., 2011). The shallow depth of these floors has been proven to impose limitations on the clear slab and beam spans. The majority of slimflor systems are not capable of spanning for long distances, they are mainly effective at spans of 6m to 10m (Lawson et al., 2015). Spanning more than 10m significantly increases the structural depth of the flooring system, hence the longer the span, the less economical the solution proves to be for multi-story buildings, as the RC slabs of such spans prove to be both deeper and heavier (Tsavdaridis et al., 2013).

To achieve longer spans, lighter flooring systems have been considered, such as the Ultra-Shallow Floor Beam (USFB), which consists of perforated steel beams designed to connect with floor slab placing within the steel flanges in order to reduce the structural depth of the composite sections (Tsavdaridis et al., 2013). These composite structures also have other advantages, including increased load carrying capacity, fire resistance, local buckling stiffness and a significant increase in the bending stiffness when compared with traditional beams. Furthermore, these structures reduce construction cost by eliminating the construction time and the amount of formwork (Tsavdaridis et al., 2009a). The most common applications of USFBs have been based on slabs with depths ranging from 180mm to 300mm, in which the concrete has been placed level with the top flange. The practical span to depth ratio of USFBs is usually in the range of 25 to 30. Consequently, the USFB is limited to a span up to 9m, with a depth of up to 300mm. When the span is extended to more than 9m, the depth will increase to more than 300mm, even when lightweight concrete is used (Tsavdaridis et al., 2009a). This leads to an uneconomical solution for flooring systems. In addition, an increase of slab spans reduces the natural frequencies of the USFBs and leads to an increase of the floor vibration (Kansinally and Tsavdaridis, 2015).

Another type of slimflor system, which is similar to the USFB, is the composite slimflor beam (CoSFB), which is based on the development of an advanced composite connection by using concrete dowels. The resulting structural solution allows for the possibility to achieve a slim-floor beam span up to 12m, with a slimflor beam centre of 10m and an overall depth of only 350mm

(Hechler et al., 2013). The average slender ratio (span/depth) of the CoSFB is about 35. This flooring system has been used with the Cofradal slab (composite floor slab), which consists of a cold rolled metal deck, a thermal insulation layer and a concrete layer. This composite floor slab is lightweight, and has better thermal and acoustic performances, along with good fire resistance. The maximum width of the Cofradal slab by using two elements connected with each other is up to 1200mm with a span up to 7.8m (COFRADAL200®). The CoSFB used with the Cofradal slab is limited to a span of up to 10.5m, with a depth up to 300mm and is suitable for residential buildings because of its low load carrying capacity.

1.2 Research Problem

Two types of prefabricated floor systems have been used with the aforementioned floor beams (USFB and CoSFB), which are a hollow core precast floor and Cofradal slab. The hollow core precast floor is fabricated using reinforced concrete. It contains voids run continuously along their length, which helps reduce dead weight and material cost. A concrete topping layer is often cast in place onto the top surface of the hollow core slabs to create a continuous level finished surface. The topping layer is typically 50mm deep. The maximum span of this floor is up to 10.5m, with a thickness below 300mm.

The Cofradal floor system is an innovative fully prefabricated floor system, developed by AreclorMittal in 2009 (COFRADAL200®). This type of floor system is suitable for lightweight industrial offices and residential buildings. This system is a prefabricated steel-concrete composite slab produced in a factory and is ready to be fixed on the construction site. It consists of a cold rolled metal deck, a thermal insulation layer and a concrete layer. Two widths can be provided of 600mm and 1200mm, with a maximum span of 7.8m. The benefit of this type of floor system is that it is two to three times lighter than an equivalent usual plain concrete floor system, which allows for fewer frame sections and fewer ground foundations.

Therefore, all existing flooring systems have span and depth limitations, along with prefabrication and site construction issues (Hicks, 2003, Tsavdaridis et al., 2009b, Hechler et al., 2013). Site construction involves further site work to complete the construction, with the exception of the precast unit system, where

the units have been prefabricated off-site and have been lifted into position with a limited width of a maximum 1200mm per lift, which increases energy consumption, CO_2 emissions, construction costs and potential site repair and maintenance costs. The trend nowadays in the industry is making the buildings of the future more flexible and adaptable to the future needs. The building requirements and specifications for column grids and facades, conditions and design parameters of the structural system include the floor-to-floor heights, spans of beams and slabs, arrangements for fire protection, live and additional dead loads, and the design of components and services spaces. Therefore, appropriate construction systems and components, as well as design fundamentals, should be selected by applying the sustainability approach.

For this purpose, this study employed a Life Cycle Assessment (LCA) methodology for selecting the materials of the prefabricated ultra shallow flooring system, which is novel in terms of applying this new methodology in the design stage (Tsavdaridis et al., 2009a, Hechler et al., 2013). This study also focuses on producing a flooring system with a span that exceeds the span limitations, with a shallower depth for other existing shallow flooring systems (RC, Cofradal and hollow core precast flooring systems).

The potential benefits of the prefabricated ultra shallow flooring system include reducing the number of erection/installation lifts by using lighter elements (lighter concrete and steel) and wider units, and reducing the extent of site work by pre-off site fabrication, by considering the material cost versus the fabrication and site erection costs being proportionally in the order of 35% and 65%, respectively (Humphreys, 1995). Therefore, an increase in speed of site construction, reduction of site work and lighter construction, along with larger clear span capacity, would be a great benefit to the construction industry.

Furthermore, the current trend in the industry is to reduce the amount of energy consumption, CO_2 emissions and cost by using prefabricated lightweight components. These prefabricated elements will not only be produced with the quality assured method of the shop fabrication, but will also reduce potential site repair and maintenance costs by eliminating onsite mistakes that could arise through bad workmanship.

1.3 Background of prefabricated ultra shallow flooring system

In recent years, the increasing demands of the prefabricated shallow floor systems due to their potential benefits in reducing the number of erection/installation lifts, the extent of site work, the amount of energy consumption, the amount of CO_2 emissions and cost, has led to the development of the hollow core precast floors and Cofradal floors. However, the span and width of these flooring systems, with a depth below 300mm are up to 7.8m in the Cofradal flooring system (COFRADAL200®) and 10.5m for hollow core precast flooring system, with a width of 1.2m (Bison). The prefabricated ultra shallow flooring system is a new prefabricated type of steel-concrete composite flooring system, which consists of two main structural components: a concrete floor and steel beams. The concrete floor is in the form of T ribbed slab sections constructed using reinforced lightweight concrete. The concrete ribbed slab of the composite flooring system has regular voids running from one side to the other side of the T-ribbed slab, which forms the T-ribs. These voids can be used for the passage of building services if it is required. This further minimises the overall floor depth and eliminates the unwanted floor depth needed to accommodate the building services passing underneath the beam structures. The construction time is also improved as the flooring system is fabricated in the factory. This method of construction eliminates the time spent on concrete hardening in traditional floor constructions. Hence, concreting is no longer required on critical paths.

Two types of unique shear transferring connection systems (web-welded stud shear connection system (WWSS), and WWSS with dowels) are used to connect the steel beam to the concrete slab. The steel edge beams encapsulate the floor slab in the middle and provide clean and straight finished edges. The floor slab spans to a maximum of 2m inclusive of the width of the steel edge, with a finished depth of 230mm, as illustrated in Figure 3-1.

(a)

(b)

Sec (A-A)

Sec (B-B)
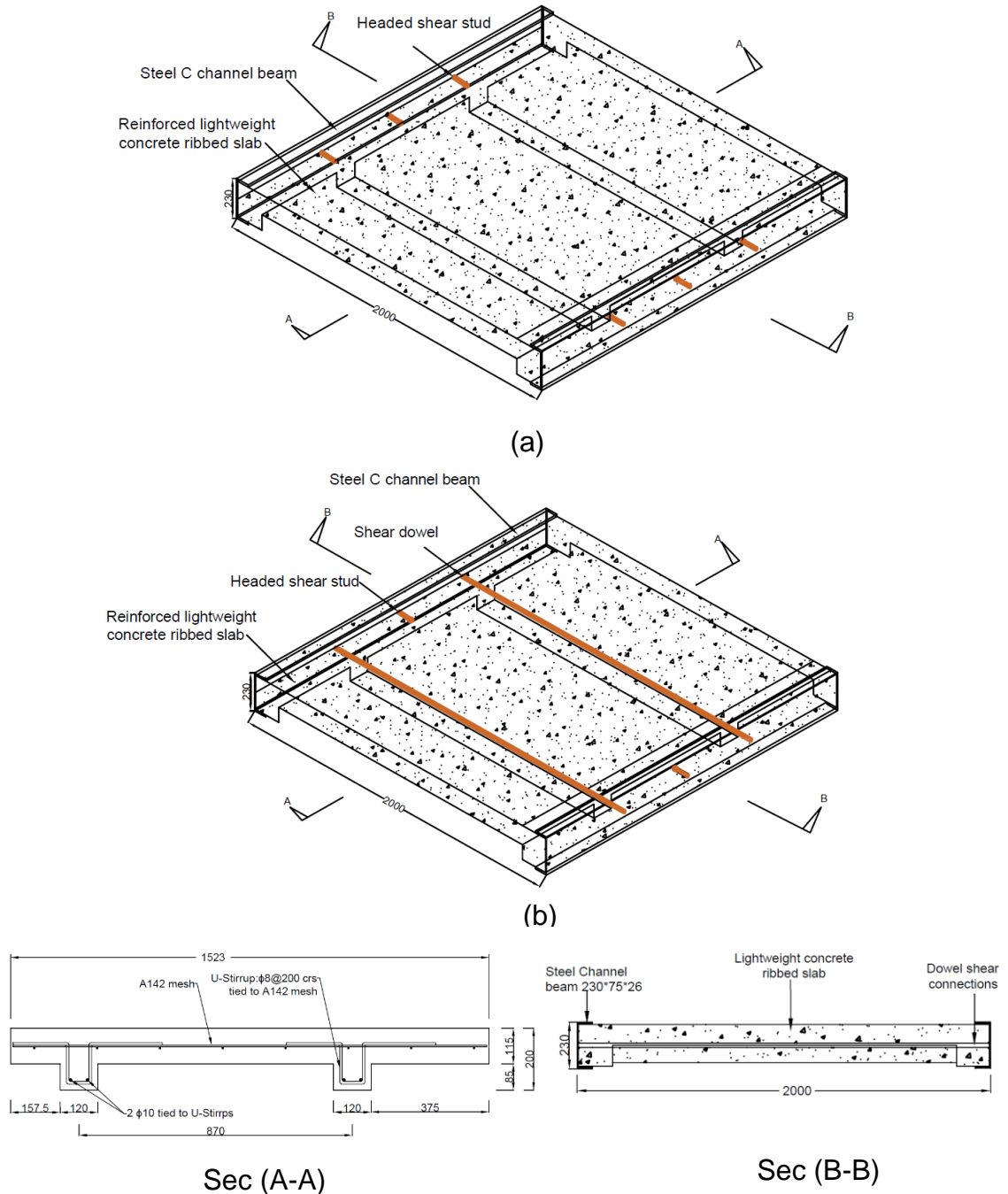
Figure 1-2: Schematic drawing of the prefabricated ultra shallow flooring system

A prefabricated ultra shallow flooring system is a construction system that fits in a range of floor beams (down standing beam, slimflor beam) and is used in steel building technologies. The prefabricated ultra shallow flooring system is similar to the shallow flooring systems (hollow core precast floors and Cofradal floors). The common feature of this flooring system is its flat ribbed slab structure, which minimises the overall floor depth and weight, in addition to the use of lightweight materials (lightweight concrete and steel). However, the manufacturing process and the compositeness of the flooring system offers three key advantages when

compared with the hollow core precast flooring system (Bison) and Cofradal flooring system (COFRADAL200®). The first advantage is a reduction in the number of erection (installation) lifts, by using lighter elements (lightweight concrete and steel members, where wider units may fit on the tracks for transportation. The second advantage is a reduction of the extent of site work, facilitated by pre-off site fabrication, by examining the material cost versus the fabrication and site erection costs, which are proportional in the order of 35% and 65%, respectively. The third advantage is a reduction of energy consumption and CO_2 emissions by using prefabricated lightweight materials.

1.4 Aim and Objectives

The aim of this research is to enable the construction of shallow lightweight low energy consumptions, low CO_2 emissions and a low-cost flooring system through the use of lightweight materials (lightweight concrete and steel). With a view to achieve this aim, an evaluation of the materials LCA and LCC is necessary. This is achieved via an LCA comparison study of the prefabricated ultra shallow flooring system, with alternative shallow flooring systems (e.g. hollow core precast slab and Cofradal slab).

Experimental, computational and analytical studies were carried out to investigate the unique shear transferring mechanism of the prefabricated ultra shallow flooring system and provide information on the behaviour and shear resisting properties of two shear connection systems. The intention is to achieve a better understanding of the failure mechanisms developed through the shear connection systems, as well as develop a design methodology for the proposed shear connection systems.

The objectives of this study are summarised below:

1. Carry out a literature review on shear connection systems and existing prefabricated shallow composite floors, with emphasis on experimental studies (i.e. push-out tests).
2. Examine the LCA and LCC of the prefabricated ultra shallow flooring system and compare it with existing similar solutions, such as the hollow core precast slab and the Cofradal slab, which have been used with the USFB and CoSFB, respectively.

3. Design and carry out two series of push-out tests. The first series of the tests was to investigate the web-welded shear stud (here called WWSS) connection system. The second series of the tests was to investigate the web-welded shear studs together with horizontally lying dowels (WWSS with dowels).

4. Analyse the results of the push-out tests to develop a design methodology for the proposed shear connection systems.

5. Conduct comprehensive FEA parametric studies to identify the effect of the shear connection systems to the prefabricated ultra shallow flooring system on the shear capacity, while varying the mechanical/material and geometrical properties of the components.

6. Develop a design methodology for the shear capacity of the proposed prefabricated ultra shallow flooring system based on the results of the push-out tests and FEA parametric studies.

1.5 Structure of the thesis

Chapter 1   Introduction

This chapter presents the background and motivation behind the proposed prefabricated ultra shallow flooring system. The aim and objectives are also emphasised.

Chapter 2   Literature review

The extant publications are reviewed on the shear connection systems and the prefabricated shallow composite flooring systems. Emphasis is given to the investigations of the push-out tests. The reviewed shear connection systems are similar or have similarities to the shear connection systems used in the prefabricated ultra shallow flooring system. The review extends to shear connectors other than the headed shear studs.

Chapter 3   Prefabricated ultra shallow flooring system

This chapter presents the background information on the prefabricated ultra shallow flooring system and shear connection systems. The methodology of the investigations is also emphasised.

Chapter 4   Life cycle assessment (LCA) and life cycle cost (LCC) of the prefabricated ultra shallow flooring system

The historical background on the LCA is provided and the publications are reviewed. Emphasis is given to the environmental performance (LCA) and economic performance (LCC) of the prefabricated ultra shallow flooring system, along with alternative prefabricated shallow composite flooring systems.

Chapter 5   Push-out test series

This chapter presents investigations on two types of shear connection systems used for the prefabricated ultra shallow flooring system. The test specimens had variables in the type of shear connection system and concrete strength. The relationship between the shear capacity of the shear connection systems and the type of the shear connection systems, along with the concrete strength, are studied. The behaviour and failure mechanisms of the shear connection systems are specifically analysed.

Chapter 6   Finite Element Analysis

This chapter presents the results of the FEA studies. An extensive parametric study is carried out, which further investigates the behaviour of the shear connection systems.

Chapter 7   Analytical study of the shear connection systems

In this chapter, the results of the push-out tests are analysed. A design method for the shear capacity of the shear connection system is developed and verified using the results of the FEA study. A design methodology for the bending capacity of the prefabricated ultra shallow flooring system is also proposed based on Eurocode 4 and BS5950 standards.

Chapter 8   Conclusions and recommendations

In this chapter, the findings of the push-out tests and FEA for the shear connection systems of the proposed prefabricated ultra shallow flooring system are summarised, together with the developed design method. Recommendations are made towards areas of improvement for the shear connection systems and interesting future research topics worth investigation.

Chapter 2 Literature Review

2.1 Introduction

In the context of investigating the shear connection systems of the prefabricated ultra shallow flooring system and evaluating the structural performance of the system, this chapter presents a review of publications focusing on shear connection systems, as well as existing prefabricated shallow composite flooring systems. Particular emphasis is given to experimental investigations, i.e. push-out tests. The current design codes of practice are also discussed.

2.2 Shear connection system

2.2.1 Codes of practice

Eurocode 4 (EN 1994-1- 1, 2004) requires that the ultimate tensile strength of headed studs, f_u, should not be greater than 500N/mm^2 for studs used in solid slabs and a concrete encasement, and 450N/mm^2 for studs used with profiled steel decking. The design shear resistance (P_{Rd}) of headed studs shear connectors used in a solid slab and concrete encasement can be calculated using the following equations given in Eurocode 4 (EN 1994-1- 1, 2004).

$$P_{Rd} = \frac{0.8 f_u \pi d^2/4}{\gamma_v} \qquad (2.1)$$

$$P_{Rd} = \frac{0.29 \alpha d^2 \sqrt{f_{ck} E_m}}{\gamma_v} \qquad (2.2) \qquad \text{(whichever is smaller)}$$

Where f_u is the specified ultimate strength of the stud (≤500MPa), d is the diameter of the stud, γ_v is the partial factor (1.25), f_{ck} is the concrete cylinder compressive strength, E_{cm} is the secant modulus of concrete, $\alpha = 0.2(hs/d +1)$ for $3 \le h_s/d \le 4$ or $\alpha = 1.0$ for $h_s/d \ge 4$, h_s is the overall height of the stud.

(BS5950-3.1, 1990) also provides detailed specifications for headed studs shear connectors in terms of dimensions and spacing. The design shear resistance is given as a value in(BS5950-3.1, 1990), with corresponding stud dimensions and concrete strength, as illustrated in Table 2-1.

Table 2-1 Characteristic shear resistance of the headed studs
(BS5950-3.1, 1990)

Dimensions of stud shear connectors			Characteristic strength of concrete			
Nominal shank diameter	Nominal height	As-welded height	N/mm^2 25	N/mm^2 30	N/mm^2 35	N/mm^2 40
mm	mm	mm	kN	kN	kN	kN
25	100	95	146	154	161	168
22	100	95	119	126	132	139
19	100	95	95	100	104	109
19	75	70	82	87	91	96
16	75	70	70	74	78	82
13	65	60	44	47	49	52
NOTE 1 For concrete of characteristic strength greater than 40N/mm^2 use value for 40 N/mm^2. NOTE 2 For connectors of height greater than tabulated use values for greatest height tabulated.						

The American Institute of Steel Construction (AISC, 1994) provides a formula for calculating the ultimate strength of headed studs, Eq. 2.3.

$$Q_u = 0.5A_{sc}\sqrt{f_c^{`}E_c} \leq A_{sc}\,F_u \qquad (2.3)$$

Where, A_{sc} is the stud cross-section area (mm^2), $f_c^{`}$ is the concrete cylinder compressive strength (MPa), E_c is the elastic modulus of concrete (MPa), and F_u is the specified tensile strength of the stud (MPa). The (AISC, 1994) offers higher predication for the shear strength of the headed stud shear connector by about 40% compared with the one obtained from the Eurocode 4 (EN 1994-1-1, 2004).

Eurocode 4 (EN1994-2, 2005) Annex C provides specifications for the design of horizontally lying shear studs. The design shear resistance of the horizontal lying shear stud that causes splitting forces in the direction of the slab thickness (as shown in Figure 2-1) should be determined for ultimate limit states other than fatigue from Eq. (2.4), if this leads to a smaller value than that of Eqs. (2.1) and (2.2):

$$P_{Rd,L} = \frac{1.4k_v(f_{ck}da_r^{`})^{0.4}(a/s)^{0.3}}{\gamma_v} \qquad (2.4)$$

Where:

$a_r^{`}$ is the effective edge distance; = a_r - cv-Ø$_s$/2 ≥ 50mm;

k_v = 1 for shear connector in an edge position,

= 1.14 for shear connector in a middle position;

y_v is a partial factor (1.25);

f_{ck} is the characteristic cylinder strength of the concrete at the age considered, in N/mm²;

d is the diameter of the shank of the stud with 19≤ d≤ 25mm;

h is the overall height of the headed stud with h/d ≥ 4;

a is the horizontal spacing of studs with 110 ≤ a ≤ 440mm;

s is the spacing of stirrups with both a/2 ≤ s ≤ a and $s/a_r' ≤ 3$;

$Ø_s$ is the diameter of the stirrups with $Ø_s ≥8mm$;

$Ø_\ell$ is the diameter of the longitudinal reinforcement with $Ø_\ell ≥10mm$;

C_v is the vertical concrete cover according to Figure 2-1 in mm.

(a) middle position
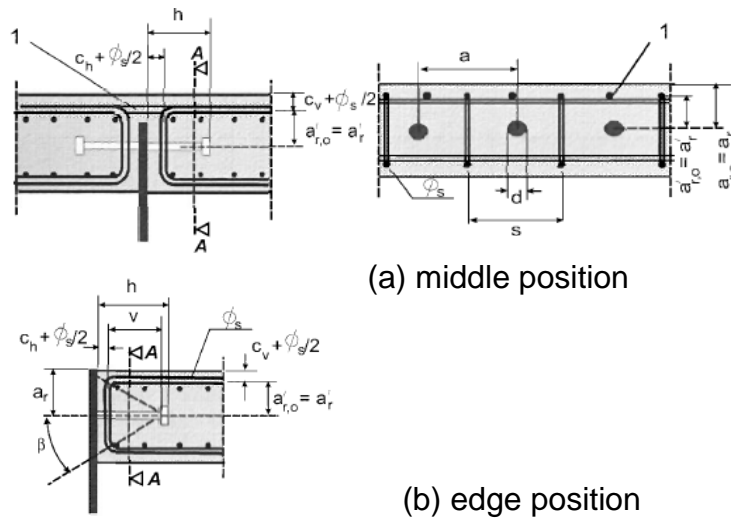
(b) edge position

Figure 2-1: Schematic of the horizontally lying shear studs Eurocode 4 (EN1994-2, 2005)

The failure of the pull-out of the stud positioned at the edge of the slab should be prevented by fulfilling the following conditions according to Eurocode 4 (EN1994-2, 2005) Annex C:

Uncracked concrete: $β ≤ 30°$ or $v ≥$ max (110mm; $1.7a_r'$; 1.7 s/2)

Cracked concrete: $β ≤ 23°$ or $v ≥$ max (160mm; $2.4a_r'$; 2.4 s/2)

The splitting force in the direction of the slab thickness should be resisted by stirrups according to Eurocode 4 (EN1994-2, 2005) Annex C, which should be designed for tensile force according to the following equation:

$$T_d = 0.3 \, P_{Rd,L} \qquad\qquad (2.5)$$

The influence of vertical shear on the design resistance of a stud connector due to vertical support of the slab should be considered. This interaction may be verified by the following equation:

$$\left(\frac{F_{d,L}}{P_{Rd,L}}\right)^{1.2} + \left(\frac{F_{d,V}}{P_{Rd,V}}\right)^{1.2} \leq 1 \qquad (2.6)$$

$$P_{Rd,V} = \frac{0.012(f_{ck}\emptyset_\ell)^{0.5}(da/s)^{0.4}(\emptyset_s)^{0.3}\left(a_{r,o}^{`}\right)^{0.7}k_v}{\gamma_v} \qquad (2.7)$$

Where, $a_{r,o'}$ is the relevant effective edge distance with $a_{r,o'} = a_{r,o} - c_v - \emptyset_s/2 \geq 50mm$. In addition to the design requirements given in Eq. (2.4), the following conditions should be satisfied:

$h \geq 100mm$; $110 \leq a \leq 250mm$; $\emptyset_s \leq 12mm$; $\emptyset_\ell \leq 16mm$.

2.2.2 Headed shear stud

Since the first use of headed studs as a shear connector in the 1950s (Davies, 1975), it has become the most common type of shear connectors in both bridge and building construction. Many investigations of headed studs have been carried out. This review focuses on the experimental studies of shear studs used in composite systems with solid slabs as well as profiled metal decking.

2.2.2.1 Headed studs used in solid slabs

Slutter and Driscoll (1965) presented nine push-out tests with solid slabs as shown in Figure 2-2, along with twelve composite beam tests with a span of 4.5m, and one two-span continuous beam test. From these tests they found that the ultimate flexural strength of the beam is related to the ultimate strength of the stud shear connector and that the stud's diameter (d_s) and concrete cylinder compressive strength ($f_c^`$) directly governs the ultimate strength of the stud as in Eq. 2.8:

$$q_u = 930d_s{}^2\sqrt{f_c^`} \qquad (2.8)$$
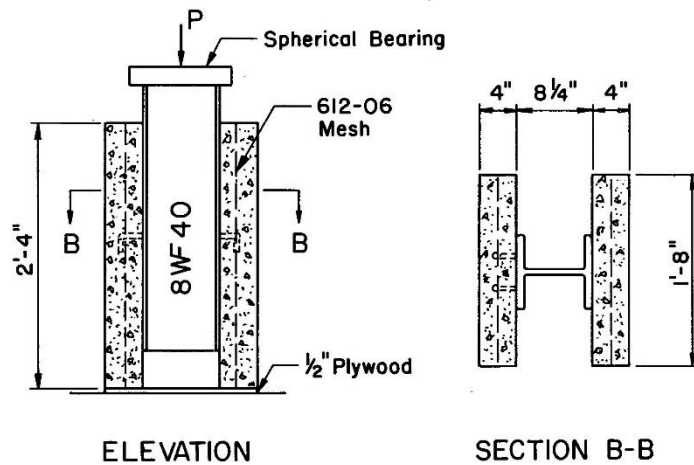
Figure 2-2: Details of the push-out test specimens
(Slutter and Driscoll, 1965)

Davies (1967) investigated the spacing and layout pattern of the studs by conducting twenty half-scale push-out tests with solid slabs. The studs were 10mm in diameter and 50mm in height. The results illustrated that two studs per flange placed perpendicular to the direction of the load had a 25% higher failure load than that of the studs placed parallel to the direction of the load, and the ultimate strength of the studs varied linearly with the longitudinal spacing of the studs.

Goble (1968) studied the behaviour of thin flange push-out specimens using 13mm, 16mm and 19mm diameter studs. Overall, 41 specimens were tested. It was found that the change in failure mode from stud shearing to stud pulling-out from the flange occurred at a stud diameter to flange thickness ratio of 2.7. The studs of the thinner flange specimens were more flexible in the lower load ranges, and there was no difference in ductility between the two failure modes. The ultimate strength of studs, as concluded by (Goble,1968) is very close to the conclusion of (Slutter and Driscoll,1965) only with a different coefficient of 882 rather than the 930 of Eq. 2.8.

Johnson and Oehlers (1981) presented statistical analyses of results of 125 push-out tests from 11 sources, 101 new push-out tests, and 4 composite beam tests. The statistical analyses conclude that the strength of studs in push-out tests is strongly influenced by the width of the slabs, and that little of the scatter found in the results is due to experimental error. One of the parameters in the new tests

is the height of the weld collar. The results show that a welded collar of $1.34d_s$ in diameter and $0.25d_s$ in height resists about 70% of the total shear, where d_s is the shank diameter. The shank failure strength of a stud increases continuously as the height of the weld collar increases from 0 to $0.35d_s$.

The overall conclusions are that the stiffness and strength of the studs are highest when shank failure occurs and that it is possible to base the spacing of studs on shank failure loads whenever sufficient breadth of a concrete slab can be provided. The minimum breadth is about twice the longitudinal spacing of the studs. Whether the maximum shear flow can be transferred to the slab without splitting the concrete depends on the layout of the studs. They should be spread as uniformly as is practicable over the whole available width of the steel flange, and should never be located in a single straight line above the web.

2.2.2.2 Headed studs used in profiled metal decking

Hawkins and Mitchell (1984) conducted 13 push-out tests to study the behaviour of headed stud shear connectors in composite beams with profiled steel sheeting perpendicular to the beam. The diameter of the stud was 19mm. The variables of the study were the type of loading (monotonic and cyclic loading), the depth of the profiled sheeting (38mm and 76mm), the type of slab (ribbed metal deck slab and solid slab), and the orientation of the metal deck (specimens with the metal deck perpendicular and parallel to the steel beams). Four different failure modes were observed during the test. The failure modes were (1) stud shearing, (2) concrete pull-out, (3) rib shearing and (4) rib punching. An equation was proposed as follows:

$$Q_p = 0.45\sqrt{f_c^`}\,A_c \qquad\qquad (2.9)$$

Where, Q_p is the shear capacity due to concrete pull-out failure (N), $f_c^`$ is the concrete compressive strength (MPa), and A_c is the area of concrete pull-out failure surface (mm^2).

Jayas and Hosain (1988) presented the results of 18 full-scale push-out test specimens and 4 pull-out specimens using profiled steel decking of 38mm thick and 16mm diameter studs, as shown in Figure 2-3. The parameters considered were the longitudinal spacing of the headed shear studs and the geometry of the metal decks' ribs. Five of the push-out specimens were cast with solid concrete

slabs, five specimens were cast with the ribbed metal deck parallel to the steel beam, and the remaining eight specimens were cast with metal deck perpendicular to the steel beam.
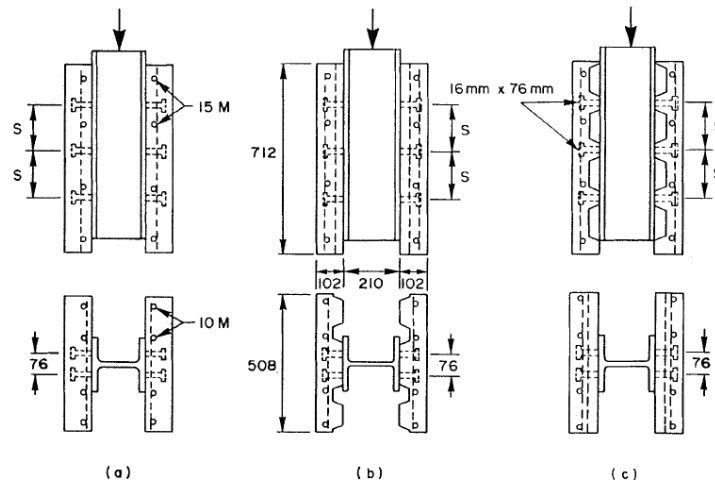
Figure 2-3: Description of push-out test specimens with profiled steel decking (Jayas and Hosain, 1988)

The results concluded that the current Canadian Standards Association (CSA, 1984) and Load and Resistance Factor Design codes (AISC, 1986) are able to predict stud strength correctly for specimens with solid slabs and with parallel ribbed slabs only when a failure occurs owing to stud shearing, i.e., when the studs are spaced sufficiently apart. The main mode of failure in the specimens with perpendicular ribbed metal decks was pulling out of the shear stud connectors. The authors have proposed two separate but similar empirical equations for specimens with a 38mm and 76mm metal deck, as follows:

For 38mm thick metal dick,

$$Q_p = 0.61\lambda\sqrt{f_c`}A_c \leq Q_u \qquad (2.10)$$

For 76mm thick metal dick,

$$Q_p = 0.35\lambda\sqrt{f_c`}A_c \leq Q_u \qquad (2.11)$$

Where, Q_p is the shear capacity due to concrete pull-out failure (N), λ is a factor that depends on the type of concrete used, fc` is the concrete compressive

strength (MPa), A_c is area of concrete pull-out failure surface (mm²) and $Q_u = 0.5A_s\sqrt{f_c`E_c}$.

Lloyd and Wright (1990) conducted 42 'through-deck' push-out tests on specimens that incorporated trapezoidal profiled steel sheets and headed shear connectors, as illustrated in Figure 2-4. This study investigated the effects of varying basic through-deck push-out test parameters to recommend a standard configuration for such tests, and further, to study the effect of practical sheeting-joint details on connector strength. The main variables were the slab width, slab height and the amount and position of reinforcement.
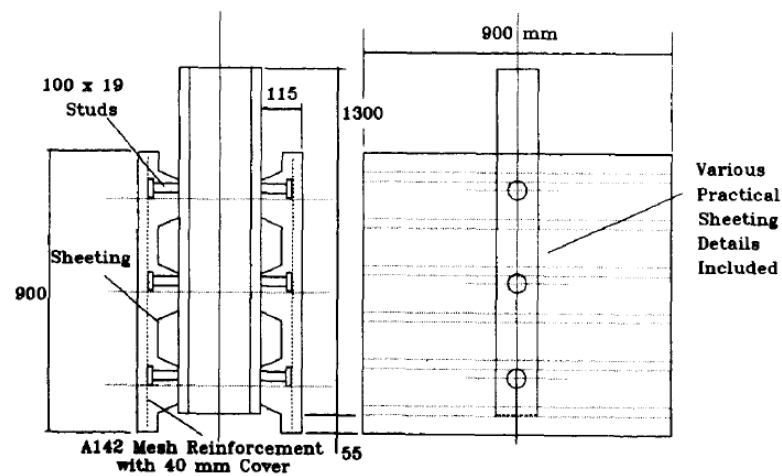
Figure 2-4: General arrangement of profiled sheet push-out
test specimens (Lloyd and Wright, 1990)

The test results showed that the capacity of the shear studs with profiled steel decking depends on the geometry of the metal deck and the stud height. It also concluded that the capacity of shear connector is considerably less than that in the solid slabs. A simplified formula for calculating the connector resistance was proposed as follows:

$$Q_p = A_p{}^{0.34}f_{cu}{}^{0.17} \tag{2.12}$$

Where Q_p is the shear capacity due to concrete pull-out failure (N), f_{cu} is the cube strength of the concrete, A_p is the concrete pull-out failure surface area dependent upon the geometry of the sheeting.

Hicks (1998) examined the longitudinal shear resistance of steel and concrete composite beams using conventional headed stud connectors through

conducting 42 push-out tests. The applicability of the existing design codes and the standard specimen used in assessing the strength of stud connector has also been examined. From the test results, it was proven that there is an additional parameter that affects the experimental strength of headed stud connectors, which has been identified as the generation of frictional forces developing at the interface between the base of the specimen and the reaction floor. The existence of such forces, which can significantly influence the apparent shear capacity that has developed, appears not to have been identified previously. In addition, detailing at the base of the specimens, which incorporate decking, also appears to affect the ability of the studs to transfer shear. A formula for calculating the connector resistance was proposed as follows:

$$Q_p = K_c \, f_c \, A_p \qquad\qquad (2.13)$$

Where, Q_p is the shear capacity due to concrete pull-out failure (N), K_c is the reduction factor for the cylinder strength of the concrete and is dependent on the number and arrangement of studs welded in a trough, f_c is the cylinder strength of the concrete, A_p is the concrete pull-out failure surface area dependent on the geometry of the sheeting.

Kim et al. (2001) conducted three push-out tests to study the behaviour of through-deck welded shear connectors. The headed stud used in the tests was 13mm×65mm and the profiled steel sheeting had a depth of 38mm, as shown in Figure 2-5.
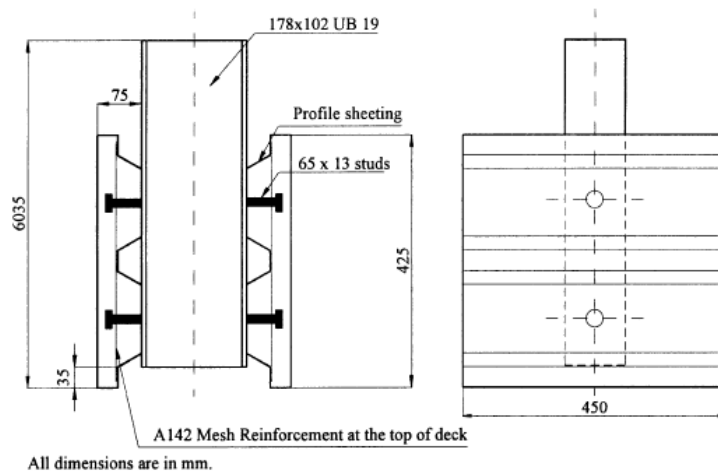
Figure 2-5: Arrangement for the push-out test (Kim et al., 2001)

Kim et al. (2001) discussed concrete pull-out failure surface area and strength. The major failure modes found in the tests were a concrete pull-out failure and local concrete crushing around the foot of the stud. It has been observed that there is some uncertainty in the existing formulae for the concrete pull-out area and strength, since the predicted concrete pull-out strengths by (Hawkins and Mitchell, 1984), and (Lloyd and Wright, 1990) are up to twice as high as the test strength. The strength predicted by (Hicks, 1998) was the closest to the test strength.

2.2.2.3 Headed studs used in lightweight concrete

Chinn (1965) examined 10 push-out tests using headed studs of 13mm, 16mm, 19mm and 22mm diameter. The stud lengths are approximately four times its diameter and the flanges of the steel section were greased. The shear failure mode was demonstrated by studs of all diameters, except for 22mm, which showed slab cracking. It was found that the ultimate strength of the studs in push-out tests was 18% to 43% higher than their direct shear strength. The conclusion was that the concrete strength had no effect on the ultimate strength of the studs, as demonstrated in the concluded formula, Eq. 2.14, where d is the stud diameter. Nevertheless, this was later disapproved by the conclusions of other studies (such as (Ollgaard et al., 1971) and (Hawkins, 1973).

$$Q_u = 39.22d^{1.766} \tag{2.14}$$

Ollgaard et al. (1971) conducted 48 push-out tests on headed studs of 16mm and 19mm diameter with normal and lightweight concrete (LWC). Seven parameters were studied: stud diameter, the number of studs per slab, the compressive and tensile strength of concrete, the elastic modulus of concrete, the density of concrete, and the type of aggregate, as shown in Figure 2-6.
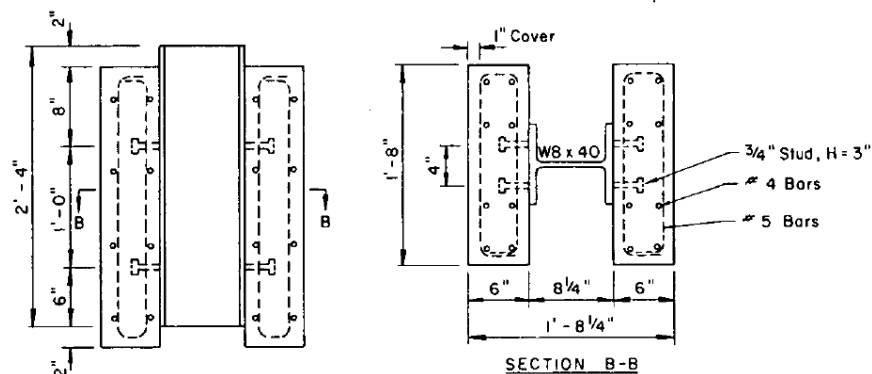
Figure 2-6: Details of push-out test specimens (Ollgaard et al., 1971)

The test results showed that the strength of the studs was more greatly influenced by the concrete compressive strength and elastic modulus than by the tensile strength and density of the concrete. Studs in both types of concrete showed significant deformation after the ultimate load's stage. The strength of the studs in the lightweight concrete was 15% to 25% lower than that when using normal concrete. Three failure modes were observed: concrete failure, stud shearing, and a combination of both. A formula was developed for the ultimate strength of the stud, Eq. 2.15. Its simplified formula, Eq. 2.16, was adopted by the AISC specifications. Moreover, the load-slip behaviour of the studs was mathematically expressed in Eq. 2.17, where Q is the load (kip) and Δ is the slip (in.).

$$Q_u = 1.106 A_s f_c^{`0.3} E_c^{0.44} \qquad (2.15)$$

$$Q_u = 0.5 A_s \sqrt{f_c^{`} E_c} \qquad (2.16)$$

$$Q = Q_u (1 - e^{-18\Delta})^{2/5} \qquad (2.17)$$

Hawkins (1973) carried out 47 push-out tests using solid slabs. The studied parameters were: type of stud steel (cold formed and hot formed), stud diameter (19mm and 22mm), concrete type (normal and lightweight), concrete strength, and slabs with or without reinforcement. The results showed that the concrete strength is the main factor governing the capacity of studs for a given slip value and that the properties of stud steel have a less significant effect. The ultimate tensile strength was found to be the most important property of the steel stud, rather than its yielding strength. Other variables have significantly less influence on the capacity of studs than the strengths of the concrete and steel. The author stated that the stress-slip curves of studs for low loads can be predicted by modelling studs as a flexible elastic dowel on an elastic foundation. For high loads, the shear stress can be predicted by empirical expression. Four unique failure modes were observed: the shearing of studs, the punch-out of studs, the pull-out of studs, and the cracking of the unreinforced slab.

Valente and Cruz (2009) conducted 12 push-out tests on headed studs of 19mm, 22mm and 25mm diameter and 9 push-out tests on Perfobond rib with lightweight concrete, as illustrated in Figure 2-7. Three parameters were studied: type of shear connector, stud diameter, the number of studs (single or double), and reinforcement arrangement of the slab.

(a) Isolated studs of 19, 22 and 25 mm diameter
(CN series)

(b) Double stud of 19 mm diameter
(CDN series)

(c) Perfobond connector
(CP series)

(d) Perfobond connector
(Specimen CP3.1)
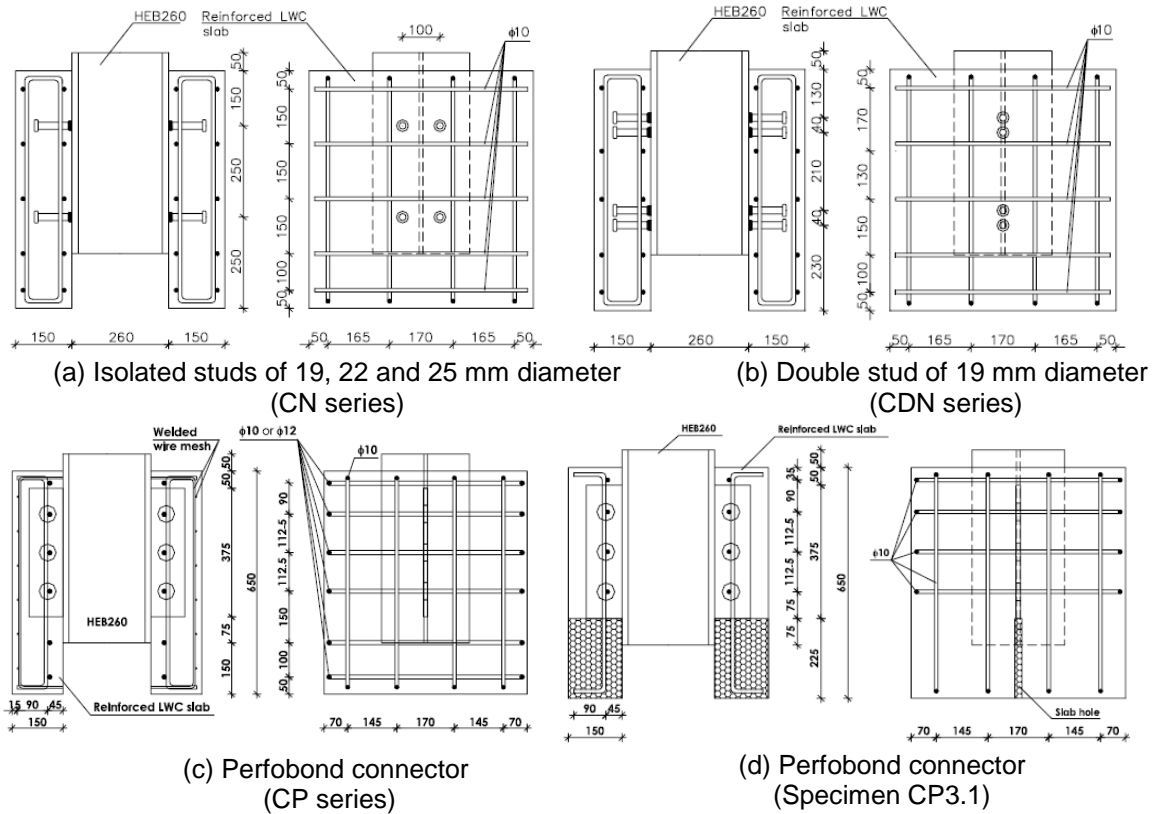
Figure 2-7: Details of push-out test specimens (Valente and Cruz, 2009)

The test results showed that LWC is adequate and can be used in composite structures. It obtained some loss in the load capacity of specimens with LWC compared with the specimens with normal concrete. The observed type of failure showed that LWC with a compressive strength of at least 55MPa to 60MPa should be used in order to ensure the stud shear failure. A ductile behaviour was showed by the headed studs as the plastic slip exceeded the value of 6mm demanded in Eurocode 4 (EN1994-1-1, 2004). The double stud shear connector showed a decrease in the load capacity of the connector, but allowed an increase in the slip deformation. This arrangement guarantees a more ductile behaviour of the shear connector. The failure mode with the Perfobond rib shear connector was verified with large cracking and crushing in some zones of the concrete slab. The rib connector itself did not suffer failure. This type of shear connector demonstrates a very high load capacity associated with a ductile behaviour. The maximum load attained depends on the area of transversal reinforcement disposed and concrete strength. It was shown that the connector load capacity tends to decrease when normal concrete is replaced by lightweight concrete. It was also confirmed that perfobond shear connector presents very stiff behaviour

at the beginning of the test. The maximum loads measured for Perfobond shear connector are much higher than those verified for headed studs.

2.2.3 Other types of shear connector

Other types of shear connectors have been developed for particular constructions with specific properties, in addition to the headed studs shear connection system. This section reviews publications on shear connection systems that are similar to those used in the proposed flooring system. The reviewed shear connectors consisted of horizontally lying studs, concrete dowels in DELTABEAM, an Ultra-Shallow Floor Beam, Composite Slimflor Beam and composite bridge girders.

2.2.3.1 Horizontally lying studs shear connector

Kuhlmann and Breuninger (2002) and Kuhlmann and Kürschner (2006) presented studies of a horizontally lying studs shear connector, where the studs are welded to the web post of a composite girder or slim-floor tee sections, as shown in Figure 2-8. This type of shear connector eliminates the less efficient steel top flange.

(a) Composite girder with horizontal lying studs without top flange

(b) Composite slim-floor tee section with horizontal lying studs
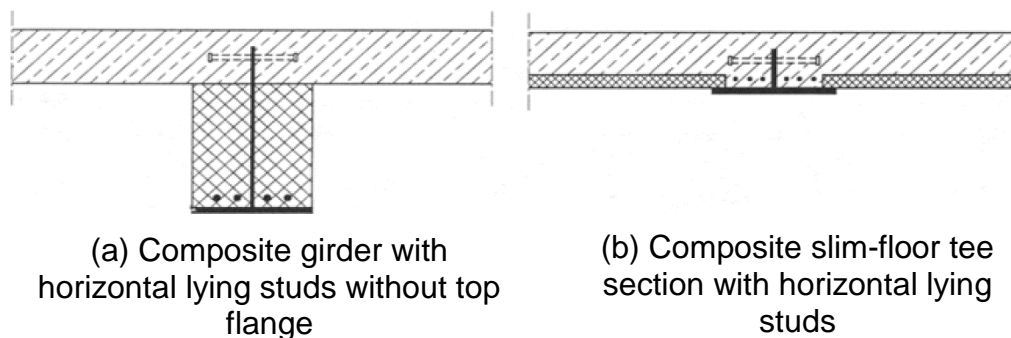
Figure 2-8: Composite girder and Composite slim-floor
(Kuhlmann and Breuninger, 2002)

Kuhlmann and Breuninger (2002) investigated the lying studs when subjected to longitudinal shear. Overall, 50 push-out tests were conducted. The main failure of these lying studs was due to the splitting of the concrete. The splitting action of the tension force creates cracks, as shown in Figure 2-9 (a). Therefore, vertical stirrups are used to prevent the concrete from expanding. The results demonstrated that the most significant affecting parameters on the shear strength of the lying studs are: concrete compressive strength, amount and arrangement of reinforcement, stud diameter, and the distance from the studs to the top surface of the concrete slab. It was found that the characteristic slip value of the

lying studs at failure is 17.4mm, which is much higher than the specified slip value of 6mm in Eurocode 4 (EN1994-1-1, 2004), which is the classification for a ductile shear connector.

In complement of the previous paper by Kuhlmann and Kürschner (2006), the lying studs shear connectors subjected to monotonic vertical shear was further investigated; a combination of monotonic vertical and longitudinal shear, along with cyclic longitudinal shear. A total of 19 cyclic push-out tests illustrated that a higher peak load close to static resistance causes a decrease of fatigue life and that a rise of concrete strength leads to a slight increase in fatigue life. However, no significant influence of the stirrup diameter could be demonstrated.

(a)   (b)
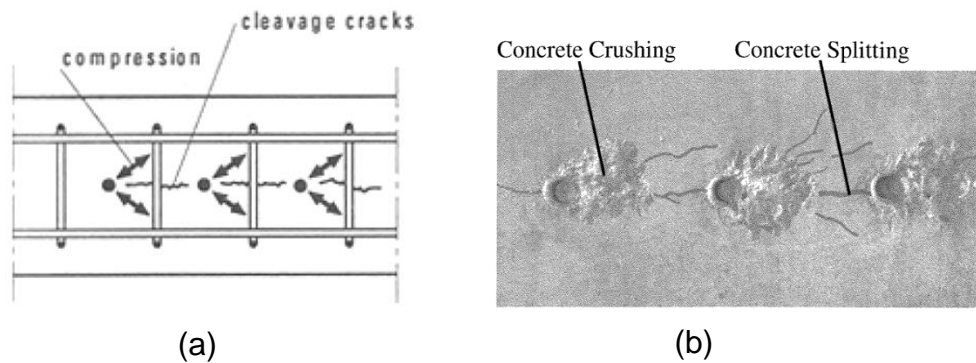
Figure 2-9: (a) Lying studs subject to longitudinal shear
(Kuhlmann and Breuninger, 2002); (b) Concrete failure due to cyclic
(Kuhlmann and Kürschner, 2006)

2.2.3.2 Concrete dowels shear connector in DELTABEAM

The Deltabeam is a type of incorporated floor beam, consisting of a steel boxed section with web holes, as shown in Figure 2-10. The holes are regularly spaced and form a shear connector with the concrete that fills the steel box section. There are two sizes of web opening in the Deltabeam: Ø75mm and Ø150mm. The openings have lipped edges that project inwards.

(a) Deltabeam Schematic   (b) Cross-section of
                                     the Deltabeam
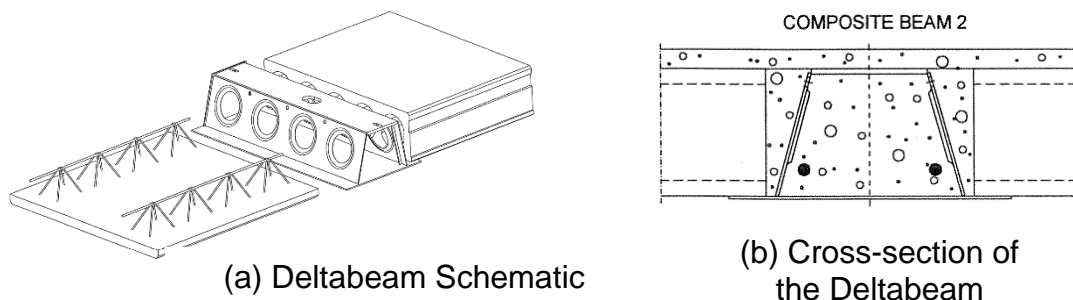
Figure 2-10: Deltabeam (Peltonen and Leskelä, 2006)

Peltonen and Leskelä (2006) conducted 75 push-out tests examining the shear-slip properties of the concrete dowel connector, using the parameters of web hole diameter, the geometry of the lip (mainly the lip depth), and concrete strength. The push-out tests, as shown in Figure 2-11 (a), were designed to simulate the shearing of the concrete infill with respect to the steel section. The tests illustrated the ductile load-slip behaviour of the concrete dowel shear connector, with average maximum slips of 6-9mm. The disassembled specimens demonstrated that the failure of all specimens was due to the shearing off of the concrete dowel, as shown in Figure 2-11(b). The effect of the depth of the lip, which is the depth of the concrete dowel on the resistance of the 75mm diameter web holes, was small. The authors developed a formula for calculating the shear resistance for the concrete dowel.

$$P_{max} = K_R(f_{ctm})f_{ctm}A_{\emptyset W} \tag{2.18}$$

Where, f_{ctm} is the mean tensile strength of the concrete, K_R is a resistance factor, which depends on the geometry of the hole (depth and diameter), and $A_{\emptyset w}$ is the area of the web hole. Three groups of the K_R were determined for both diameters.

(a) Push-out test arrangement

(b) Shearing off failure of the concrete dowel
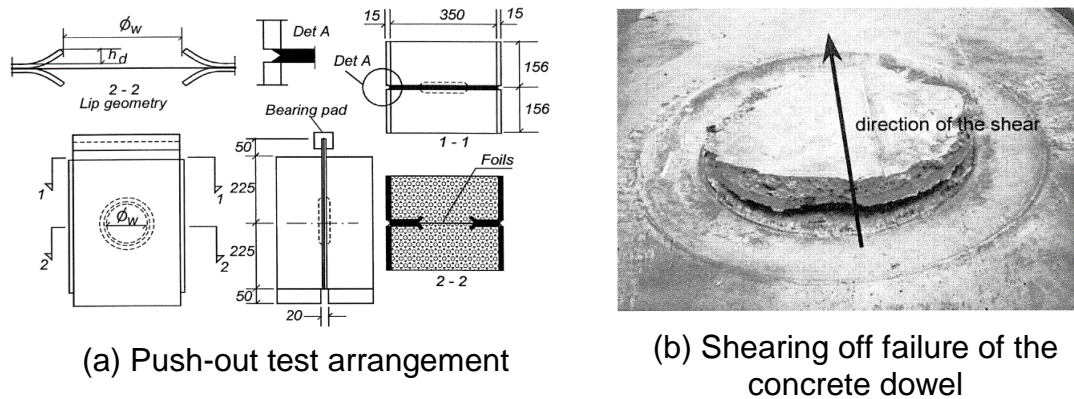
Figure 2-11: Push-out test (Peltonen and Leskelä, 2006)

2.2.3.3 Concrete dowels shear connector in Ultra Shallow Floor Beam (USFB)

Huo (2012) examined the longitudinal shear behaviour of ultra-shallow floor beams through 16 full-scale push-out tests. Four types of new shear connectors were studied, which are concrete infill only shear connectors, tie bar shear connectors, ducting shear connectors and horizontal shear stud connectors with two types of concrete (normal and fibre reinforced concrete) as shown in Figure 2-12.

(a) Ducting   (b) concrete infill   (c) horizontal studs   (d) tie bar
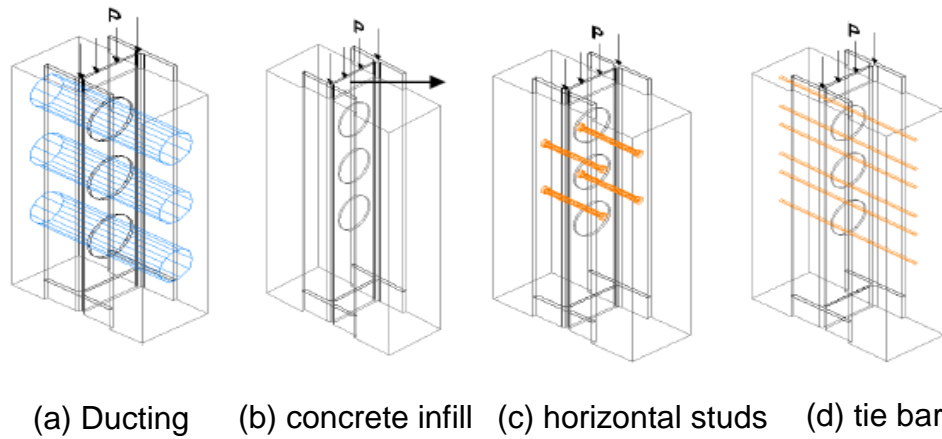
Figure 2-12: Push-out tests with different types of shear connectors
(Huo, 2012)

The test results concluded that uniform behaviour was demonstrated by each type of shear connectors. The use of tie bars and studs increased the shear capacity, slip, and ductility capacity of the shear connectors. The shear capacity of the shear connectors increased with increasing diameters of the web opening and with higher strengths of concrete infill. The authors proposed an empirical formula for calculating the shear capacity of the new shear connectors.

$$P_{us} = \frac{\left[2f_{ct}\left(\frac{\pi D^2}{4}\right) + 1.5f_{cu}(tD) + R_{add} \right]}{1.5} \tag{2.19}$$

Where, P_{us} is the design shear resistance of the shear connector, f_{ct} is the tensile splitting strength of concrete, f_{cu} is the compressive strength of concrete, D is the diameter of the web opening, t is the thickness of the web, R_{add} is the additional resistance of the tie-bar or studs.

2.2.3.4 Concrete dowels shear connector in Composite Slimflor Beam (CoSFB)

Hechler et al. (2013) investigated the capacity and the shear connectors' characteristics of the concrete dowels in the composite slimflor beams through 6 push-out tests, as shown in Figure 2-13. These tests studied the influence of varying the concrete compressive strength, the thickness of the steel beam web, the hole diameter in the slimflor beam and the reinforcement bar diameter that passes through the web. The authors found that concrete strength barely influenced the shear capacity of the connectors, while a small effect on the shear capacity has been recognised when changing the web thickness. In addition, they

recognized a significant increase in bearing capacity by doubling the diameter of the bar. Therefore, the influence of the reinforcement bar seems to be crucial in design for the bearing capacity. The results demonstrated that concrete infill around the web hole has a great effect on the bearing capacity of the concrete dowels' shear connectors.
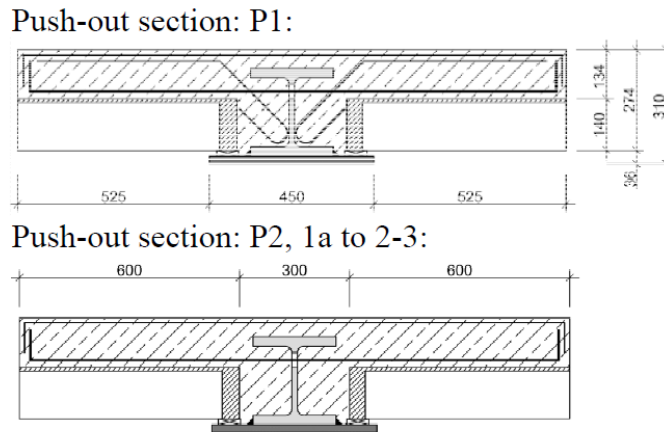
Figure 2-13: Specimen details of push-out test
(Hechler et al., 2013)

2.2.3.5 Concrete dowels shear connector in composite bridge girders

Mangerig and Zapfe (2003) carried out 102 push-out tests to investigate the effects of concrete dowels in composite bridge girders, with a view to develop a design procedure for the concrete dowels, as shown in Figure 2-14. An additional 16 push-out tests were implemented with cyclic loading investigating the fatigue properties of the concrete dowels. The parameters of the study were: the geometry of the perforation, concrete strength, and reinforcement. Six flexural tests were also carried out on composite girders without top flange, see Figure 2-14 (a). The variables of the specimens were: span, dowel arrangement and degree of the concrete dowel.

One of the failure modes of the concrete dowel, which results from the transverse tensile stress, was the punched cone, as demonstrated in Figure 2-15 (a). The criterion of this type of failure can be defined by applying shear stress to the surface of a regular cone. The authors disagree with the general concept of the double-shearing off of the concrete dowels along the planes of the web. It is suggested that the shearing surfaces are not completely parallel to the web plane, as shown in Figure 2-15 (b). The authors recognise that big concrete dowels require a reduction of the shear surface. The test results and failure mechanisms of the composite girder tests show the effective shear transferring mechanism of

the concrete dowel. A design formula of local pressure (or compressive) failure, as shown in Figure 2-15 (c), was developed:

$$P_{RD} = 72.7 h_d t_w \sqrt{f_{ck}} \, \frac{1}{\gamma_v} \qquad (2.20)$$

Where h_d is the concrete dowel height, t_w is the web thickness, f_{ck} is the concrete cylinder compressive strength and $\gamma_v = 1.25$.

(a) Top-flangeless girder   (b) Girder with open circular (c) Compressed concrete
    with web side filing   shaped plate welded on the   in the zone of maximum
                                       top flange   local pressure
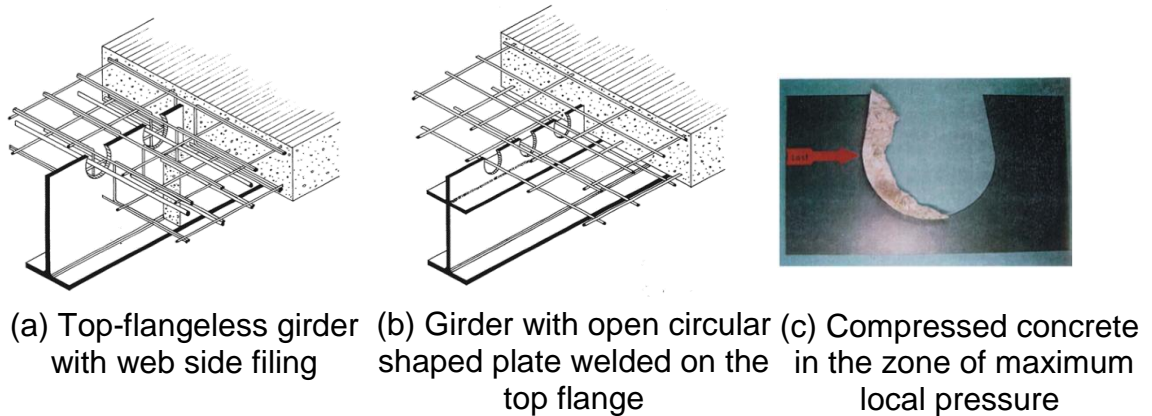
Figure 2-14: Different types of composite bridge girders
(Mangerig and Zapfe, 2003)

(a) Punch cone failure   (b) Bearing surface of
    mode   the concrete dowel in
                                      plane view
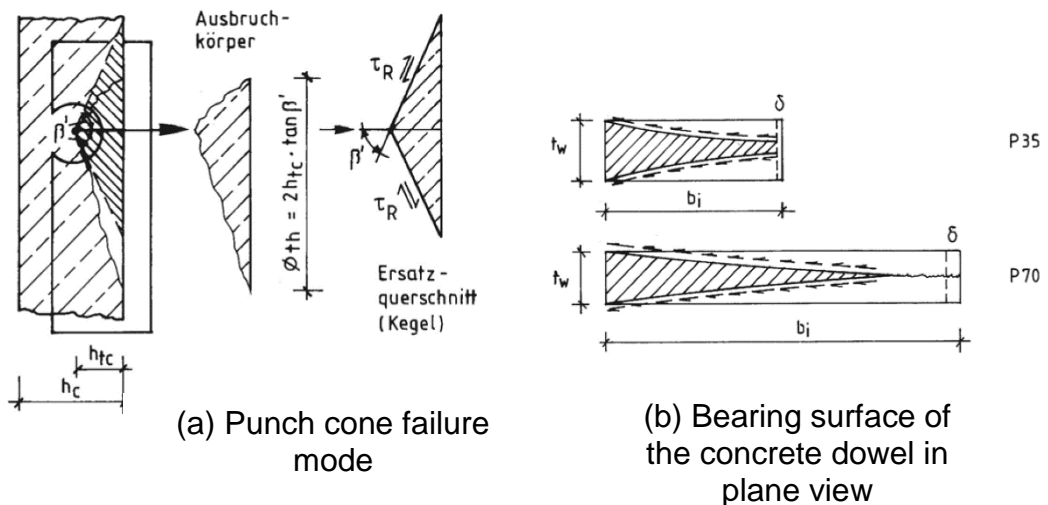
Figure 2-15:Failure modes of composite bridge girder
(Mangerig and Zapfe, 2003)

The shear connection system is important, since it characterises the performance of the steel-concrete composite structures. The shear connection of the prefabricated ultra shallow flooring system is formed by (a) web-welded shear studs (WWSS) and (b) WWSS with dowels. Such shear connection systems have not been investigated previously.

Headed shear studs connectors have been widely investigated since their initial use as the first shear connectors in the 1950s. The current codes of practice provide detailed specifications on the use and design of headed studs. Other types of shear connection system have also been developed for particular constructions. Publications for both headed shear studs and other types of shear connectors are reviewed here, particularly the experimental investigations (push-out tests). The codes of practice are also discussed herein to identify the critical characteristics that provide strength and ductility to the system.

2.3 Prefabricated shallow composite flooring systems

2.3.1 Hollow core precast slab

Hollow core precast slabs were developed in the 1950s when long-line prestressing techniques evolved, and for more than 30 years the type of units produced changed very little-the typical units in Europe were a maximum of 450mm thick. The hollow core precast slabs have been used in a variety of structural applications, including residential and commercial buildings, parking structures, and short-span bridges. The slabs contain voids that run continuously along their length, which help to reduce dead weight and material cost. Figure 2-16 shows hollow core precast slabs with two different top surface conditions.

(a) Specimen with machine-finished   (b) Longitudinally raked slab

Figure 2-16: Hollow Core floors (Mones and Breña, 2013)

Precast concrete units can be fabricated in a large range of shapes and sizes. Complex geometric configurations requiring difficult forming procedures, especially architectural concrete, can be fabricated and installed more economically by precasting than by forming and casting the concrete in place.

Precast concrete units are fabricated under controlled factory conditions. Hence, precast producers can fabricate their units with precise dimensional accuracy and consistency in finishes and textures.

Hollow core slabs are economical, and have good sound insulation and fire resistance properties. Common depths of hollow core slabs range from 150mm to 250mm for spans of approximately 10m (see Table 2-2).

In fact, a concrete topping layer is often cast in place onto the top surface of hollow core slabs in order to create a continuous level finished surface. The topping layer is typically 50mm deep. The concrete topping may increase the flexural strength, shear strength, and bending stiffness of the slab if the composite action is developed with the hollow-core units (Mones and Breña, 2013).

Table 2-2: Load Span of Hollow Core Precast Units with the depth of 250mm (Bison)

Floor Type	Maximum Span (m)	Unit Depth (mm)	Overall Floor Depth (mm)	Total Floor Weight (kN/m^2)	Live Load (kN/m^2)	Unit Width (mm)
Hollow Core Precast Units	12.92	250	300	4.8	3.5	1200
Hollow Core Precast Units	11.94	250	300	4.8	5.0	1200
Hollow Core Composite Precast Units	10.5	250	300	6.0	3.5	1200
Hollow Core Composite Precast Units	9.5	250	300	6.0	5.0	1200

Yee (2001) reviewed the structural and economic benefits of precast concrete construction, such as substantial savings in structural concrete and steel quantities, along with savings in the formwork due to the precast slab serving as formwork, which becomes a large portion of the composite slab structure. The initial formwork costs of precast units may be high, however by using the formwork repetitively on a mass production scale, the formwork cost per unit produced would be insignificant when compared with the accumulated savings in material quantity in the precast elements. This benefit is important not only for its immediate economic savings, but also for its long-term environmental benefits in

terms of conserving energy, saving natural resources, and preserving the world's ecosystem.

Due to the fact that hollow-core precast floors typically do not have any transverse shear reinforcement, the longitudinal shear strength of these units must be carefully observed during the design stage. Furthermore, with the use of relatively deeper units, the size effect on the shear strength becomes more significant. Therefore, the longitudinal shear strength of hollow-core precast units has been studied extensively.

Hawkins and Ghosh (2006) investigated the shear strength of hollow core precast slabs with depths greater than 320mm through shear strength tests performed by three U.S. manufacturers, as well as European research relating to hollow-core shear strength. It was found that the web-shear strength of relatively deep hollow core units can be smaller than those predicted by Eqs. 11 and 12 of ACI 318-05. The analysis of the results for tests on units with depths up to 410mm suggests that the location of the critical section for the evaluation of web-shear strengths should be a function of unit geometry.

Another type of hollow core precast unit is the hollow core composite floor, which consists of hollow core slabs with a cast-in-situ screed or concrete topping. A technical and economical alternative can be made by reducing the thickness of the precast units and increasing the thickness of the concrete topping by maintaining the load-carrying capacity for the whole composite section (Girhammar and Pajari, 2008). The expensive screed can be replaced by a cheaper concrete and installations could be embedded in the topping layer. Proper shear and bond strength of the interface is required for composite action. Earlier studies on prestressed hollow core slabs with concrete topping have been conducted by (Scott, 1973) and (Ueda and Stitmannaithum,1991).

Scott (1973) examined the composite action between the precast and cast-in-place portions through a load test. They found that composite action was evident up to the ultimate load. Three types of top surface of the precast slab were investigated: smooth, even, and machine cast finish. No reinforcing steel projecting from the precast slab into the topping concrete was used in this test. The results further demonstrated the substantial shear strength capabilities for

the hollow core units when used in combination with a 50mm concrete topping of modest strength.

Ueda and Stitmannaithum (1991) investigated the shear carrying capacity of precast prestressed hollow core slabs with concrete topping. The parameters under examination were the thickness of concrete topping, prestressing force, tensile reinforcement ratio and shear span-to-effective depth ratio. The complete composite action has been observed in their tests, although only rough surface finishing was provided. Only small slips were measured between the precast and topping concrete elements, and there was no evidence that their interface was an initiator of ultimate failure. For both thick and thin concrete topping, web shear cracking always took place in the precast element.

The effect of the presence (or absence) of steel bar reinforcement in the concrete topping of the composite hollow core floors was investigated by (Bayasi and Kaiser, 2003). The shear studs have been used to transfer forces among composite system components. The results revealed the need for an adequate number of shear studs to reduce failure potential due to inadequate stress transfer, and further revealed that concrete topping with added steel bars were needed to sustain the bending resistance of the generally brittle precast carbon fibre decks.

Dowell and Smith (2006) proved that the precast concrete panels act compositely in flexure, with a cast-in-place topping slab. No reinforcing bars have used in the topping concrete crossing the interface between slabs. The results verified that no horizontal shear slip occurred between the precast concrete panels and the cast-in-place slabs, and that the deck acted as a fully composite member to failure. The testing was conducted with different roughening levels applied to the top of the precast concrete slab.

Therefore, the shear and bond strengths of the interface between the two portions are critical for the full composite action of the hollow core slab with concrete topping. The shear and bond strengths of interfaces and contact surfaces in different composite concrete structures have been investigated (e.g. (Tassios and Vintzēleou, 1987) (Bayasi and Zeng, 1997) (Gohnert, 2000); (Beushausen, 2001); and (Silfwerbrand, 2003).

Studies focusing on the flexural behaviour of composite hollow-core units are very limited. Baran (2015) investigated the flexural response of precast prestressed concrete hollow-core slabs with cast-in-place concrete topping. Five precast concrete hollow-core units have been tested. The flexural response determined from the numerical analysis of testing specimens was later compared with the behaviour that was ascertained through experiment. The results demonstrate that a major composite action is valid between the hollow-core unit and the topping slab under load levels corresponding to the uncracked state of the cross-section.

The existence of a topping slab resulted in improvements in the cracking moment and initial stiffness of hollow-core units. The beneficial effect of the topping slab on the ultimate moment capacity was observed to be limited, mainly because of the loss of composite action prior to reaching the ultimate moment capacity. Horizontal shear strength at the interface between the hollow-core unit and topping slab was determined through a limited number of push off load tests and through calculations considering the load level corresponding to the initiation of significant relative slip using the basic mechanics of materials approach and the simplified code expression. The measured and computed interface shear strength values were observed to be significantly lower than the horizontal shear strength values specified by the (ACI-318-05, 2005) and (AASHTO, 2010) specifications.

These hollow core precast slabs have been integrated into slimflor construction. These structures benefit from slender ceilings, fast erection, a small dead load and a high level of quality. The most common type of slimflor construction consists of precast hollow core slabs supported on the lower flange of transverse shallow steel beams (Slimflor beam). The Slimflor beam consists of a Universal Column section connected with a plate welded to the bottom flange, as shown in Figure 2-17; the bottom plate supports the floor slabs directly.
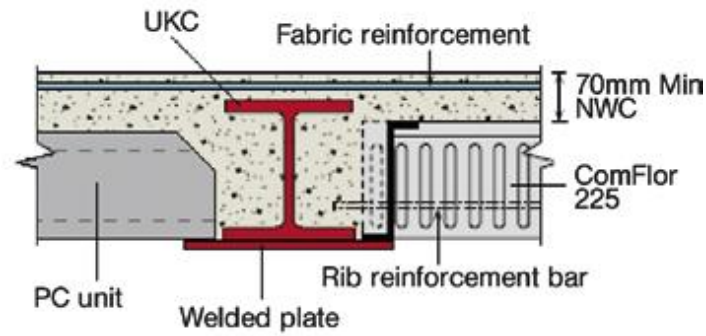
Figure 2-17: Cross section of the Slimflor beam with
precast units (Lawson et al., 1999)

Mullett (1992b) introduced design guidance for Slimflor beams with hollow core precast units in agreement with the (BS5950: Part 1, 1990). The shear capacity of the hollow core precast slabs is considerably reduced due to transverse stresses when they are bedded on slender beams (flexible supports), such as Slimflor beam.

Hechler et al. (2013) investigated the effects of different support conditions on shear capacity, the effects of full-scale tests on floor systems, consisting of ten slabs on flexible supports, and further, reference tests on single slabs on rigid supports were performed. The present paper describes the development and calibration of nonlinear three-dimensional finite element (FE) models with the available test data to numerically determine the influence of support type and stiffness on load-bearing behaviour. The results reveal the slabs' failure mechanism and identifies a range of flexible supports.

Another type of slimflor beam, which integrates the precast units with it, is the Asymmetric Slimflor Beam (ASB). This slimflor beam is a rolled section with a thin flange where the additional plate is not required in this type, as shown in Figure 2-18. Rackham et al. (2006) introduced guidance on the design of ASB using precast hollow core concrete slabs, which cover two types of structures, with or without concrete topping. Practical guidance is determined by the effect of tolerance on the PC units' bearing capacity and the end preparation that provides clearance for the concrete encasement.

Figure 2-18: Asymmetric Slimflor beam (ASB) with precast
units (Rackham et al., 2006)

The hollow core precast slabs have been incorporated with a new type of shallow floor beam, which is an Ultra-Shallow Floor Beam. An Ultra-Shallow Floor Beam (USFB) is a perforated beam designed to act compositely with floor slabs lying within the steel flanges, which is developed by ASD Westok. It has been fabricated by welding two highly asymmetric cellular tee-sections together along the web (Tsavdaridis et al., 2009b). The top and bottom tee-sections have been cut from different parent plain sections, where the top tee is smaller than the bottom tee-section, as presented in Figure 2-19. This configuration reduces the weight of the beam and increases moment capacity. The circular and elongated web openings provide a channel for tie-bars, ducting and building services to pass through the structural depth of the beam. This minimises the structural depth of the composite sections and produces lighter members for economy reasons. In USFBs, the concrete slab lies within the steel flanges and has been connected through the web opening. These concrete dowels enhance longitudinal and vertical shear resistance. As a result, fire resistance is increased.

Figure 2-19: Schematic of USFBs with tie- bar shear connection
and precast units (Tsavdaridis et al., 2009b)

2.3.2 Arcelor Cofradal slab

The Cofradal slab is an innovative pre-fabricated slab system developed in France by AreclorMittal in 2009 (COFRADAL200®). This type of slab is suitable for light industrial offices and residential buildings. This system is a prefabricated steel-concrete composite slab produced in a factory and is ready to fix on the construction site, as shown in Figure 2-20.

(a) Cross section of
Cofradal slab
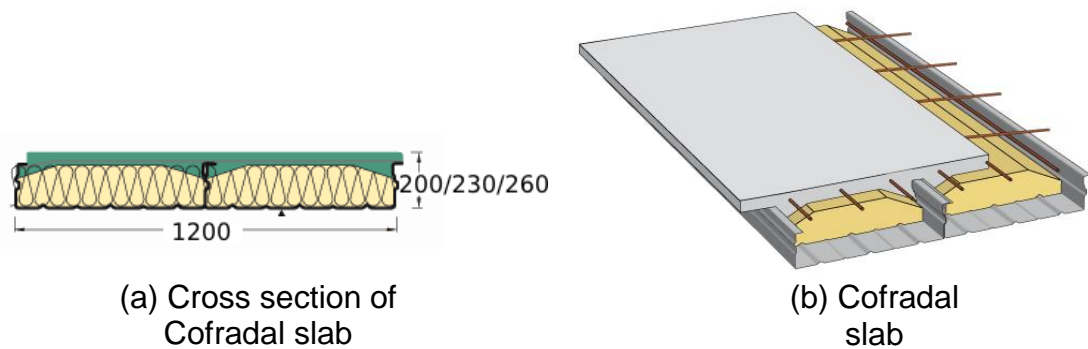
(b) Cofradal
slab

Figure 2-20: Cofradal slab (COFRADAL200®)

The slabs come completed with a steel and concrete top and do not require any structural on-site concreting on the floor. Only a small amount of concrete is needed for embedding the support's perimetrical joint area and light concrete is required on top of the floor for the circulation surface. The depth of the unit is fixed at a total thickness of 260mm and weight 2.8kN/m^2. Two widths can be provided of 600mm and 1200mm with a span of 7.8m. The benefits of this type of slab are that it is two to three times lighter than an equivalent usual plain concrete slab. It allows for fewer frame sections and fewer ground foundations. It can be used for ground slabs, provided that air circulation is effective and moisture is avoided beneath the slab. As it is a fully prefabricated slab, there is no need for propping on site, which allows for simple circulation on the construction site and rapidly available area for stocking during the construction process. This contributes to the economy of the process by reducing death periods of works due to there being no need for concrete curing.

Cofradal slab consists of a galvanised profiled steel sheeting with a tensile strength of 320N/mm² fitted with a mineral wool insulation layer and reinforced concrete top layer with C30 (f_{ck} = 30N/mm²) and reinforcing bars welded onto the steel sheeting. This welding provides a connection point between the tensioned steel and the compressed concrete, creating composite behaviour between the

steel sheeting and the top concrete. The mineral wool layer, with a density of $50kg/m^3$, is an effective shuttering bed for the concreting of the top of the slab. This layer provides thermal insulation between levels if needed, acoustic resistance, and finally provides the desired fire resistance.

The slab resistance depends on the live load to be used on the slab. The element can span from 3m for a live load of 8.8kN/m² to 7m for a live load of 4.3kN/m², see Table 2-3. Other types of Cofradal slab are available with different depths, such as 230mm and 260mm.

Table 2-3: Load Span of Cofradal Slab with depths less than 300mm
(COFRADAL200®)

Floor Type	Maximum Span (m)	Unit Depth (mm)	Overall Floor Depth (mm)	Total Floor Weight (kN/m²)	Live Load (kN/m²)	Unit Width (mm)
Cofradal 200	7.0	200	200	2.4	4.3	1200
Cofradal 230	7.5	230	230	3.1	3.5	1200
Cofradal 260	7.8	260	260	2.8	2.5	1200

Cofradal slabs have been used with an advanced type of slimflor beam, known as a Composite Slimflor Beam (CoSFB). Composite slimflor is the most recent type of slimflor and integrated beam structure. It consists of a steel section with circular openings filled with concrete and a plate, which is welded to the bottom flange, as illustrated in Figure 2-21. The use of concrete dowels was to assure a controlled shear transmission between the slimflor beam and the concrete slab (Hechler et al., 2013).

The possibility of combining concrete dowel technology with SFB technology has been identified and developed by the AreclorMittal. The relevant tests have been performed at the University of Stuttgart.

The load-bearing behaviour of deep embedded concrete dowels in CoSFBs and their parameters have been investigated through experimental tests (Baran, 2015). A specific focus has been given to the effect of the ratio of the resistance of concrete dowel to the concrete compression class. The results showed that using concrete dowels provides a considerable increase to the load-

bearing capacity of the floor beam. Further investigations have been done by using an FE analysis.

Lawson et al. (2015) reviewed the performance characteristics and some recent improvements in slim-floor and integrated beam structure, such as CoSFB. This type of construction provides a flat floor using precast concrete slabs, Cofradal slabs or deep composite decking. This shows benefits over other forms of construction in many sectors.
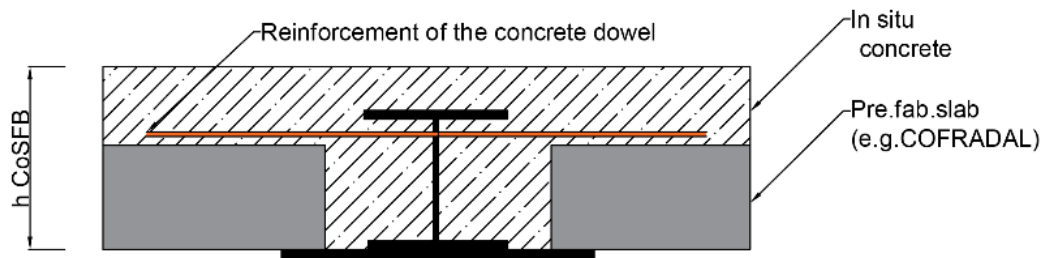
Figure 2-21: Typical CoSFB-composite slimflor beam section with Cofradal slab (Hechler et al., 2013)

2.4 Summary

In this chapter, a detailed literature review of different types of shear connectors and existing prefabricated shallow flooring systems have been presented, which is important to the objectives of this thesis. Although, the shear transferring mechanism of the prefabricated ultra shallow flooring system had not been examined previously, the review of publications on other types of shear connectors and prefabricated shallow composite flooring systems has provided many useful guidelines. The collected information used in the later research was:

- Methodologies of testing and analysis.
- Findings of testing, i.e. characteristic behaviour, failure mechanism, shear capacities and flexural strengths.
- Findings of the analysis, i.e. design formulas and methods.
- Benefits and drawbacks of other forms of shear connectors and shallow flooring systems.

The properties of the shear connector are fundamentally important for the behaviour and the strength of a steel-concrete composite flooring system, as large longitudinal shear forces are transferred along the interface of the concrete and steel elements. This thesis presents several investigations of unique shear

transferring mechanisms of prefabricated ultra shallow flooring systems. For such systems, the shear transferring mechanism can be significantly different to the system using conventional shear studs, which is yet to be investigated.

The information on push-out tests provided by the review on the shear connector was used in the current study. The shear capacity of the traditional headed studs was dependent on different parameters, such as the stud diameter, the ultimate tensile strength of the steel stud, and the concrete compressive strength. The method for investigating the shear connection systems in this thesis was first to identify the parameters that would be effective for the shear resistance of the new shear connection system, and then push-out tests were designed and carried out. The review on the shear connector was similar to that used for the ultra-shallow flooring system, which also provided comparable information, such as modes of failure, slip values and design formulas. For example, the horizontally lying studs' shear connector had a similar arrangement. The links between the publications and the information used for the later research are summarised in Table 2-4.

Limited experimental work and a lack of research of the issue of using lightweight concrete in shallow composite flooring systems is evident. Moreover, all existing shallow composite flooring systems have weight, span and depth limitations, along with prefabrication and site construction issues. Findings from the research carried out for the shear connectors used with shallow composite flooring systems have shown that the shear capacity of the shear connectors is dependent on the type of shear connector and concrete strength. New types of shear connectors with new concrete materials need to be developed for the use of shallow composite flooring systems to reduce weight, depth and increase the span. Therefore, new types of shear connection systems with new concrete materials have been developed and are used in the current study. This thesis has presented the experimental and analytical studies of the novel shear connection systems (WWSS and WWSS with dowels) used with lightweight aggregate concrete for the prefabricated ultra shallow flooring system.

Table 2-4: Links between the publications and information used in the later research

Information used for later research			Publications
Codes of practice for headed studs		Design formulas and design table	Eurocode 4 (EN 1994-1-1, 2004), British Standard (BS5950-3.1, 1990), American Institute of Steel Construction (AISC, 1994)
Push-out tests	Headed studs	Parameters effect to the shear composite and design formulas	(Chinn, 1965),(Slutter and Driscoll, 1965), (Davies, 1967), (Goble, 1968), (Ollgaard, 1971), (Hawkins, 1973)
	Horizontal lying studs	Important parameters and characteristic slips	(Kuhlmann and Breuninger, 2002), (Kuhlmann and Kürschner, 2006)
	Concrete dowel in Deltabeam, USFB and CoSFB	Load-slip behaviour, slips, failure mechanism and design formula	(Peltonen and Leskelä, 2006), (Huo, 2012), (Hechler et al., 2013)
Existing lightweight prefabricated shallow composite flooring systems	Precast hollow core slab	Advantages, Disadvantages	(Yee and Eng, 2001)
	Arcelor Cofradal slab	Advantages, Disadvantages	(Braun et al., 2015)

Chapter 3 : Experimental programme

3.1 Introduction

The properties of the shear connectors are fundamentally important for the behaviour and the strength of a steel-concrete composite flooring system, since large longitudinal shear forces are transferred along the interface of the concrete and steel elements. This chapter presents the shear transferring mechanism, along with the methodologies of the investigations of the shear connection systems used for the prefabricated ultra shallow flooring system.

3.2 Background of lightweight concrete used for the prefabricated ultra shallow flooring system

The prefabricated ultra shallow flooring system is fabricated using lightweight concrete. The main reason for the use of lightweight concrete (LWC) is to reduce the dead load of the flooring system, which results in a reduction in the size of the columns, beams, foundations and other load-bearing elements, in addition to improving the thermal properties of the elements, improving the fire resistance, saving time in transporting and handling prefabricated units on site, and further, reducing both formwork and propping. Lightweight concrete provides better thermal performance than normal weight concrete, and its application may significantly reduce energy consumption in buildings. Real et al. (2015) argued that the application of structural lightweight concrete in buildings located in European countries could reduce heating energy consumption by 15% when compared with normal weight concrete, due to its superior thermal performance, thereby reducing various costs of operation, such as heating and air-conditioning. In addition, lightweight concrete has good acoustic properties, whereby sound is absorbed and not reflected, as is the case with dense concrete. Moreover, it is non-combustible and has good resistance to fire. As such, with good planning, using structural lightweight concrete may achieve an economic benefit to many engineering applications (NRMCA, 2003).

Lightweight concrete (LWC) can be defined as the concrete of a substantially lower unit weight than that made of gravel or normal weight crushed aggregates. The dry densities are normally in the range of 800kg/m^3 to 2000kg/m^3 (El Zareef and Schlaich, 2008). Lightweight concrete is manufactured by either using lightweight aggregates or through the formation of voids in concrete by

omitting sand or by formation of voids in cement via the addition of substances causing foam. There are three categories of LWC, namely structural LWC, low density LWC and moderate strength LWC (Neville and Brooke, 2005). According to (NRMCA, 2003), structural LWC has an in-place density of between 1440kg/m^3 and 1840kg/m^3. Clarke (2002) defines structural LWC as having densities in the range of 1200kg/m^3 to 2000kg/m^3. Normal density concretes range from 2200kg/m^3 to 2600kg/m^3 depending on the type of aggregates used (Neville and Brooke, 2005). According to the above literature, structural LWC should have a minimum compressive strength of 17N/mm^2. Low density lightweight concrete has a density between 300 and 800 kg/m^3. This type of concrete is used for non-structural purposes, mainly for thermal insulation purposes (Neville and Brooke, 2005). The moderate strength lightweight concrete lies between structural LWC and low density LWC. Its compressive strength is between 7 and 17 MPa and the thermal insulation characteristics are in-between those of low-density concrete and structural lightweight concrete (Neville and Brooke, 2005).

LWC is manufactured by combination of fine and coarse lightweight aggregates, or coarse lightweight aggregates with normal weight fine aggregates. The complete replacement of normal weight aggregates with lightweight aggregates reduces air dry density to about a half that of normal weight concrete (Clarke, 2002); (NRMCA, 2003). Neville and Brooke (2005) define three classes of LWC, which can be made available according to their method of production: (i) No fines concrete obtained by omitting the finer fraction of normal weight or lightweight aggregates to create air filled voids, (ii) Aerated concrete produced by the inclusion of air bubbles in cement paste or a cement mortar matrix to form a cellular structure that contains 30–50% voids, and (iii) Lightweight concrete obtained by replacing either wholly or partially normal weight aggregates in a concrete mix with lightweight aggregates of low apparent specific gravity (porous aggregates containing large proportion of voids). This last type is used in the present investigation where all course aggregates were replaced with lightweight aggregates of pumice or scoria in order to obtain the lightweight concrete (LWC). LWC does not provide only lighter structures, but also creates structures with better insulation against heat and sound, and such structures are more resistant to earthquakes (lower seismic impact due to their lower weight).

To achieve sustainable development, researchers have attempted to identify the waste or by-product materials that can replace the materials in lightweight concrete without consuming limited natural resources (Pelisser et al., 2011). Lytag is a lightweight aggregate that is manufactured from pulverised fuel ash and sintered fly ash: a by-product of coal-fired power stations. Lytag is up to 50% lighter than normal weight aggregate. The bulk density of lytag aggregate is 700-800kg/m^3 compared with the bulk density of a normal aggregate of 1550kg/m^3. The sustainability of LWA (Lytag) assists with diverting materials going to landfill and reduces the demand for virgin, normal weight natural aggregate. For instance, every tonne of Lytag used saves the extraction of two tonnes of natural aggregate (Doel, 2007). There is also a positive impact on our environment, since more LWA can be transported in one load, reducing the number of vehicle movements and associated emissions.

Another type of lightweight aggregate is the lightweight expanded clay aggregate (Leca), which is a manufactured and artificial lightweight aggregate. After heating at 1150°C in a rotary kiln, the clay expanded to about four to five times its original size and took the shape of pellets. Leca is up to 50% lighter than lightweight aggregate (Lytag). The bulk density of Leca aggregate is 250-450kg/m^3, which when compared with the lytag aggregate is 700-800kg/m^3.

Table 3-1 shows the span limits for the prefabricated ultra shallow flooring system.

Table 3-1: Span limits for the prefabricated ultra shallow flooring system

Floor Type	Concrete Type	Concrete density kg/m^3	Maximum Span (m)	Overall Floor Depth (mm)	Total Floor Weight (kN/m^2)	Live Load (kN/m^2)	Unit Width (mm)
Prefabricated ultra shallow flooring system	LWC	1700	8.0	230	2.67	2.5	2000
			8.0	260	2.71	3.5	2000
			9.5	300	2.81	5.0	2000
			10.0	300	2.81	3.5	2000

3.3 Concrete mix and material details

For further reduction in the weight of the concrete floor system, lightweight materials (two types of lightweight concrete with a density approximately half the density of normal weight concrete) are used. This aforementioned weight reduction is in addition to the weight reduction achieved due to the shape of the ribbed slab, which will considerably reduce the amount of concrete volume and weight, while allowing for the structural strength performance of the system. Therefore, the lightweight concrete ribbed slab is expected to be more economical than the existing precast concrete slab and the Cofradal slab and could assist with the steel composite edge beams of the prefabricated ultra shallow flooring system to achieve a longer span than other systems.

Many available design mixes were investigated to find the most appropriate mix of the prefabricated ultra shallow flooring system (Brooks et al., 1987; Alengaram et al., 2013). Consequently, the lightweight concrete mixes proposed by (Brooks et al., 1987) with a density of 1705kg/m^3 and a density of 1300kg/m^3 are adopted in this study, with a compressive strength of 30N/mm^2 and 16N/mm^2 at 28 days, which are capable of providing the required strength based on the calculation of the ribbed slab design. The mix proportions of lightweight concrete mixes are illustrated in Table 3-2. These mixes used two types of lightweight aggregate (Lytag and Leca). In addition, normal weight concrete is also used, with a density of 2325kg/m^3 and a compressive strength of 30N/mm^2 as shown in Table 3-2. Steel bars with a yielding strength of 420N/mm^2 will be used for reinforcing the specimens.

3.3.1 Materials properties

The main raw materials of lightweight concrete (LWC) are cement, lightweight fine aggregate, lightweight coarse aggregate and water. The materials used for this investigation can be explained as follows. Combinations of the following constituent materials were used to produce lightweight concrete in this research. Figure 3-2 shows different types of aggregates used to prepare the various types of concrete.

- **Portland cement:** CEM I-52,5 N, 3.15 specific gravity (S.G.), conforming to (BS EN 197-1:2011).

- **Lightweight fine aggregate:** LYTAG lightweight aggregate conforming to (BS EN 13055-1:2002) with a saturated surface dry specific gravity of 1.40 in its fine (0-5mm) size is used in the mixes. The bulk density of the fine Lytag is 1000kg/m^3. It is manufactured from pulverised fuel ash (provided by Lytag Ltd, UK) and sintered fly ash, a by-product from coal-fired power stations (Cheeseman et al., 2005). The gradation of the used lightweight aggregate is illustrated in Figure 3-3.

- **Lightweight coarse aggregate:** LYTAG lightweight aggregate conforming to (BS EN 13055-1:2002) with a saturated surface dry specific gravity of 1.64 in its coarse (5-10mm) size is used in mixes. The bulk density of the coarse Lytag is 700kg/m^3. The gradation of the used lightweight aggregate is illustrated in Figure 3-4.

- **Lightweight fine aggregate:** LECA lightweight aggregate conforming to (BS EN 13055-1:2002) with a saturated surface dry specific gravity of 0.32 in its fine (0-5mm) size is used in the mixes. The bulk density of the fine Leca is 620kg/m^3. It is manufactured from high-temperature burnt clay nodules. The gradation of the used lightweight aggregate is illustrated in Figure 3-5.

- **Lightweight coarse aggregate:** LECA lightweight aggregate conforming to (BS EN 13055-1:2002) with a saturated surface dry specific gravity of 0.44 in its coarse (5-10mm) size is used in the mixes. The bulk density of the fine Leca is 280kg/m^3. The gradation of the used lightweight aggregate is illustrated in Figure 3-6.

- **Fresh, clean and drinkable water**.

(a) Natural gravel   (b) Natural sand   (c) Lytag coarse aggregate   (d) Lytag fine aggregate

(e) Leca coarse aggregate   (f) Leca fine aggregate

Figure 3-1: Different types of aggregates used in preparing concrete mixes
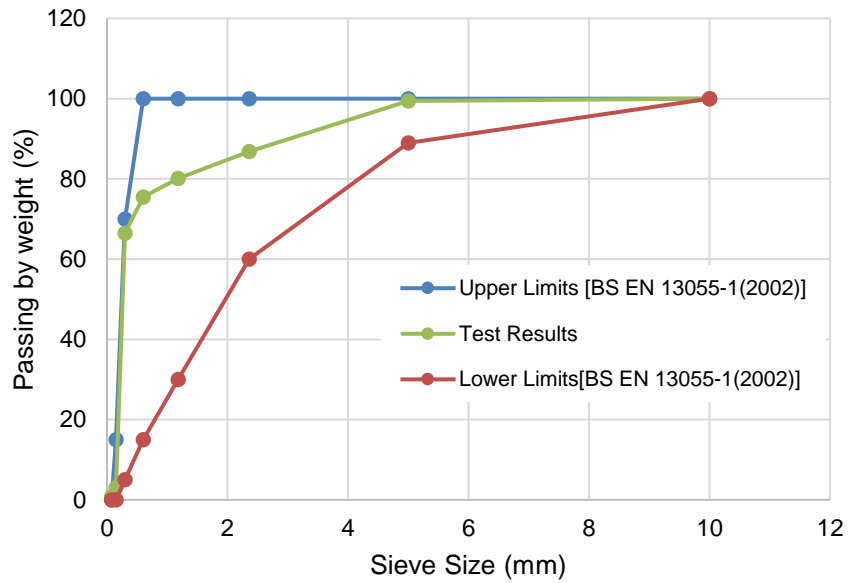
Figure 3-2: Grading curves for standard requirements and lightweight fine aggregate used (Lytag)
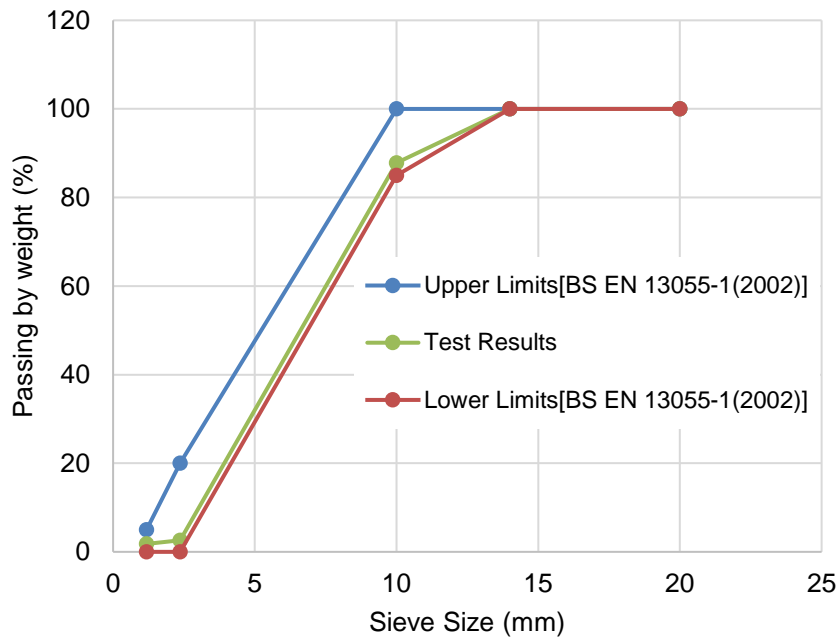
Figure 3-3: Grading curves for standard requirements and lightweight coarse aggregate used (Lytag)
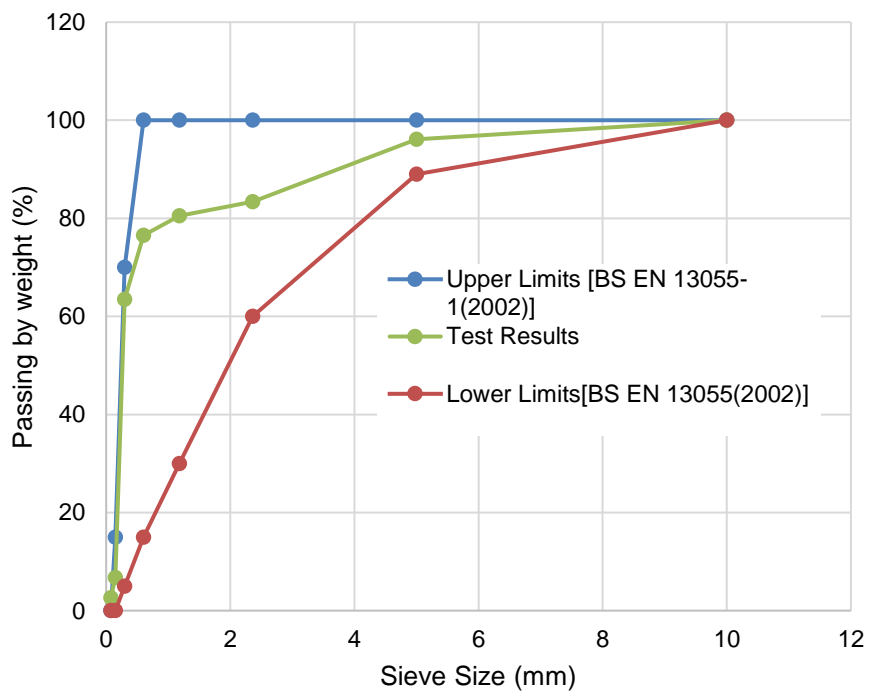
Figure 3-4: Grading curves for standard requirements and lightweight fine aggregate used (Leca)
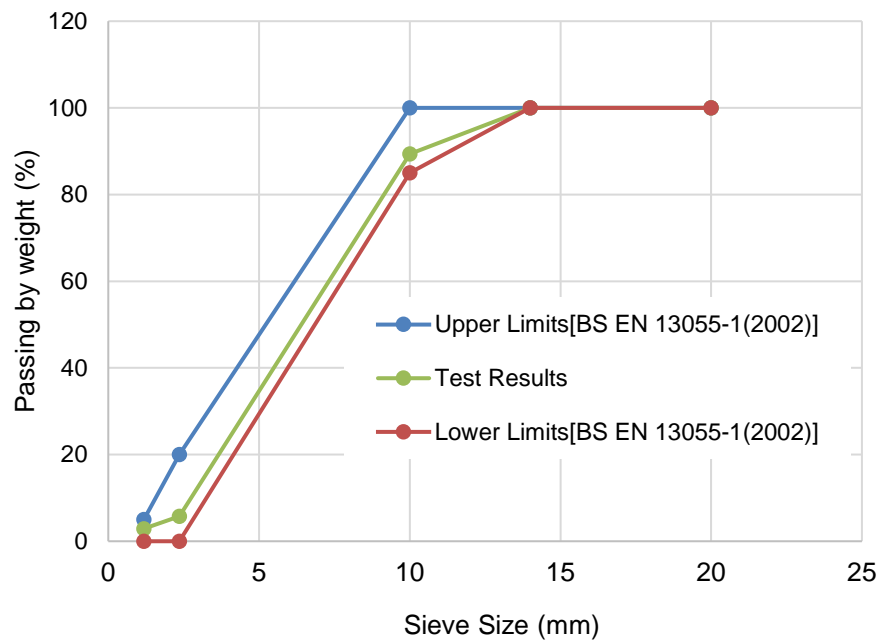
Figure 3-5: Grading curves for standard requirements and lightweight coarse aggregate used (Leca)

In addition, the main raw materials of Normal Weight Concrete (NWC) are cement, sand, gravel and water. The materials used for this investigation can be explained as follows. Combinations of the following constituent materials were used to produce normal weight concrete in this research.

- **Portland cement:** CEM I-52,5 N, 3.15 specific gravity (S.G.), conforming to (BS EN 197-1:2011).

- **Fine aggregate:** sand with 2.65 specific gravity, conforming to (BS 882:1992) is used in the mixes. The bulk density of the sand is 1800kg/m^3. The gradation of the used sand is illustrated in Figure 3-7.

- **Coarse aggregate (gravel):** coarse aggregate with specific gravity of 2.79, conforming to (BS 882:1992) is used in the mixes with a maximum aggregate size of 10mm is used in mixes. The bulk density of the gravel is 1600kg/m^3. The gradation of the used coarse aggregate is illustrated in Figure 3-8.

- **Fresh, clean and drinkable water**.
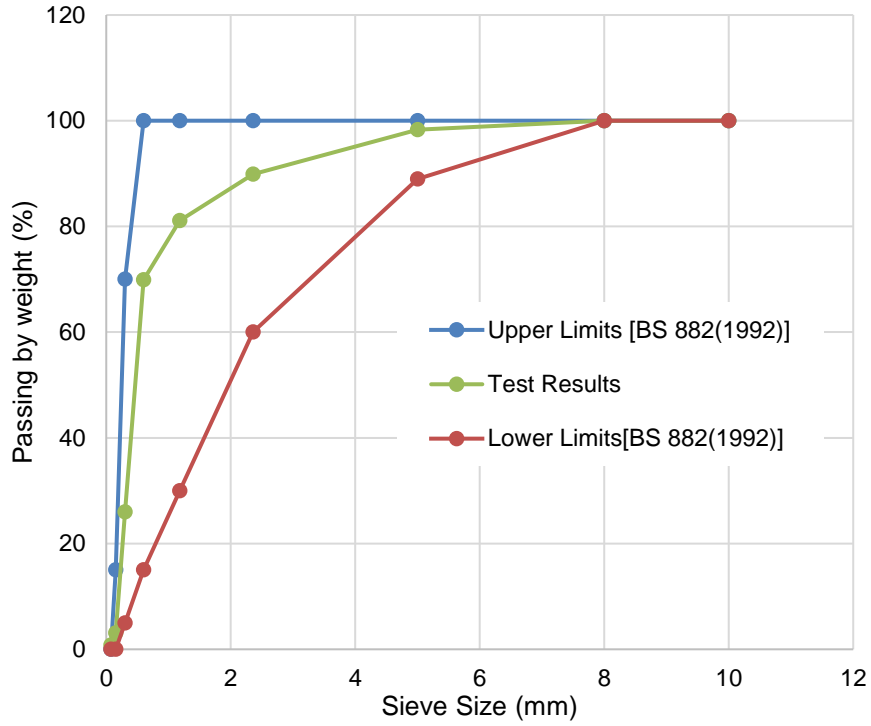
Figure 3-6: Grading curves for standard requirements and sand used
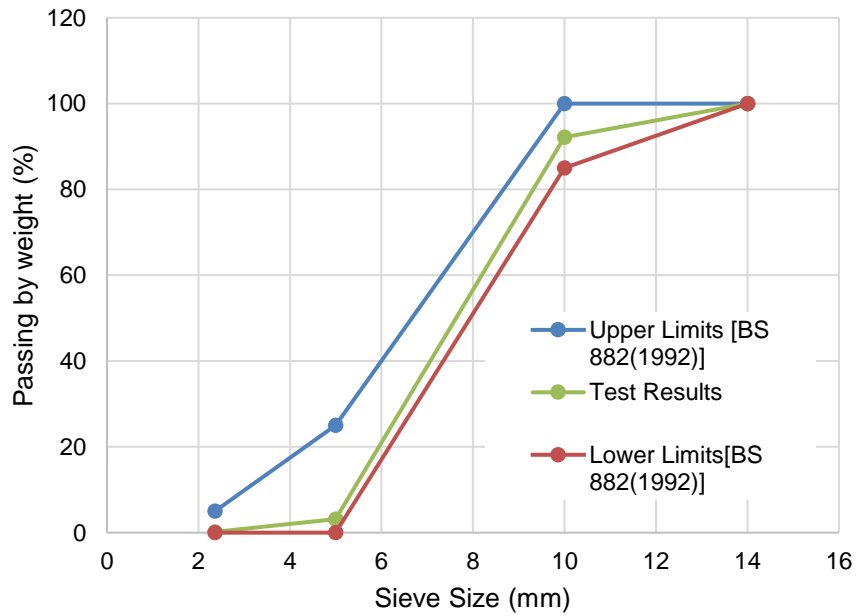
Figure 3-7: Grading curves for standard requirements and normal coarse aggregate used

Table 3-2: Concrete mixture proportions

Concrete type	W/C ratio	Cement (kg/m^3)	FA (kg/m^3)	CA (kg/m^3)	CA type	FA type	Density (kg/m^3)
NWC	0.75	300	810	990	NA	NS	2325
LWC	0.79	250	625	520	RA	RA	1700
ULWC	0.98	450	324.5	229	EC	EC	1300

W/C water to cement ratio, CA coarse aggregate, FA fine aggregate, NS natural sand, NG natural aggregate, RA recycled aggregate, EC expanded clay.
[a] NA: natural aggregate has a dry density of 1600kg/m^3
[b] NS: natural sand has a dry density of 1800 kg/m^3
[c] RA: recycled aggregate (coarse Lytag) has a bulk density of 700 kg/m^3
[d] RA: recycled aggregate (fine Lytag) has a bulk density of 1000 kg/m^3
[e] EC: expanded clay (coarse Leca) has a bulk density of 280 kg/m^3
[f] EC: expanded clay (fine Leca) has a bulk density of 620 kg/m^3

3.4 Concrete compressive strength of push-out tests

The concrete strength of the push-out specimens was determined at 7-day, 14-day, 28-day and on-the-day of the push-out tests. The concrete cube compressive tests and cylinder tensile splitting tests were carried out in accordance with (BS 1881-116, 1983). The results are listed in Table 3-3.

Figure 3-9 shows the stress-strain curve of normal weight concrete, lightweight concrete and ultra lightweight concrete under compression up to failure.

Table 3-3: Concrete strength of push-out specimens

Testing day	Normal weight concrete		Lightweight concrete		Ultra lightweight concrete	
	Cube Compressive Strength, f_{cu}, (N/mm^2)	Cylinder Tensile Splitting Strength, f_{ct}, (N/mm^2)	Cube Compressive Strength, f_{cu}, (N/mm^2)	Cylinder Tensile Splitting Strength, f_{ct}, (N/mm^2)	Cube Compressive Strength, f_{cu}, (N/mm^2)	Cylinder Tensile Splitting Strength, f_{ct}, (N/mm^2)
7-day	21	2.00	17	1.43	11	0.69
14-day	26	2.11	22	1.60	14	0.86
28-day	30	2.31	30	1.99	16	1.25
Push-out test (on-the-day)	37.3	2.45	36	2.12	20.0	1.38
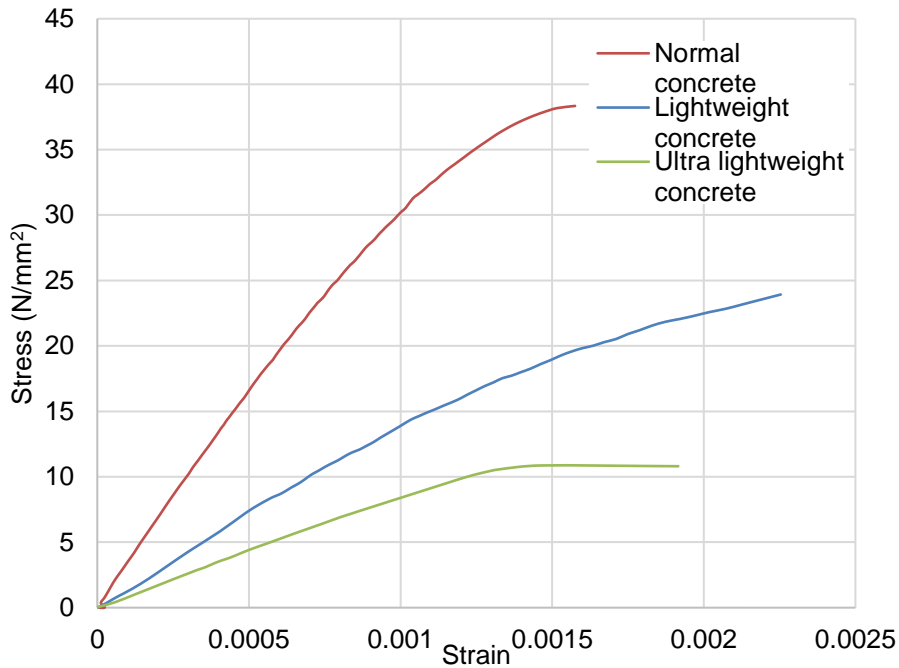
Figure 3-8: Stress-strain curves of normal and lightweight
concretes under compression

3.5 Steel section of push-out test series

Four coupons were machined from the steel section of the push-out test series.
Two of the coupons were cut from the flanges and two were cut from the web
post. The steel parts used in manufacturing the tested specimens i.e. the steel
reinforcement, steel plate, stud and dowel shear connectors are tested under
uniaxial tension according to (ISO 6892-1:2009). The overall average strengths
were:

- Yield strength, 406N/mm^2
- Ultimate strength, 570N/mm^2

Figure 3-10 shows the stress-strain curve of the steel section coupons.
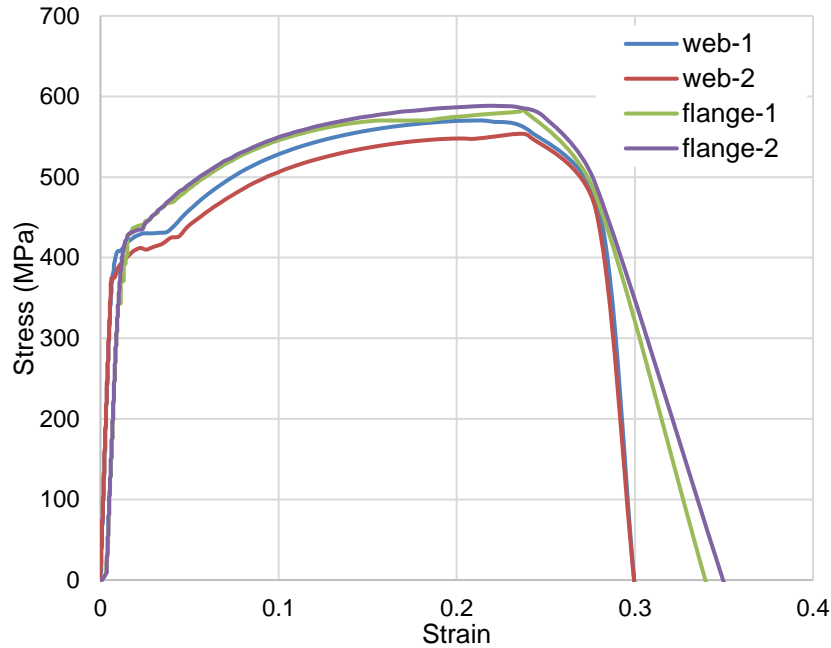
Figure 3-9: Stress-strain curves of steel section coupons

3.6 Reinforced concrete ribbed slab

The reinforced concrete ribbed slab is designed according to Eurocode 2 (EN1992-1-1, 2004), which is a one-way spanning ribbed slab that consists of a "reinforced concrete slab" (RCS) and reinforced concrete ribs (RCRs). For ease of manufacture, straight lines were adopted. A maximum span of flat slabs was achieved. Slabs were designed as secondary and ribs were designed as primary beams for RC design. RCS has been kept to a maximum depth of 75mm, spanning between RCRs, which are set at a uniform spacing of 870mm. The slab general arrangements are given in Table 3-4.

Table 3-4: Reinforced concrete ribbed slab properties

Sample	Top slab depth mm	Ribs depth mm	Total depth mm	Ribs width Mm	Clear gap between ribs mm	Slab span mm	Concrete Density kg/m³	Compressive strength of concrete N/mm²
Ribbed slab	75	85	160	120	750	870	2325	30.0
							1705	30.0
							1300	16.0

This slab connects with the steel beam by using H20 dowels at rib locations and shear studs between the rib locations. These dowels tie the steel beam and the slab at every 435mm with shear studs fixed at alternate centres.

The steel reinforcements are tested under uniaxial tension according to (ISO 6892-1, 2009). Figure 3-11 shows the stress-strain curve of the steel reinforcing bars.
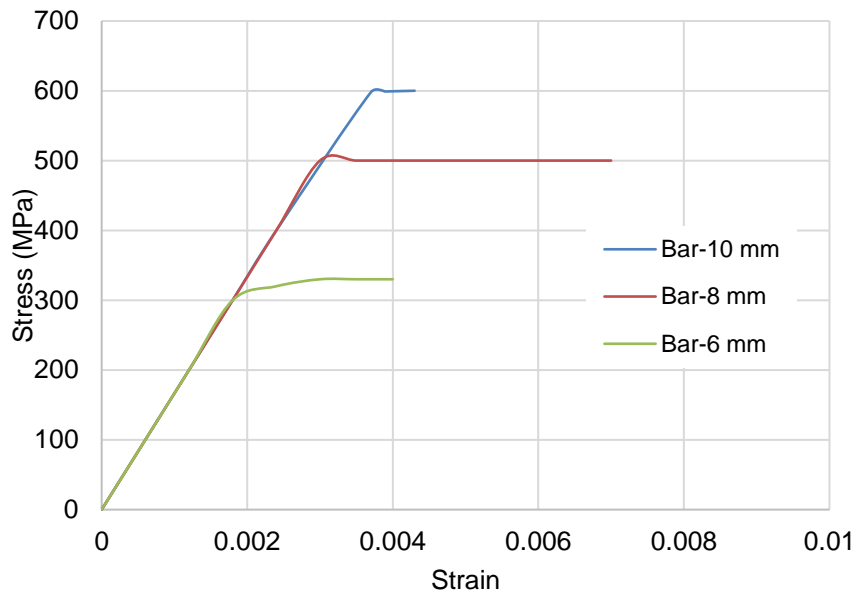
Figure 3-10: Stress-strain curve of reinforcing bars used for the prefabricated ultra shallow flooring system

3.7 Shear transferring mechanism

A shear connector is an interconnecting element between the concrete and steel of a composite structure that has sufficient strength and stiffness to enable the two elements to be designed as a single structure-see Eurocode 4 (EN1994-1-1, 2004). The most common type of shear connectors is the headed shear stud, which is normally welded on the top flange of the downstand composite beams. The shear transferring mechanism of the prefabricated ultra shallow flooring system is formed uniquely by WWSS and WWSS with dowels.

3.8 Web-welded stud shear connectors (WWSS)

The headed shear studs used for the prefabricated ultra shallow flooring system are to provide shear resistance in the region where the thin slab is. The headed shear studs are welded to the centre of the web post of the parallel flange channel, as illustrated in Figure 3-1. The studs resist the longitudinal shear force. Coupon test results of the headed studs are illustrated in Table 3-5.

Table 3-5: Headed studs properties

Ø19mm headed stud coupon test	
Diameter	6.6 (mm)
Cross-sectional area	34.22(mm^2)
Failure load	18.14
Yield strength (N/mm^2)	452.1
Tensile strength (N/mm^2)	530.2

3.9 Dowels shear connectors

One of the functions of the dowels used in the prefabricated ultra shallow flooring system is to provide the tying force for the concrete slabs on both sides of the web post. Generally, high yield reinforcing bars of Ø20mm with 2m in length are welded to the centre of the web post of the parallel flange channel. The combination of the WWSS with dowels forms this type of shear connector; its shear transferring mechanism is illustrated in Figure 3-1. Coupon test results of the dowels are illustrated in Table 3-6 and Figure 3-12.

Table 3-6: Dowels properties

Ø20mm dowel coupon test	
Diameter	19.83(mm)
Cross-sectional area	314.16 (mm^2)
Failure load	143.94 kN
Yield strength (N/mm^2)	322.5
Tensile strength (N/mm^2)	455.5
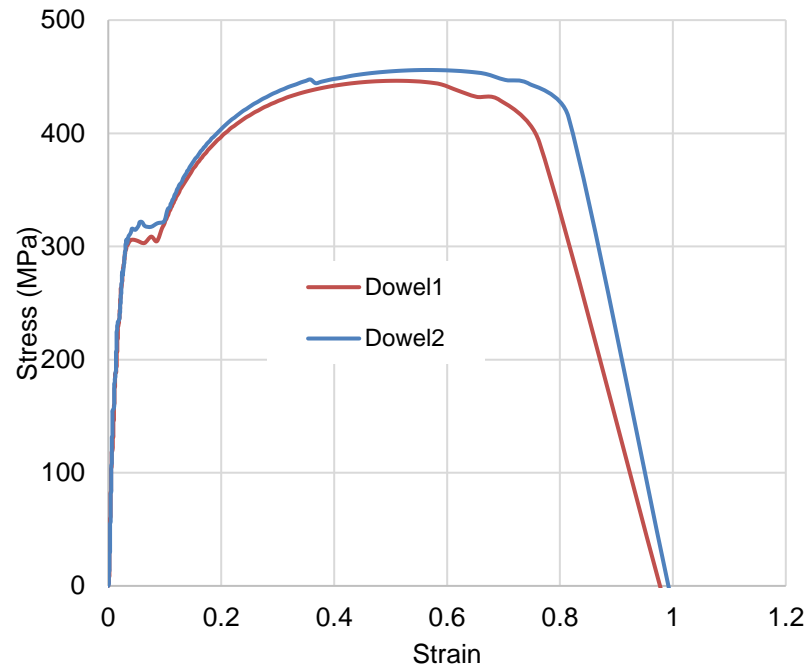
Figure 3-11: Stress-strain curve of Ø20mm dowel coupon

3.10 Composite action

The unique shear transferring mechanism used for the prefabricated ultra shallow flooring system consists of WWSS and WWSS with dowels. The shear transferring mechanism enables the steel beam and concrete elements to interact with each other. This interaction makes the slabs behave compositely. As a result of the composite action, the steel beam and concrete slab act together to resist bending. The moment resistance and stiffness of the composite beam are more greatly increased when compared with the bare steel section. The amount of increase in strength and stiffness is also dependent on the degree of composite action.

3.11 Methodologies of investigation

The shear connection system of the prefabricated ultra shallow flooring system is different from the conventional headed shear studs. The behaviour and shear resisting properties of the shear connection systems have not been investigated previously. In order to provide information for design and further research on the shear connection systems, this research is carried out by using the methods of a push-out test. Details of this methodology are summarised in the following section.

3.11.1 Push-out tests

The push-out test is a fundamental test that applies direct longitudinal shear force to the shear connector. The shear resisting capacity and load-slip behaviour of the shear connector can be obtained from the push-out test. The standard push-out test for the headed shear studs and its load-slip curve are shown in Figure 3-13. Eurocode 4 (EN1994-1-1, 2004) provides detailed specifications for the push-out test of the headed shear studs. Push-out tests were carried out in this research to investigate the shear-resisting capacity and load-slip behaviour of the shear connector used for the ultra shallow flooring system. Specimens of the push-out tests were designed to represent the actual configurations and shear behaviour of the shear connector. Set up and testing procedures were designed to create the desired loading conditions and to be in compliance with the specifications of Eurocode 4 (EN1994-1-1, 2004).

(a)   (b)
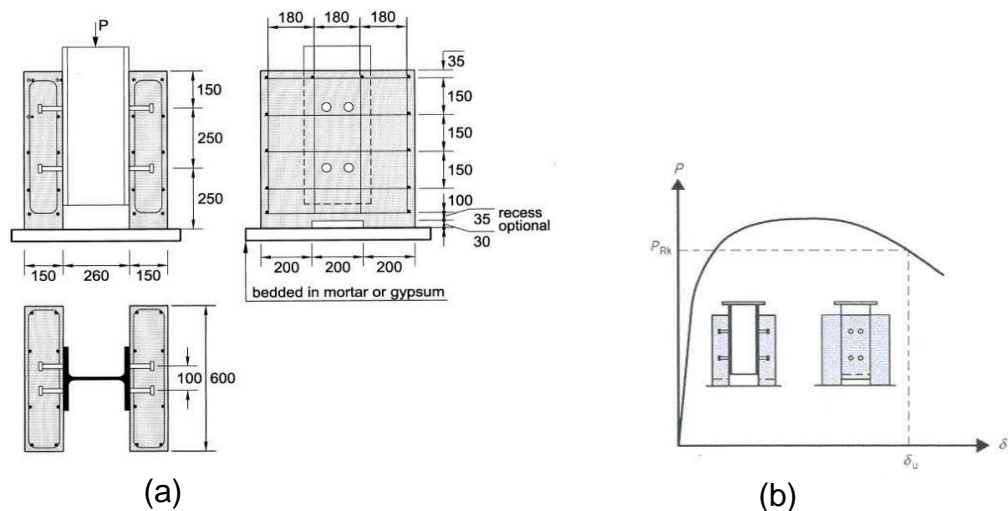
Figure 3-12: (a) Standard push-out test for the headed studs; (b) Load-slip curve of the headed studs Eurocode 4 (EN1994-1-1, 2004)

3.12 Summary

This chapter has presented the background of the lightweight concrete used for the prefabricated ultra shallow flooring system. A summary of the material properties (steel beam, shear connection systems and concrete, etc.) used for the study was also presented. Then, the methodology of investigation into the prefabricated ultra shallow flooring system using push-out test was described in this chapter.

The findings from the research carried out for lightweight aggregate concrete have shown that the lightweight aggregate concrete is a sustainable material in terms of reducing the dead load of the flooring system, improving the thermal properties and fire resistance of the elements, saving in transporting and handling prefabricated units on site and reducing formwork and propping. This material has been used for the prefabricated ultra shallow flooring system for the aforementioned reasons. However, there is a lack of test specimens for the composite flooring systems used with the lightweight aggregate concrete. This thesis has provided the experimental and analytical studies of the novel shear connection systems used with lightweight aggregate concrete for the prefabricated ultra shallow flooring system.

An analytical LCA and LCC studies of three types of prefabricated shallow composite flooring systems were presented in **Chapter 4**. This analysis focused on semi and fully prefabrication methods for flooring systems. The semi prefabrication method was represented by a hollow core composite precast flooring system with casting in place of a finishing layer, whereas the full prefabrication method was represented by the Cofradal flooring system and the prefabricated ultra shallow flooring system using lightweight aggregate concrete.

The experimental studies included push-out tests of two new types of shear connection systems (WWSS and WWSS with dowels) of the prefabricated ultra shallow flooring system were presented in **Chapter 5**. Three types of concrete, normal concrete, lightweight aggregate concrete, and ultra lightweight concrete has been used for casting the push-out test specimens in order to study the effects of concrete properties on the behaviour of the novel shear connection systems.

An FEA parametric study has also been provided in **Chapter 6**, which further investigated the behaviour of the shear connection systems used for the prefabricated ultra shallow flooring system.

Chapter 4 : Life Cycle Assessment (LCA) and Life Cycle Cost (LCC) Studies

4.1 Introduction

A new flooring system has been developed in this research thesis, which is primarily optimised for material usage aiming towards a sustainable and resilient solution suitable for multi-storey buildings. This chapter presents a comprehensive view of the Life Cycle Assessment (LCA) and Life Cycle Cost (LCC) studies of three types of prefabricated shallow composite flooring systems. It outlines the methods of calculating the LCA and LCC performance levels, the existing standards for LCA and LCC, and the impact assessment of the LCA and LCC results.

4.2 Sustainable design

Various factors influence the impact of building construction on the environment and the responsibility is shared by owners, developers, architects and engineers, finance institutions, government authorities, contractors, material suppliers, labourers, tenants, building managers, operation and maintenance personnel, recyclers salvagers, and landfill/incinerator managers (Dong et al., 2015). Designers (architects and engineers) have an important role in terms of the selection of materials and construction systems.

When it comes to flooring systems, Lopez-Mesa et al. (2009) claimed that in the case of residential buildings, the environmental impact of a structure with precast hollow core concrete floors is 12.2% lower than that of cast in-situ floors for the defined functional unit using the (LCA) methodology. Dong et al. (2015) compared the carbon emissions of precast and traditional cast in-situ construction methods based on a case study of a private residential building in Hong Kong and performed an LCA study to consider the system processes from cradle-to-site of the construction. The comparison was conducted based on eight scenarios at four levels, for example, cubic meter concrete, precast facade, a group of façade elements, and an entire apartment. It was found that the precast construction method can lead to 10% carbon reduction for one cubic meter concrete. Jaillon et al. (2009) stated that the use of the precast method could lead to 52% of waste reduction and 70% of timber formwork reduction.

Wong and Tang (2012) compared the precast and cast-in-situ concrete with the system boundary from cradle-to-site and concluded that the precast method can reduce carbon emissions. van den Dobbelsteen et al. (2007) found that in the case of office buildings, energy consumption during building operation accounts was on average 77.5% of the environmental impact, whereas the use of building materials was responsible for 19.5%. It was also found that the supporting structure is responsible for almost 60% of the environmental impact caused by the building materials. Therefore, the supporting structure is responsible for about 11.7% of the whole environmental impact.

Reza et al. (2011) investigated three types of block joisted flooring systems (concrete, clay, and expanded polystyrene (EPS) blocks) using a life cycle analysis (LCA). The selection of three sustainable flooring systems in Tehran (Iran) was based on the triple bottom-line (TBL) sustainability criteria. The analytical hierarchy process (AHP) is used as a multi-criteria decision making technique that helps to aggregate the impacts of the proposed (sub) criteria into a sustainability index (SI) through a five-level hierarchical structure. The detailed analysis shows that the EPS block is the most sustainable solution for block joisted flooring systems in Tehran.

Moreover, the use of lightweight materials in various applications adds great advantages when compared to heavyweight construction, such as in the case of partition walls, as it has been proven that they contribute to the overall material inputs of the built environment (Mateus et al., 2013). A new lightweight sandwich membrane (new lightweight partition wall) was recently developed and evaluated using the LCA methodology, which comprises of an environmental, functional and economic life cycle analysis. Two reference partition walls were used to compare the new lightweight partition wall to identify the advantages of the new lightweight partition wall: (i) the traditional heavyweight partition wall (hollow brick wall); and (ii) the lightweight gypsum panels wall (plasterboard wall). Based on this comparison, it has been found that a new lightweight solution could be more sustainable than both standard solutions of hollow brick partition walls and plasterboard partition walls.

In conclusion, the environmental impact of the construction materials does not only depend on the material itself, but also the way the components are put in place, its maintenance requirements and the system's longevity, along with the

travel distance from purchasing to the site, etc. (González and Navarro, 2006). This means that the selection of materials and the design of the structural system requires a rigorous LCA study. As Malin (2005) illustrates, this type of evaluation is a task for expert scientists and consulting companies specialised in environmental impact. Calculation of the environmental indicators (Life Cycle Impact Assessment-LCIA) requires a detailed appreciation of the life cycle inventory databases, especially their composition and the critical inclusion of the system's boundary and allocation rules (Assefa et al., 2007).

When LCA is applied to study a building, the product studied is the building itself, and the assessment is defined according to a certain level, while it contains all material processes. This level is known as the "whole process of building" and there is a plethora of available tools to work at this level, such as BREEAM (Vukotic et al., 2010). When the LCA is applied to study part of the building, a building component or a material, the level is called "building material and component combination" (BMCC), and in this case, it is important to recognise the component's impact equivalent according to the functional unit of the building. The functional unit could be one of many (e.g. m^2, m^2 internal space, m^3, each, number of occupants, etc.) in the case of whole building LCAs. The most commonly used functional unit in the life cycle assessment of buildings is the square meter floor area (Khasreen et al., 2009). It is important to note that all the environmental impacts calculated within one LCA study should refer to the chosen functional unit.

There are a few available life cycle inventory (LCI) databases, such as ATHENA, Ecoinvent version 3.4, and AusLCI (Islam et al., 2015). The most recognised databases for material embodied energy and carbon dioxide in the UK is the Inventory of Carbon and Energy Beta 2, developed by the University of Bath (Hammond et al., 2008). ATHENA is most suitable for use in the USA and Canada, as it contains the most comprehensive database of American products and processes. Ecoinvent contains Swiss and European product and process data. Data quality in LCA studies on buildings is a major concern, due to the high rate of change and high technical improvements involved in the building industry. Therefore, the age, regional origin, and accuracy of the inventory data influences the accuracy and validity of the studies. A major focus over the last two decades

in Europe, Canada, and the USA has been to produce region specific LCI databases.

So far, the LCA of different building materials has been discussed. The problems and solutions involved in reducing the CO_2 emissions from building materials such as concrete have been explained through specific studies. A summary of the findings are presented in Table 4-1.

Table 4-1: Summary of LCA of the building sector

Building materials and construction process	Problems	Solutions	Prefabricated ultra shallow flooring system Solutions
Concrete	- Higher energy consumption from the production of cement - Higher CO_2 emissions from the production of cement	- Using alternative materials (lime mortars instead of cement mortars) - Using foamed concrete - Using green concrete - Using precast units	Using green concrete such as lightweight aggregate concrete
Steel	- Higher energy consumption from the production of steel - Higher CO_2 emissions from the production of steel	- Using optimized steel elements - Using lightweight steel elements - Manufacturing small metal components without any scraps - Re-use steel elements without recycling	Using lightweight steel elements.
On-site construction process	- Higher energy consumption from the fuel consumption in material transportation and heavy equipment, waste treatment management - Higher CO_2 emissions from the fuel consumption in material transportation and heavy equipment, waste treatment management	Prefabrication construction process	The fully prefabricated flooring system

4.3 Integrated environmental-economic performance

4.3.1 Environmental performance (LCA)

A cradle-to-grave approach was adopted for the LCA study to determine the environmental impact of the three aforementioned distinctive types of flooring systems, by considering the following stages: raw materials acquisition, product manufacture, transportation, installation, and eventually, recycling and/or waste management. The use and maintenance stage (operation stage) is not included in this study due to lack of information (data) about this stage.

Most LCA methods employ the principles of the International Standards Organization (ISO) series, which are known as series 14040 within the more general ISO 14000 series on environmental management systems (Defra, 2008). These documents describe four general steps that must be carried out in any LCA:

(a) Initially, the researcher defines the aims, boundaries, and limitations of the study, and sets significant assumptions-generally definitions of system boundaries, such as the full lifetime of the product or one phase of its manufacturing; functional units such as m^2 of floor area; quality of the data, etc. All of these assumptions should be specified at this early stage, as they determine the direction of the study. The study will be assessed in the interpretation stage.

(b) Life cycle inventory is the second step of the LCA. It includes a collection of the data and calculation methods, and it is considered the most important and time-consuming stage since this data will be the basis for the study. It has also been connected with the scoping exercise as the data collection, and other cases may lead to redefinition or refinement of the system limitations. For instance, the lack of data may result in changing the objectives or the scope of the study. Therefore, data completeness is pivotal. The life cycle inventory phase (LCI) usually uses databases of building materials and component combinations.

(c) The impact assessment evaluates potential environmental impacts. The purpose of this phase is to estimate the importance of all environmental burdens obtained in the LCI by analysing their influence on selected environmental loads.

An impact assessment is used by the ISO series 14040 (ISO, 2006b, ISO, 2006a, ISO, 2012) to characterize and normalize the environmental impacts. The first stage of the life cycle impact assessment is to select the impact categories, category indicators, and characterization. The next stage is to assign the LCI results to the selected impact categories and the last stage multiplies the inventory results by the characterization factors. The impact categories are divided into two types: the midpoint categories and the endpoint categories. Midpoints are concerned with environmental problems, whereas endpoints are concerned with the damage that these environmental problems can cause. In the ISO 14042 standard, a distinction is made between obligatory elements, such as classification and characterization, and optional elements, such as normalisation, ranking, grouping, and weighting. According to ISO 14042, the general framework of a life cycle impact assessment (LCIA) method is composed with obligatory elements (classification and characterization), which convert the LCI results into an indicator for each impact category that leads to a unique indicator using numerical factors based on value-choices.

(d) The final stage of the LCA is the interpretation, which aims to analyse the results and reach conclusions by explaining the boundaries and providing recommendations. These recommendations are based on the outcomes of the previous phase of the LCA or LCI study. Life cycle interpretation also intends to provide an easily understandable, complete, and harmonious presentation of the results of an LCA or an LCI study, in agreement with the scope definition of the study.

The framework of the current LCA study is shown in Figure 4-1 and consists of four major steps:

- **Step 1**: Identify the scope and define the boundaries and the functional unit.
- **Step 2**: Model the processes and resources involved in the product system, collate the Life Cycle Inventories of these processes and resources and generate any new inventories required.
- **Step 3**: Analyse the life cycle impacts in terms of mid-points (impact categories) and end-points (system categories).

- **Step 4**: Evaluate and interpret results, as well as generate a report for decision-making.

The framework of the LCA study is shown in Figure 4-1.
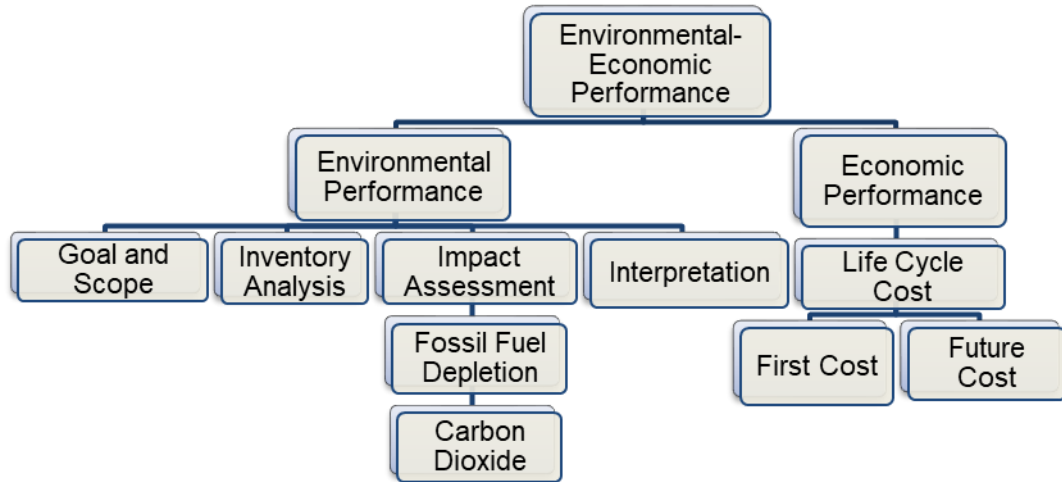
Figure 4-1: Overall performance steps (Ahmed and Tsavdaridis, 2018)

4.3.2 Scope

The scope of the present study is to evaluate the prefabricated ultra shallow flooring system and compare it with the current state-of-the-art sustainable flooring systems.

4.3.3 Functional Unit

The functional unit is the unit of comparison in the LCI. In this study, one square meter (m^2) of the flooring system fulfilling similar requirements regarding a live load of $2kN/m^2$ and a span of 7.8m is chosen. This is chosen according to the maximum span of the Cofradal slab, which is 7.8m, and can take a live load of $2kN/m^2$. Therefore, the same live load was applied to all studied flooring systems and with the same span regardless of their capacity. All emissions, energy consumption and materials are based on this functional unit (e.g. MJ/m^2, $kgCO_2e/m^2$ etc.).

4.3.4 System Boundaries

The system under study includes the entire life cycle of the flooring systems listed above, including the manufacturing of building materials, construction and

demolition. Transportation for each life cycle phase is also included. The impact categories studied are Embodied Energy and Global Warming Potential (GWP).

4.3.5 Definition of Impact Categories and Calculations Methodology

The scope step also includes the specification for which impact categories are to be covered in the impact assessment step. This is typically done by selecting one of the available calculation methodologies. Each methodology defines the impact categories that are used to generate results. Some methodologies also define a weighting scheme by which different impact categories are combined into more generic results. The calculation methods are classified according to regions, such as European and North American (Goedkoop and Oele, 2006).

This study is focused on the environmental problems that these flooring systems will cause during their lifetime. Therefore, the LCIA results are calculated at the midpoint level using the TRACI method (Bare, 2002).

The embodied energy and embodied carbon calculation procedure for the flooring systems are summarised below.

- The production phase includes the materials of studied flooring systems, the compaction of each concrete mix and the installation of the studied flooring systems. Hence, the embodied energy EE-P and EC-P, in the production phase can be calculated using the following equations (Yang et al., 2013):

$$EE_{-P} = \sum_{i=1}^{n} \left(W_i \times EE_{(i)-LCI}\right) + \sum_{i=1}^{n} \left(W_i \times EE_{(i)-CE} \times t\right) \qquad (4.1)$$

$$EC_{-P} = \sum_{i=1}^{n} \left(W_i \times EC_{(i)-LCI}\right) + \sum_{i=1}^{n} \left(W_i \times EC_{(i)-CE} \times t\right) \qquad (4.2)$$

Where i represents a raw material constituting the flooring system, n is the number of raw materials added for each flooring system production, and W_i, EE_{i_LCI} , EC_{i_LCI}, $EE_{i\text{-}CE}$ and $EC_{i\text{-}CE}$ are the unit weight (kg/m^2), embodied energy inventory (MJ/kg), embodied carbon inventory (kgCO$_2$e/kg) of raw material i, respectively, embodied energy inventory (MJ/hr) of the operation of construction equipment and embodied carbon inventory (kgCO$_2$e/hr), and t is the operation time for the equipment.

- The transportation phase includes the transportation of materials and prefabricated units to the building site applicable to each solution. Overall, the embodied energy and embodied carbon from the transportation phase can be obtained from:

$$EE_{-T} = \sum_{i=1}^{n} \left(W_i \times D_i \times EE_{(i)-LCI(TR)} \right) \tag{4.3}$$

$$EC_{-T} = \sum_{i=1}^{n} \left(W_i \times D_i \times EC_{(i)-LCI(TR)} \right) \tag{4.4}$$

Where W_i is the unit weight (tonne/m^2), D_i is the transportation distance of each flooring system constituent material i from the manufacturing plant to the building site (km), $EE_{(i)-LCI(TR)}$ is the embodied energy inventory related to the heavy haulage vehicle (MJ/km.tonne). $EC_{(i)-LCI(TR)}$ is the embodied carbon inventory related to the heavy haulage vehicle (kgCO$_2$e/km.tonne).

- The end of life phase includes the steel recycling and transportation of recycled steel and concrete demolition and the transportation of crushed concrete. The embodied energy from the end of life phase of steel can be obtained from:

$$EE_{-ST-EOL} = \sum_{i=1}^{n} \left(W_i \times EE_{(i)-LCI(RC)} \right) + \sum_{i=1}^{n} \left(W_i \times D_i \times EE_{(i)-LCI(TR)} \right) \tag{4.5}$$

$$EC_{-ST-EOL} = \sum_{i=1}^{n} \left(W_i \times EC_{(i)-LCI(RC)} \right) + \sum_{i=1}^{n} \left(W_i \times D_i \times EC_{(i)-LCI(TR)} \right) \tag{4.6}$$

Where W_i is the unit weight of (kg), $EE_{(i)-LCI(RC)}$ is the embodied energy inventory form the recycling process (MJ/kg), $EC_{(i)-LCI(EOL)}$ is the embodied carbon inventory form the recycling process. W_i is unit weight (tonne), D_i is the transportation distance of recycled material i from the construction site to the recycling plant (km), $EE_{(i)-LCI}$ is the embodied energy inventory and $EC_{(i)-LCI(TR)}$ is the embodied carbon inventory related to the vehicle (kgCO$_2$e/km.tonne). Steel recycling according to the substitution method (Hammond et al., 2008).

The substitution method is an opposite to the recycled content method. In the substitution method the creation of recyclable material is allocated the full benefit of recycling at end of life (called recyclability) (Hammond et al., 2008). This leaves

no benefit for incoming recycled materials, which are effectively neglected. The substitution method can be modelled as an effective recycled content, with the "effective recycled content" defined by the fraction of new recycled material that arises from the end of life recovery processes (i.e. a measure of its recyclability).

- The end of life phase of concrete can be obtained from:

$$EE_{-CON-EOL} = \sum_{i=1}^{n}(W_i \times EE_{(i)-LCI(EOL)}) + \sum_{i=1}^{n}(W_i \times D_i \times EE_{(i)-LCI(TR)})$$ (4.7)

$$EC_{-CON-EOL} = \sum_{i=1}^{n}(W_i \times EC_{(i)-LCI(EOL)}) + \sum_{i=1}^{n}(W_i \times D_i \times EC_{(i)-LCI(TR)})$$ (4.8)

Where W_i is the unit weight of (kg), $EE_{(i)-LCI(EOL)}$ is the embodied energy inventory (MJ/kg), and $EC_{(i)-LCI(EOL)}$ is the embodied carbon inventory ($kgCO_2e/kg$) for the demolition of concrete. W_i is the unit weight (tonne), D_i is the transportation distance of demolished material i from the construction site to the landfill (km), $EE_{(i)-LCI(TR)}$ is the embodied energy inventory related to the heavy haulage vehicle ($kgCO_2e/km.tonne$).

4.3.6 Characteristics of studied flooring systems

The selected flooring systems include the Cofradal 260mm flooring system, the hollow composite precast flooring system and the prefabricated ultra shallow flooring system. The Cofradal 260mm flooring system is constructed using galvanized profiled steel sheeting with a tensile strength of 320N/mm² fitted with a mineral wool insulation layer and a reinforced concrete top layer with C30/37 and reinforcing bars welded on the steel sheeting. This welding provides a connection point between the tensioned steel and the compressed concrete, creating composite behaviour between the steel sheeting and the top concrete. The mineral wool layer, with a density of 50kg/m³ is an effective shuttering bed for concreting the top of the slab. This layer provides thermal insulation between the levels if needed, along with acoustic resistance. The overall depth of the slab is 260mm with a width of 1200mm and maximum span of 7.8m. This system is a fully prefabricated steel-concrete composite slab produced in-house and ready to be fixed on site.

Hollow composite precast flooring system is fabricated from normal concrete C40/50 with voids that run continuously along its length. The overall depth of the slab is 300mm including the concrete topping layer (50mm) with a width of 1200mm and maximum span of 10.5m. This system was constructed under controlled factory conditions. The concrete topping layer was placed on site, on the top surface of hollow core slabs to create a continuous level finished surface. Therefore, this system is a semi-prefabricated slab and is ready to be fixed on site.

The prefabricated ultra shallow flooring system was explained in **Chapter 3**.

The depth for the three flooring systems for a 7.8m span (max. for Cofradal slab) and an imposed load of 2kN/m^2 was presented in Table 4-2.

Table 4-2: The characteristics of material inputs for the flooring systems (Ahmed and Tsavdaridis, 2018)

Flooring systems	Description	Thickness, width, span, Dimensions	Overall floor weight kN/m^2	Live load kN/m^2
Cofradal 260mm slab	Cofradal260 slab (composite floor slab)	260mm x 1.2m x 7.80m	2.8	2.0
Hollow composite slab	Reinforced concrete floor slab with finishing	200mm x 1.2m x 7.8m	5.1	2.0
Prefabricated ultra shallow flooring system	Composite flooring system with lightweight reinforced concrete T ribbed slab connected with two steel edge C-channel beams using studs and dowels	230mm x 2.0m x 7.8m	2.61	2.0
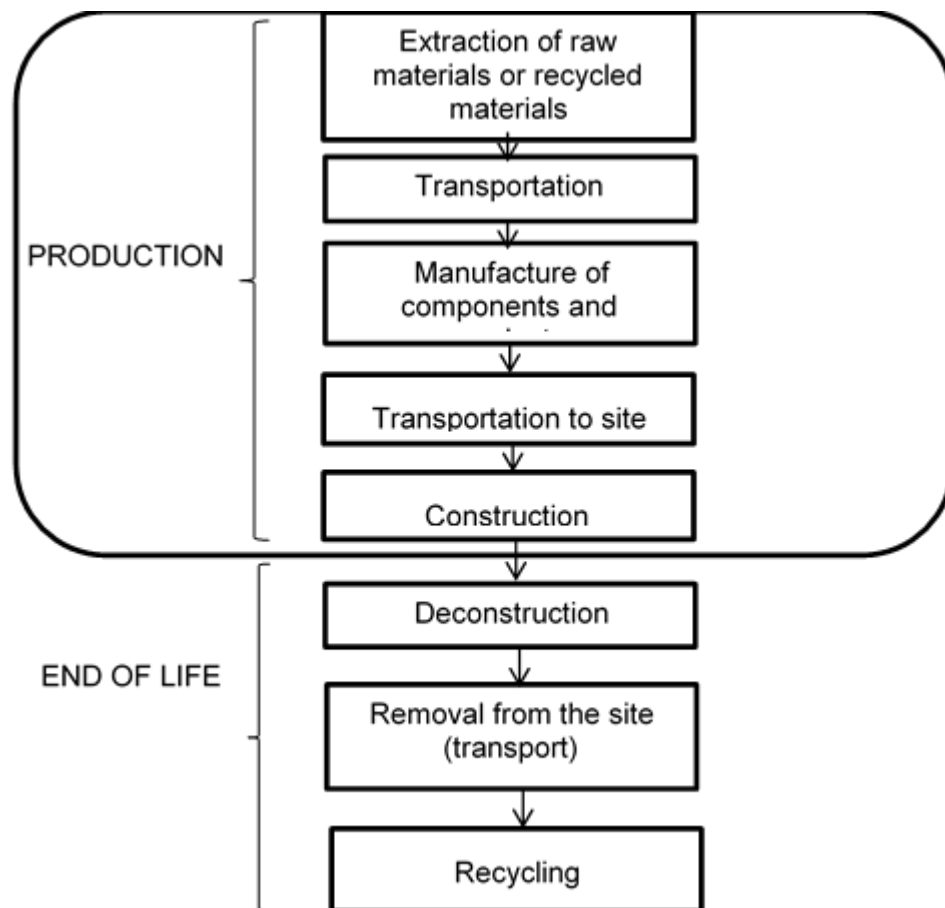
Figure 4-2: A simplified lifecycle process flow chart showing production
boundary for the case study (Ahmed and Tsavdaridis, 2018)

4.3.7 Life cycle inventory analysis

The inventory analysis accurately quantifies the inventory flows with inputs such as the raw materials, water, and energy, as well as outputs, including the air emissions, releases to land and water effluents for a product system. In this study, carbon emission coefficients and embodied energy coefficients for materials, processes, and fuels were derived where possible from the UK, or otherwise relating to the country of production as shown in Tables 4-3, 4-4 & 4-5. A number of sources and databases were used, including:

- The Inventory of Carbon and Energy, Beta 2 (Hammond et al., 2008).
- Life cycle assessment of concrete, master thesis (Sjunnesson, 2005).
- CO_2 Emissions and energy consumption during the construction of concrete structures (Gorkum, 2010).

The latter two references have been used to provide detailed information about the embodied energy and embodied carbon data for concrete demolition and the operation of construction equipment from the European counties.

4.3.7.1 Pre-use phase

The embodied energy and air emissions associated with construction materials during their extraction, processing, and manufacture represent the largest portion of the total embodied energy and air emissions in buildings. Yohanis and Norton (2002) demonstrated that this is about 78% in a residential building and about 92% in an office building. These figures have nearly a 15% discrepancy, mostly arising from a wide variety of building materials used, different building sizes, and their different functions (Vukotic et al., 2010, Blengini, 2009, Asif et al., 2007, Huberman and Pearlmutter, 2008).

4.3.7.2 Use and maintenance phase

Embodied energy and air emissions associated with the maintenance of flooring system activities (e.g., refurbishment) were ignored due to the lack of information about this particular stage.

4.3.7.3 End of life phase

The last phase of the flooring system life involves energy and emissions related to demolition, recycling processes, and transportation. The emissions from this stage mainly owe to the energy consumption of the mechanical demolition equipment. All data on the energy consumption of demotion equipment were derived from various sources (Sjunnesson, 2005, Gorkum, 2010).

Table 4-3: Embodied carbon and embodied energy coefficients for the production and transportation of materials (Hammond et al., 2008)

Type of flooring systems	Material	Material Weight (W) (kg/m²)	Embodied Energy Coefficient (MJ/kg)	Embodied Carbon Coefficient (kg CO₂e/kg)	Transportation distance (D) (km)	Embodied Energy Coefficient for transportation (MJ/kg)	Embodied Carbon Coefficient for transportation (kg CO₂e/kg)
Cofradal260 slab	Reinforcing concrete (32/40N/mm²) with a density of 2360kg/m³	278.5	1.0761	0.1664	155	2.4	0.15
	Rock wool Insulation	27.5	16.8	1.12	155	2.4	0.15
	Metal Deck	13.55	22.6	1.54	155	2.4	0.15
Hollow composite precast slab	Precast concrete (40/50N/mm²)	519.87	1.5255	0.1819	155	2.4	0.15
	Concrete finishes layer (40/50N/mm²)	120	1.0	0.151	155	2.4	0.15
Prefabricated ultra shallow flooring system	Reinforcing concrete (25/30N/mm²) with a density of 1700kg/m³	239.65	0.8044	0.1148	155	2.4	0.15
	19mm Stud	0.034	17.4	1.4	155	2.4	0.15
	20mm Dowel	0.67	17.4	1.4	155	2.4	0.15
	Steel Section	26	21.50	1.53	155	2.4	0.15

Table 4-4: Embodied carbon and embodied energy coefficients for the operation of construction equipment (Gorkum, 2010)

Type of flooring systems	Equipment	Number of hours(t)/unit	Embodied Energy Coefficient (MJ/hr)	Embodied Carbon Coefficient (kg CO_2e/hr)
Cofradal260 slab	Tower crane of 100 ton	1.6	720	53.23
Hollow composite precast slab	Tower crane of 100 ton	1.6	720	53.23
	Pumps	0.158	540	46.12
Prefabricated ultra shallow flooring system	Tower crane of 100 ton	1.0	720	53.23
	Equipment	Concrete depth (m)	Embodied Energy Coefficient (MJ/m^3)	Embodied Carbon Coefficient (kg CO_2e/m^3)
Hollow composite precast slab/ finishing layer	Concrete compactor	0.63	1.18	0.2

Table 4-5: Embodied carbon and embodied energy coefficients for the end of life of materials (Hammond et al., 2008, Sjunnesson, 2005)

Type of flooring systems	Material Weight (W) (kg/m^2)	Material	Embodied Energy Coefficient (MJ/kg)	Embodied Carbon Coefficient (kg CO_2e/kg)
Cofradal260 slab	13.55	Steel recycling	13.1	0.75
	17.72	Reinforcing steel bar recycling	11	0.74
	524.28	Concrete demolition	0.007	0.00054
Hollow composite precast slab	3.06	Reinforcing steel bar recycling	11	0.74
	581.42	Concrete demolition	0.007	0.00054
Prefabricated ultra shallow flooring system	323.57	Steel recycling	13.1	0.75
	0.58	Reinforcing steel bar recycling	11	0.74
	562.85	Concrete demolition	0.007	0.00054

4.3.8 Life cycle impact assessment

The LCIA results are calculated at the midpoint level using the TRACI method (Bare, 2002). The LCIA phase initially focused on the characterisation step and thus the following indicators are considered:

• EE (Embodied Energy): as an indicator relevant to the total primary Energy resource consumption;

• GWP (Global Warming Potential): as an indicator relevant to the greenhouse effect. Characterisation factors for the embodied energy and global warming potential from the TRACI method are used in this study. This method has been used instead of IPCC method as there is no difference between the two methods for evaluating the GWP. The characterization factor for GWP is the same for both methods which is equal to 1.57kg CO_2-eq (Frischknecht et al., 2007).

4.3.9 Impact assessment of the LCA results

4.3.9.1 Pre-use Phase

• Manufacturing:

Material embodied energy relating to the acquisition of raw materials, their processing, and manufacturing. Paradoxically, Figure 4-3 demonstrates that the three flooring systems have completely different embodied energy during this stage. The prefabricated ultra shallow flooring system has 817.49 MJ/m^2 lower than the precast flooring system, which has 976.96 MJ/m^2, and lower than the Cofradal flooring system, which has 1142.68 MJ/m^2.

Table 4-6 presents the embodied energy and global warming potential of the studied flooring systems at each life cycle stage.

Table 4-6: Embodied energy, global warming potential at each life cycle stage (Ahmed and Tsavdaridis, 2018)

Life cycle phase	Cofradal260 slab		Hollow composite precast slab		Prefabricated ultra shallow flooring system	
	Embodied Energy (MJ/m^2)	Global Warming Potential (kg CO$_2$ Eq/m^2)	Embodied Energy (MJ/m^2)	Global Warming Potential (kg CO$_2$ Eq/m^2)	Embodied Energy (MJ/m^2)	Global Warming Potential (kg CO$_2$ Eq/m^2)
Manufacture	1142.68	125.11	976.96	120.56	817.49	70.40
Transportation	164.11	10.25	296.96	18.56	138.07	8.7
Onsite construction	1152	73.79	1238.06	81.20	720	46.12
Demolition	3.67	0.28	4.07	0.31	3.94	0.304
Recycling	-363.60	-22.68	-33.66	-2.26	-329.96	-19.15
Total	2098.86	186.75	2482.39	218.37	1349.54	106.37

• Transportation:

The embodied energy and global warming potential of material transportation includes, herein, the fuel combustion arising from the transportation of materials by a 20ton diesel fuel truck from manufacturing plant to the construction site. The transportation distance considered for the flooring systems was 155km, according to Beta 2 (Hammond et al., 2008). The values for Cofradal slab transportation impacts are 164.11 MJ/m^2, 296.96 MJ/m^2 for the hollow composite precast slab values and 138.07 MJ/m^2 for the prefabricated ultra shallow flooring system representing approximately 7% of total embodied energy.

Vukotic et al. (2010), reported that the value for transportation of materials to the construction site may vary between 7% and 10% of the total embodied energy. Bribián et al. (2011) demonstrated that this value is approximately 6% of the total embodied energy. In this paper, the values for material transportation is 7% of the total embodied energy.

• Onsite construction equipment:

The construction and erection of building assemblies requires the use of a range of manual and power operated tools and equipment, such as compressors, saws, welders, and drills (Cole, 1998). The values of embodied energy and air emissions of related equipment are derived from their source (Gorkum, 2010).

Figures 4-3 - 4-6 depict the Embodied Energy and Global Warming Potential of the studied flooring systems.
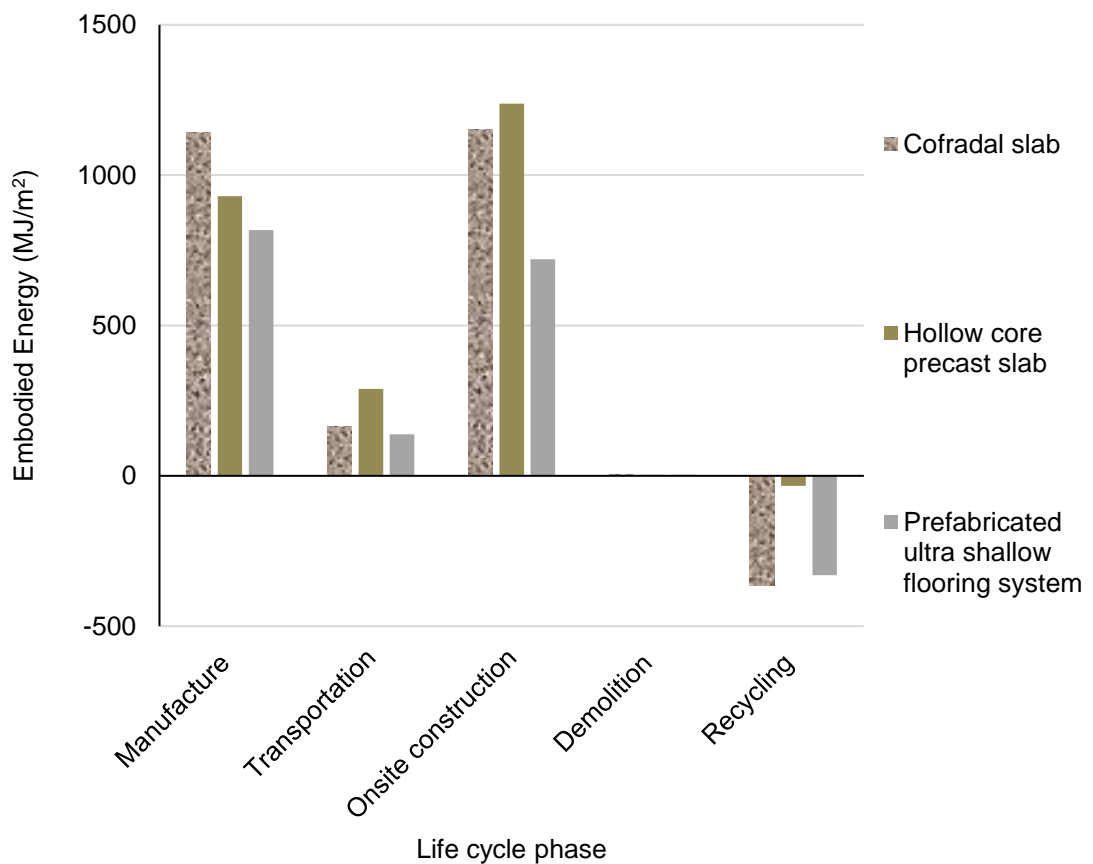
Figure 4-3 Embodied Energy by life cycle phase
(Ahmed and Tsavdaridis, 2018)
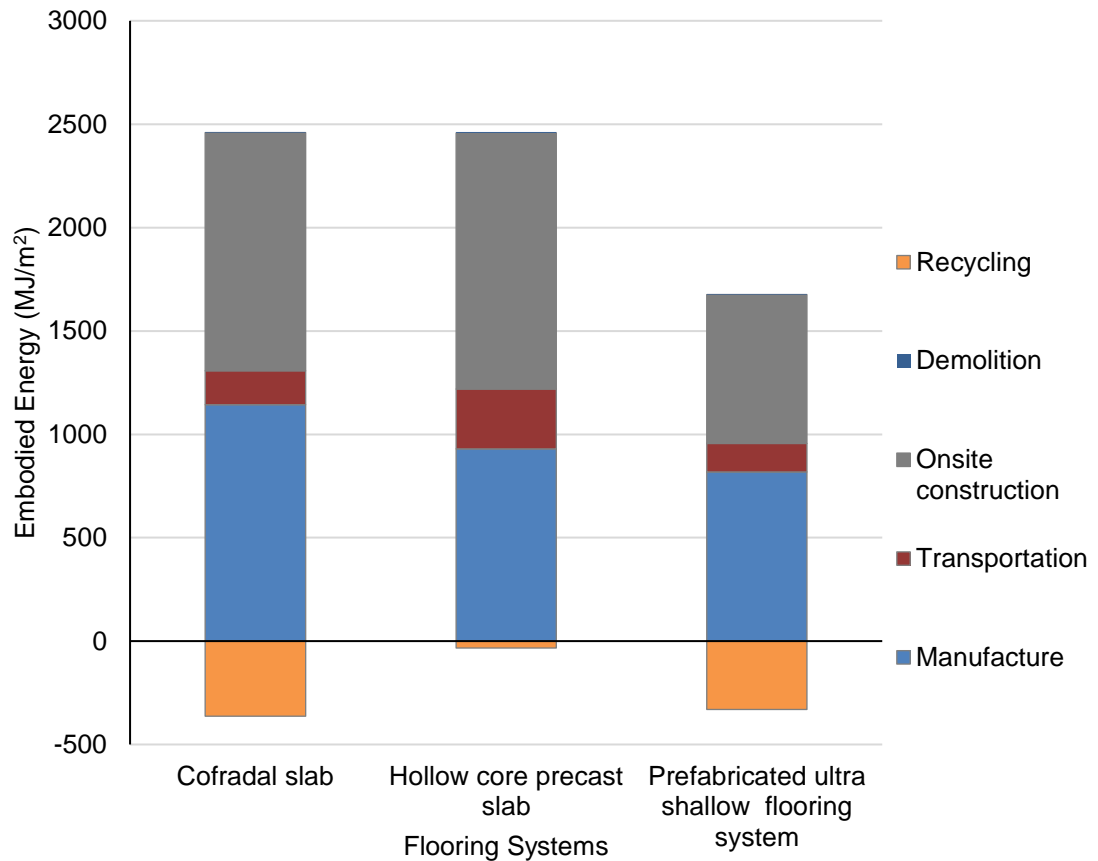
Figure 4-4: Embodied Energy by flooring systems
(Ahmed and Tsavdaridis, 2018)

4.3.9.2 End-of-life

End-of-life embodied energy accounts for impacts associated with building demolition, including waste transportation and Recycling potential. For this study, the ICE inventory provides information about the Recycling values of building materials. For steel beams and metal decks, approximately 95% can be reused for full benefits, while 5% is lost and goes to landfill. Regarding the reinforcement bars, 75% is reusable. Concrete is only considered at the demolition stage (Sjunnesson, 2005), since no information has been provided by the ICE inventory (Hammond et al., 2008) about its demolition and recycling method.

Energy consumed during the demolition stage proved to be the least important parameter of the building's life cycle. Any changes in demolition practices do not have a direct impact on the reduction of air emissions associated with it, due to the marginal value of energy consumed during the demolition of flooring systems.

As previous discussed, the recycling process is considered for the steel components only due to uncertainties associated with the prediction of concrete

recycling. The embodied energy was 363.60 MJ/m², 33.66 MJ/m², and 329.96 MJ/Mm² for Cofradal260 slab, hollow composite precast slab, and prefabricated ultra shallow flooring system, respectively. This highlights how end-of-life Recycling can play a significant role in the embodied energy analysis and the reduction of air emission. However, it is worth noting that the prediction of future demolition seems to be one of the major difficulties in the selection of the best method for waste management.

Figures 4-5 and 4-6 show a breakdown of Global Warming Potential by each phase of the life cycle of flooring systems. A prefabricated ultra shallow flooring system emits less than 60% of the emissions of the Cofradal260 slab and less than 65% of the hollow composite precast slab. This is due to the energy intensity of reinforced concrete with high cement content.
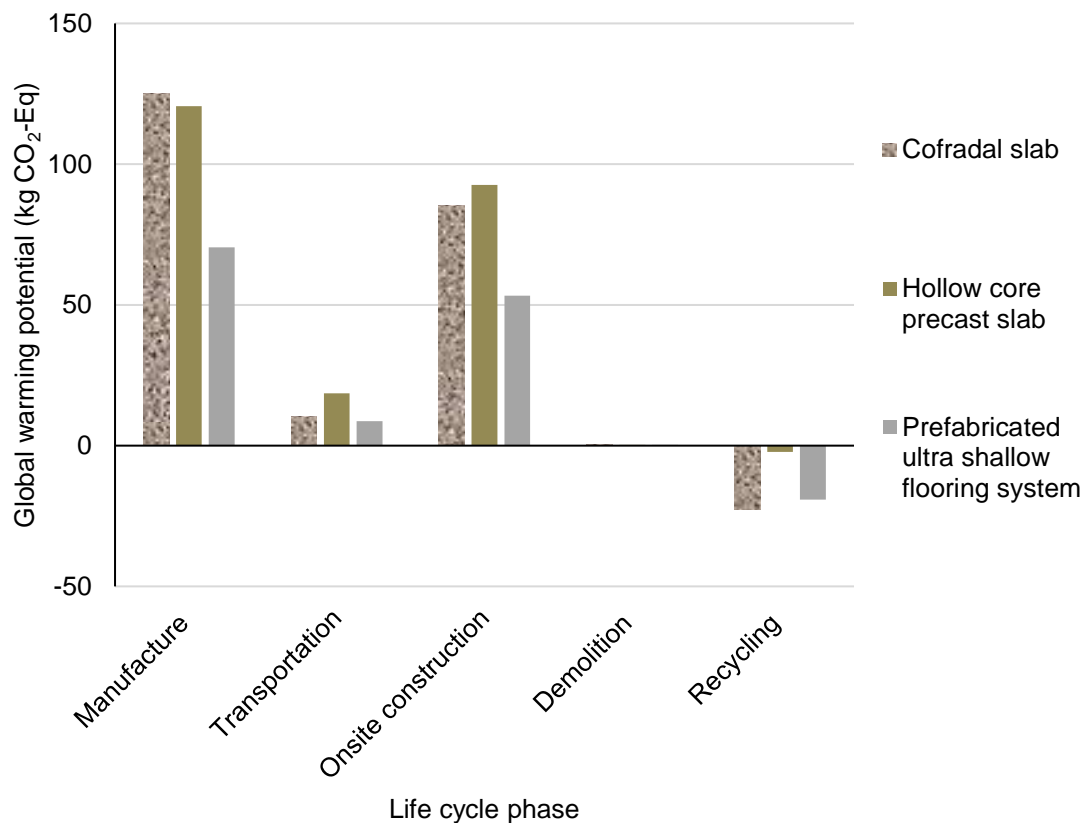
Figure 4-5: Global Warming Potential by life cycle phase
(Ahmed and Tsavdaridis, 2018)
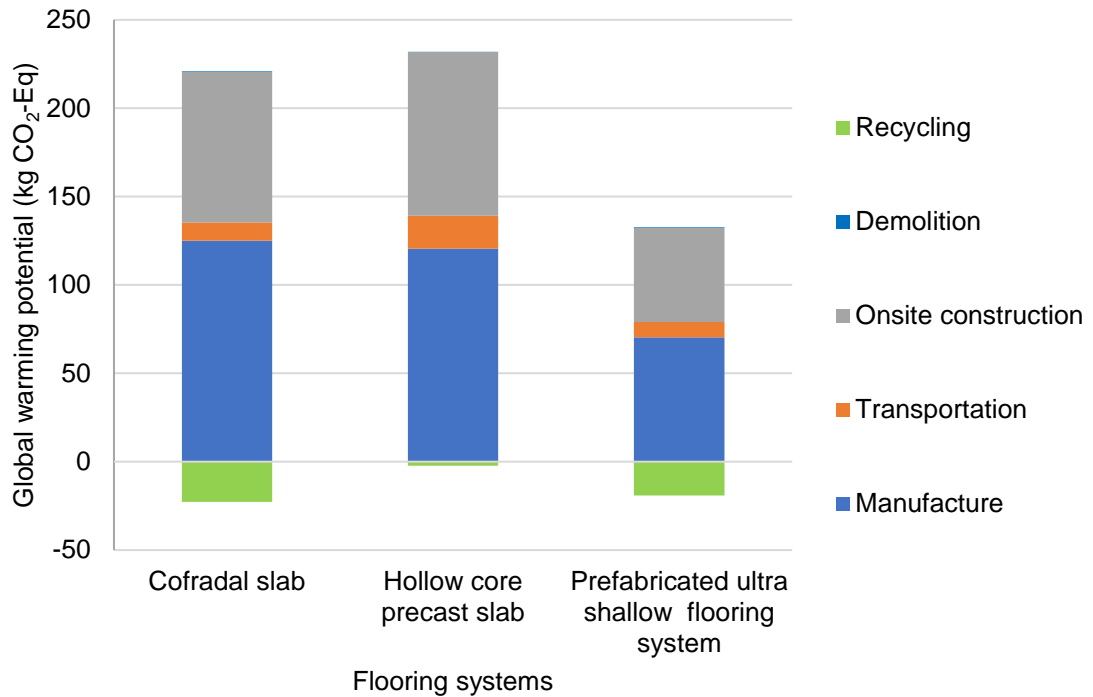
Figure 4-6: Global Warming Potential by flooring systems
(Ahmed and Tsavdaridis, 2018)

4.4 Economic performance (LCC)

4.4.1 Importance of LCC

It is important that the fundamental arguments supporting life cycle costing, its core principles and the restrictions on how it can be used, are understood by everyone involved in scoping, designing, and delivering the project. For public sector procurement, the government has set out a policy of making decisions on the basis of best value rather than lowest initial cost, which is the essence of life cycle costing. This is emphasised in the UK Construction 2025 strategy document, dated July 2013. By working in partnership, the construction industry and Government jointly aspire to achieve, by 2025, a 33% reduction in both the initial cost of construction and the life cycle cost of assets (Tse, 2016).

The economic analysis of building design solutions can be used in two different ways. When a range of possible designs is still being considered, then life cycle costing can be used as a comparison tool to work out the life cycle costs of each design as part of the decision-making process, and further select the best alternative. LCC can also be used for predicting and assessing the cost performance of constructed assets (ISO15686-5, 2008).

4.4.2 Existing standards for LCC

An international code of practice for life cycle costing is provided by (ISO15686-5, 2008) in relation to the built environment. This code is part of a series of standards covering service life planning, the long-term understanding of building elements, components, and equipment. ISO15686-5 (2008) makes the distinction between life cycle costing and whole life costing, as explained in Figure 4-7.

According to the ISO definition, life cycle costing includes the initial construction and through-life activities associated with a built asset, while whole life costing also includes non-construction activities and income generation, such as receiving rent from tenants. The implication is that life cycle costing will be more relevant to designers, contractors, and facility or asset managers, whereas whole life costing will be more appropriate to owner-occupiers, developers, and landlords.
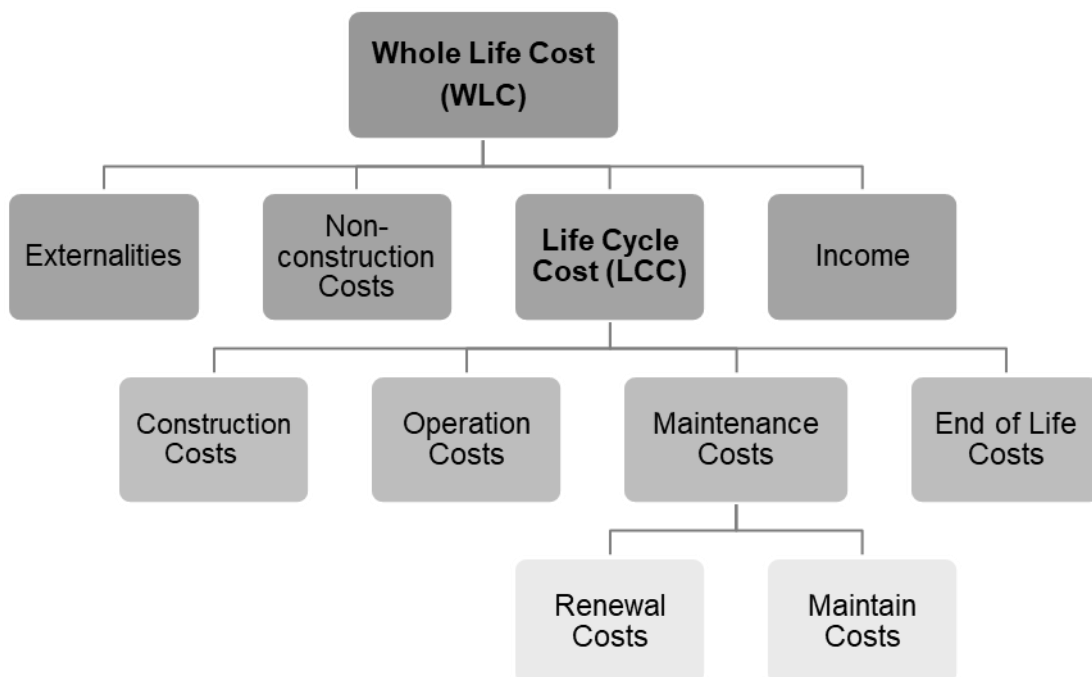
Figure 4-7: Definitions of whole life cost and life cycle cost based on (ISO15686-5, 2008)

4.4.3 Discount Rate selection

The discount rate is a fundamental characteristic of the analysis. The same discount rate must be applied to all the models within the analysis so that the comparison is valid. This rate reflects the time value of money, which is used to

evaluate future costs in relation to present costs, accounting for the prevailing interest rate and (indirectly) the inflation rate.

Therefore, the discount rate is variable with time. In the UK, the Treasury (UK government practice) rules specifies a discount rate to be used for a given year; similar rates are established in other countries (Treasury, 2003). For life cycle costing on public sector projects, a discount rate of 3.5% per annum is stipulated by Treasury rules for all projects up to 30 years. For longer timescales and public sector projects (typically infrastructure buildings), a series of lower discounts rates are applied to different project years. This study used a 3.5% discount rate for 0–30 years, in line with UK government practice.

4.4.4 Study period selection

The study period is another fundamental factor in the life cycle cost analysis. The usual situation is that a single study period is applied to all the alternatives being assessed. There are special circumstances when different study periods are applied to different alternatives, but in this study, the calculated results must be presented as equivalent annual costs. The study period may be defined by the client or may be proposed by the project team. As shall be seen, the outcomes of life cycle costing can be extremely sensitive to the study period, and the choice should always be backed up with a strong argument. For new build or refurbishment projects, study periods of between 15 and 25 years are commonly used, but longer or shorter periods can be used. Shorter periods may be used for projects concerned with building services systems or interior fit-out. For the life cycle costing of building services installation, the life expectancy of the equipment is often used as the study period. Longer periods may be used for infrastructure works. In all cases, the study period should be informed by the client's business plan.

4.4.5 Costs data collection

The construction costs have been derived from a common industry reference, which is the SPON's price books (Langdon, 2014).

4.4.6 Calculations of LCC

Similar to the environmental (LCA) studies, the LCC studies of a product is to evaluate its economic influence. It estimates all relevant costs, including

construction, use (i.e., operation, maintenance, repair, and replacement) and end-of-life waste management (disposal) throughout the life period at their present value (PV) as in Eq.(4.9). Future costs (i.e., operation, maintenance, and disposal) are calculated using Eq.(4.10) for present values at an estimate of future inflation, and are then discounted using Eq.(4.11) to present value at a suitable discount rate. In this study, the construction cost and end-of-life costs were considered; the operation cost was not considered due to a lack of information for the operation stage.

$$\text{LCC} = C_C + C_u + C_{EOL} \tag{4.9}$$

Where LCC is the total life cycle costs of a flooring system, Cc is the construction costs, Cu is the usage costs, C_EOL is the end of life costs.

$$\text{FC} = \text{PV} \times (1 + f)^n \tag{4.10}$$

$$\text{DPV} = \text{FC}/(1 + d)^n \tag{4.11}$$

Where FC = future cost, PV = present value, DPV = discounted present value, f = inflation rate, d = discount rate, and n = number of years.

The construction costs Cc include the costs of the production and transport of construction materials, as well as the labour and energy costs for the construction of the flooring system and developer's profits:

$$C_C = C_{CM\&T} + C_{L\&OH} + C_{MF} \tag{4.12}$$

Where C_CM&T costs of extraction, production, and transport of construction materials C_L&OH labour and overhead costs C_MF fuel costs for the machinery used in the construction of the flooring systems.

4.4.7 Impact assessment of the LCC results

Economic performance was evaluated at the beginning of the purchase of a product and its installation. The study period ends at a fixed date in the future, which is the end-of-life time for flooring systems. The time value of money was accounted for in the LCC method by considering a real discount rate. This discount rate converted the future costs to their equivalent present value. The

unit costs for the flooring system, including installation costs, were extracted from SPON's price books (Langdon, 2014). The end-of-life costs were derived from various sources (Langdon, 2014, HMRC, 2011, SilverCrest, 2010). A 3.5% real discount rate was used to adjust cash flows to present values with a projection lifetime of 30 years (Treasury, 2003). Table 4-7 shows the first and future costs for the analysed flooring systems. The construction cost and end-of-life cost of prefabricated ultra shallow flooring system are less than the Cofradal260 slab costs by about 11% and 42%, and less than the construction and end-of-life costs of the hollow composite precast slab by about 13% and 19%, respectively. Figures 4-8 and 4-9 show the first and future costs of the studied flooring systems.

Table 4-7: First and future costs of flooring systems

Cofradal slab		Hollow composite precast slab with finishing		Prefabricated ultra shallow flooring system	
Construction phase	End of life phase	Construction phase	End of life phase	Construction phase	End of life phase
Cost (£)	Cost (£)	Cost (£)	Cost (£)	Cost (£)	Cost (£)
3079	294	2727	211	2676	171
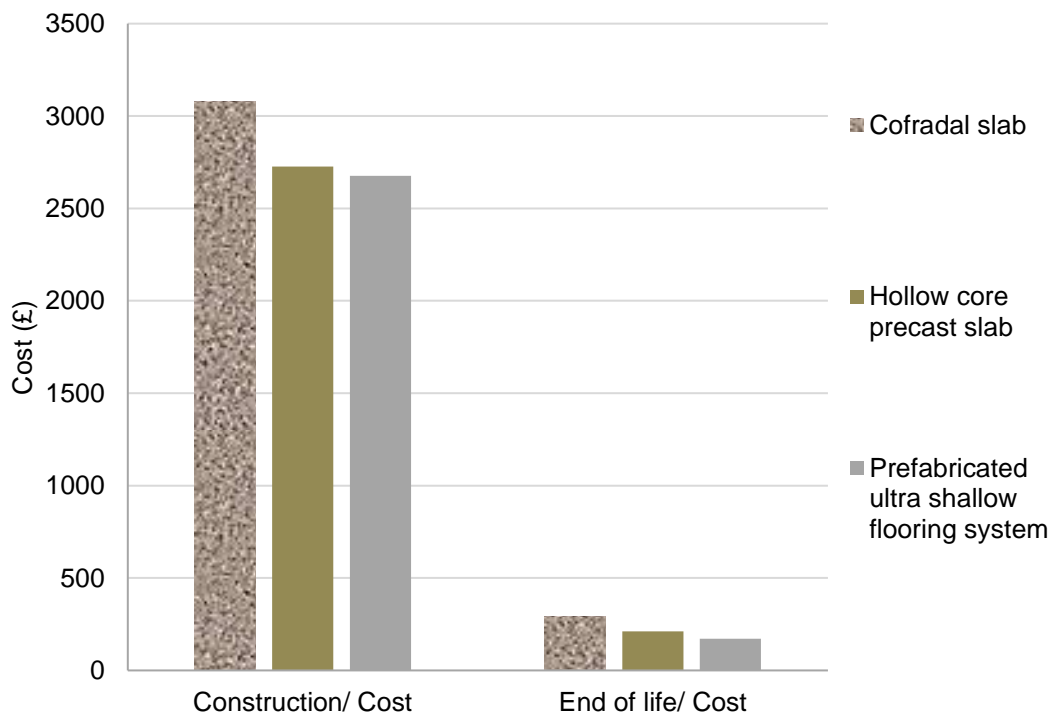
Figure 4-8: Costs of life cycle phase (Ahmed and Tsavdaridis, 2018)
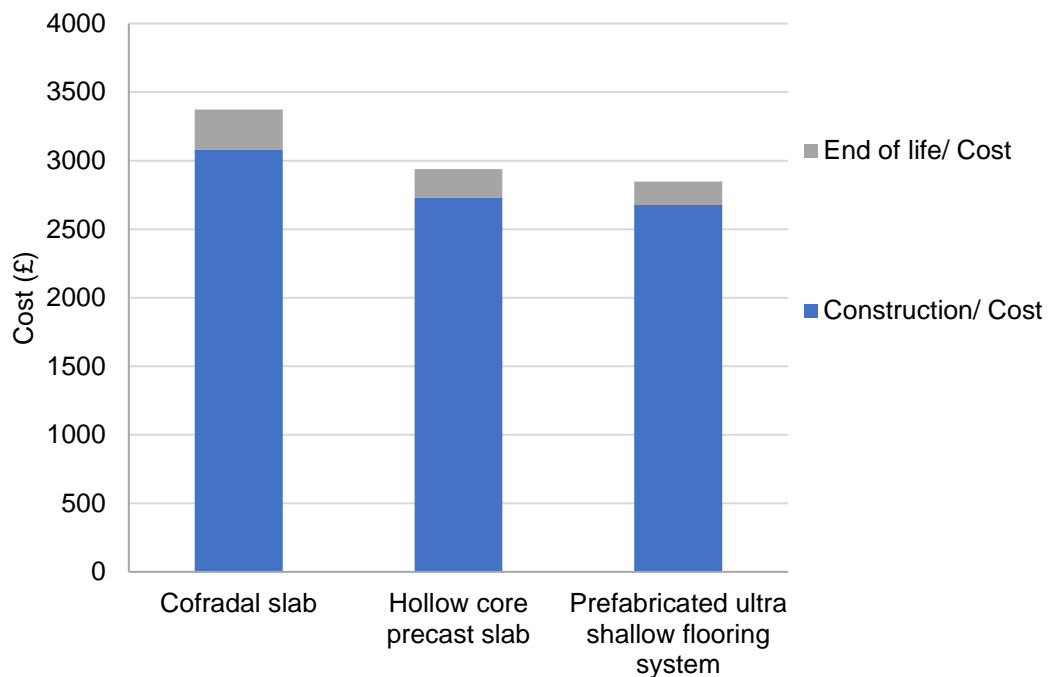
Figure 4-9: Costs by flooring systems (Ahmed and Tsavdaridis, 2018)

4.5 Summary

In this chapter, analytical LCA and LCC studies of three types of prefabricated shallow composite flooring systems have been presented. This analysis focused on semi and fully prefabrication methods for flooring systems. The semi prefabrication method was represented by a hollow core composite precast flooring system with casting in place of a finishing layer, whereas the full prefabrication method was represented by the Cofradal flooring system and the prefabricated ultra shallow flooring system was presented in **Chapter 3**.

Specifically, this study identifies a calculation boundary and five energy consumptions and carbon emission sources for semi and full prefabrication. These included embodied energy and embodied carbon emissions of manufacturing, transportation of building materials, transportation of construction waste, transportation of prefabricated components, and the operation of equipment and construction techniques, demolition and Recycling. In addition, this study also investigated the life cycle cost of these flooring systems, including both the construction and end-of-life phases. A comparison of these flooring systems that adopts semi and fully prefabrications was employed to illustrate the differences and characteristics of energy consumptions, carbon emissions, and cost.

- **Concluding remarks**

  Based on the presented analytical study, the following conclusions can be made:

- The results indicate that the proposed fully prefabricated flooring system reduced 28.45% of embodied energy and 43.73% of embodied carbon emissions compared with the Cofradal260 slab, 16.32% of embodied energy and 41.60% of embodied carbon emissions compared with the hollow composite precast slab for the manufacturing phase.

- For onsite construction, the proposed fully prefabricated flooring system reduced 37.5% for both embodied energy and embodied carbon emissions, compared with the Cofradal slab, and 53.50% for embodied energy and 53.12% for embodied carbon emissions compared with the hollow composite precast slab.

- For transportation, the proposed fully prefabricated flooring system reduced 15.86% for embodied energy and 15.12% embodied carbon emissions compared with the Cofradal slab, and 52.28% for embodied energy and 51.9% for embodied carbon emissions compared with the hollow composite precast slab.

- Regarding Recycling, the proposed fully prefabricated flooring system has a reduction of 9.25% of embodied energy and 15.56% of embodied carbon emissions compared with the Cofradal260 slab.

- The reduction percentage in embodied energy and embodied carbon emissions for the prefabricated ultra shallow flooring system compared with the hollow composite precast slab was higher than the Cofradal slab for both transportation and onsite construction phases, based on this data analysis. This is related to the fact that a hollow composite precast slab is a semi-prefabricated slab with a cast in-situ finishing layer, while the proposed flooring and Cofradal slabs are fully prefabricated flooring systems, including the finishing layer; this raises the amounts of embodied energy and embodied carbon emissions.

- The reduction percentage in embodied energy and embodied carbon emissions for the prefabricated ultra shallow flooring system compared with the Cofradal slab was higher than the hollow composite precast slab for both manufacture and Recycling phases. The reason for this is based on the use

of materials with high intensity of embodied energy and embodied carbon emissions, such as rock wool insulation material and concrete with a high cement content.

- The key approach to enhance embodied energy and embodied carbon emission reductions in semi prefabrication is in reducing the amount of offsite casting work, making reasonable and economically efficient proportions of concrete, and selecting off-site factories that are near the projects or material distribution centres. In the full prefabrication, the main methods to enhance the reduction in embodied energy and embodied carbon emissions reduction are as follows:

  - Reducing the amount of used concrete by optimising the design of reinforced concrete through changing the shape, such as using ribbed slab in the prefabricated ultra shallow flooring system.

  - Reducing the use of high intensity embodied energy, and embodied carbon emissions' materials - for instance, using lightweight aggregate concrete with lower amounts of cement content and recycled aggregate, as used in the prefabricated ultra shallow flooring system.

  - Increasing the width of the prefabricated elements - this will reduce the amount of embodied energy and embodied carbon emissions of onsite construction, with an increase in the width from 1.2m (for Cofradal260 slab and hollow core composite precast slab) to 2.0m (for the prefabricated ultra shallow flooring system). These aspects will gain increased recognition by more governments and clients as competition in the prefabrication market increases.

- The life cycle cost of these three flooring systems was also investigated in this study. The outcomes show that the prefabricated ultra shallow flooring system reduced by 13.08% of the construction cost and 41.83% of the end-of-life cost in comparison with the Cofradal260 slab, 1.87% of construction cost and 18.95% of end-of-life cost, in comparison with the hollow composite precast slab. The reduction percentage of the cost is not too high, which is related to the fact that the life cycle cost study only covers two phases. Therefore, as further work, it is recommended to extend the life cycle cost of this study to cover all phases, which represents a challenging task in finding the necessary data for the whole life cycle cost phases from the industry.

Chapter 5 : Push-out test series

5.1 Introduction

This chapter presents the push-out test series of the prefabricated ultra shallow flooring system. The experimental series of this thesis required the construction of eight prefabricated ultra shallow flooring systems. All test specimens were tested to failure under monotonic loading. This chapter outlines the design and construction of the test specimens, the test set-up, the instrumentation employed to measure the slip, separation of the specimens, test observations and the results.

5.2 Details of push-out test

Push-out tests investigate the shear resistance of the shear connectors by applying a direct longitudinal shear force to the shear connectors. The shear connectors of the prefabricated ultra shallow flooring system are different in comparison to the typical headed shear studs, formed uniquely by (1) WWSS and (2) WWSS with dowels.

The push-out test series involved 8 full-scale specimens investigating the WWSS and WWSS with dowels, with three types of concrete normal weight concrete, lightweight concrete using (lytag aggregate) and ultra lightweight concrete using (leca aggregate), as shown in Table 5-1. The test specimens were designed to represent the actual configurations of the shear connectors in the construction practice. The design principle is that the shear connectors of the test specimens are subjected to direct longitudinal shear force. Hence, the shear-resisting capacity and load-slip behaviour of the shear connectors were obtained. The set-up and procedures of the push-out tests were carried out to create the desired static loading conditions in order to be in compliance with the specifications of Eurocode 4 (EN1994-1-1, 2004).

The plan for the number of specimens of the push-out test was set up according to the availability of the lightweight aggregate materials, since the cost of these materials is expensive. Therefore, the intention is to have one specimen with normal weight concrete, two with lightweight concrete, and one with ultra lightweight concrete, for each group. It is worth to note that one of the specimens of the first groups (specimen with normal weight concrete) failed from one side

rather than two sides as the load was concentrated on one side only due to technical issues. As a result, this specimen was repeated with normal weight concrete. Therefore, the first group has two specimens with normal weight concrete, one with lightweight concrete and one with ultra lightweight concrete.

Table 5-1: Push-out test parameters

Test Group	Specimen No.	Type of shear connector	Concrete Type
Group1	T1-NWC-1	WWSS	Normal weight Concrete
	T1-NWC-2	WWSS	Normal weight Concrete
	T1-LWC	WWSS	Lightweight Concrete
	T1-ULWC	WWSS	Ultra Lightweight Concrete
Group2	T2-NWC	WWSS with dowels	Normal weight concrete
	T2-LWC-1	WWSS with dowels	Lightweight Concrete
	T2-LWC-2	WWSS with dowels	Lightweight Concrete
	T2-ULWC	WWSS with dowels	Ultra Lightweight Concrete

5.3 Concrete preparation

The push-out test specimens consisted of a steel section and concrete slabs, as shown in Figure 5-1. There were two types of shear connectors (WWSS and WWSS with dowels) welded to the web post of the steel sections. Concrete passed from one side to other side connecting the steel edge beams (parallel flange channel) on both sides. The steel sections were applied with grease to prevent the development of a bond between the concrete and steel. All the push-out test specimens were cast in the Heavy Structures Laboratory of the University of Leeds. Cube and cylinder specimens were prepared from the same mix of concrete used for the push-out test specimens. All the push-out test specimens,

along with the cubes and cylinders, were cured under the same condition and were covered with wet sacks and plastic sheets.

(a)

(b)
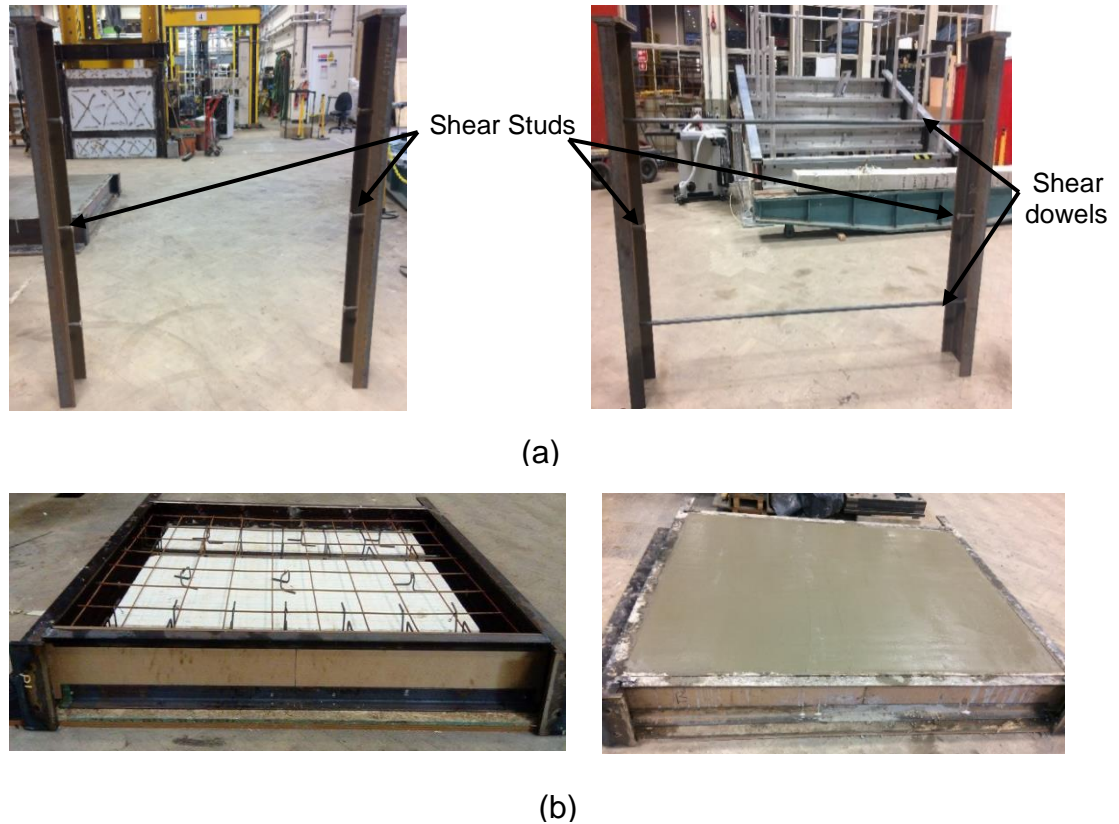
Figure 5-1: (a) Steel sections of the push-out test specimen; (b) Cast specimen for the push-out tests

5.3.1 Steel profiles

The steel section of the push-out test specimen was a short parallel flange C-channel. Three studs/horizontally lying dowels were welded to the web post. In order to study the relationship between the shear-resisting capacity of the shear connector and the type of shear connector, the steel sections were designed to have two types of shear connectors. The studs of Ø19mm and horizontally lying dowels of Ø20mm were welded to the sections of 230x75x26PFC, as shown in Figure 5-2. A steel beam (254x254x73UC) was connected to the top of the steel section to evenly spread the load.

(a)

(b)
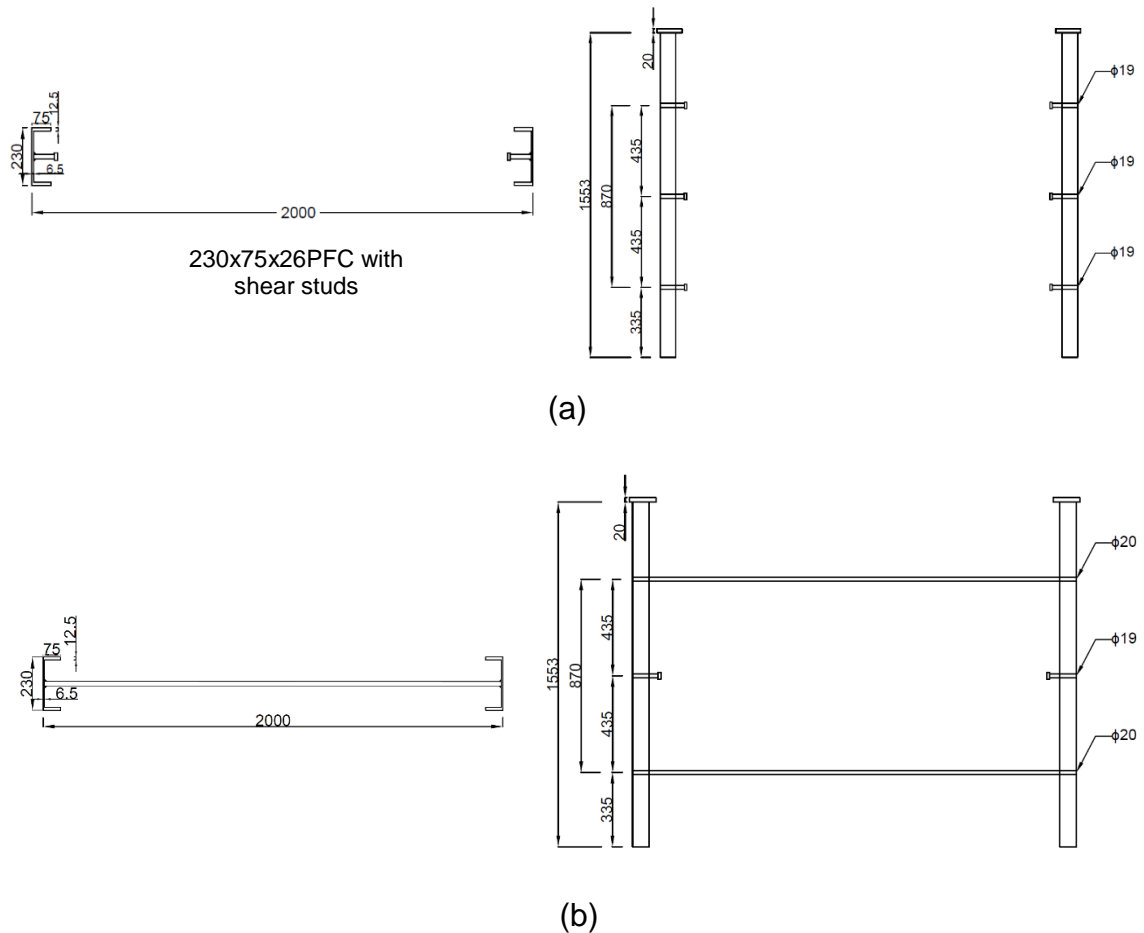
Figure 5-2: (a) The steel section of 230x75x26 PFC with Ø19mm studs; (b) the steel section of 230x75x26 PFC with Ø20mm horizontally lying dowels and Ø19mm studs

5.3.2 Slab systems

The total width of the concrete slabs of all specimens in the push-out test series was 2000mm. It was designed to represent the effective width of the concrete slab of the test specimen and to avoid undesirable variables due to the different width of the concrete slab. The depth of the infill part of the slabs was 217.5mm. The depth of ribbed slabs was 75mm, with ribs of 85mm at 870mm, in addition to the finishes of 40mm. The overall slab's depth, including finishes, was 200mm, as depicted in Figure 5-3.

Three types of concrete were used to cast the slabs: normal weight concrete, lightweight concrete (using Lytag aggregate) and lightweight concrete (using leca aggregate). The purpose of using the three types of concrete was to study the relationship between the shear-resisting capacity of the shear connection systems and the concrete strength. The tensile strength of normal weight

concrete was higher than that of the lightweight concrete with different compressive strength. This was concluded from the concrete strength tests carried out in the present research. The concrete strength comparison for the three types of concrete was presented in **Chapter 3**.
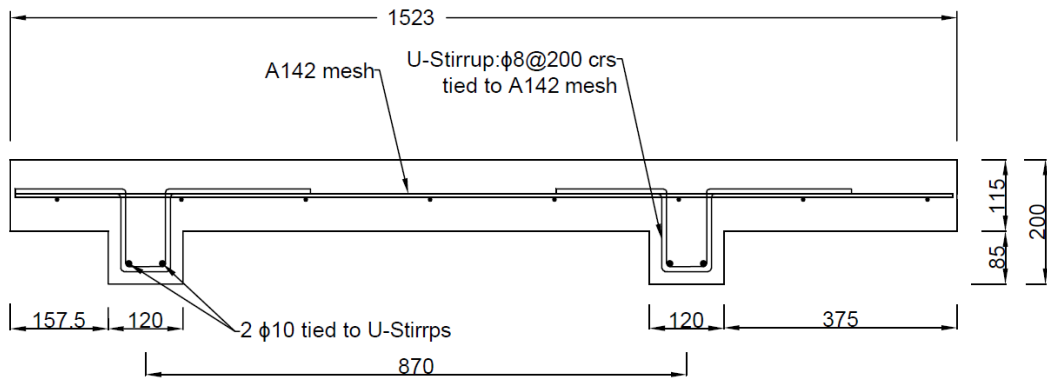
Figure 5-3: Cross section of ribbed slab

5.3.3 Test groups

Two types of shear connectors used for the prefabricated ultra shallow flooring system were investigated in the push-out test series. There were two test groups representing each type of shear connector: WWSS and WWSS with dowels. Each test group had three push-out test specimens. The variable parameters of the test specimens and their labels were summarised in Table 5-2.

Table 5-2: Specimen labels and variable parameters of the test groups

Test Group	Specimen No.	Concrete Type
T1, T2*	T1-NWC	Normal weight concrete(NWC)
	T1-LWC	Lightweight Concrete (LWC)
	T1-ULWC	Ultra Lightweight Concrete(ULWC)
*T1: WWSS T2: WWSS with dowels		

5.3.3.1 Specimens of test group T1, WWSS

The specimens of test group T1 comprised of three headed studs welded on one side of the web post, as shown in Figure 5-4. These shear studs would resist the longitudinal shear force applied on top of the steel section. The diameter of the studs was 19mm and the height was 95mm, as shown in Figure 5-4.
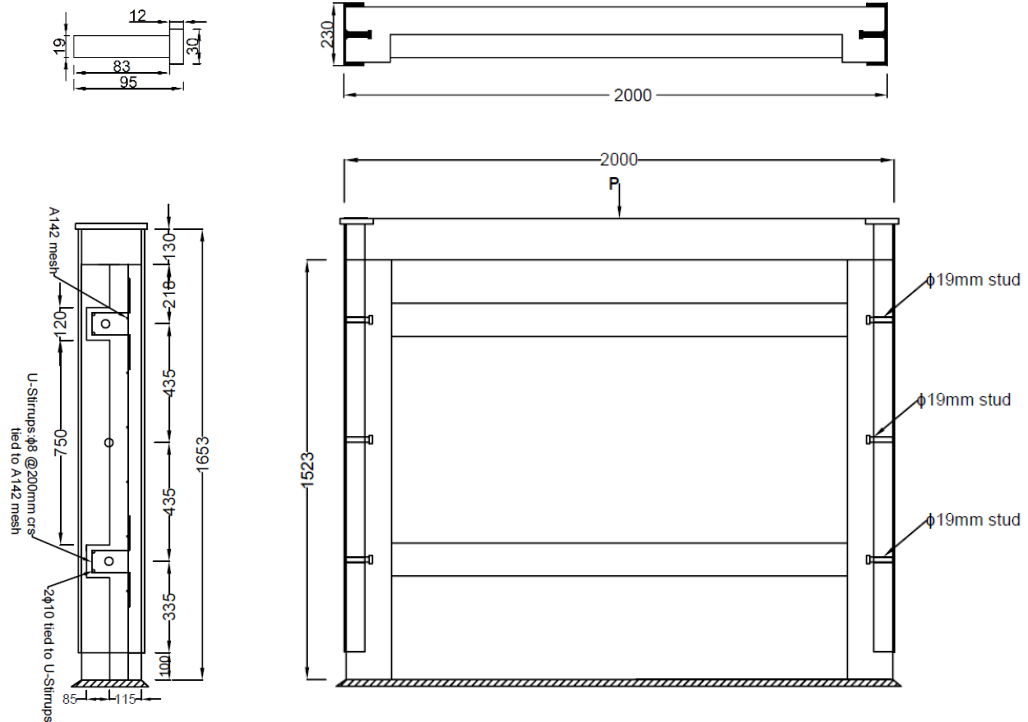
Figure 5-4: Drawings of the T1 specimens

5.3.3.2 Specimens of test group T2, WWSS with dowels

The horizontally lying dowels of test group T2 are represented by Ø20mm dowel welding to the steel edge beams (parallel flange C-channel), tying the concrete slab and steel edge beams together and passing through the centre of the slab ribs. The two horizontally lying dowels were positioned at 870mm centres, as shown in Figure 5-5. The studs were positioned at 435mm centres passing through the thin slab. The WWSS with dowels simultaneously resisted the longitudinal shear force.
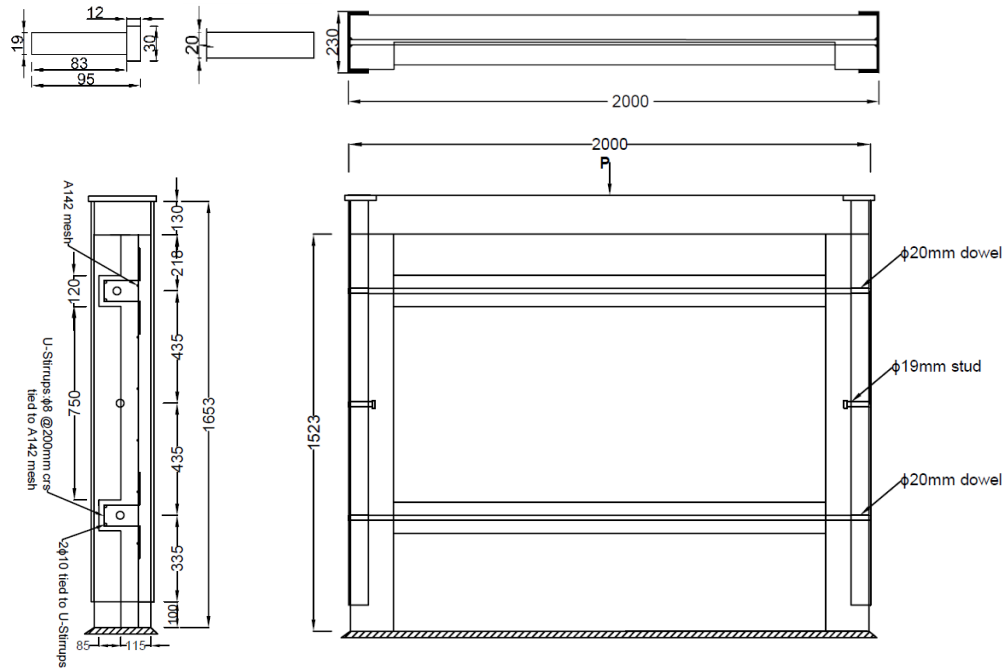
Figure 5-5: Drawings of the T2 specimens

5.4 Test apparatus

A rig of 1000kN (100ton) capacity, as shown in Figure 5-6 (a), was used for the push-out tests. One identical 1000kN (100ton) hydraulic jack was used to apply the load. A load cell was placed under the jack, as shown in Figure 5-6 (b). Digital dial gauges were used to obtain the measurements of slips and separations. Six digital dial gauges were positioned on both sides of the slab measuring the slips in a vertical direction. Two digital dial gauges were positioned on both sides of the slab measuring separations in the horizontal direction. One digital dial gauge was positioned in the z-direction for recording movement in this direction. The resolution of the digital dial gauges was 0.01mm.

A data logger machine linked to a computer recorded all the readings at different load levels. All the specimens were loaded until failure. During this process, any failure associated with unloading the specimen was also observed. The failure patterns were captured using a digital camera.
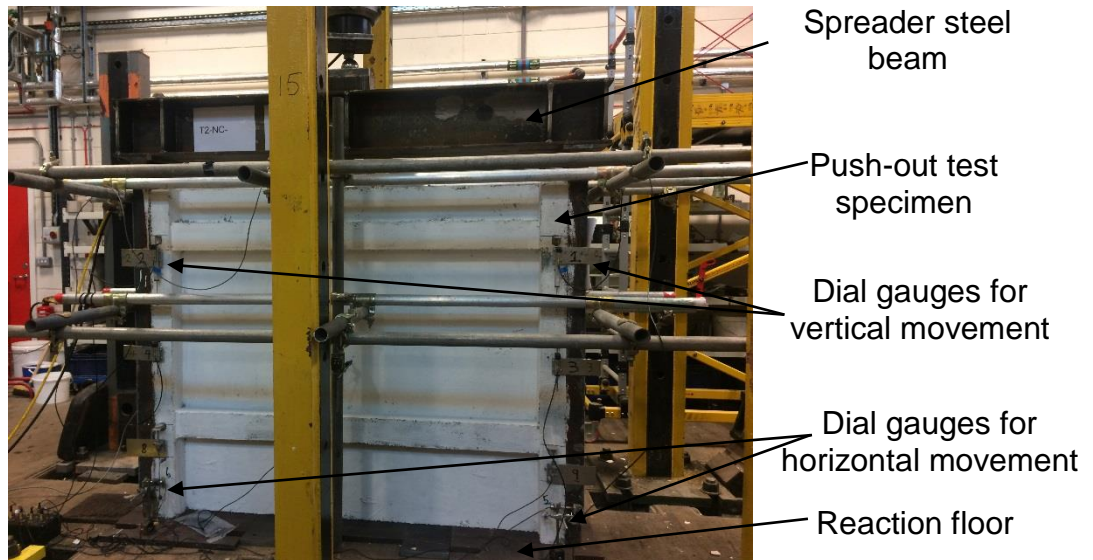
(a)

(b)

Figure 5-6: (a): The rig for the push-out tests; (b): Set up and instrumentations of the push-out tests

5.4.1 Testing procedure

The push-out tests were carried out in accordance with the specifications of Eurocode 4 (EN1994-1-1, 2004). The specimens were bedded onto a steel plate. This was done to eliminate any uneven contact between the specimens and the reaction floor. Monotonic loading was applied to the steel sections, and incremental shear force was applied to the shear connectors. The push-out tests were load-controlled. The load increments for the specimens of each test groups are listed in Table 5-3. The specimens were tested until the destructive failure of the shear connectors. The duration of the push-out tests was 2 hours on average, with a load rate of 0.5kN/sec, which was more than the minimum duration of 15 minutes specified in Eurocode 4 (EN1994-1-1, 2004). The slips were measured until the load dropped to at least 20% below the maximum load.

Table 5-3: Load increments of the test groups

Test Group	Load Increment	As % of the Expected Failure Load
T1 (WWSS)	20kN (2ton)	4%
T2 (WWSS with dowels)	20kN (2ton)	4%

5.5 Results

Load-slip and load-separation curves were obtained from the push-out tests. The load-slip curves represented the characteristic behaviour of the shear connectors in response to the direct longitudinal shear force. The load-separation curves represented the tie-resisting behaviour of the shear connectors. The concrete strengths of all specimens at the day of the push-out test are presented in Tables 5-6 & 5-7. The test results were evaluated with the aim to provide information on the specific properties of the shear connectors. The criteria of the evaluation were based on Eurocode 4 (EN1994-1-1, 2004). The behaviour and failure mechanisms of the shear connectors are studied in particular, with the aim of optimising and improving the design details. The shear resisting capacities of the shear connectors were further analysed in **Chapter 7** to establish a shear resistance design model.

5.5.1 Load-slip curves

The load-slip curves of all test groups are shown in Figures 5-7 & 5-8. The load shown in these load-slip curves was the load per shear connector. The load–slip curves selected for the discussion are based on: (1) the type of shear connector and (2) the type of concrete (NWC, LWC, and ULWC).

5.5.2 Load-separation curves

The load-separation curves of all test groups are shown in Figures 5-9 & 5-10. The load shown in the load-separation curves was the load per shear connector. Load-separation curves represent the tie-resisting behaviour of the shear connector to the longitudinal shear force. The scales of the load-separation curves were the same as those of the load-slip curves. Hence, a comparison between the slips and separations can be shown.
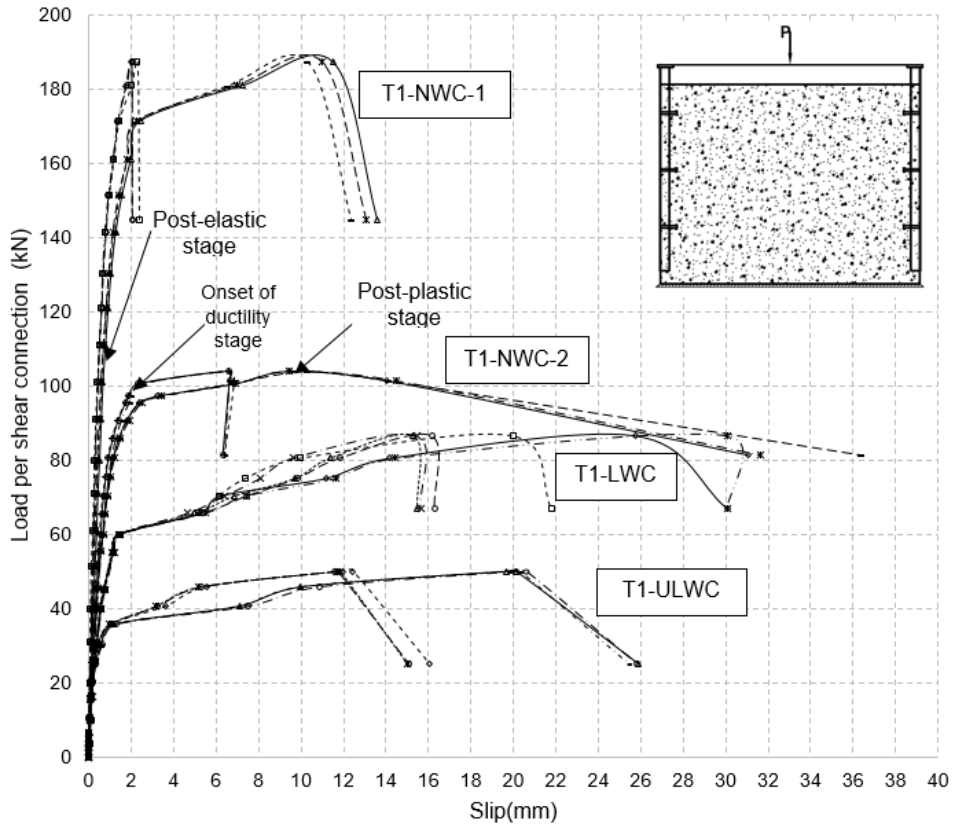
Figure 5-7: Load-slip curves of WWSS (test group T1)
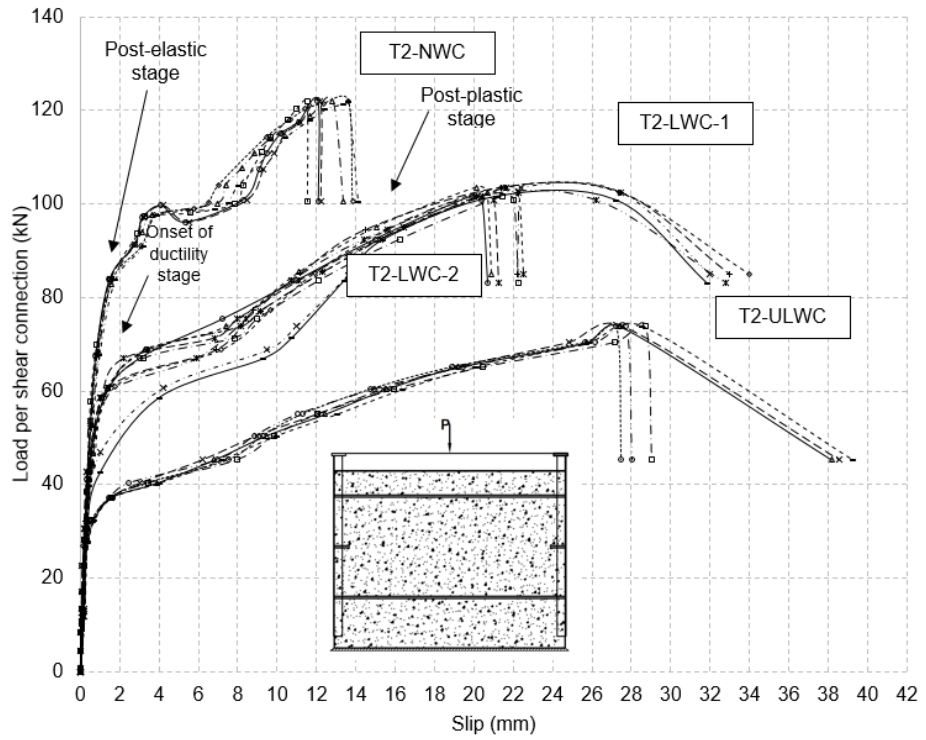
Figure 5-8: Load-slip curves of the WWSS with dowels
(test group T2)
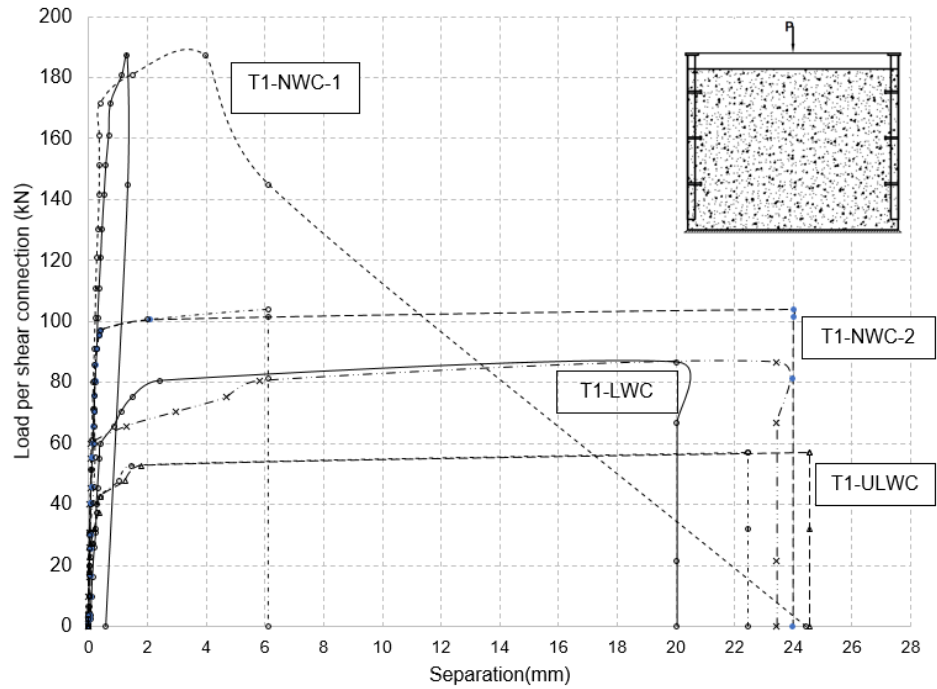
Figure 5-9: Load-separation curves of WWSS (test group T1)
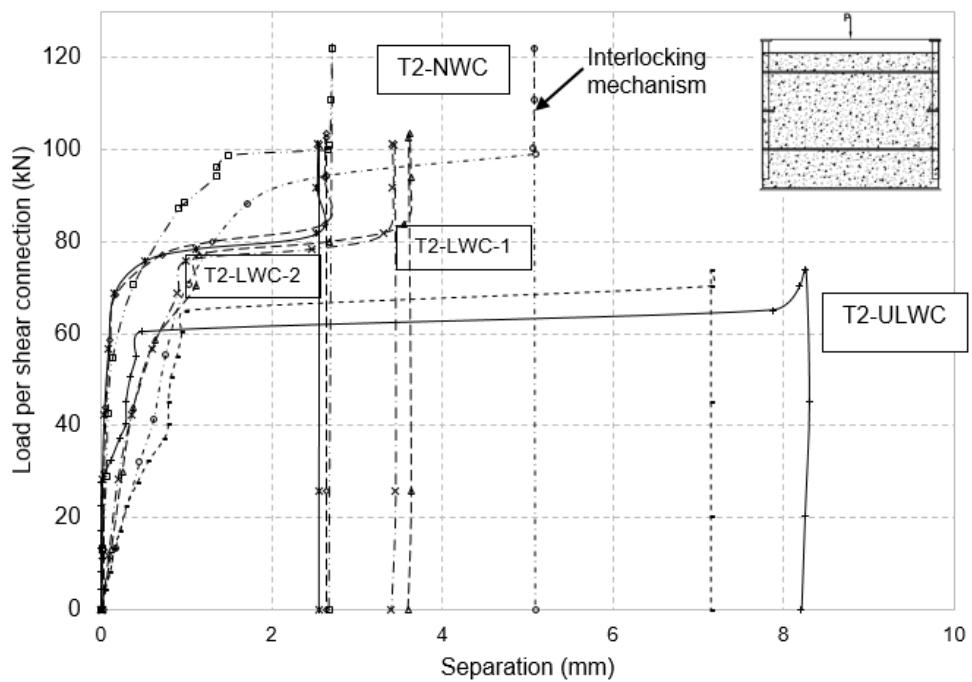
Figure 5-10: Load-separation curves of WWSS with dowels
(test group T2)

5.5.3 Results evaluation according to Eurocode 4 (EN1994-1-1, 2004)

The results of the push-out tests were evaluated in accordance with Eurocode 4 (EN1994-1-1, 2004), see Tables 5-4 & 5-5. The methods and criteria used in the evaluation are outlined below.

- The ultimate shear capacity of the shear connector, P_u, was obtained by dividing the ultimate load of the specimens by the number of shear connectors.

- The slip capacity of the shear connector, δ_u, was the slip value at the load level, which dropped 10% below the ultimate load Eurocode 4 (EN1994-1-1, 2004).

- Characteristic slip capacity, δ_{uk}, is the slip capacity reduced by 10%. If it is greater than 6mm, the shear connector is classified as ductile Eurocode 4 (EN1994-1-1, 2004). Furthermore, the load-slip curve of the shear connector should show plastic deformation after the maximum load is reached.

- The stiffness of the shear connector, K, is the linear stiffness of the load-slip curves.

- The criterion of the tie resistance check is that the transverse separations at 80% of the ultimate load should be less than half of the slip at that load level Eurocode 4 (EN1994-1-1, 2004).

Table 5-4: Result evaluation of the push-out test group (T1)

Specimen No.	Ultimate shear capacity, P_u,(kN)	Shear Connectors	Slip capacity, δ_u (mm)	Characteristic slip capacity, δuk, (mm)	Stiffness,K, (kN/mm)	Ductility classification (pass/fail)	Tie resistance check (pass/fail)
T1-NWC-1*	187.17	Right top stud	2.37	2.13	78.97	fail	fail
	187.17	Right middle stud	2.06	1.85	90.85	fail	fail
	187.17	Right bottom stud	2.06	1.85	90.85	fail	fail
	187.17	Left top stud	13.59	12.23	13.77	pass	pass
	187.17	Left middle stud	13.09	11.78	14.29	pass	pass
	187.17	Left bottom stud	12.33	11.09	15.18	pass	pass
T1-NWC-2	103.97	Right top stud	21.60	19.44	5.34	pass	pass
	103.97	Right middle stud	21.30	19.17	4.88	pass	pass
	103.97	Right bottom stud	23.20	20.88	4.48	pass	pass
	103.97	Left top stud	6.58	5.92	15.80	fail	pass
	103.97	Left middle stud	6.58	5.92	15.80	fail	pass
	103.97	Left bottom stud	6.63	5.97	15.68	fail	pass
T1-LWC	86.70	Right top stud	16.28	14.65	5.32	pass	pass
	86.70	Right middle stud	15.45	13.90	5.61	pass	pass
	86.70	Right bottom stud	15.63	14.06	5.54	pass	pass
	86.70	Left top stud	30.07	27.06	2.88	pass	pass
	86.70	Left middle stud	30.07	27.06	2.88	pass	pass
	86.70	Left bottom stud	21.82	19.63	3.97	pass	pass
T1-ULWC	57.02	Right top stud	20.63	18.56	2.76	pass	pass
	57.02	Right middle stud	20.29	18.26	2.81	pass	pass
	57.02	Right bottom stud	20.12	18.10	2.83	pass	pass
	57.02	Left top stud	12.41	11.16	4.59	pass	pass
	57.02	Left middle stud	11.85	10.66	4.81	pass	pass
	57.02	Left bottom stud	11.73	10.56	4.86	pass	pass
* The specimen, T1-NC-1 was failed from one side rather than two, therefore the ultimate load is taken by three shear connectors only rather than six shear connectors, and the ultimate shear capacity is per shear connector of the three shear connectors							

Table 5-5: Result evaluation of the push-out test group (T2)

Specimen No.	Ultimate shear capacity, P_u,(kN)	Shear Connectors	Slip capacity, δ_u (mm)	Characteristic slip capacity, δuk, (mm)	Stiffness,K, (kN/mm)	Ductility classification (pass/fail)	Tie resistance check (pass/fail)
T2-NWC	121.9	Right top dowel	12.18	10.96	10.0	pass	pass
	121.9	Right stud	11.55	10.36	10.58	pass	pass
	121.9	Right bottom dowel	12.09	10.88	10.08	pass	pass
	121.9	Left top dowel	13.64	12.27	8.93	pass	pass
	121.9	Left stud	12.83	11.55	9.50	pass	pass
	121.9	Left bottom dowel	13.64	12.27	8.93	pass	pass
T2-LWC-1	101.65	Right top dowel	22.10	19.89	4.59	pass	pass
	101.65	Right stud	21.50	19.35	4.72	pass	pass
	101.65	Right bottom dowel	21.10	18.99	4.81	pass	pass
	101.65	Left top dowel	31.10	27.99	3.63	pass	pass
	101.65	Left stud	30.10	27.09	3.37	pass	pass
	101.65	Left bottom dowel	30.10	27.09	3.37	pass	pass
T2-LWC-2	103.51	Right top dowel	22.20	19.98	4.66	pass	pass
	103.51	Right stud	21.00	18.90	4.92	pass	pass
	103.51	Right bottom dowel	22.20	19.98	4.66	pass	pass
	103.51	Left top dowel	31.20	28.08	3.31	pass	pass
	103.51	Left stud	30.10	27.09	3.43	pass	pass
	103.51	Left bottom dowel	30.90	27.81	3.34	pass	pass
T2-ULWC	73.83	Right top dowel	31.90	28.71	2.31	pass	pass
	73.83	Right stud	30.70	27.63	2.40	pass	pass
	73.83	Right bottom dowel	30.90	27.81	2.38	pass	pass
	73.83	Left top dowel	29.00	26.10	2.54	pass	pass
	73.83	Left stud	27.30	24.57	2.70	pass	pass
	73.83	Left bottom dowel	28.00	25.20	2.63	pass	pass

5.5.4   Results of test group T1: WWSS

The WWSS of test group T1 consisted of three Ø19mm headed studs shear connectors welded on one side of the web post of each steel channel. There were three headed studs welded on both sides of the web post, as shown in Figure 5-4. Hence, each side of the specimen has three shear connectors. The WWSS would be in direct contact with the longitudinal shear force, as the studs are welded to the steel C-channels. The results of the ultimate loads and slips are listed in Tables 5-6 & 5-7. The load-slip and load-separation curves of each specimen are shown in Figures 5-11-5-13. The load values of these curves were the load per shear connector. The results of the ultimate load and slip are summarised in Table 5-6.

Table 5-6: Result summary of the test group T1

Specimen No.	Concrete Type	$f_{cu}{}^*$ (MPa)	$f_{ct}{}^\sim$ (MPa)	Ultimate Load (kN)	Slip (mm) at Ultimate Load	Separation (mm) at Ultimate Load
T1-NWC-1	Normal	31.60	2.26	561.51	2.32	3.96
T1-NWC-2	Normal	38.52	2.88	623.82	2.10	23.98
T1-LWC	Lightweight (lytag)	32.20	1.61	520.23	13.73	23.43
T1-ULWC	Lightweight (leca)	20.0	1.36	342.42	20.15	24.55
* cube compressive strength of concrete ~ tensile splitting strength of concrete at the day of the push-out test						

The slips of the WWSS at the ultimate load were significant - between 2-21mm. Large slips were demonstrated by all specimens. This demonstrated the desired ductility for the shear connector. The slip stiffness of the WWSS among the three specimens was different. It has been shown that the slip stiffness was influenced by the strengths of the concrete. The separation of all the specimens were large, between 3-25mm, which indicates the weak tie resistance of the WWSS. All the specimens demonstrated that the separation started at a load level of the sudden slip increase. The separations at the ultimate loads were 23.98mm for the T1-NWC-2 specimen, 23.43 mm for the T1-LWC specimen and 24.55mm for the T1-ULWC specimen.

The relationship between the shear-resisting capacity of the shear connector and concrete strength was shown from the results. The failure load of the specimen

with a higher strength of concrete (T1-NWC-2) was higher than that of specimens with a lower strength of concrete: T1-LWC and T1-ULWC, respectively. This comparison was based on the same type of shear connector. This comparison was made between the specimens with the same type of shear connectors.

5.5.4.1 Behaviour analysis

The ductile behaviour was shown by the WWSS, which initially deformed elastically before it underwent plastic deformations with significant slips. The load dropped gradually and extensive slips also occurred after the ultimate load was reached. The ultimate failure of the shear connectors, as the shear stud sheared off, occurred after the load dropped to 85-93% of the maximum loads.

The slip behaviour of the WWSS was similar to that of the headed studs in the standard push-out tests, as illustrated in Figure 3-13 (Figure of the load-slip curve from Eurocode 4 (EN1994-1-1, 2004). This similar behaviour indicated that the behaviour of the WWSS was greatly influenced by the headed studs. The specimens with lightweight concrete (T1-LWC and T1-ULWC) demonstrated additional ductility when compared with specimen T1-NWC-2. However, the specimen T1-NWC-2 has reached higher failure load than the failure loads of specimens T1-LWC and T1-ULWC. This is related to the fact that the failure loads of the specimens are depending on the compressive strength of the concrete type rather than its ductility.

Loud cracking was heard as the ultimate loads were reached. The cracking noise then became intensified. Sudden destructive failure occurred, as the web welded studs were sheared off on the left side of the specimen.

It was clearly demonstrated, by all specimens of the test group, that no interlocking mechanism occurred at the ultimate load levels. This indicated that the contribution of the shear resistance of web welded studs shear connectors in holding the whole system from failure was very small.
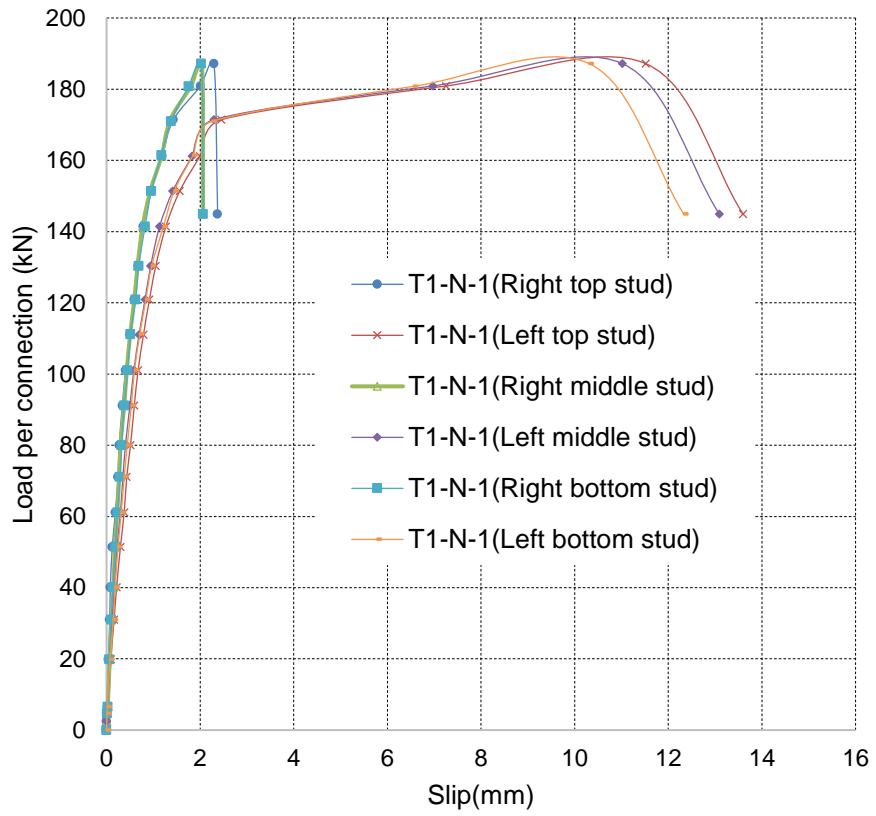
(a)
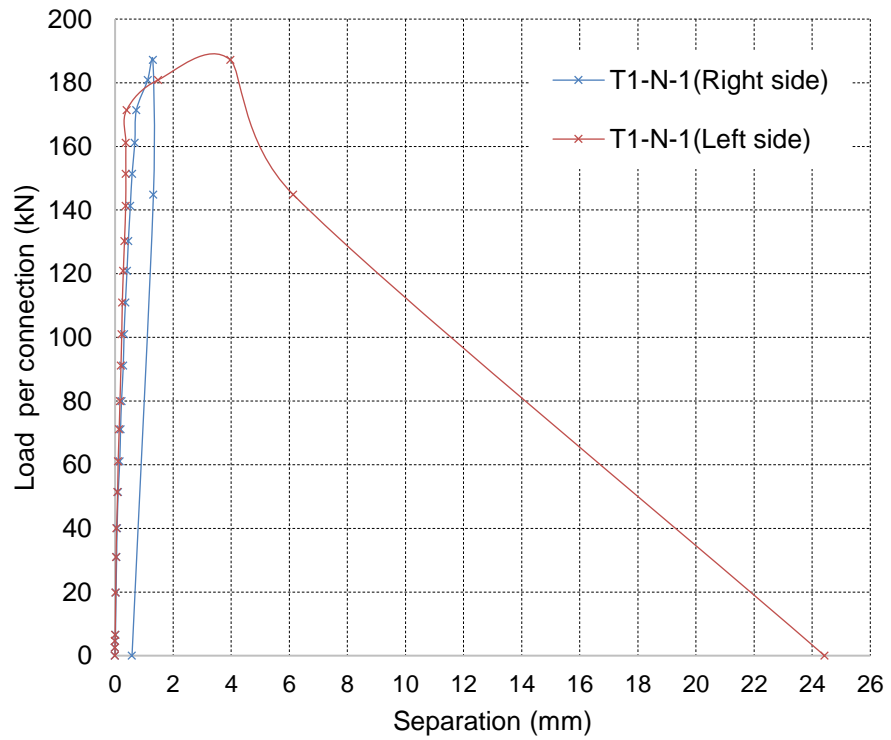
(b)

Figure 5-11: (a)Load-slip, (b) load-separation curves of specimen T1-NWC-1 (WWSS-normal weight concrete)
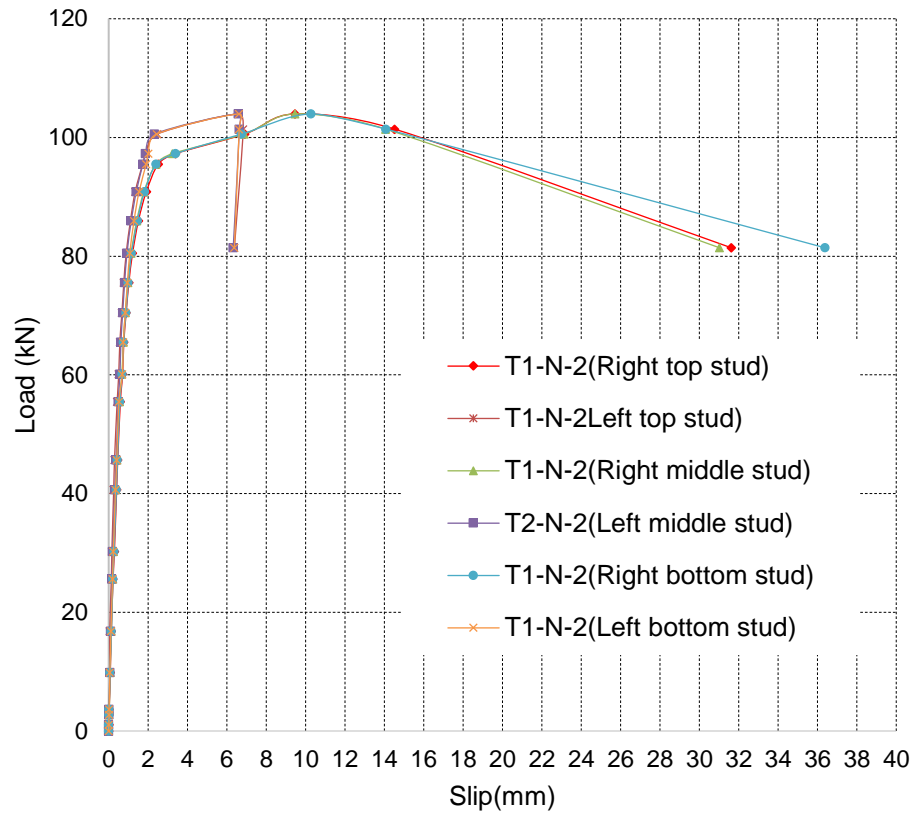
(a)
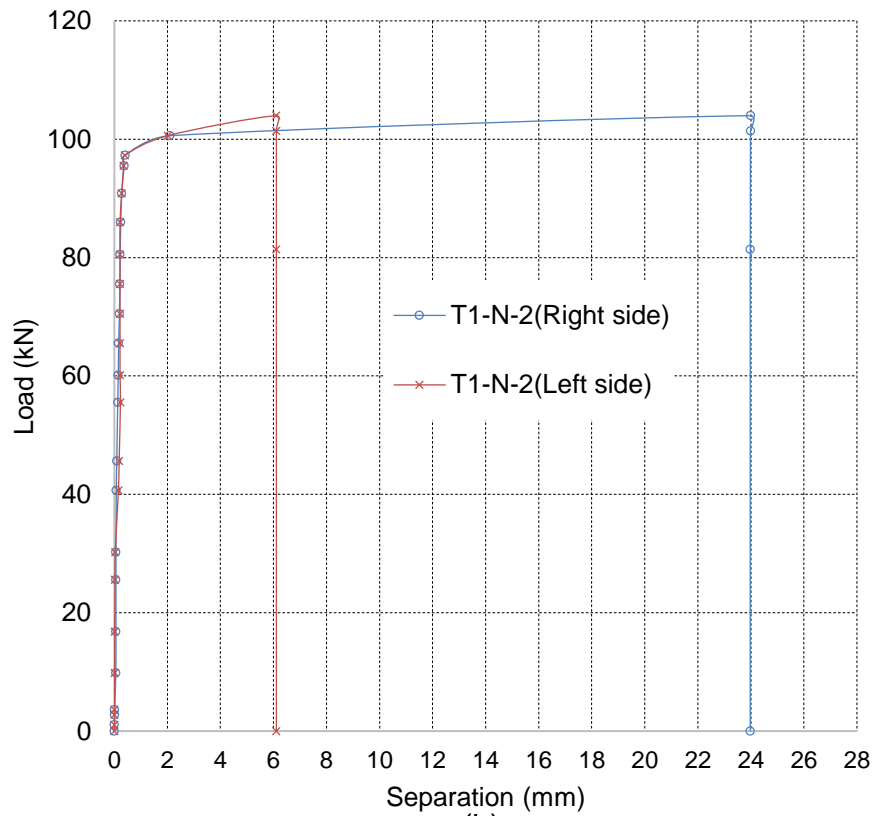
(b)

Figure 5-12: (a): Load-slip, (b) load-separation curves of specimen T1-NWC-2 (WWSS-normal weight concrete)
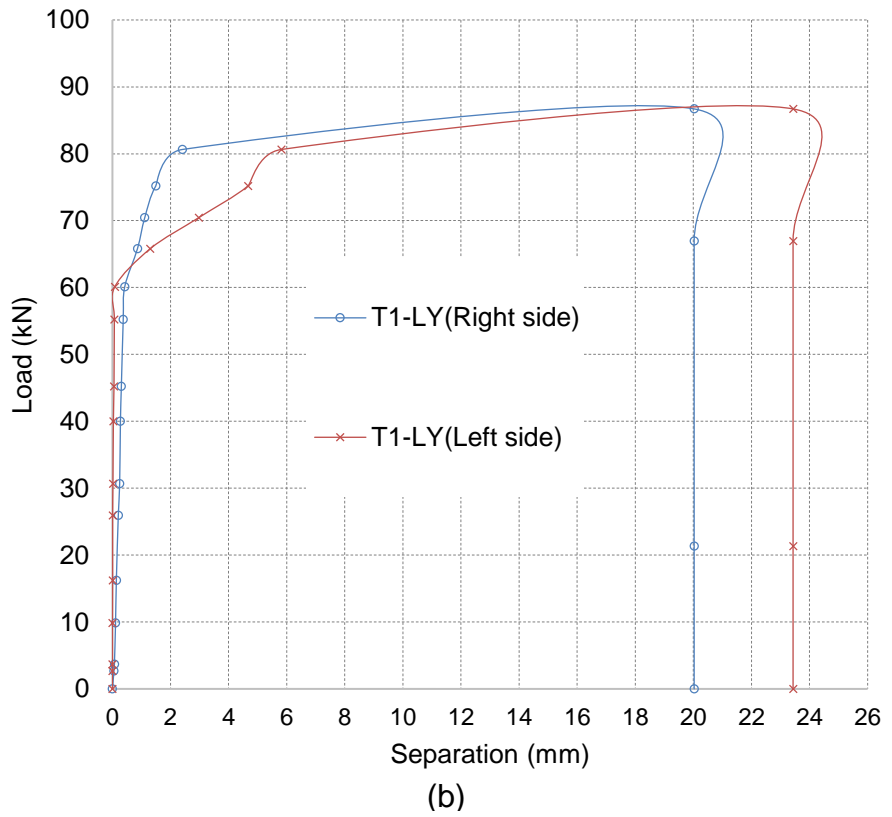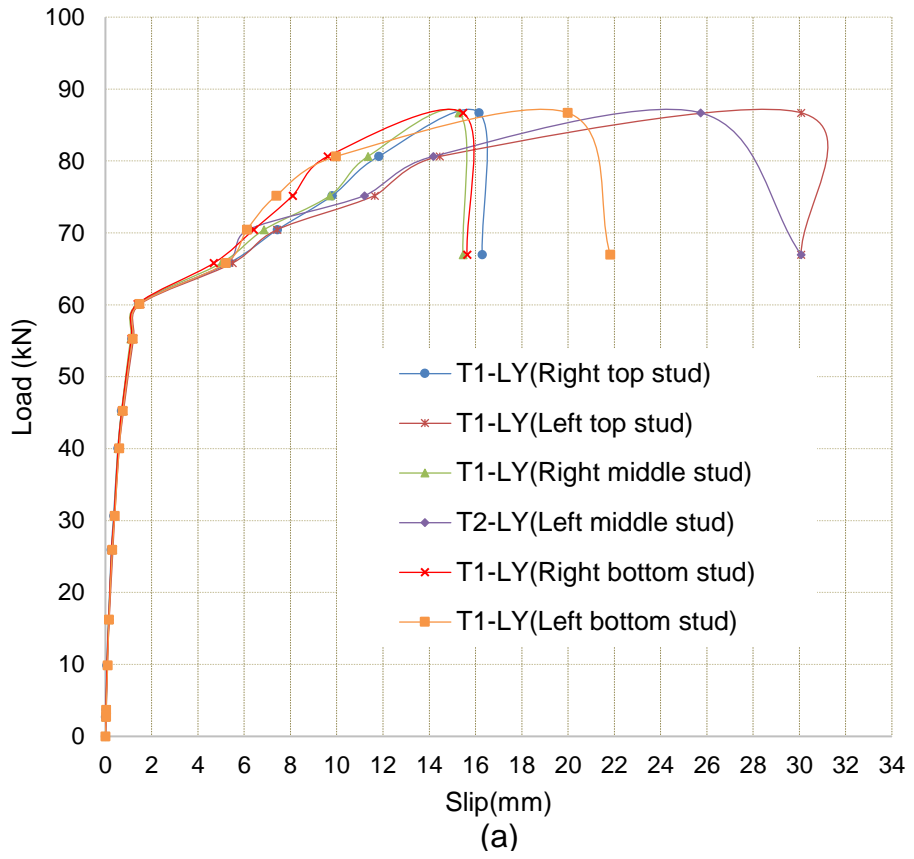
Figure 5-13: (a) Load-slip, (b) load-separation curves of specimen T1-LWC (WWSS-lightweight concrete)
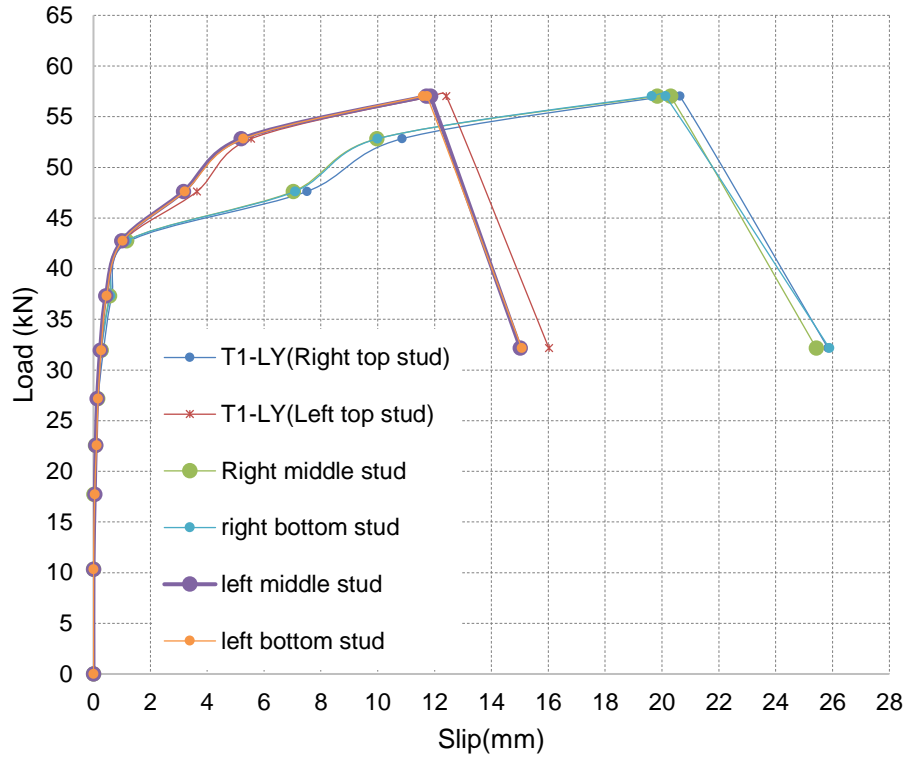
(a)
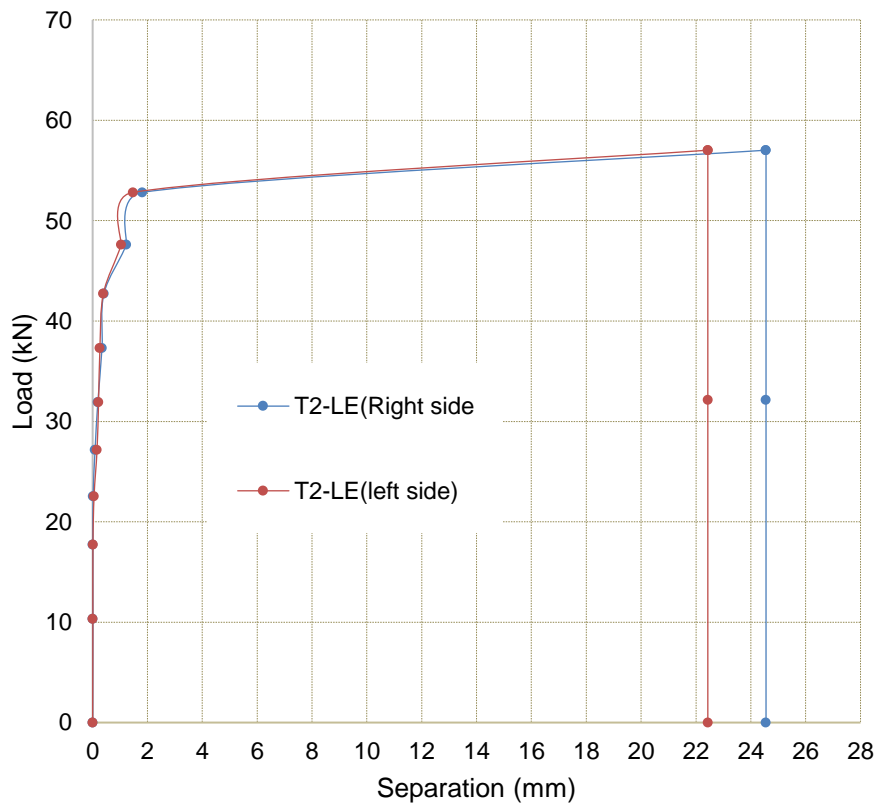
(b)

Figure 5-14: (a) Load-slip, (b) load-separation curves of specimen T1-ULWC (WWSS-ultra lightweight concrete)

5.5.4.2 Failure mechanisms

For specimen T1-NWC-1, the studs on the left side sheared off with small bending near their root, however, the studs on the right side were not bent and not sheared off, as shown in Figure 5-15. This was because the load was not distributed evenly on both sides. As a result, the failure was concentrated on one side (left side), rather than two sides. The bending length of the shear studs was 20mm.
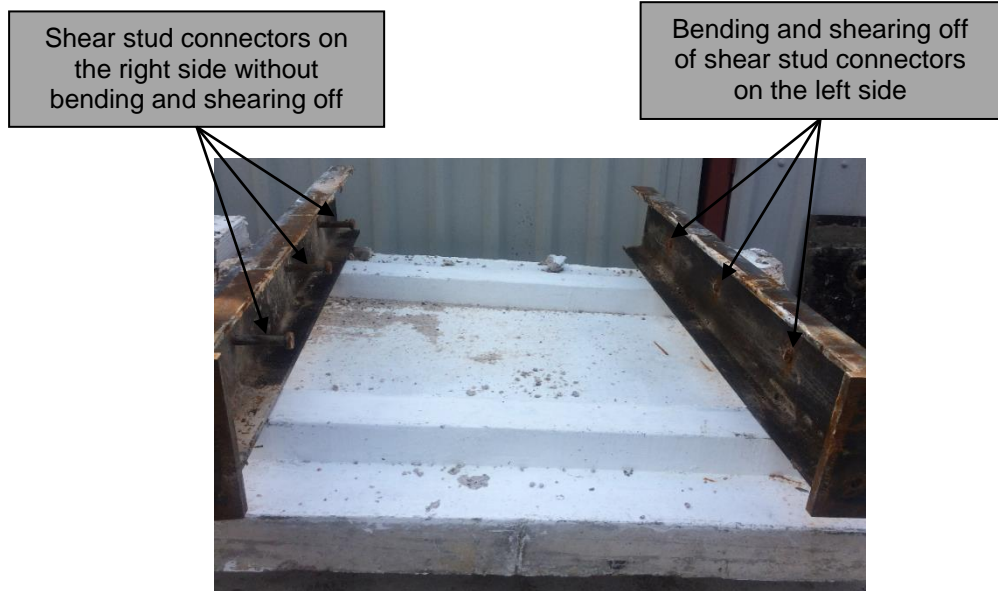
(a): Bending and shearing off of the shear stud connectors
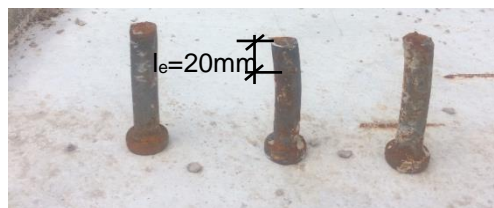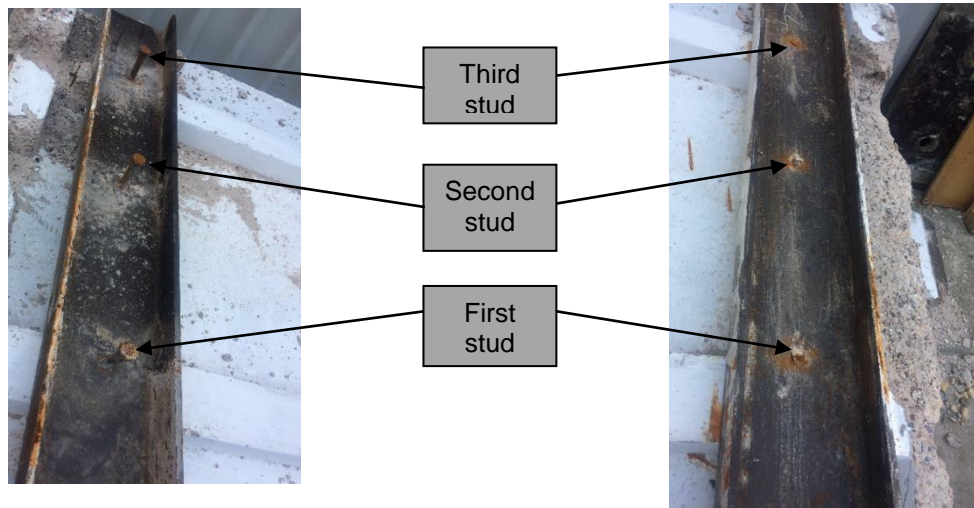
(b): Bending length of the shear connector

Figure 5-15: Shear connectors' failure of T1-NWC-1 specimen

The concrete cracks of specimen T1-NWC-1 were concentrated on one side (left side), which started with concrete cracking near the top studs' position, near the position of the ribs, at a load of 520kN. These cracks continued towards the position of the middle shear stud connectors. Then, the concrete near the bottom studs' position started cracking at a load of 540kN. The concrete failure profile is presented in Figure 5-16. Sudden failure occurred at the end of the test, as the top, middle and bottom studs on the left side were sheared off at a load of 560kN.
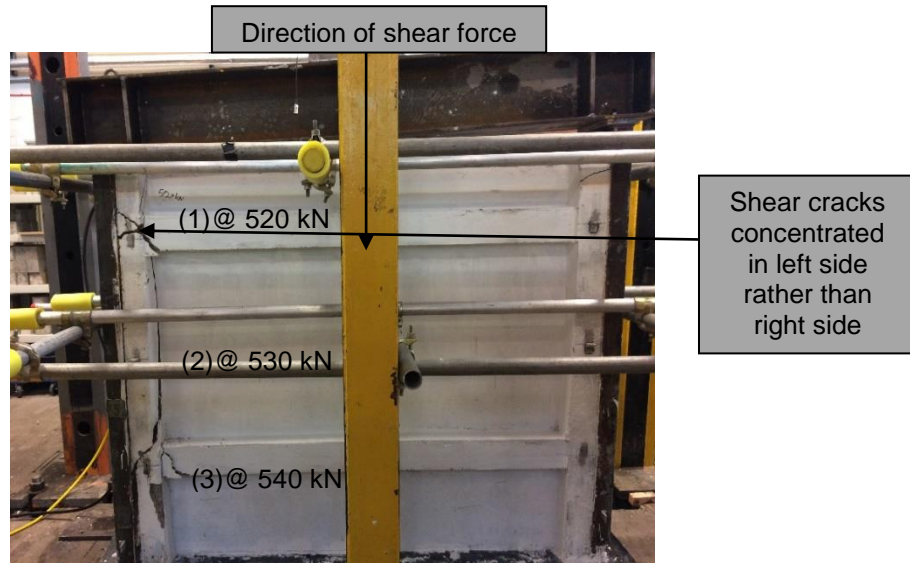
(a): Full specimen view
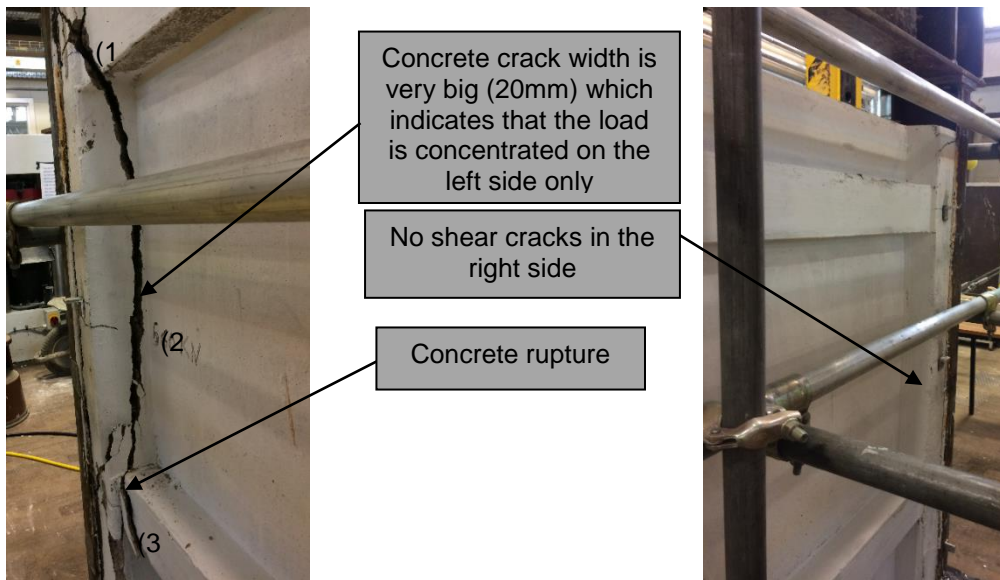
(b): Left and right sides view of the specimen

Figure 5-16: Concrete failure profile of specimen T1-NWC-1

For specimen T1-NWC-2, the studs on the right side were sheared off with bending near their root, however, the studs on the left side were bent without being sheared off, as depicted in Figure 5-17. The bending length of the shear studs was 40mm.
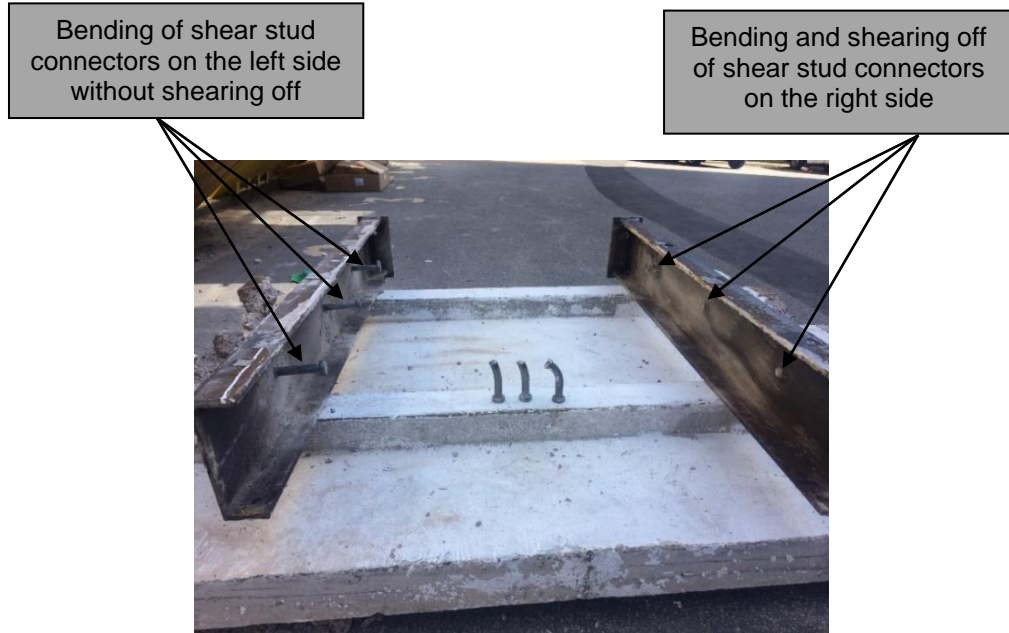
(a): Bending and shearing off of the shear stud connectors
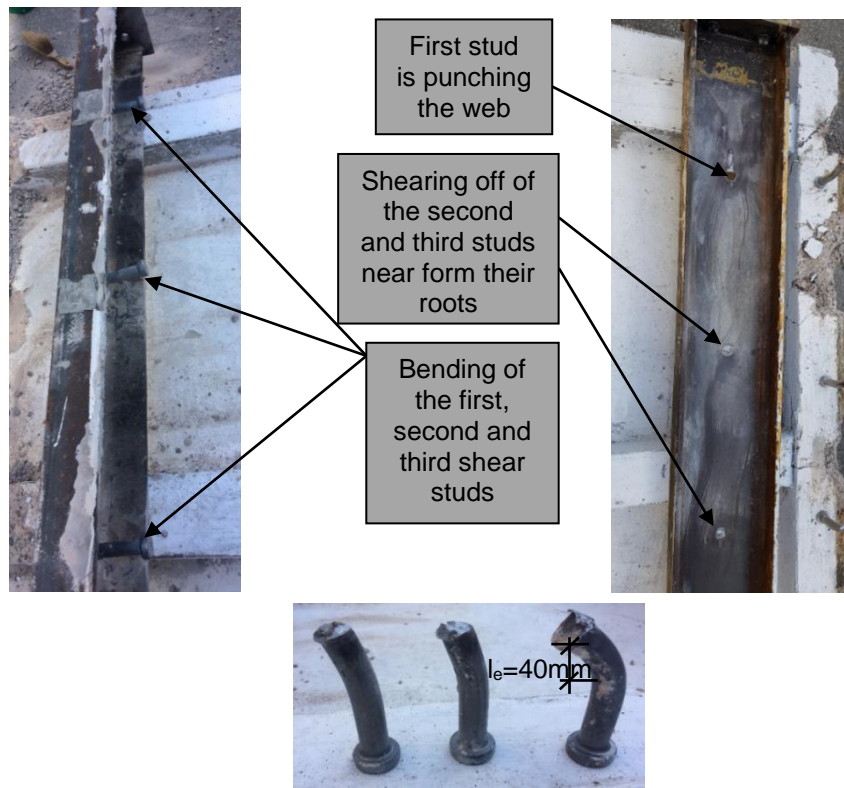
(b): Bending length of the shear

Figure 5-17: Shear connectors' failure of T1-NWC-2 specimen

The concrete failure of specimen T2-NWC-2 began from the top studs' position, at the ribs at both sides at a load of 580kN. These cracks continued towards the position of the shear stud connectors in the middle of the specimen at a load of 600kN. Then, the concrete near the bottom studs' position started cracking at a load of 620kN, the concrete failure profile is shown in Figure 5-18. The cracking sound was initially heard at the end of the elastic deformations. Then, it intensified during the plastic deformations. Sudden failure occurred at the end of the test, as the top, middle and bottom studs on the right side were sheared off.
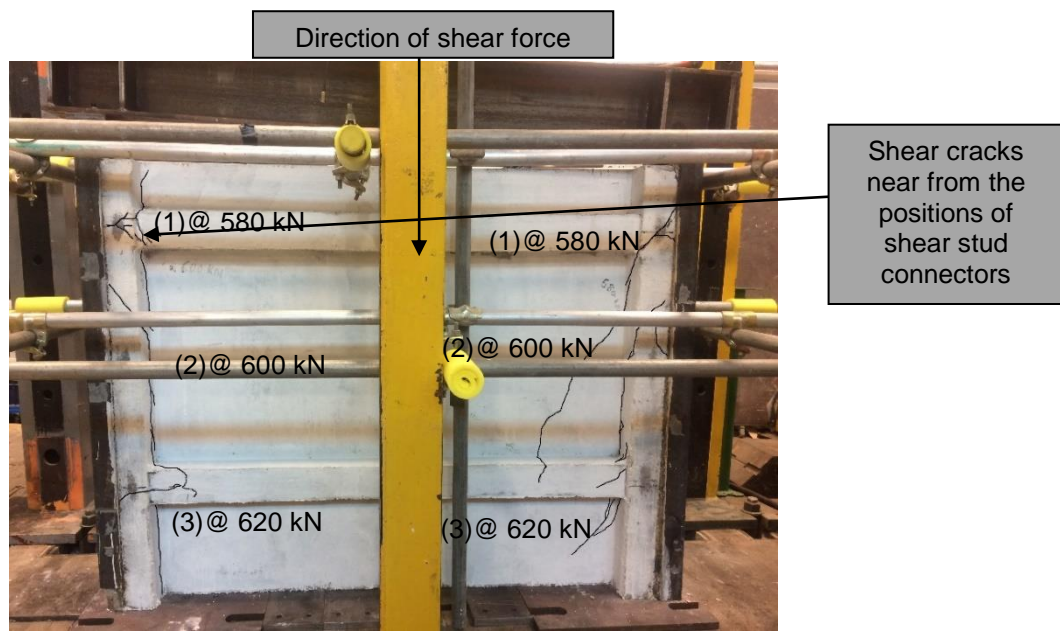
(a): Full specimen view
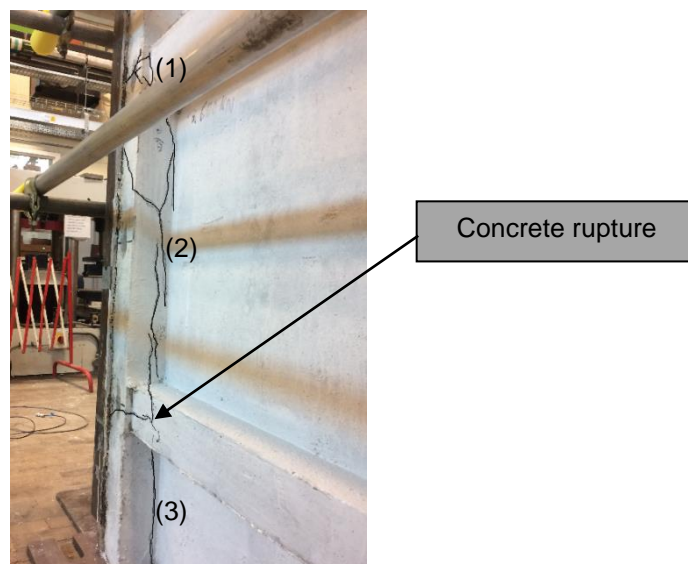
(b): Left side view of the specimen

Figure 5-18: Concrete failure profile of specimen T1-NWC-2

For specimen T1-LWC, the studs on the left side were sheared off with bending near their root, however, the studs on the right side were bent without being sheared off, as depicted in Figure 5-19. The bending length of the shear studs was 10mm.

(a): Bending and shearing off of the shear stud connectors

$l_e=10mm$

| Bending and shearing off of shear stud connectors on the left side | Bending of shear stud connectors on the right side |
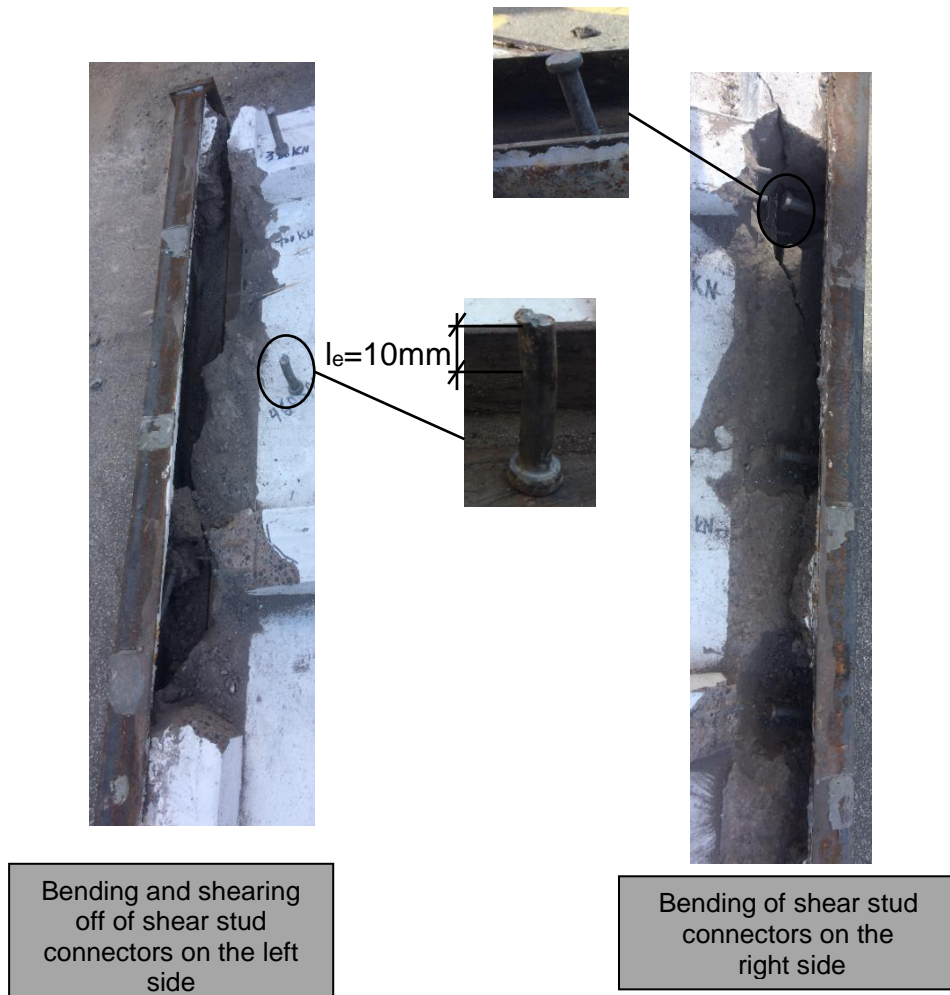
(b): Bending length of the shear connector

Figure 5-19: Shear connectors' failure of T1-LWC specimen

The concrete failure of specimen T1-LWC started with the concrete cracking near the top studs' position, near the position of the ribs in both sides, at a load of 380kN. These cracks continued towards the position of the middle shear stud connectors. Then, the concrete near the bottom studs' position started cracking at a load of 460kN; the concrete failure profile is presented in Figure 5-20. Sudden failure occurred at the end of the test, as the top, middle and bottom studs on the left side were sheared off at a load of 520kN.
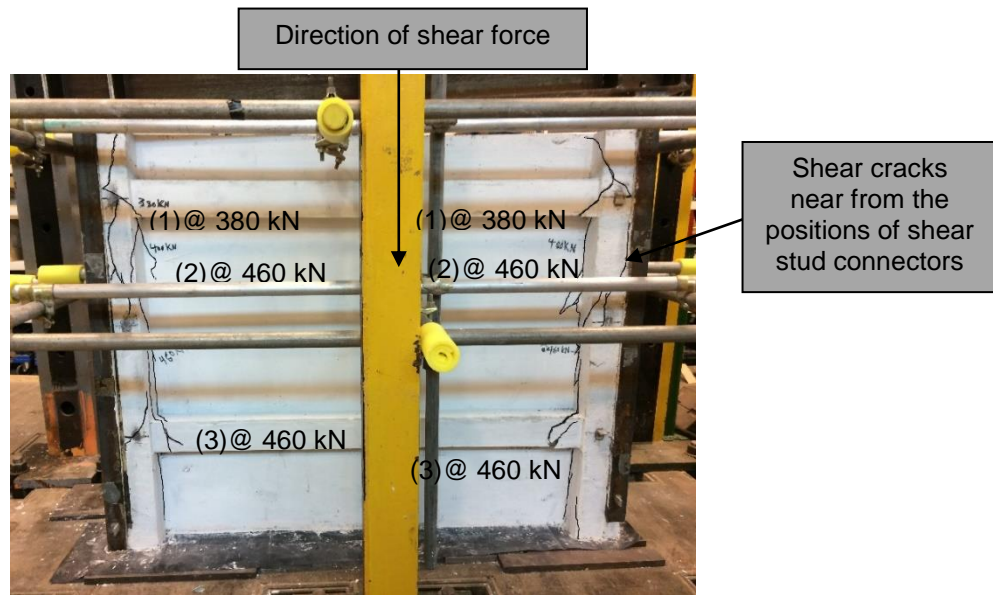
(a): Full specimen view
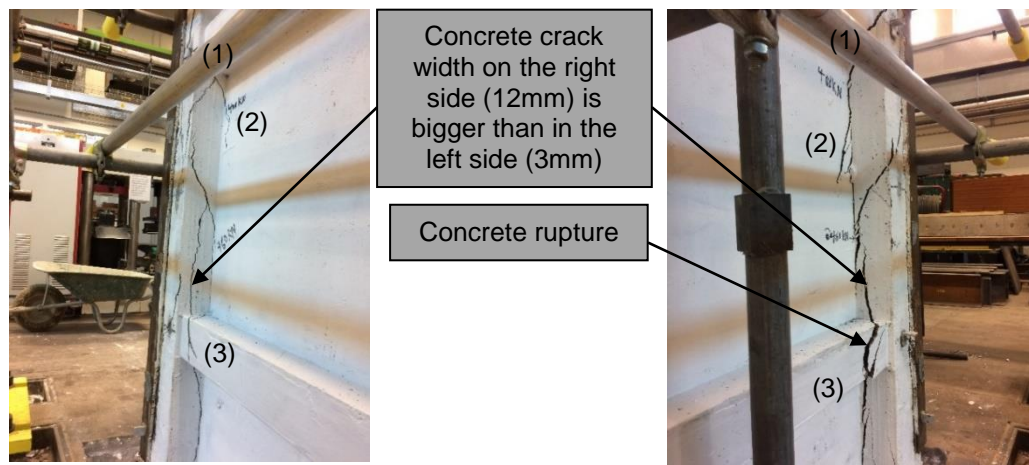
(b): Left and right sides view of the specimen

Figure 5-20: Concrete failure profile of specimen T1-LWC

For specimen T1-ULWC, the studs on the right side were sheared off with minor bending near their root. However, the studs on the left side were bent without being sheared off, as depicted in Figure 5-21. The bending length of the shear studs was 10mm.
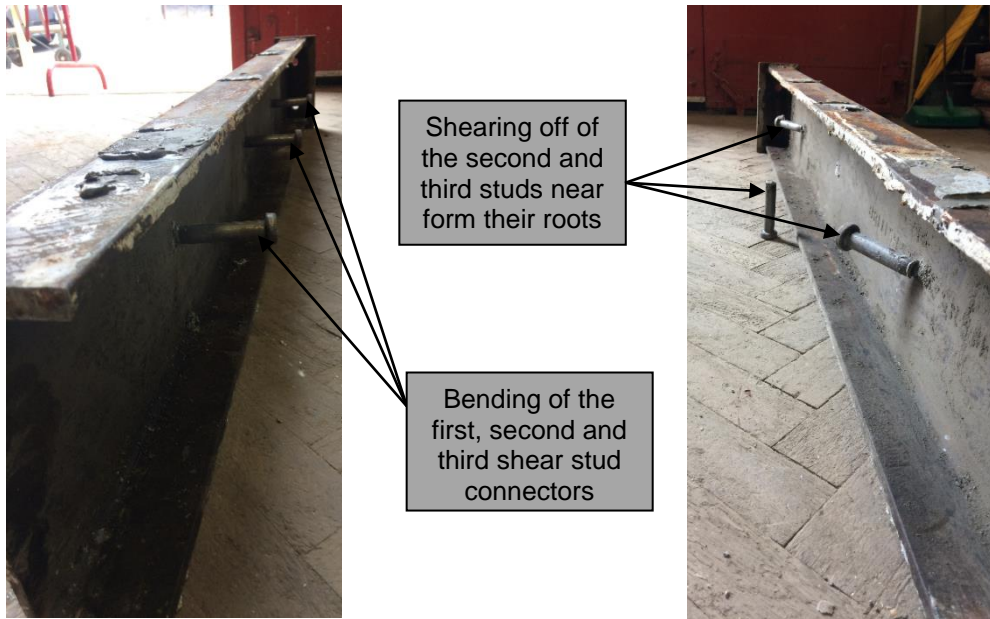
Shearing off of the second and third studs near form their roots

Bending of the first, second and third shear stud connectors

(a): Bending and shearing off of the shear stud connectors

l_e=10mm

(b): Bending length of the shear connector

Figure 5-21: Shear connectors' failure of the T1-ULWC specimen

The concrete failure of specimen T1-ULWC started with concrete cracking near the top studs' position, near the position of the ribs in both sides, at a load of 260kN. These cracks continued towards the position of the middle shear stud connectors at a load of 300kN. Then, the concrete near the bottom studs' position started cracking at a load of 320kN; the concrete failure profile is presented in Figure 5-22. Sudden failure occurred at the end of the test, as the top, middle and bottom studs on the right side were sheared off at a load of 342kN.
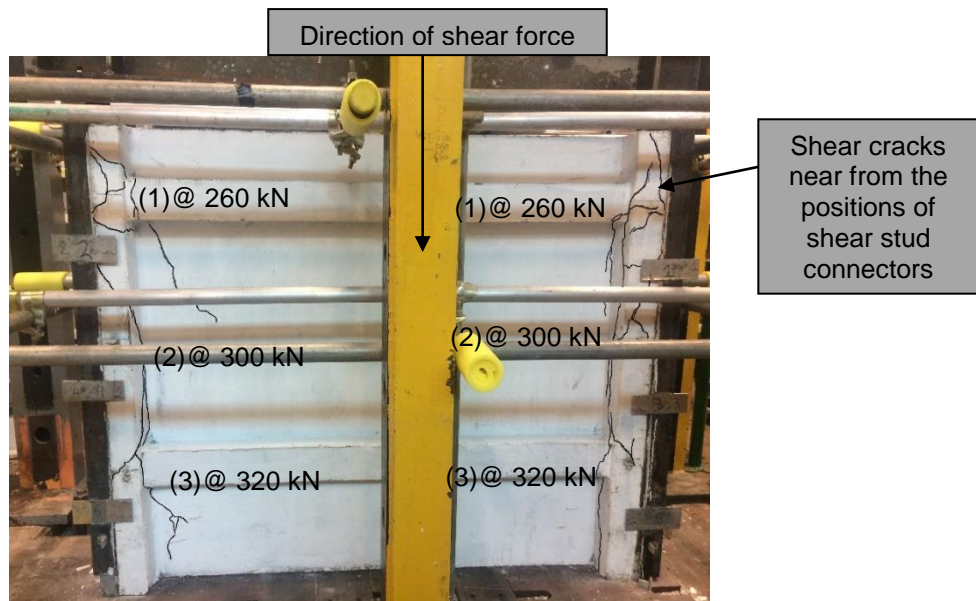
(a): Full specimen view
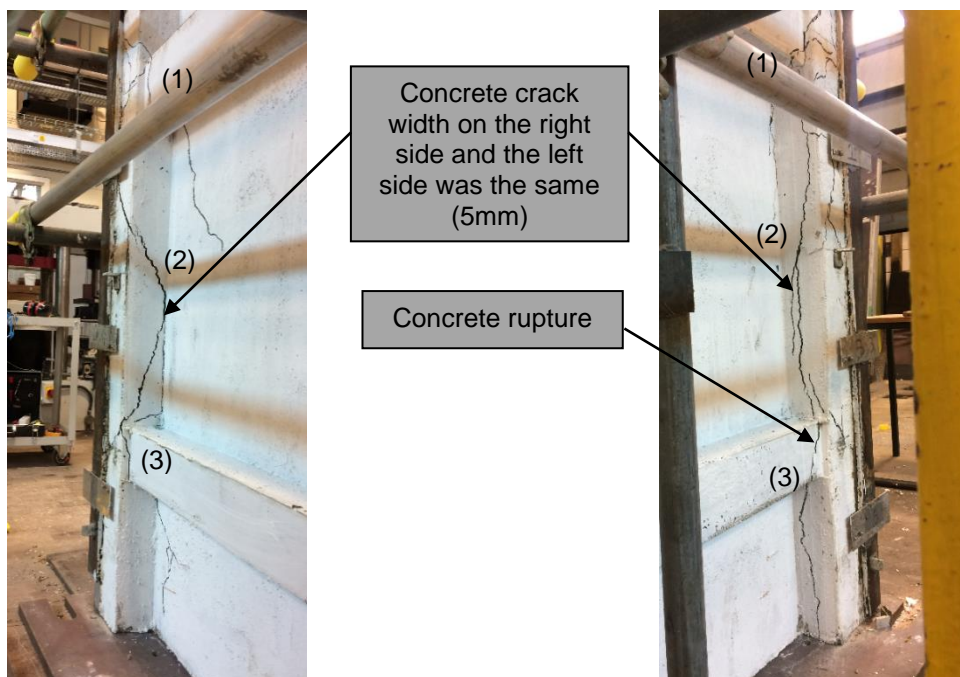
(b): Left and right sides view of the specimen

Figure 5-22: Concrete failure profile of specimen T1-ULWC

5.5.5 Results of test group T2, WWSS with dowels

The shear connection system of test group T2 were formed as the horizontally lying dowels combined with the headed studs in resisting the longitudinal shear force. There were two horizontally lying dowels of Ø20mm and two headed studs of Ø19mm welded on both sides of the steel channels, as shown in Figure 5-5.

Hence, each side of the specimen has three shear connectors. The results of the ultimate load and slip are summarised in Table 5-7. The load-slip and load-separation curves of each specimen are shown in Figures 5-23-5-26. The load of these curves was the load per shear connector.

Large slips were observed in all specimens. The separations of all the specimens were no more than 9mm, which indicated a strong tie resistance of WWSS with dowels.

The results of test group T2 showed that the shear-resisting capacity of the shear connector increased with an increase of concrete strength. The failure load of the specimen with a higher strength of concrete (T2-NWC) was higher than that of the specimens with a lower strength of concrete (T2-LWC-1, T2-LWC-2, and T2-ULWC), respectively. This comparison was based on the same type of shear connectors.

The slips of the WWSS with dowels at the ultimate load were significant, between 13-29mm. This indicated the desired ductility for the shear connectors. The slip stiffness of the WWSS with dowels was different among the three specimens. It is observed that the slip stiffness was influenced by the strengths of the concrete. All specimens demonstrated that the separation started at a load level of the sudden slip increase. The separations at the ultimate loads were 5.07mm for specimen T2-NWC, 3.41mm for specimen T2-LWC-1, 3.62mm for specimen T2-LWC-2 and 8.25mm for specimen T2-ULWC.

Table 5-7: Result summary of the test group T2

Specimen No.	Concrete Type	f_{cu}* (MPa)	f_{ct}~ (MPa)	Ultimate Load (kN)	Slip (mm) at Ultimate Load	Separation (mm) at Ultimate Load
T2-NWC	Normal	37.3	2.45	731.97	13.64	5.07
T2-LWC-1	Lightweight	34.6	2.11	609.90	15.79	3.41
T2-LWC-2	Lightweight	36.8	2.12	621.09	15.47	3.62
T2-ULWC	Ultra Lightweight	20.0	1.38	443.02	28.55	8.25
* cube compressive strength of concrete ~ tensile splitting strength of concrete at the day of the push-out test						

5.5.5.1 Behaviour analysis

The ductile behaviour of the WWSS with dowels was shown by the failure behaviour of the specimens. The shear connectors deformed elastically, which was then followed by plastic deformations. Large slips were induced during the plastic deformations before and after the ultimate loads were reached. The ultimate failure of the shear connectors, as the horizontally lying dowels and the shear stud sheared off, occurred after the load dropped to 85-93% of the maximum loads.

The slip behaviour of the WWSS with dowels was similar to that of the headed studs in the standard push-out tests. The specimens with lightweight concrete (T2-LWC-1, T2-LWC-2 and T2-ULWC) demonstrated additional ductility when compared with the specimen with normal weight concrete (T2-NWC).

Intensive cracks were shown as the ultimate loads were reached. Large sudden destructive failure occurred as the dowel and web welded studs were sheared off on the right side of the specimen.

It was clearly demonstrated by all specimens of the testing group that an interlocking mechanism occurs between the concrete and the shear connectors at ultimate load levels. This mechanism indicated that the failure resistance (or shear strength) of the horizontally lying dowels' shear connectors contributed towards holding the whole system from failure. This indicates that the failure of the horizontally lying dowels shear connectors occurred after the failure of the studs' shear connectors at the end of the test.
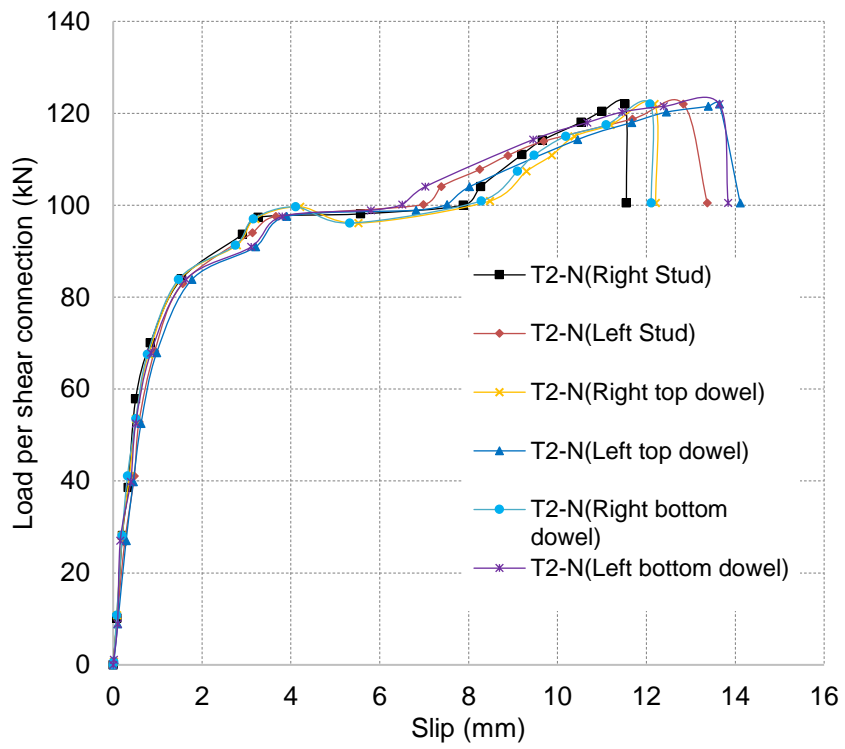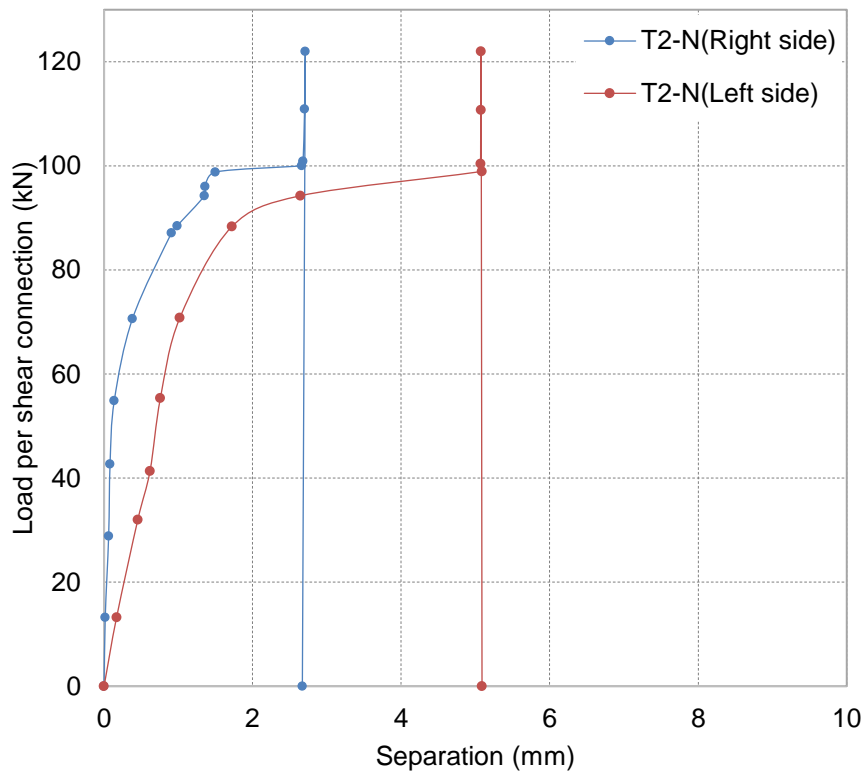
Figure 5-23: (a) Load-slip, (b) load-separation curves of specimen T2-NWC (WWSS with dowels-normal weight concrete)
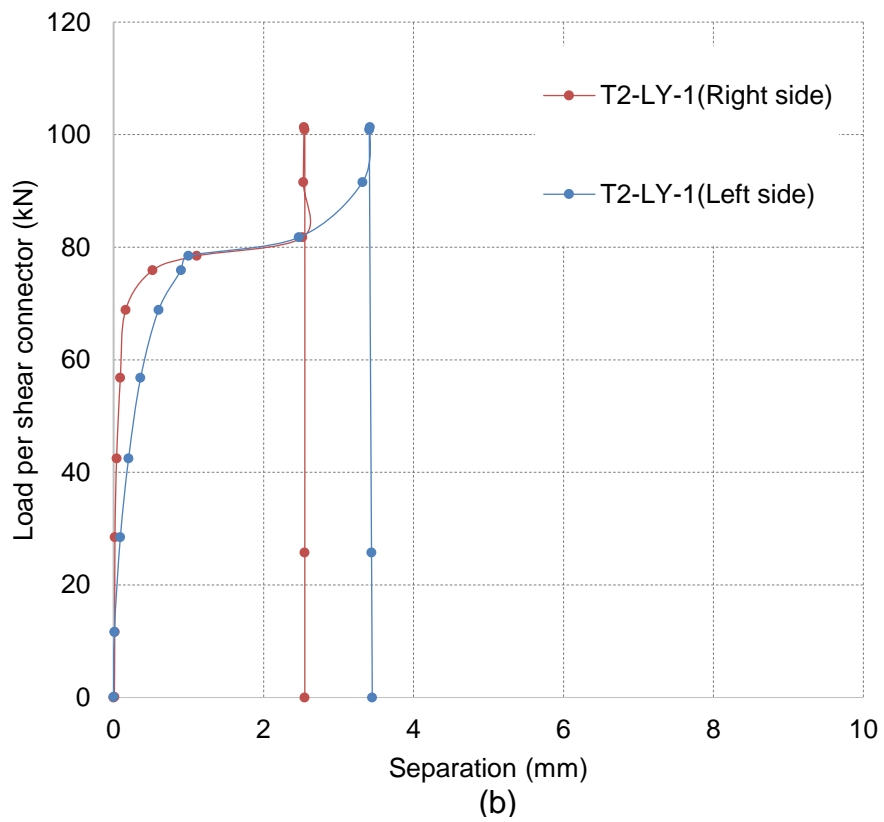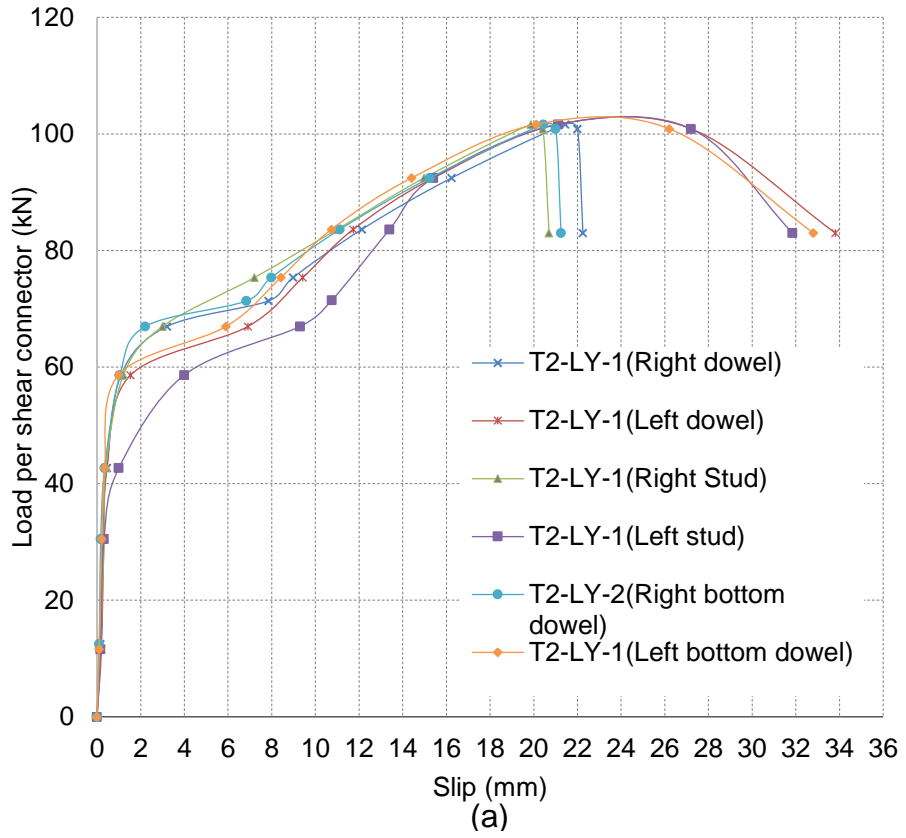
Figure 5-24: (a) Load-slip, (b) load-separation curves of specimen T2-LWC-1
(WWSS with dowels-lightweight concrete)
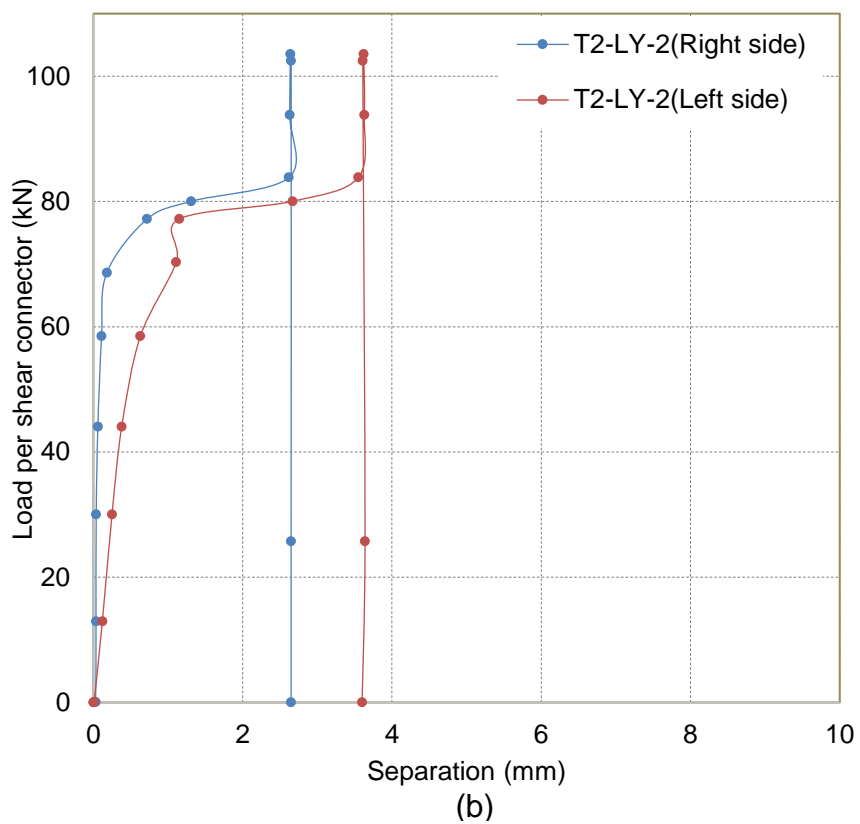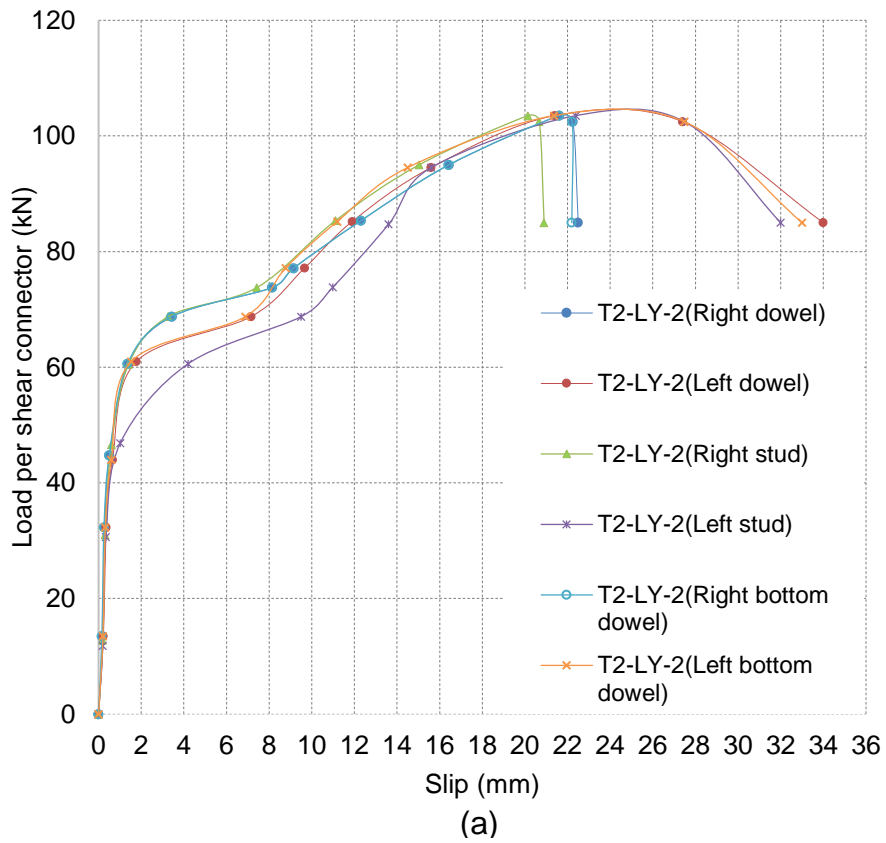
Figure 5-25: (a) Load-slip, (b) load-separation curves of specimen T2-LWC-2 (WWSS with dowels-lightweight concrete)
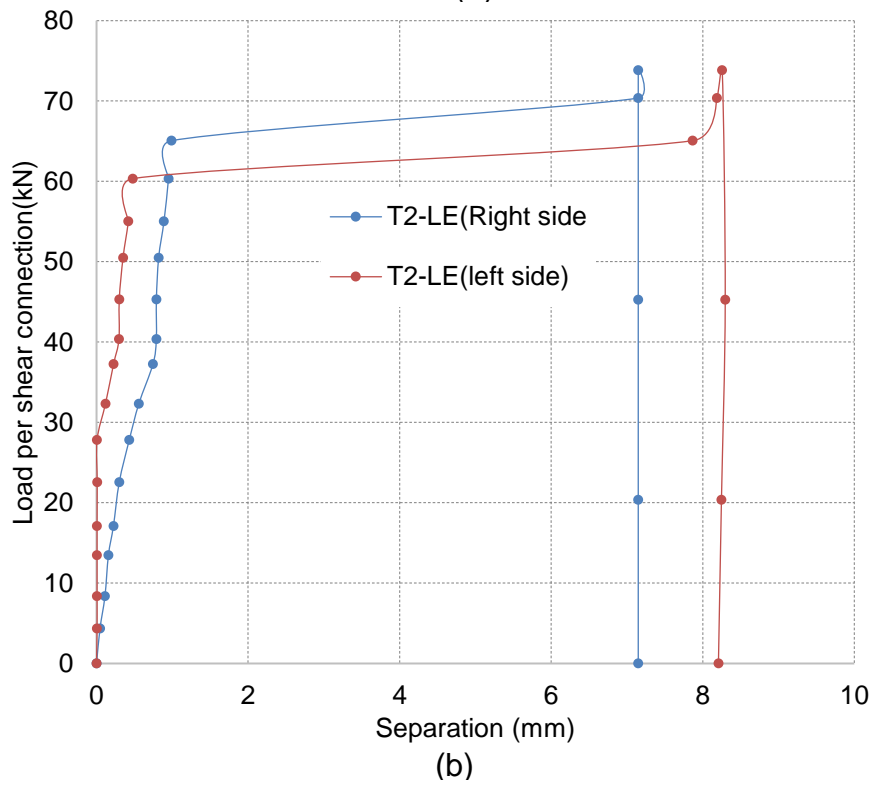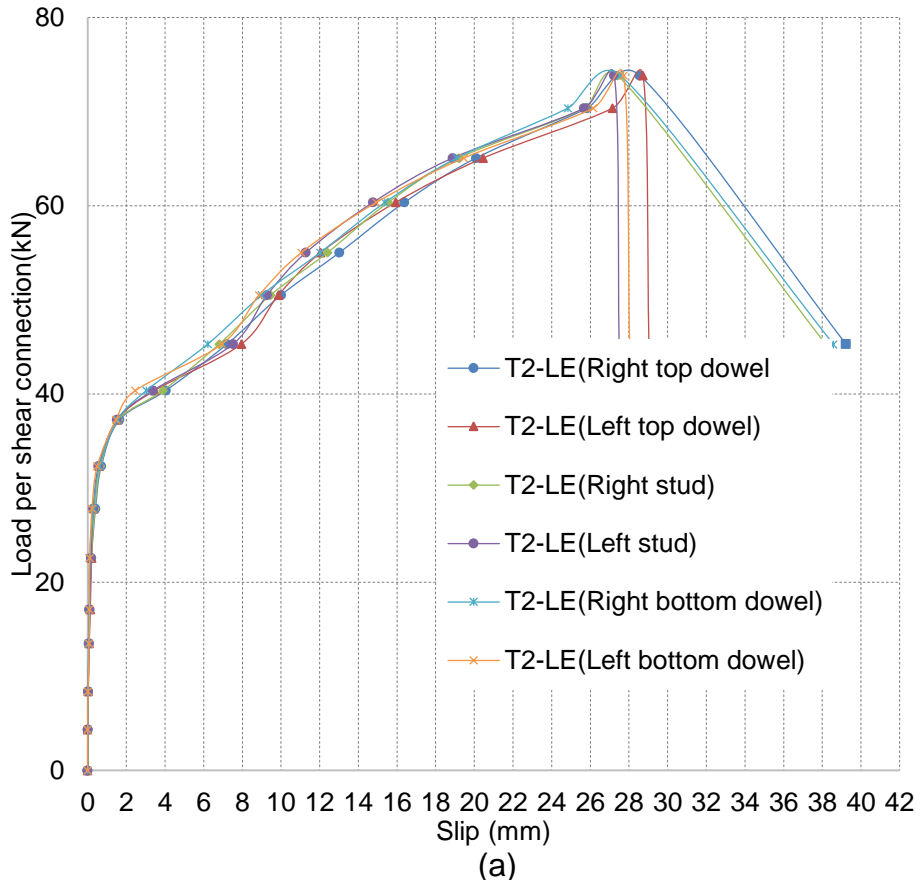
Figure 5-26: (a) Load-slip, (b) load-separation curves of specimen T2-ULWC (WWSS with dowels-lightweight concrete)

5.5.5.2 Failure mechanisms

The second dowel and headed shear stud connectors on the left side of specimen T2-NWC were sheared off with bending near their root, while the welding of the first dowel failed with bending in the dowel, as depicted in Figure 5-27. However, the horizontally lying dowels on the right side of the specimen were only bent, without being sheared off. This was due to the distribution of stresses over the slab width, which results in the concentration of the stresses on the left side of the specimen, more than on the right side of the specimen. The bending length of the horizontally lying dowels and the stud was 80mm.
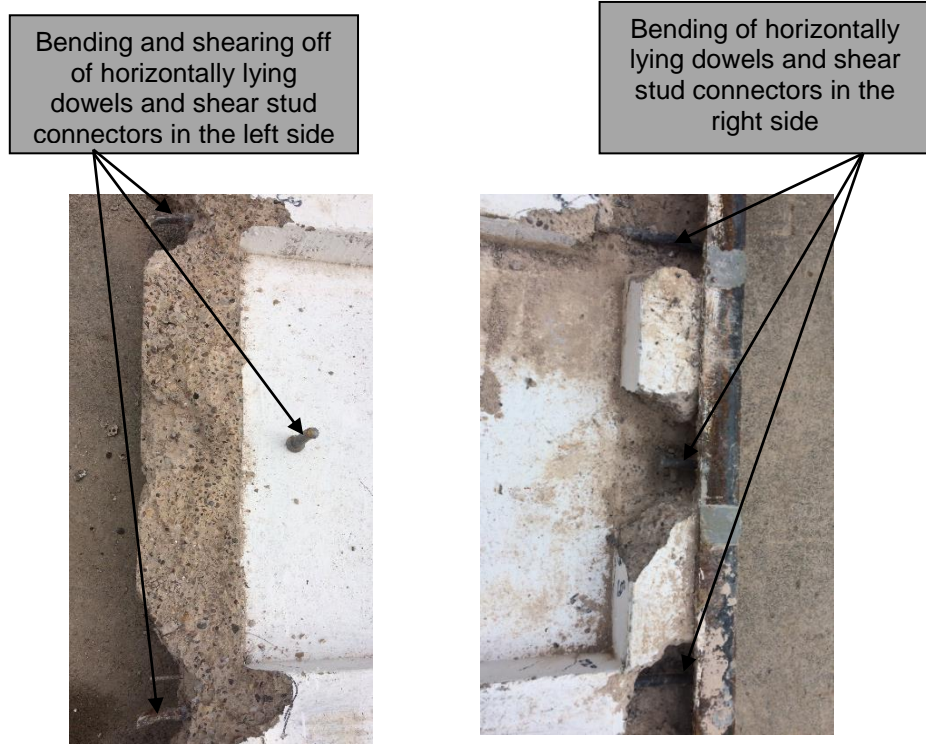
(a): Bending and shearing off of the shear connectors
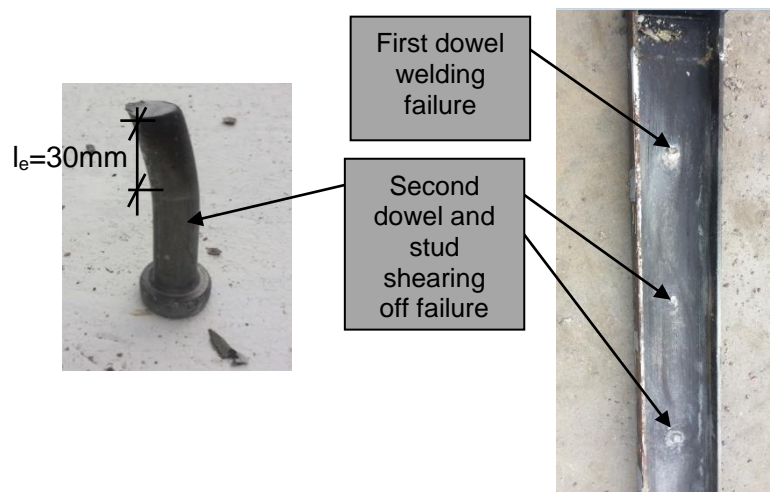
(b): Bending length of the shear connector

Figure 5-27: Shear connectors' failure of the T2-NWC specimen

The concrete failure of specimen T2-NWC started from top horizontally lying dowels' position, near the position of the ribs in both sides, at a load of 600kN. These cracks continued towards the position of the shear stud connectors in the middle of the specimen at a load of 620kN. Then, the concrete near the bottom horizontally lying dowels' position showed cracking at a load of 640kN; the concrete failure profile is shown in Figure 5-28. The cracking noise was initially heard at the end of the elastic deformations. Then, it intensified during the plastic deformations. Sudden failure occurred at the end of the test, as the top, bottom horizontally lying dowels and stud on the left side were sheared off at a load of 732kN.
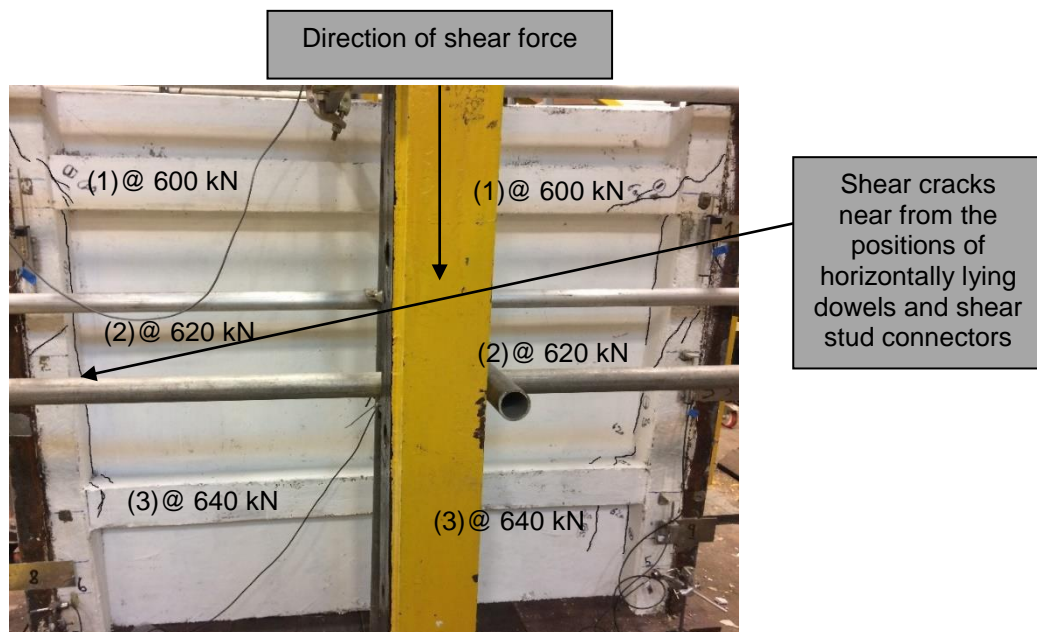
Figure 5-28: Concrete failure profile of specimen T2-NWC

For specimen T2-LWC-1, the welding of the horizontally lying dowels on the right side failed, with horizontally lying dowels' bending near their root, however, the welding of the stud failed without bending the stud, as depicted in Figure 5-29. The bending length of the horizontally lying dowels and the stud was 40mm, which is half of the bending length of the horizontally lying dowels and stud of specimen T2-NWC.
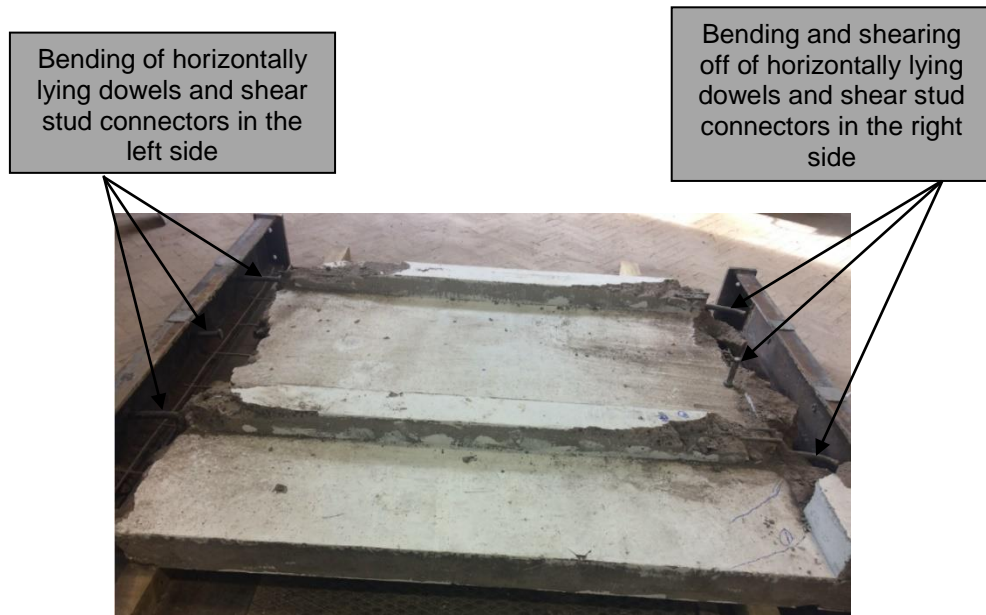
(a): Bending and shearing off of the shear connectors
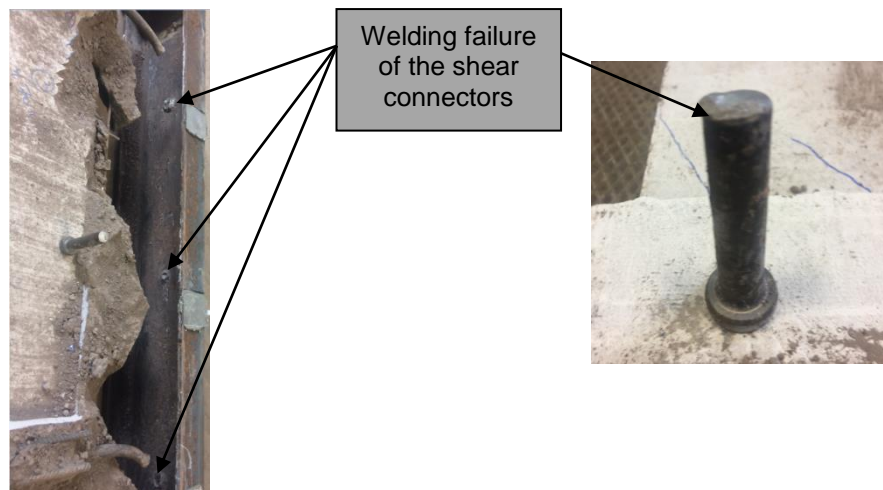
(b): Welding failure of the shear connector

Figure 5-29: Shear connectors' failure of T2-LWC-1 specimen

The concrete failure began with concrete cracking near the top horizontally lying dowels' position, where the position of the ribs in both sides, at a load of 370kN. These cracks continued towards the position of the shear stud connectors at a load of 420kN. Then, the concrete near the bottom horizontally lying dowels' position started cracking at a load of 560kN; the concrete failure profile is presented in Figure 5-30. Sudden failure occurred at the end of the test, as the top, bottom horizontally lying dowels and stud on the right side were sheared off at a load of 609.90kN.
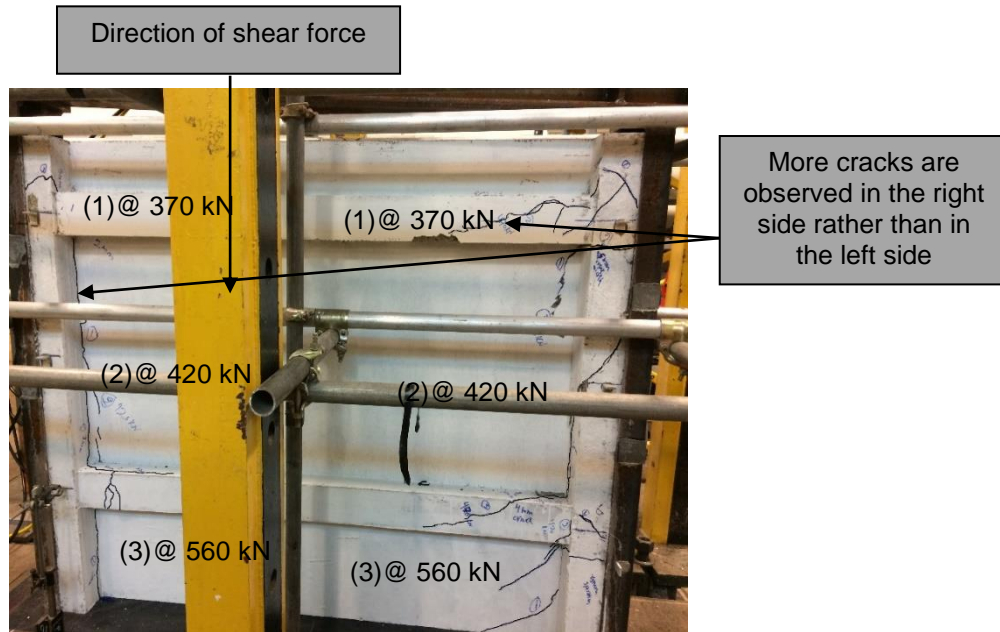
(a): Full specimen view
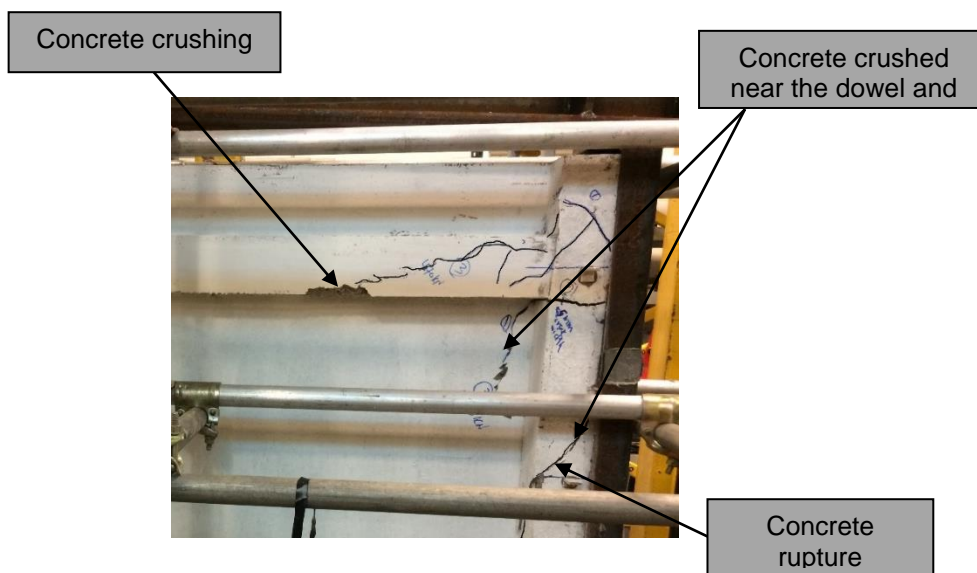
(b): Right sides view of the specimen

Figure 5-30: Concrete failure profile of specimen T2-LWC-1

For specimen T2-LWC-2, the first dowel on the left side was sheared off with the dowel bending near its root; the welding of the second dowel failed, with the dowel bending near its root, where the stud punched the web through without bending, as depicted in Figure 5-31. The bending length of the horizontally lying dowels and the stud was 40mm, which is half of the bending length of the horizontally lying dowels and stud of specimen T2-NWC.

Bending of horizontally lying dowels and shear stud connections in the right side

Bending and shearing off of horizontally lying dowels and shear stud connections in the left side

(a): Bending and shearing off of the shear connectors

Shearing off failure of the first dowel

Stud is punching the web through

Welding failure of second dowel

(b): Welding failure of the shear connector
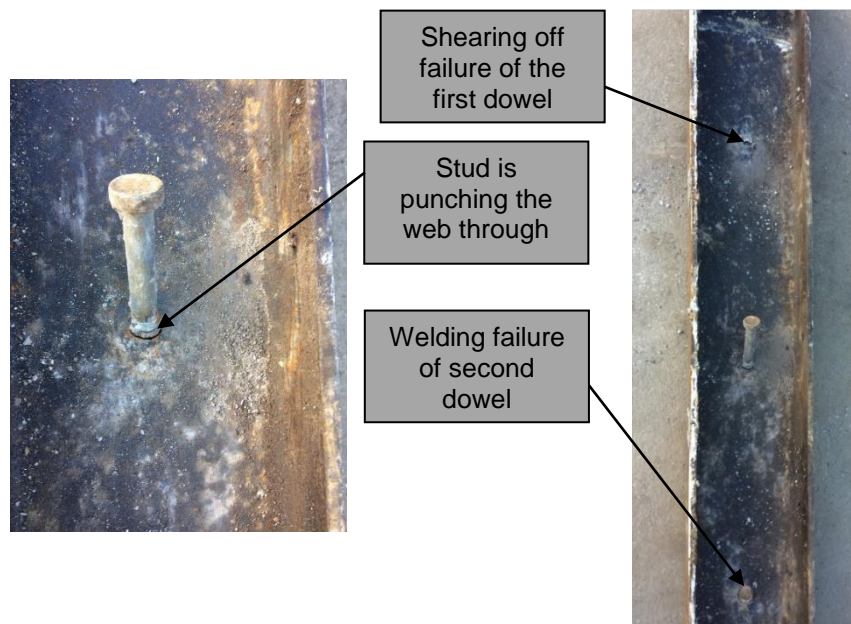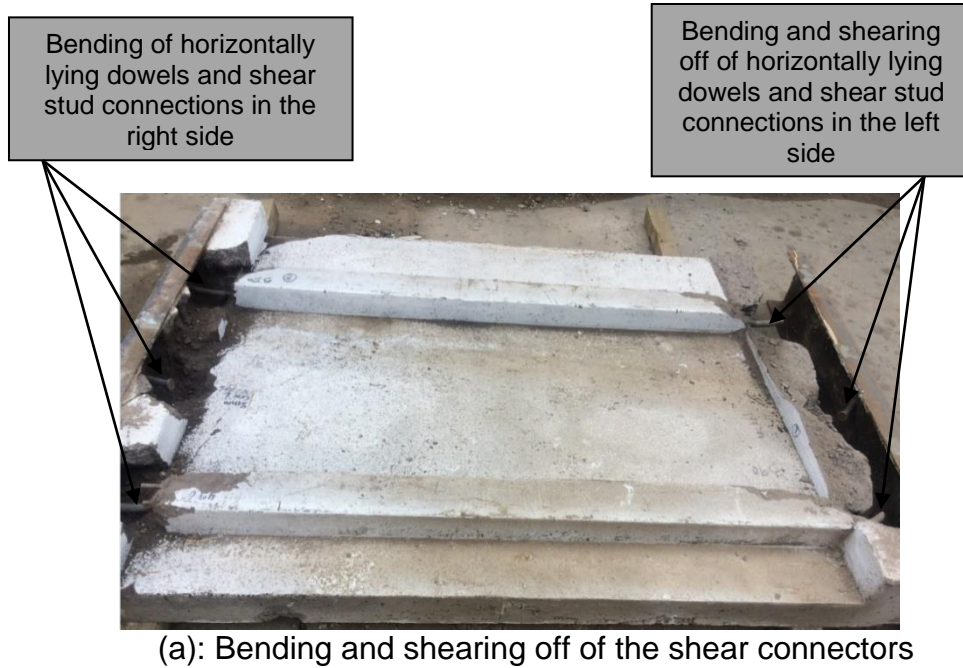
Figure 5-31: Shear connectors' failure of T2-LWC-2 specimen

The concrete failure of specimen T2-LWC-2 started with cracks near the top horizontally lying dowels' position, where the position of the ribs in both sides, at a load of 390kN. These cracks continued towards the position of the shear stud connectors at a load of 440kN. Then, the concrete near from the bottom horizontally lying dowels' position started cracking at a load of 580kN. Sudden failure occurred at the end of the test, as the top, bottom horizontally lying dowels

and stud on the right side were sheared off at a load of 621kN, as shown in Figure 5-32.
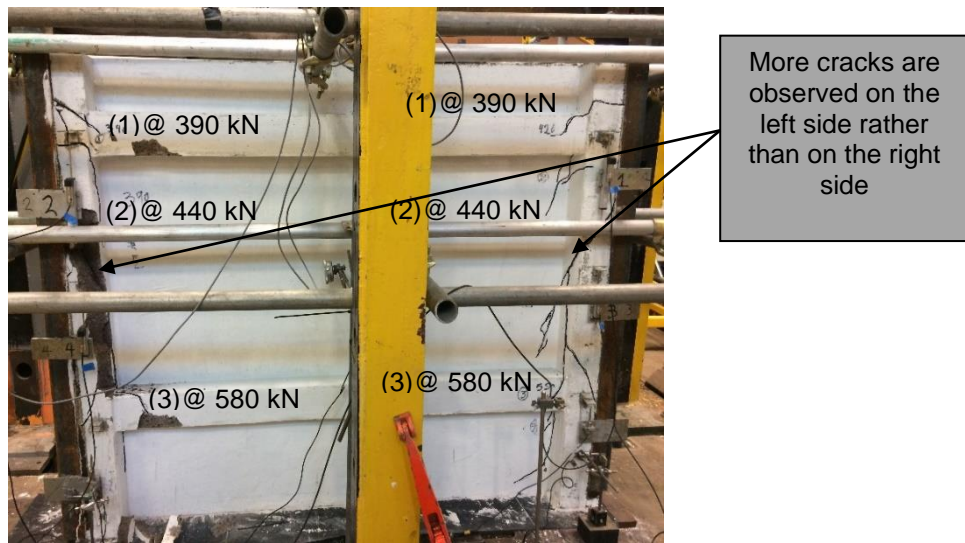
(a): Full specimen view
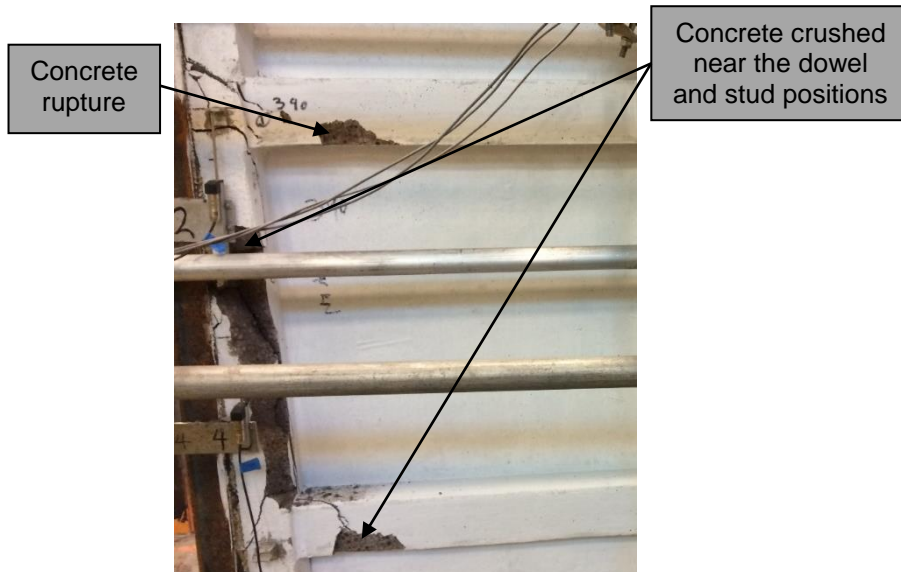
(b): Left side view of the specimen

Figure 5-32: Concrete failure profile of T2-LWC-2 specimen

The failure of specimen T2-ULWC started with shearing off the first dowel on the right side with bending near its root; the welding of the second dowel failed with bending where the position of its root and the stud was sheared off with a small amount of bending - no more than 10mm near its root, as depicted in Figure 5-33. The bending length of the horizontally lying dowels and stud was 40mm, which is half the bending length of the horizontally lying dowels and stud of specimen T2-NWC.

(a): Bending and shearing off of the shear connectors
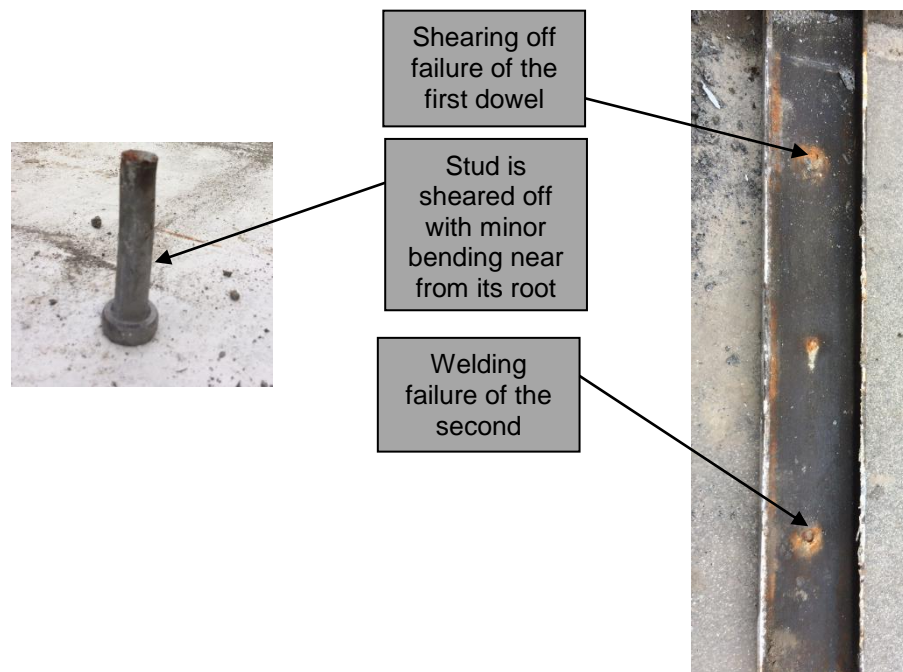
(b): Welding failure of the shear connector

Figure 5-33: Shear connectors' failure of T2-ULWC specimen

The concrete failure of specimen T2-ULWC started with cracks near the top horizontally lying dowels' position, where the position of the ribs in both sides, at a load of 261kN. These cracks continued towards the position of the shear stud connectors in the middle of the specimen at a load of 300kN. Then, concrete cracks appeared near the bottom horizontally lying dowels' position at a load of 360kN. Sudden failure occurred at the end of the test, as the top, bottom

horizontally lying dowels and stud on the right side were sheared off at a load of 443kN, as shown in Figure 5-34.
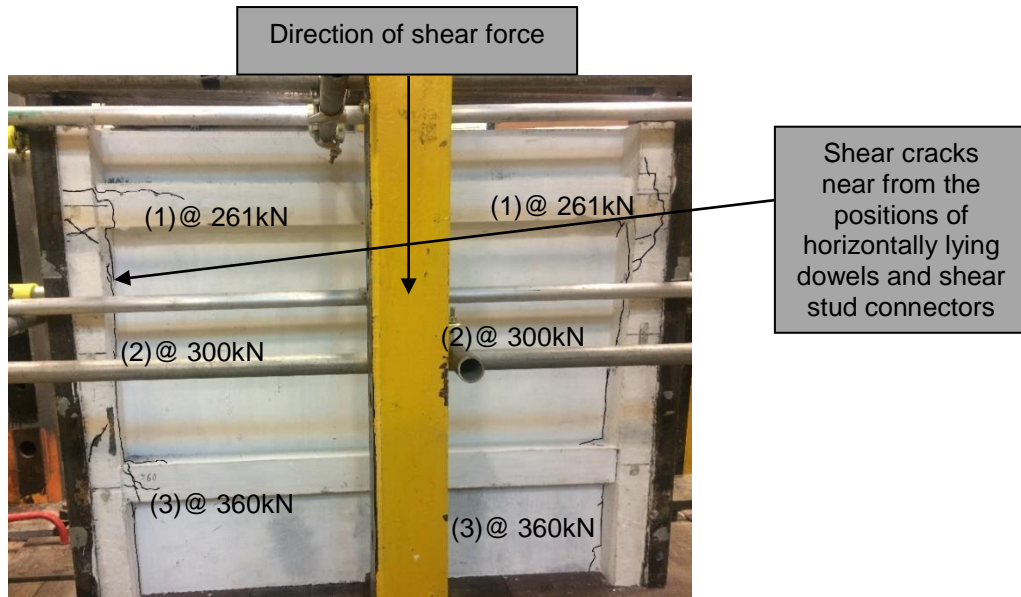
(a): Full specimen view
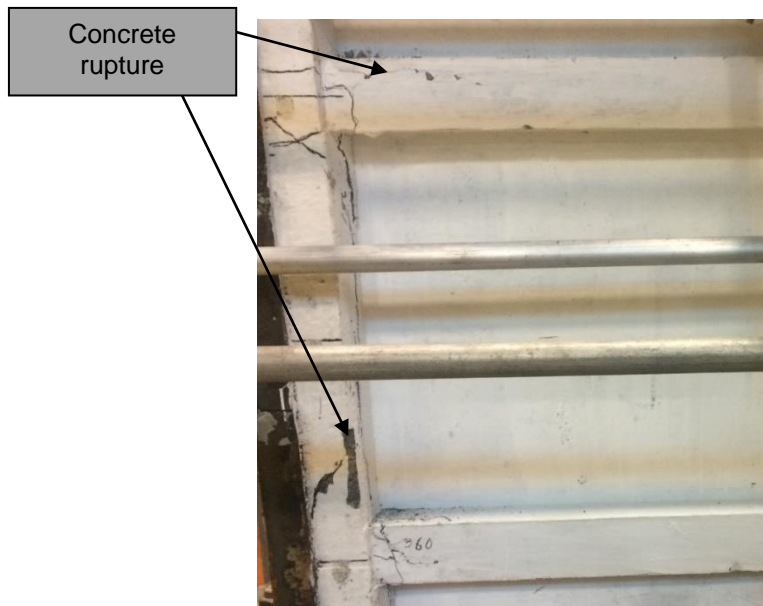
(b): Left side view of the specimen

Figure 5-34: Concrete failure profile of T2-ULWC specimen

5.5.6 Effect of connector type

Figure 5-35 shows the effect of the connector type on the maximum applied load. It can be observed that changing the type of the shear connector from WWSS to a combination of WWSS with dowels leads to a higher capacity. This is because the larger diameter of the dowel has a larger cross-sectional area and thus a larger bearing area of the concrete as it passes from one side to the other side of

the flooring system tying it all together, which in turn increases the maximum shear resistance of the connection system.

However, the maximum capacity load of the shear connector is also influenced by the yield strength of the steel connectors and the mechanical properties of the concrete used. If the diameter of the connector is large (> 12mm), the maximum resistance of the shear connector depends on the strength of the concrete materials. However, when the diameter of the shear connector is small (< 10mm), the failure is controlled by shank shear and not affected much by the strength and type of concrete (Yan et al., 2016).
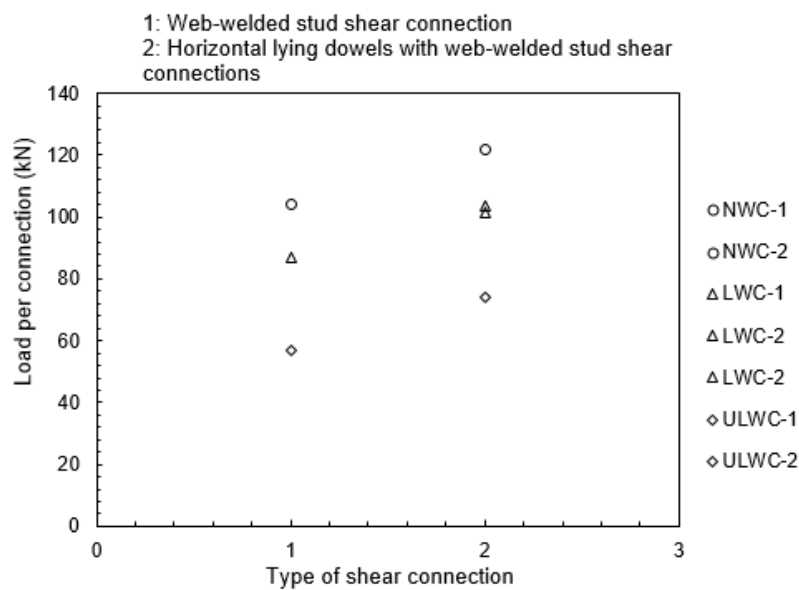
Figure 5-35: : Effect of type of shear connector on shear resistance of the shear connection system

5.5.7 Effect of concrete type

Figure 5-36 shows the influence of the concrete type on the maximum shear strength of both connection systems. The shear strength of the connector is defined as the ratio of the maximum applied (capacity) load to the number of shear connectors per specimen.

It is apparent that the maximum applied load increased by 15% when NWC was used in comparison with the LWC of a similar compression strength (see Tables 5-4 & 5-5). Subsequently, the maximum applied load increased by 14% when LWC was used in comparison with the ULWC of a similar compression strength.

(a) WWSS   (b) WWSS with dowels
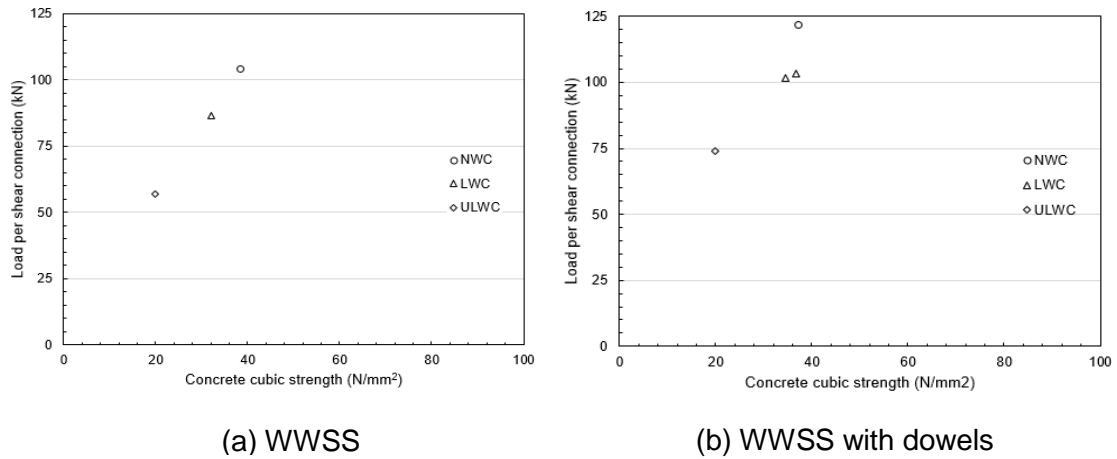
Figure 5-36: Effect of concrete type on shear resistance of the shear connection system

5.6 Summary

The results of the push-out tests were evaluated according to Eurocode 4 (EN1994-1-1, 2004). A particular emphasis was given to the slip behaviours and failure mechanisms of the shear connectors with the aim of optimising and improving the design details of the prefabricated ultra shallow flooring system. The shear resistance of the shear connection systems were analysed in **Chapter 7** to develop the design method for calculating the shear resistance of the shear connection systems.

This chapter has presented the experimental results of the push-out test series with two types of shear connection systems (WWSS and WWSS with dowels) used for prefabricated ultra shallow flooring systems. The following conclusions were made.

- Three types of failure were observed from the push-out tests: (a) shear failure with bending near the roots of the connectors, (b) shear failure of the weld toe of shear studs, and (c) concrete cracking. Brittle weld failure should be avoided by ensuring the quality of the welding during the installation of the connectors.

- The concrete strength, f_{ck}, influences the failure modes. The shear resistance of each connection system increased with increases of the concrete strength.

- The larger diameter of dowels (up to 20mm in the present study) increases the shear interaction area, as well as the concrete bearing area, thus enhancing its shear resistance.

- The horizontally lying steel dowels, together with the WWSS, increases the shear resistance and the slip capacity of the shear connector.

- The connection system with the WWSS demonstrated the ductile failure mode of the entire slab system under direct longitudinal shear force, with slip capacities ranging between 2mm and 30mm for different concrete strengths.

- The connection system with the horizontal lying steel dowels, together with the WWSS demonstrated the more ductile failure mode of the entire slab system under direct longitudinal shear force in comparison with the system having studs only, with slip capacities ranging between 13mm and 29mm for different concrete strengths.

- An interlocking mechanism was found at ultimate loads between the concrete and the shear connectors of the specimens in group T2. This mechanism demonstrates the strong tie-resistance of the steel dowels, since very little separation in the transverse direction was observed when compared with the large separation of the specimens in group T1 (shear studs only).

Chapter 6 : Finite Element Analysis

6.1 Introduction

The finite element method (FEM) is used firstly to replicate the experimental behaviour and consequently investigate further the structural performance of the prefabricated ultra shallow flooring system through the undertaking of the parametric study. This chapter describes the development of a 3-D finite element model capable of simulating the push-out test of the prefabricated ultra shallow flooring system when subjected to the direct longitudinal shear slip. The model is developed using the finite element software ABAQUS 6.14. The 3-D finite element model is validated with experimental results described in **Chapter 5**. It is proved to be able to simulate the overall behaviour of the prefabricated ultra shallow flooring system. Therefore, a parametric study is carried out in this chapter using the model which is properly calibrated to investigate other parameters such as different diameters and heights of the shear connection systems, along with different concrete strengths.

6.2 ABAQUS – Selection of modelling tool

ABAQUS is a general purpose finite element analysis (FEA) program for the use of modelling structural responses. Stress problems can be divided into two types, static and dynamic response, depending on whether the inertial effects are significant. It permits the same analysis to be used for both the static and dynamic problems. The program is designed for ease of use on complex problems, and has a simple input language, along with comprehensive data checking, in addition to a wide range of pre-processing and post-processing output display options. Therefore, it is used to implement numerical analysis for the design and behaviour of the prefabricated ultra shallow flooring system subjected to longitudinal shear slip. ABAQUS modules consist of ABAQUS/Standard, ABAQUS/Explicit and ABAQUS/CAE.

ABAQUS has a wide range of element types, for example, continuum elements, which comprise one-dimensional, two-dimensional and three-dimensional beams, membrane and shell elements. The element compositions in ABAQUS are suitable for representing large displacements, rotations and strains. The material models can be used for metals, concrete, sand, clay, jointed rock,

plastics and rubber. ABAQUS/Standard is employed in this study, as it is an ideal solution technology for static even where highly accurate stress solutions are critically important, such as the push-out test series.

6.3 Modelling procedure

ABAQUS/CAE offers a wide range of input options for modelling, such as geometry, material properties, element types, loads, solution controls, graphic user interfaces, automatic meshing, boundary conditions, contact and post processing controls.

The procedure in ABAQUS can be divided into four major steps:

- Step 1 - Geometry and material modelling
- Step 2 - Boundary and constraint conditions
- Step 3 - Output analysis
- Step 4 - Post-processing of the results

Figure 6-1 illustrates the modelling procedure of ABAQUS for the current study. Step 1 comprises the part, material property, assembly and mesh fields of the procedure.

- The part field comprises the concrete slab, shear connection systems, structural steel beam, reinforcing steel and base block.
- The material property field comprises the input of the nonlinear material stress-strain curves of each component in the part field.
- The mesh field consists of the meshing of the components using different element types and is assigned the number of mesh required for the analysis.

Step 2 provides the constraints, contacts and surface interaction model used in ABAQUS. Load and boundary conditions are also allocated in this step.

Step 3 defines how to start the analysis and obtain the output from ABAQUS after the analysis process, such as the stress distribution of the steel-concrete composite push-out test, ultimate shear resistance and slips. A step field is provided in this stage to input the load case, the time period of the step, and time increment of the analysis.

Step 4 processes the model results into figures and tables for validation and comparison with the test results.
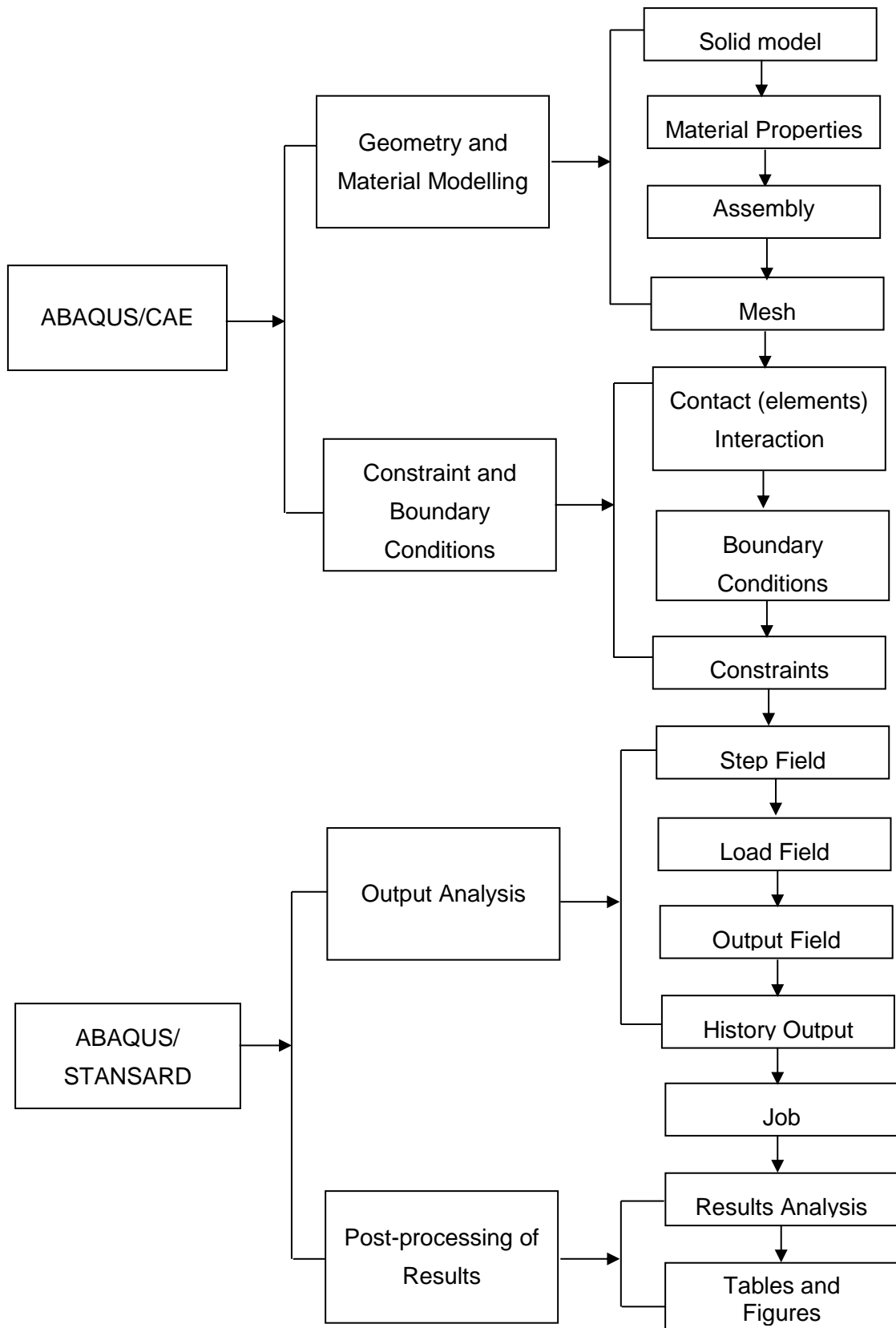
Figure 6-1: Abaqus modelling procedure

6.4 Material constitutive relationships

The material constitutive laws are used to define the stress-strain characteristics of each material used in ABAQUS. The accuracy of the analysis is dependent on the constitutive laws used to define the mechanical properties of the components. The aim of this section is to develop a reliable understanding of the mechanical properties for developing finite element steel-concrete composite models that can accurately predict their behaviour, along with ultimate shear resistance, when they are subjected to longitudinal shear slip. The main elements affecting the behaviour of steel-concrete composite push-out specimens are the concrete slab, steel beam, shear connection systems and reinforcing bars. These elements should be carefully modelled to obtain accurate results from the finite element analysis.

6.4.1 Concrete

One of the main elements of the steel-concrete composite push-out specimens is the concrete slab. The material properties of the concrete can be obtained from concrete cylinder compression and splitting tests (BS 1881-116:1983). Nevertheless, only the average concrete compressive and tensile strengths can be determined from the two tests. Consequently, in order to input the full stress-strain property of the concrete into ABAQUS, a concrete property model is required.

6.4.1.1 Concrete smeared cracking

There are two main options in ABAQUS for concrete plasticity models. Karlsson and Sorensen (2006a) illustrated that these plasticity models are appropriate to model the inelastic behaviour of concrete. Most of these models are incremental, where the total strain is separated into two parts: elastic and plastic. The solution in ABAQUS to model the nonlinear problems is to apply the loading in steps, where the load in each step is being divided into increments. Using the Newton-Raphson method, the response of the structure to a load increment is solved by iteration.

The concrete smeared cracking model has been used firstly to model the concrete's behaviour. This model does not track the individual macro cracks. Rather, constitutive calculations are made independently at each interaction of the FEA model to consider the presence of cracks by the way in which the cracks

affect the stress and material stiffness associated with the integration point. An isotropically hardened yield surface is active when the stress is dominantly compressive and an independent crack detection surface is used to determine if a point fails by cracking. The failure surface is a linear relationship between the equivalent pressure stress and the Von Mises equivalent deviatoric stress. Once a crack forms, crack orientation is stored for subsequent calculations; subsequent cracking at the same point is orthogonal to this direction. No more than three cracks can occur at any point. The failure ratios option in ABAQUS can be used to define the shape of the biaxial failure surface by specifying four ratios for ultimate stress and strain values of biaxial and uniaxial stress states.

6.4.1.2 Concrete damaged plasticity

The concrete damaged plasticity model is used in the current study over the concrete smeared cracking model because it is better at representing the inelastic behaviour of concrete. The concrete damaged plasticity model uses isotropic damaged elasticity in combination with isotropic tensile and compressive plasticity. This option in ABAQUS is used to define yield function, flow potential and viscosity parameters.

Lubliner et al. (1989) suggested that using the concrete model uses the yield function with the modifications proposed by Lee and Fenves (1998) to consider different progressions of strength characteristics under tension and compression. The evolution of the yield surface is defined by hardening variables, known as equivalent tensile and compressive plastic strains. The equivalent tensile and compressive plastic strains can be automatically calculated by ABAQUS after the definitions of elastic material behaviour. The tensile and compressive stress-strain behaviour outside the elastic range uses concrete tension stiffening and concrete compression hardening options respectively. The tensile and compressive damage uses the concrete tension damage and concrete compression damage options, respectively.

This concrete model follows the non-associated plasticity flow rule, using the Drucker-Prager hyperbolic function for the flow potential. In the concrete damaged plasticity model, the plastic potential function and the yield surface do not coincide with each other. Concrete can show a significant volume change, commonly referred to as dilation, when subjected to severe inelastic stress states.

This dilation can be represented by the appropriate plastic potential function. Conversely, the yield surface can be defined by the hardening rule. In this study, the dilation angle is taken as 38°. The material dilation angle (ψ) and eccentricity (ε) were taken as 38, and 0.1, respectively. The ratio of biaxial compressive strength to uniaxial compressive strength (f_{b0}/f_{c0}) is taken as 1.16.

6.4.1.3 Normal concrete

The compression behaviour of the normal concrete is presented by an equivalent uniaxial stress-strain behaviour curve, as shown in Figure 6-2, which is determined from Eq. 6.1 Eurocode 2 (EN 1992-1-1, 2004).

$$\frac{\sigma_c}{f_{cm}} = \left(\frac{k\eta - \eta^2}{1 + (k-2)\eta}\right)$$

(6.1)

Where:

σ_c : is the compressive stress of the normal concrete,

f_{cm}: is the characteristic compressive cylinder strength of normal concrete,

$f_{cm} = f_{ck} + 8$

$\eta = \frac{\varepsilon_c}{\varepsilon_{c1}}$

ε_{c1}: is the compressive strain of the normal concrete at the peak stress f_c,

$\varepsilon_{c1} = 0.7 f_{cm}^{0.31} \leq 2.8$

$k = \frac{1.05 E_{cm} \times |\varepsilon_{c1}|}{f_{cm}}$

$E_{cm} = 22 \times (\frac{f_{cm}}{10})^{0.3}$

The expression 6.1 is valid for $0 < |\varepsilon_c| < |\varepsilon_{cu1}|$ where ε_{cu1} is the nominal ultimate strain. The nominal ultimate strain, ε_{cu1} for concrete characteristic compressive cylinder strength of 12–50 MPa can be taken as 0.0035 Eurocode 2 (EN 1992-1-1, 2004). For a characteristic compressive strength greater than 50MPa, the ultimate compressive strain can be calculated from the following expression.

$$\varepsilon_{cu1} = 2.8 + 27 \left[\frac{(98 - f_{cm})}{100}\right]^4$$

(6.2)
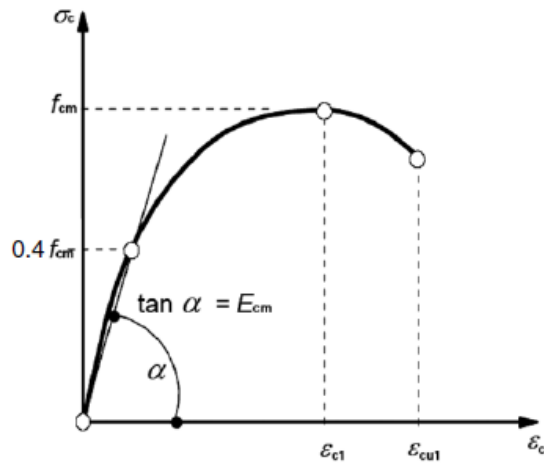
Figure 6-2: Schematic of the stress–strain relation for
concrete material Eurocode 2 (EN 1992-1-1, 2004)

Stiffness degradation on account of crushing the concrete is assumed to be zero. Consequently, no compression damage data is specified in the input. According to the ABAQUS manual, in the absence of compression damage, the plastic strain of concrete can be taken as equal to the inelastic strain. The uniaxial stress-plastic strain curve for the push test specimen, with a mean compressive cylinder strength, f_{cm} of 38.8MPa, is shown in Figure 6-3.
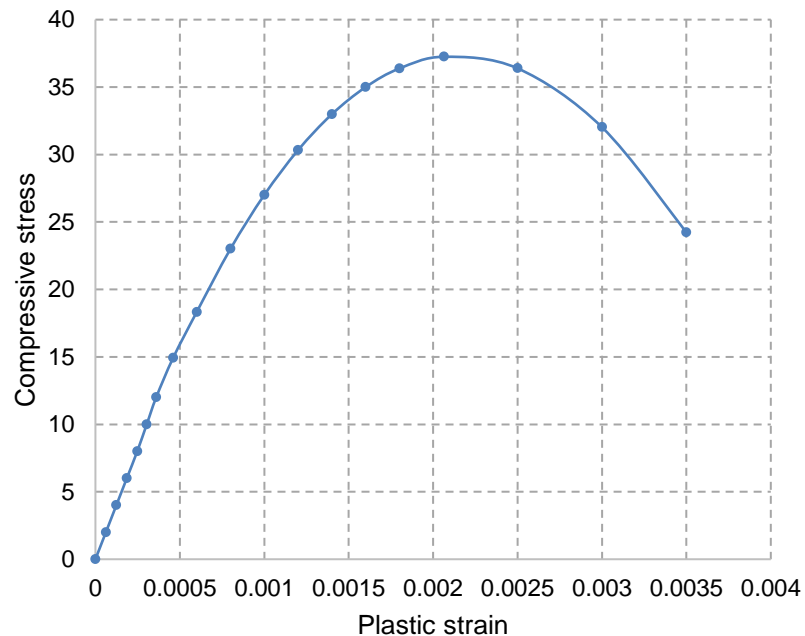
Figure 6-3: Stress-strain curve in compression for normal
concrete material

For concrete in tension, the tensile stress is assumed to increase linearly with respect to strain, until the concrete crack occurs. After the crack, the tensile stress

decreases to zero with the tension stiffening effect. Tension stiffening can be defined by means of a post-failure stress-strain relationship, or by applying a fracture energy cracking criterion. As mentioned in the ABAQUS manual (Karlsson and Sorensen, 2006a), in cases with little or no reinforcement, the stress-strain tension stiffening approach often causes mesh-sensitive results.

Consequently, the fracture energy cracking criterion is used in this study. In this approach, the brittle behaviour of concrete is represented by a stress-displacement response, rather than a stress-strain response. Different methods can be used to define the brittle behaviour of concrete using the fracture energy concept. The most appropriate approach is to define tensile cracking using a linear approximation, in which the linear loss of strength takes place after cracking, as presented in Figure 6-4(a). The brittle behaviour of concrete in tension can be expressed in a more detailed approach using a bilinear function, as established by Hillerborg (1985), and as shown in Figure 6-4(b). A more accurate method of defining brittle behaviour is to use an exponential expression, which was experimentally established by (Cornelissen et al., 1986) and is explained in Figure 6-4(c), which can be calculated using the following Eques.

$$\frac{\sigma_t}{f_t} = f(w) - \frac{w}{w_c} f(w_c) \tag{6.3}$$

$$f(w) = \left[1 + \left(\frac{c_1 w}{w_c} \right)^3 \right] \exp\left(-\frac{c_2 w}{w_c} \right) \tag{6.4}$$

Where:

w: is the crack opening displacement,

w_c: is the crack opening displacement at which stress can no longer be transferred

$w_c = 5.14 G_f / f_t$ for normal weight concrete,

c_1: is a material constant and $c_1 = 3.0$ for normal weight concrete,

c_2: is a material constant and $c_2 = 6.93$ for normal weight concrete.

(a) Linear function   (b) Bilinear function   (c) Exponential function
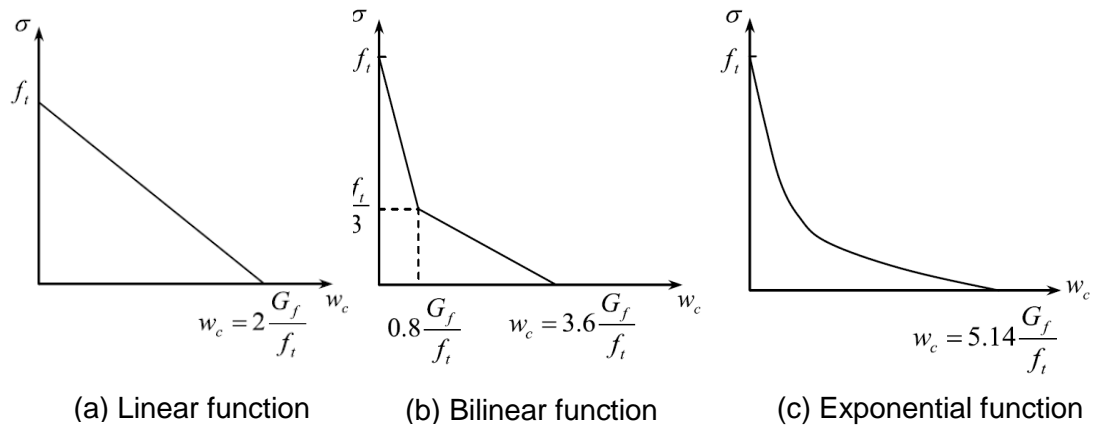
Figure 6-4: (a): Linear concrete tension softening model (Karlsson and Sorensen, 2006a) , Bilinear (Hillerborg, 1985) and exponential (Cornelissen et al., 1986)

Concrete damage in tension is included in the material modelling. The elastic stiffness of the material is degraded when a concrete crack occurs. The degradation of the elastic stiffness is characterized by two damage parameters, d_c and d_t, which are assumed to be functions of the plastic strains. The damage parameters can take values from zero (representing the undamaged status) to 1 (representing the total loss of strength). It is observed from the experiment that the concrete cracking failure mode is dominant in the push–out test. Therefore, in the FE analysis, only the tension damage variable d_t is applied.

Figures 6-5 & 6-6 show tensile stress versus the cracking displacement curve and tensile damage versus the cracking displacement curve for normal concrete material. The same formulas for representing normal concrete properties in tension and compression were used for the parametric study.
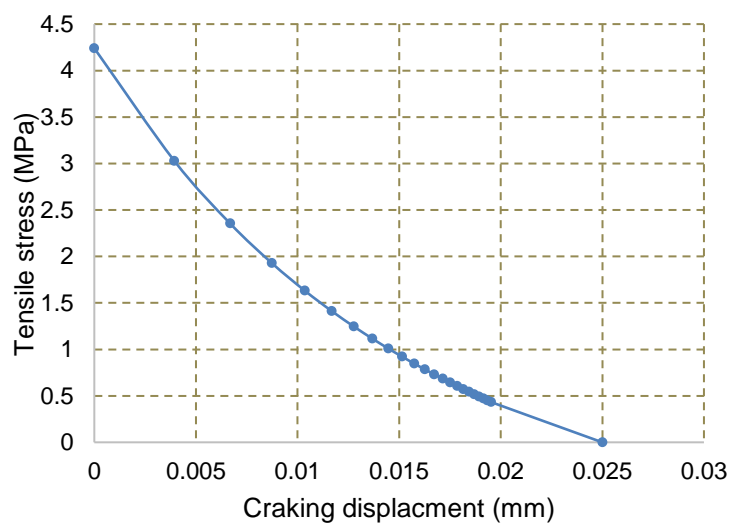
Figure 6-5: Tensile stress versus cracking displacement curve of normal concrete
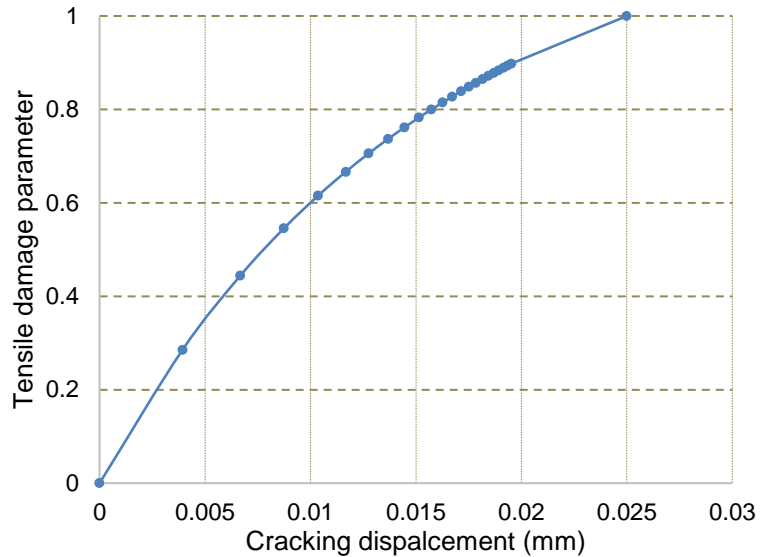
Figure 6-6: Tensile damage versus cracking displacement curve
of normal concrete

The same formulas for representing normal concrete properties in tension and compression were used for the parametric study.

6.4.1.4 Lightweight and ultra lightweight concretes

The stress-strain behaviour in the compression of lightweight and ultra lightweight concretes are represented by a mathematical model established by (Almusallam and Alsayed, 1995), which is given by Eq. 6.5.

$$f_c = \frac{(K - K_p)\varepsilon_c}{\left[1 + \left(\frac{(K - K_p)\varepsilon_c}{f_0}\right)^n\right]^{1/n}} + K_p\varepsilon_c \tag{6.5}$$

Where:

f_c is the concrete stress corresponding to the strain ε_c,

K: is the initial slope of the curve,

K_p, is the final slope of the curve,

f_0: is the reference stress,

n: is a curve-shape parameter.

These parameters are shown in Figure 6-7.
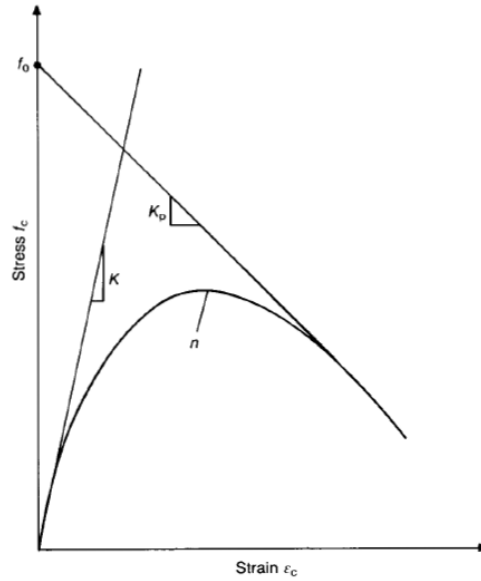
Figure 6-7: Schematic of the stress-strain model showing its parameters (Almusallam and Alsayed, 1995)

$$n = -\frac{\ln 2}{\ln\left(\frac{f_1}{f_0} - \frac{K_p}{K - K_p}\right)}$$

(6.6)

Where:

$$f_1 = f_c'\left[2\frac{\varepsilon_c}{\varepsilon_0} - \left(\frac{\varepsilon_1}{\varepsilon_0}\right)^2\right]$$

(6.7)

$$\varepsilon_1 = \frac{0.65f_0}{K - K_p}$$

(6.8)

$$f_0 = 19.1 + 1.3f_c' - K_p\varepsilon_0$$

(6.9)

$$K_p = 1374.5 - 871.1f_c' \quad \text{for } f_c' \geq 15\text{MPa}$$

(6.10)

$$K = E_c = 180.9\,f_c' + 7770.7$$

(6.11)

In addition, the relationship between the ultimate compressive strength and the corresponding strain is given by Eq. 6.12.

$$\varepsilon_0 = (0.398f_c' + 18.147) \times 10^{-4}$$

(6.12)

Figures 6-8, 6-9 represent the stress-strain curves of lightweight concrete and ultra lightweight concrete material in compression.
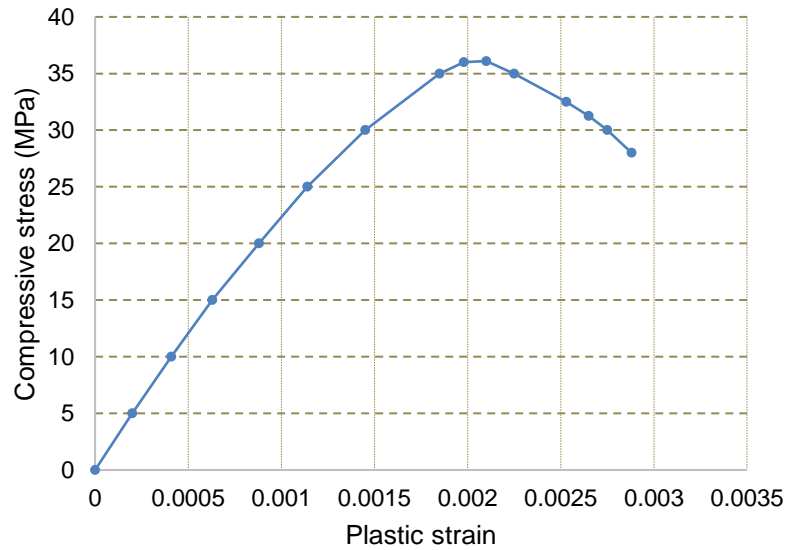
Figure 6-8: Stress-strain curve in compression for lightweight concrete material
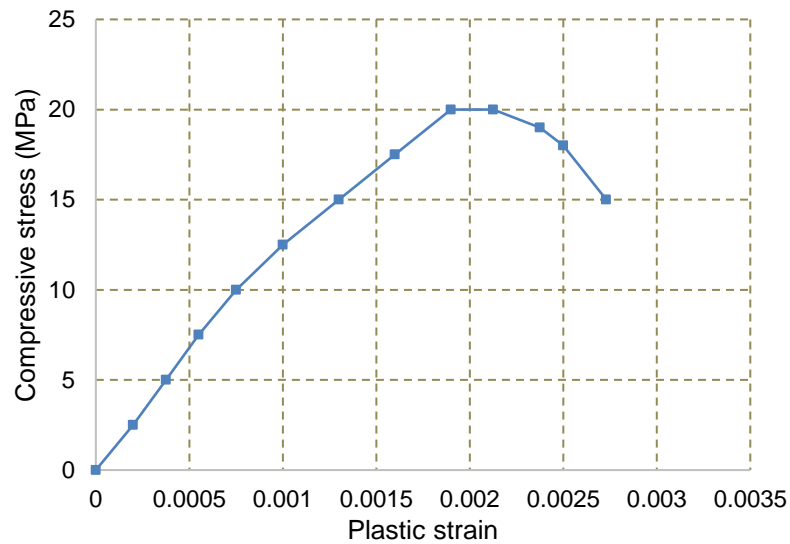
Figure 6-9: Stress-strain curve in compression for ultra lightweight concrete material

The stress-strain curve in tension of lightweight concrete is presented by the mathematical model (Cornelissen et al., 1986), which is given by the following Eques.

$$\frac{\sigma_t}{f_t} = f(w) - \frac{w}{w_c} f(w_c) \tag{6.13}$$

$$f(w) = \left[1 + \left(\frac{c_1 w}{w_c}\right)^3\right] \exp\left(-\frac{c_2 w}{w_c}\right) \tag{6.14}$$

Where:

w: is the crack opening displacement,

w_c: is the crack opening displacement at which stress can no longer be transferred

$w_c = 5.14G_f /f_t$ for normal weight concrete,

c_1: is a material constant and $c_1 = 1$ for lightweight concrete,

c_2: is a material constant and $c_2 = 5.64$ for lightweight concrete.

Figures 6-10-6-13 show tensile stress versus the cracking displacement curve and tensile damage versus the cracking displacement curve of lightweight concrete and ultra lightweight concrete material in tension. The same formulas for representing lightweight and ultra lightweight concretes properties in tension and compression were used for the parametric study.
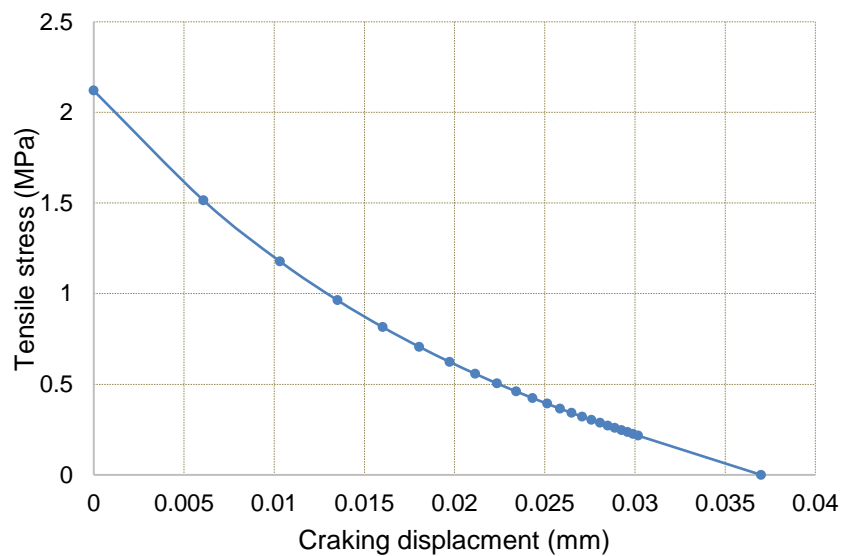
Figure 6-10: Tensile stress versus cracking displacement
curve of lightweight concrete material
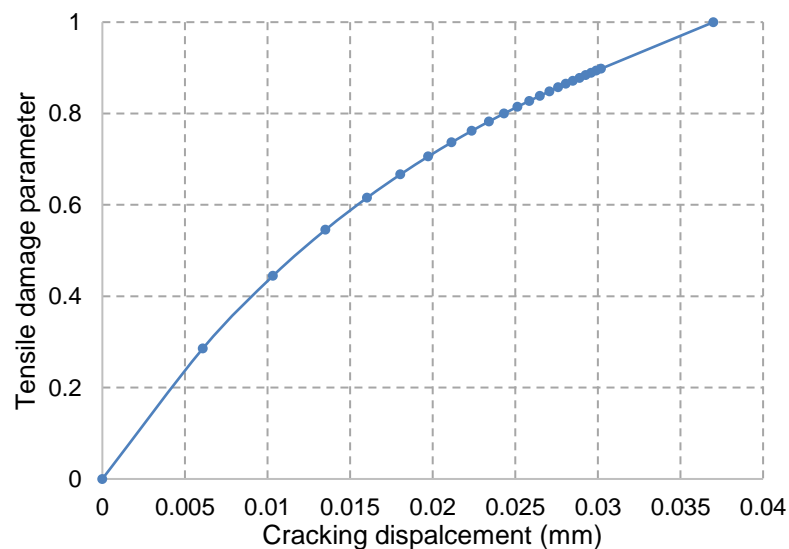
Figure 6-11:Tensile damage versus cracking displacement
curve of lightweight concrete material
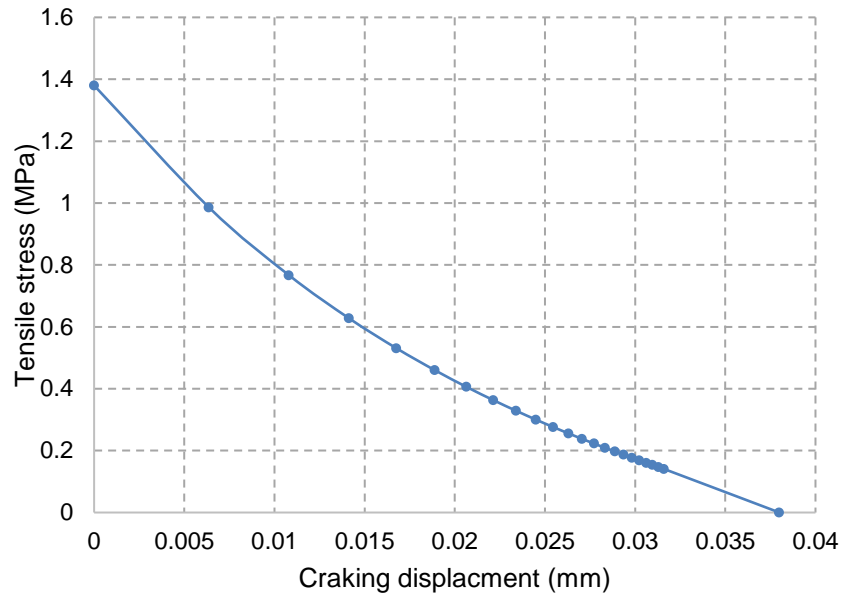
Figure 6-12:Tensile stress versus cracking displacement
curve of ultra lightweight concrete material
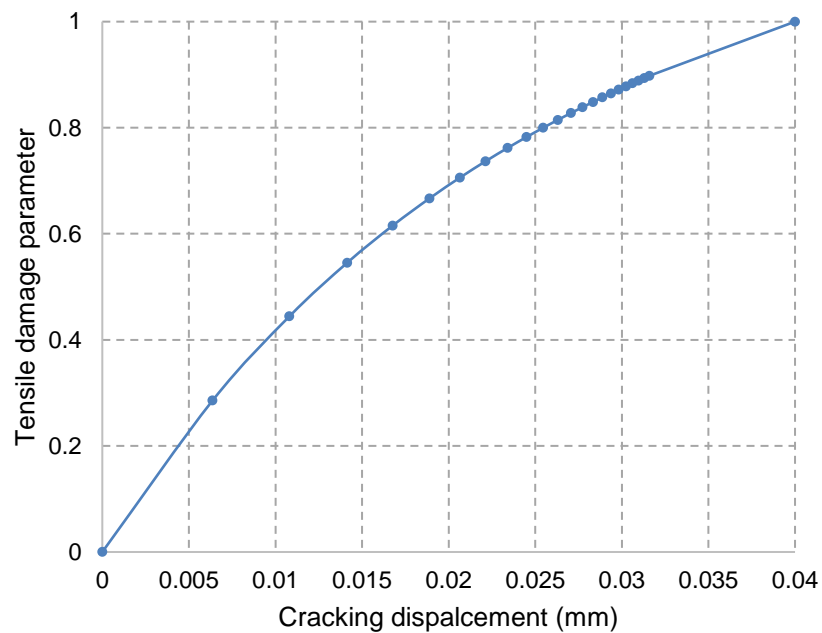
Figure 6-13: Tensile damage versus cracking displacement
curve of ultra lightweight concrete material

6.4.2 Structural steel

The material properties for the steel beam and reinforcing steel are other main components of the model. The stress-strain curve for both steel beam and reinforcing steel can be obtained from the steel tensile tests (ISO 6892-1:2009). For the push-out test specimens, the stress-strain curves were obtained and presented in **Chapter 3**. The data is input into two different material behaviours:

elastic and plastic options of the ABAQUS. Table 6-1 presents a summary of the steel components properties.

Table 6-1: Steel Components properties

Steel components	Yield Stress N/mm^2	Yield Strain	Ultimate Strain
6mm Steel Bar	550	0.0025	0.15
8mm Steel Bar	598	0.0034	0.173
10mm Steel Bar	503	0.0026	0.205
230x75x26PFC	406	0.013	0.22
20mm Steel Dowel	322.5	0.05	0.56
19mm Steel Stud	421.0	0.0125	0.1125

6.4.3 Shear connection systems

The shear connection material is of great importance in the model. The material is modelled by a tri-linear stress-strain curve, as shown in Figure 6-14 (Nguyen and Kim, 2009). The behaviour of the shear connectors' material is initially elastic, followed by strain softening and then yielding. The yield stress (σ_{ys}) is determined at ε_{ys}=0.2% and the ultimate stress (σ_{us}) achieves ε_{us} =0.6%.
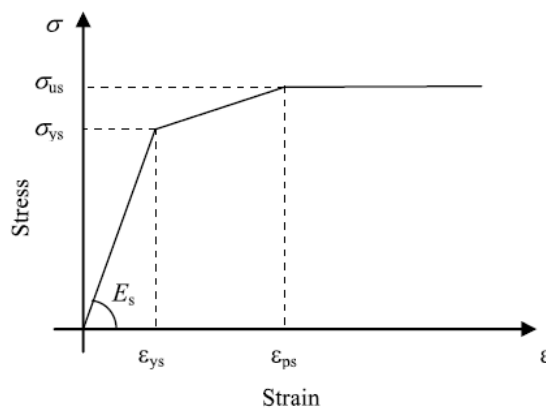
Figure 6-14: Stress-strain relationship for shear connectors
(Nguyen and Kim, 2009)

For the headed shear stud connectors, the material properties presented by (Xu et al., 2012) are used for the FEA and parametric study. From **Chapter 3**, the steel dowels were tested (ISO 6892-1, 2009) and their stress-strain curves were plotted. Similar to the structural steel, the material inputs of the shear studs were

divided into elastic and plastic regions, based on the stress-strain relationship from the tests.

The material damage and failure options were used in the material model for the shear connection systems in order to achieve the exact load-slip relationship. Modelling the failure of the material requires two specifications: the damage initiation criterion and the damage evolution response. In general, the damage initiation criterion specifies a critical equivalent plastic strain, where the stiffness of the material starts to degrade, and the damage evolution describes how the stiffness of the material degrades.

As for the damage model of shear connection systems, the metal fracture strain is actually decided by several factors, including strain rate, thermal effect, stress triaxiality, etc. Since the loading rate of 0.25 mm/s is considered slow enough to ignore the influence of strain rate and thermal effect, stress triaxiality is viewed as the primary factor. The relationship between stress triaxiality σ_m/σ_{eq} and the equivalent fracture strain P_R is expressed in Eq. 6.15 (Xue et al., 2012), where ε_R refers to the fracture strain under uniaxial load; σ_m is the mean stress; σ_{eq} is the equivalent Mises stress; S_0 is a material constant with the same magnitude of 1, $S_0=1.5$, and v is the Poisson ratio.

$$P_R = \varepsilon_R \left[\frac{2}{3} + (1 + v) + 3(1 - 2v) \left(\frac{\sigma_m}{\sigma_{eq}} \right)^2 \right]^{S_o} \tag{6.15}$$

Additionally, it is assumed that the ratio of P_R to ε_R is approximately equal to the ratio of P_D to ε_D, where ε_D equals the uniaxial strain related to the onset of fracture, and P_D equals the spatial stress status of fracture initiation. Consequently, the relationship between P_D and ε_D is based on P_R and ε_R can be established. In the present study, the criteria of fracture initiation is used as shown in Figure 6-15. The exponential correlation between damage variable D and plastic displacement has been established based on ABAQUS (2008). The exponential law parameter is 0.01 and the equivalent plastic displacement is related to the dimension size of the discrete elements.
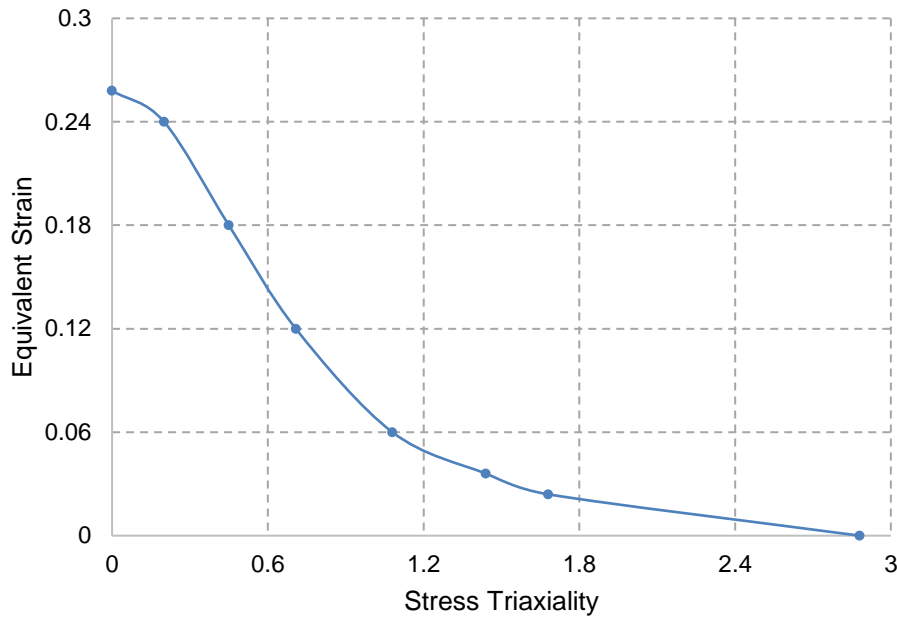
Figure 6-15: Criteria of damage initiation of shear connection systems

6.5 Contact interaction and boundary conditions

Contact interactions and boundary conditions are important characteristics in FEM, since the numerical simulations must consider the physical processes in the surface to surface interactions and boundary conditions. Inadequate definitions of boundary conditions may introduce non-physical influences into the simulation, especially in this study, where more than two components were considered in the simulation, such as the concrete slab, steel beam, shear connection systems and reinforcing steel.

Boundary conditions can be used to define the values of basic solution variables, such as warping amplitude, displacements, fluid pressures, rotations, temperatures, electrical potentials, normalised concentrations or acoustic pressures at nodes. In this study, symmetry boundary conditions in the x-axis at the end of concrete slab and the immovable restraints at the base block are applied.

Most contact problems are modelled using surface-based contact (Karlsson and Sorensen, 2006c). The structures can be either 2-D or 3-D and they can experience either small or finite sliding, such as the interface surface between the concrete slab and steel beam or shear connector. Contact interactions can also be certain types of kinematic constraints, such as surface-based tie and surface-based coupling constraints. Even boundary conditions are also a type of kinematic constraint in stress analysis, because they define the support of the

structure or given fixed displacements at the nodal points. The contact interactions for the FE model are shown in Figure 6-16.

6.5.1 Steel beam and concrete slab interface

As most contact problems are modelled by using surface-based contact, therefore this is also used for modelling the contact interface between the steel beam and the concrete slab. In the push-out test, the steel beam surface contact with the concrete slab is usually greased to reduce friction. In the analysis, the frictionless contact pair algorithm is used to define surface to surface contact between the steel beam surfaces and the surfaces of the concrete slab, as shown in Figure 6-16(b). Generally, the harder material is selected as the master surface and the softer as a slave. However, the ABAQUS manual suggests that the master and slave surface should not be chosen only on the basis of being either soft or hard material, but the stiffness of the material should also be taken into account. The steel beam is stiffer than the concrete slab. For this reason, the surface of the steel beam is taken as a master surface, while the surface of the concrete slab is treated as a slave surface.

The interaction properties of the steel beam and concrete slab surfaces are defined by normal behaviour and it is tangential to the surfaces. The default normal behaviour is assumed, which consists of a 'hard' contact pressure-over closure relationship. This type of normal behaviour allows for minimum penetration of the slave surface into the master surface. The penalty frictional formulation is used and the coefficient of friction between the steel beam and the concrete slab is taken as 0.0.

6.5.2 Steel beam and shear connection systems interface

To prevent relative slip between the steel beam and the shear connections, the steel beams are merged with the dowel and headed shear stud connectors to form one part. This is equivalent to the actual push test experiments, where shear connectors remain tied to the steel beam by welding (Nguyen and Kim, 2009).

6.5.2.1 Concrete slab and reinforcing steel interface

The contact interface between the concrete and reinforcing steel is of less importance compared with the other interfaces. It is assumed that no slip takes place between the concrete slab and the reinforcing steel bars during the analysis. Therefore, the embedded constraint method is applied in the FE model,

as shown in Figure 6-16(d). This embedded technique is used to specify the reinforcing bar elements that lie embedded in the host element, which in this case is the concrete slab that needs to be constrained. When a node of the reinforcing truss element lies within the host element, the degrees of freedom at the node are eliminated and the node becomes an "embedded node". The degrees of freedom of the reinforcing steel embedded node are constrained to the interpolated values of the degrees of freedom of the host element.

6.5.3 Concrete slab and shear connection systems interface

The surface-based contact technique is used to simulate the contact interface between the concrete slab and the shear connection systems. Since one of the objectives of this study is to investigate the behaviour of shear connection systems under longitudinal shear slip, therefore the FE model must be able to model or consider the longitudinal interface slip of the shear connection systems. This is because the shear connection systems are stiffer than the concrete slab. Therefore, the surface of the shear connection systems is taken as a master surface, while the surface of the concrete slab is treated as a slave surface, as shown in Figure 6-16(a).

The interaction properties of the concrete slab and shear connection systems surfaces are also defined by normal behaviour and are tangential to the surfaces. The penalty frictional formulation is used and the coefficient of friction between the steel beam and the concrete slab is taken as 0.5 (Qureshi et al., 2010). Different values of the coefficient of friction were applied to find the appropriate value.

6.5.4 Concrete slab and base block interface

Contact interaction is applied at the interface between the concrete slab and the base block, as shown in Figure 6-16(c). In this interaction, the friction coefficient is taken as 0.25, which is based on the study of (Ellobody et al., 2006).
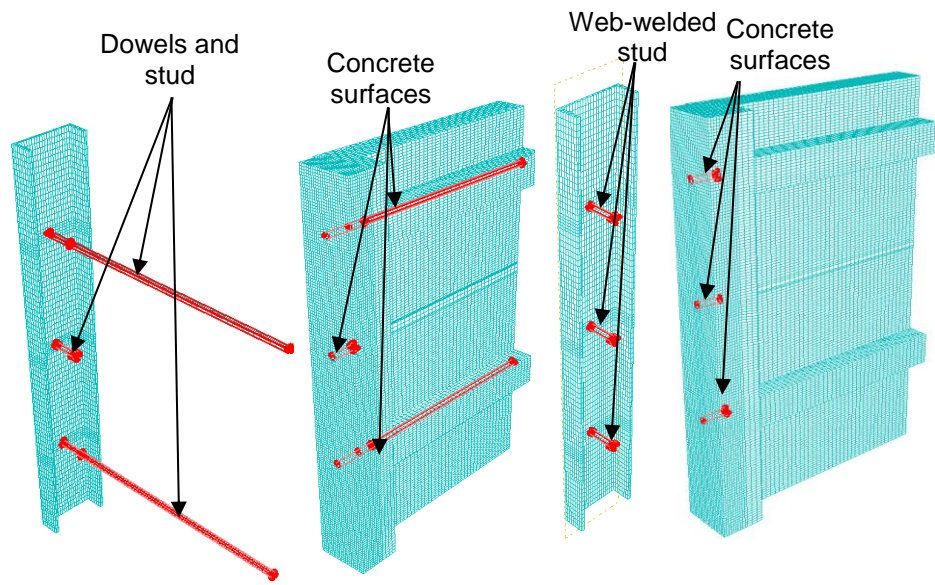
(a): Surfaces in tie constrain between
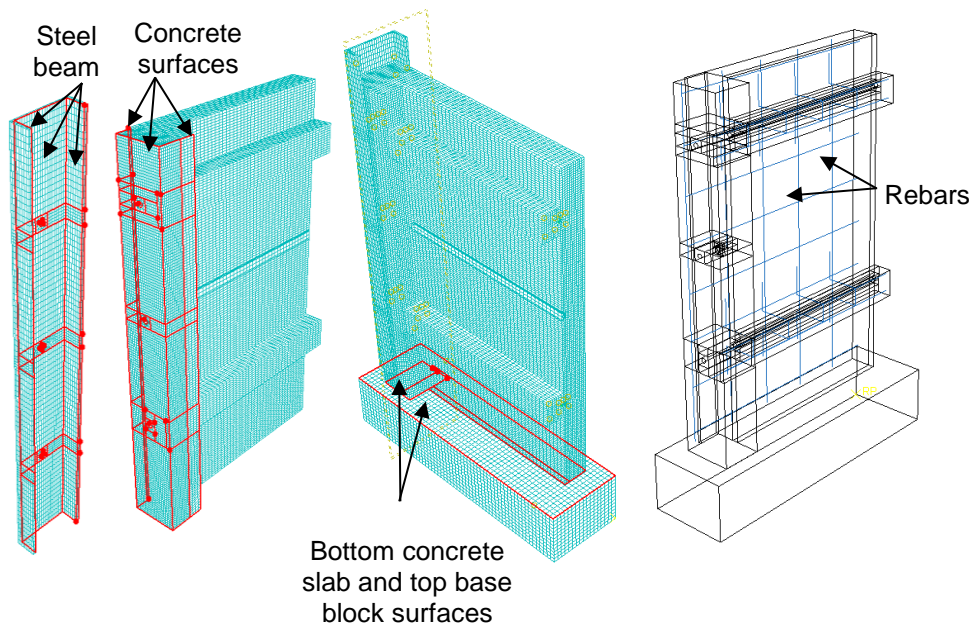
(b): Surfaces in contact interaction between steel beam and concrete slab

(c): Surfaces in contact interaction between concrete slab and base block

(d): Rebars embedded in concrete slab

Figure 6-16: Constrain and interaction surfaces

6.5.5 Symmetric and base block boundary conditions

Due to the symmetry of the push-out test arrangement, the symmetric boundary condition (BC) is applied to the surfaces at the symmetric planes of the specimen. The axis symmetric BCs were applied to surface 1, as shown in Figure 6-17(a), for which the translational displacement U1 and rotational displacements (R2 and R3) of all nodes on surface 1, and U3 and the rotational displacements (R1 and

R2) of all nodes on surface 1 were restrained. The base block is assumed to be immovable, so all DOF of the reference node of the base block is restricted.

6.6 Load application

In this analysis, displacement control is applied. Loading is downward enforced displacement applied to the top surface of the steel beam, as shown in Figure 6-17(b). ABAQUS/Explicit is a dynamic analysis program, and in case of the push test, a static solution is required. It is important to keep the inertia effects at a minimum level via slow load application in order to obtain a quasi-static solution from the explicit dynamic procedure. This is particularly essential for brittle materials, such as concrete, which failed by a sudden drop in their load carrying capacity, and as a result, the kinetic energy of the system increased extremely. Consequently, uniform displacement is slowly applied to the surface of the push-out test specimen, using a smooth amplitude function to ensure a quasi-static solution. Primarily, the quasi-static solution limits the kinetic energy of the push test to a small value throughout the analysis. Different loading rates have been tried and the optimum rate is found to be 0.25 mm/s.

(a): Axis symmetric boundary condition

(b): Base block boundary condition and loading surface
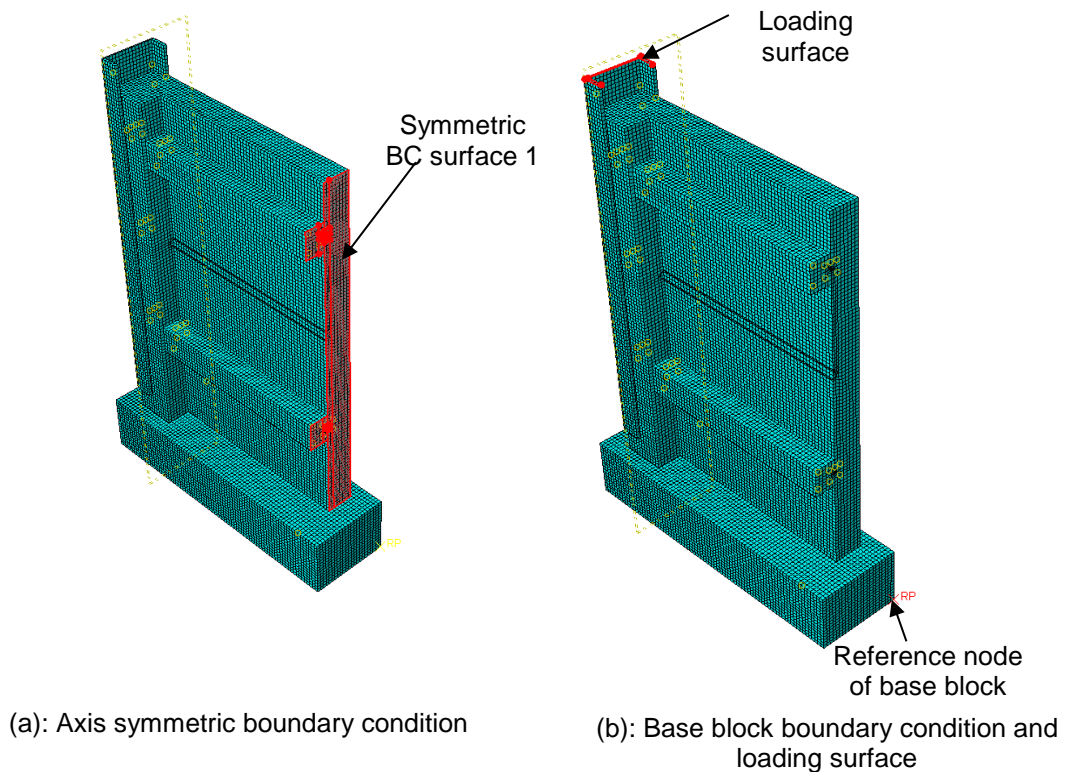
Figure 6-17: Boundary condition and loading surfaces

6.7 Mesh type

The basic modelling concepts, such as defining the nodes and surfaces, the conventions and input formats that should be followed when ABAQUS is used, are all discussed by (Karlsson and Sorensen, 2006a). After inputting the material properties of the several parts created for each component, the assembly of the model is followed.

Finally, the next step is the meshing of the assembly. A good detailed mesh is a major issue in FEM. The finer the mesh given to the component, the better the end results will be. However, the number of mesh in the model determines the computation time that is required to complete the simulation. A good mesh should have well-shaped elements with mild distortion and moderate aspect ratios.

Due to the symmetry of the push-out test specimens, only half of the push-out test arrangements with the three shear connectors have been modelled. Figure 6-18(a) shows a full view of the specimen. The push-out specimen is composed of six components: the concrete slab, steel channel, dowels, headed stud, reinforcing bars, reinforcing stirrups, and the mesh reinforcement. The components were modelled as separate parts, as presented in Figure 6-18(a).

In order to reduce the analysis time, a coarse mesh is applied to the overall size. The fine mesh is applied to the region around the interface between the concrete and the studs to achieve accurate results. In the headed stud, the mesh size is also reduced at the joint between the stud and steel beam where the stud would usually fail under shear force. A convergence sensitivity study has been conducted to specify the best mesh size to be used (see Section 6.9). The overall mesh size is 20mm and the smallest size is about 10mm. The finite element mesh of the specimen is presented in Figure 6-18(b).

6.7.1 Solid elements

The 3-D solid elements are volume elements that consist of a single homogeneous material or can contain several layers of different materials. This element type is an 8-node brick element with reduced integration stiffness. Each node has three translational degrees of freedom (DOF). Karlsson and Sorensen (2006b) illustrated how the solid elements can be used for both linear and complex nonlinear analysis, including contact, large deformation, plasticity and failure.

For the concrete slab, structural steel beam, and the shear connection systems parts, a 3-D eight node element (C3D8R) is used. The element profiles of the concrete slab, steel beam and shear connection systems are shown in Figure 6-18(c).

6.7.2 Truss elements

Truss elements can be used in either 2-D and 3-D to model slender, line-like structures that support loading only along the axis or the centre line of the element. No moment or forces perpendicular to the centre line are supported. A 2-node straight truss element that uses linear interpolation for position and displacement and has a constant stress is available in ABAQUS/Standard. In addition, a 3-node curved truss element that uses quadratic interpolation for position and displacement so that the strain varies linearly along the element is also available in ABAQUS/Standard.

For the reinforcing bars, reinforcing stirrups and reinforcing welded wire mesh parts, a 2-D two-node truss element (T3D2) with linear approximation of displacement, two nodes and three translational degrees of freedom are all used, as shown in Figure 6-18(c).

6.7.3 Block Elements

Block elements are bilinear rigid quadrilateral elements. They are used in different applications, such as defining the surfaces of the rigid bodies for contact applications and multibody dynamic simulations, constraining model parts, and applying loads to rigid structures associated with rigid body reference nodes. R2D2 elements are used for the plane strain or plane stress analysis, RAX2 elements are used in axisymmetric planar geometries, and R3D3 and R3D4 elements are used in three-dimensional analysis.

For the base block part, a 4-node, bilinear quadrilateral element (R3D4) is used, as shown in Figure 6-18(c).

(a): A half of the push-out specimen

(b): Full view of the push-out

Steel beam and shear connectors Element type C3D8R

Concrete slab Element type C3D8R

Base block Element type R3D4

Rebar Element type T3D2

(c): element types
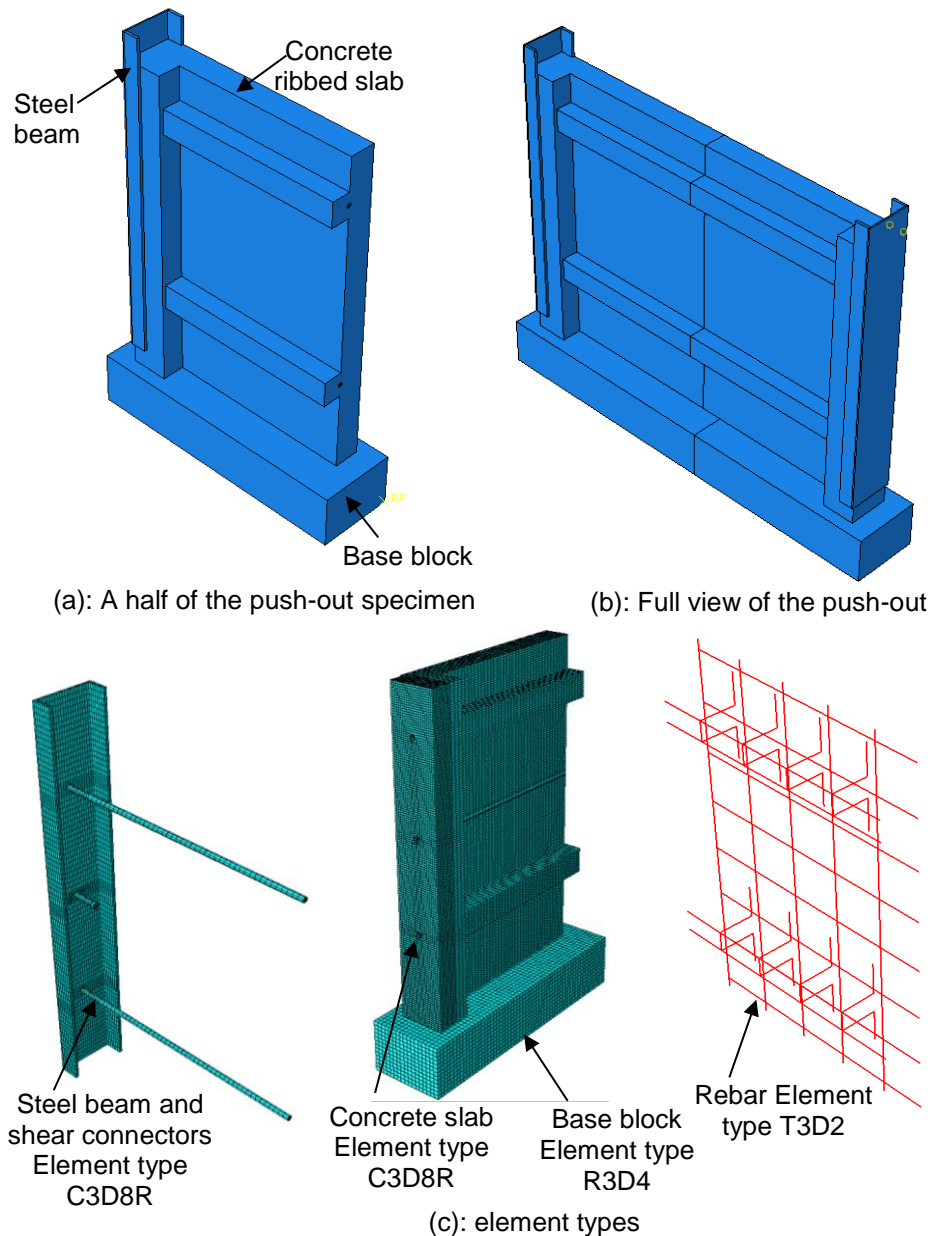
Figure 6-18: Finite element mesh type

6.8 Analysis method

The RIKS method is frequently used to study the behaviour of the shear connectors in the push-out test (Nguyen and Kim, 2009). The RIKS method is generally used to predict the unstable and nonlinear collapse of a structure. It is an implicit load control method. In the RIKS method, the load is applied proportionally in several load steps. In each load step, the equilibrium iteration is performed and the equilibrium path is tracked in the load-displacement space. This method is often used in static analysis and has been shown to be a strong method for nonlinear analysis. However, due to the equilibrium iteration, the RIKS

method consumes much time and computer resources for a relatively large model. In addition, the convergence problem is often encountered when material damage and failure are included, and thus the ultimate load could not be obtained.

In this study, the dynamic explicit analysis method is used, which is a time control method. It is usually used for problems relating to metal forming, impact and progressing damage and failure of the material. It has been shown to be an efficient solution scheme for contact interaction, discontinuous mediums and large deformations. It has been used in many problems such as metal sheet forming(Jung, 1998), crack and failure of concrete material (Algaard et al., 2005), composite laminate impact (Nguyen et al., 2005), among others. Despite being a dynamic method, the dynamic explicit analysis is also used for quasi-static analyses.

The global mass and stiffness matrices in the dynamic explicit analysis method not to be formed and inverted as a result each increment is relatively inexpensive compared to the implicit analysis. The size of the time increment is specified according to the mesh size and material properties. The time of the analysis can be reduced by using mass scaling. The explicit analysis is very efficient for solving contact and discontinuous problems, therefore, it is adequate for the simulation of push-out test. It can be used for the simulation of the push-out test with the same loading rate as in the real experiment. Nevertheless, in order to reduce the time of analysis, the approach of increasing loading rate is used in this study. Different loading rates have been used and the most appropriated rate has been determined as 0.25 mm/s.

6.9 Convergence sensitivity study

A push-out test specimen with a dowels and studs shear connection system is used to carry out the mesh convergence study (element size analysis). Only one half of the push-out test is modelled using the symmetric boundary conditions. Four different element sizes were used to determine the optimum size of the push-out test specimen for the FEA. The smallest three element sizes were 15mm, 10mm and 8mm, with an overall mesh size of 20mm. The normal weight concrete strength for the model is 37.3MPa. A slip of 13.67mm is applied to the model, which is the same slip obtained from push-out test specimen T2-NWC.

The load-slip of specimen T2-NWC and the models of different element sizes are shown in Figure 6-19. The summation of the measured reaction force on the loading surface at a slip of 6mm Eurocode 4(EN1994-1-1, 2004) were compared between the models of different element sizes, as shown in Figure 6-20.
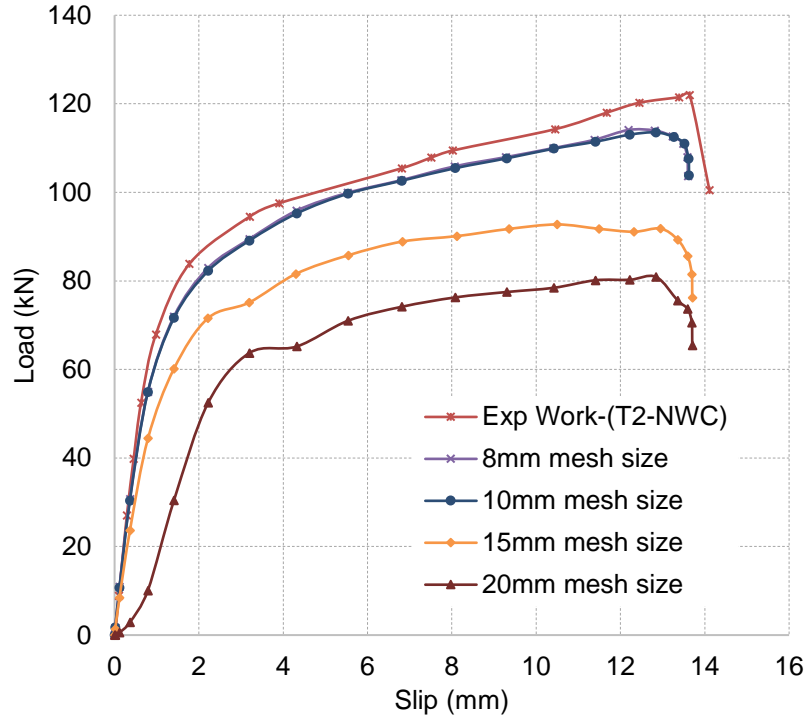
Figure 6-19: Load-slip of specimen T2-NWC and models with different element sizes
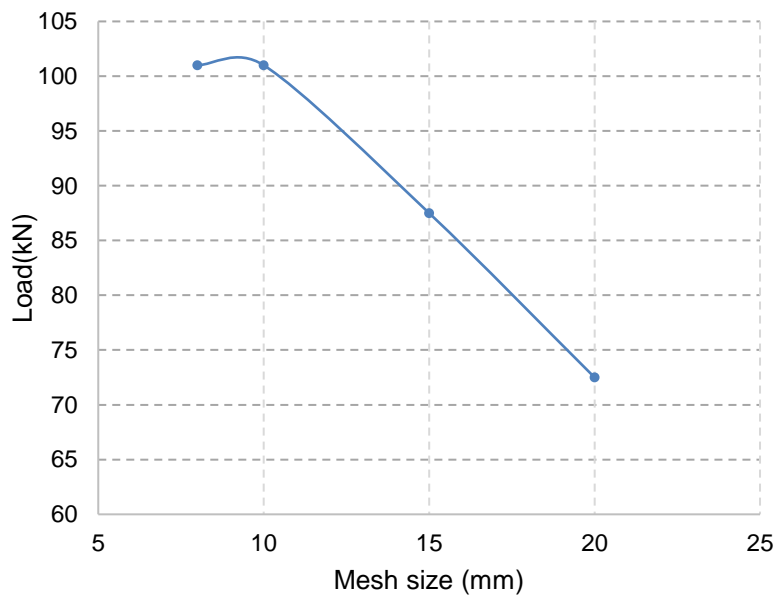
Figure 6-20: Load-mesh size of models with different element size at slip of 6mm

The results of the reaction force were almost identical between the models of element sizes (10mm & 8mm). Hence, these two element sizes could be used to model the FEA push-out tests. However, the computational time increases using the fine element size of 8mm. Therefore, an element size of 10mm has been chosen as the optimum element size for the FEA push-out tests.

6.10 Validation study

The FEA of the shear connection systems is carried out by using the material strengths obtained in the push-out tests. The results of the FEA were compared with the results of the push-out tests.

The comparisons for the failure loads and slips between the push-out tests and the FEA are summarised in Table 6-2. The identical slip stiffness between the results of the FEA and push-out tests are illustrated in Figures 6-21 & 6-22. Both the failure loads and slips of the FEA were very close to those of the push-out tests. The average ratio for the failure loads between the results of the FEA and push-out tests is 1.06. The average ratio for the slips between the results of the FEA and push-out tests is 1.04.

Table 6-2: Comparisons between the results of the push-out test specimens and FEA models

Test Reference	Concrete strength f_c (MPa)	Failure Load			Slip		
		Push-out test (kN)	FEA (kN)	Ratio (Test/FEA)	Push-out test (mm)	FEA (mm)	Ratio (Test/FEA)
T1-NWC	38.52	103.97	96.78	1.07	10.28	9.27	1.10
T1-LWC	32.20	86.70	78.75	1.10	19.98	17.90	1.11
T1-ULWC	20.0	57.02	55.74	1.02	20.15	19.45	1.03
T2-NWC	37.3	121.90	113.54	1.07	13.64	12.84	1.06
T2-LWC-1	34.6	101.65	95.46	1.06	20.45	20.04	1.02
T2-LWC-2	36.8	103.51	96.62	1.07	21.62	21.79	0.992
T2-ULWC	20.0	73.83	69.12	1.06	28.72	28.04	1.02
Mean CV				1.064 2.23			1.047 4.22

The bending failure mode of the WWSS and dowels and the concrete failure mode were demonstrated by the FEA, as illustrated in Figures 6-23-6-34. The slip and stress contour plots of the FEA for the models with NWC-fc of 37.3MPa, LWC-fc of 36.8MPa and ULWC-fc of 20MPa are shown in Figures 6-23-6-34, respectively.

A comparison between the FEA model and the experimental work failure modes is illustrated in Figures 6-35-6-40. The stress plots clearly demonstrated the bending of WWSS and dowels and the cracking of the concrete in the shear direction when subjected to the longitudinal shear slip, as shown in Figures 6-23-6-34.

The above validation has shown excellent agreements between the results of the FEA and the push-out tests, in the terms of the failure load, slip, stress results and failure mode. It has been demonstrated that the FEA model used for the validation is reliable and could be used to carry out a parametric study on the shear connection systems.
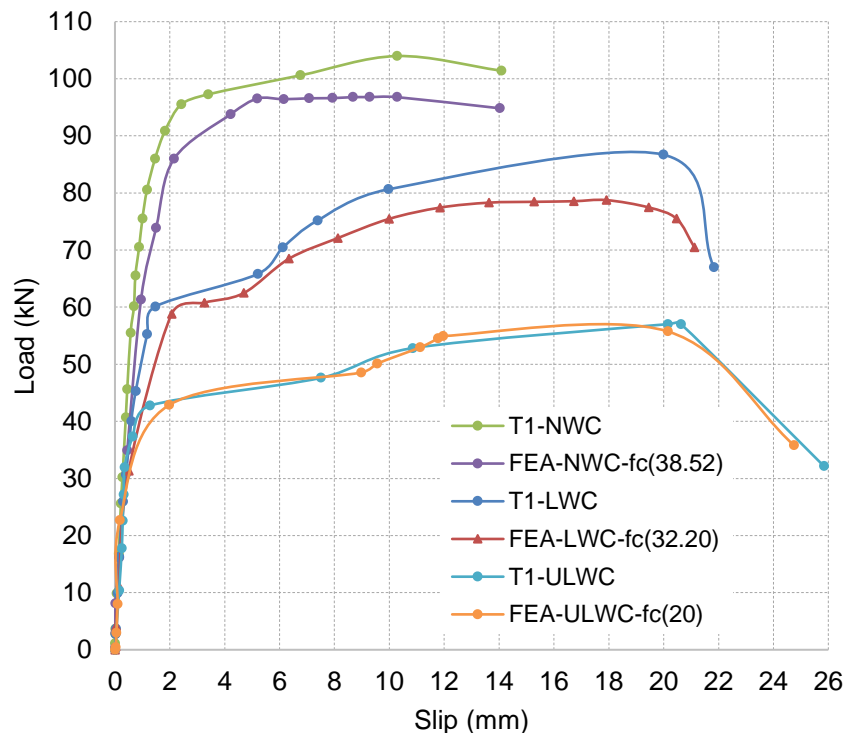
Figure 6-21: Comparison of load-slip curves between FEA models and push-out test specimens with WWSS
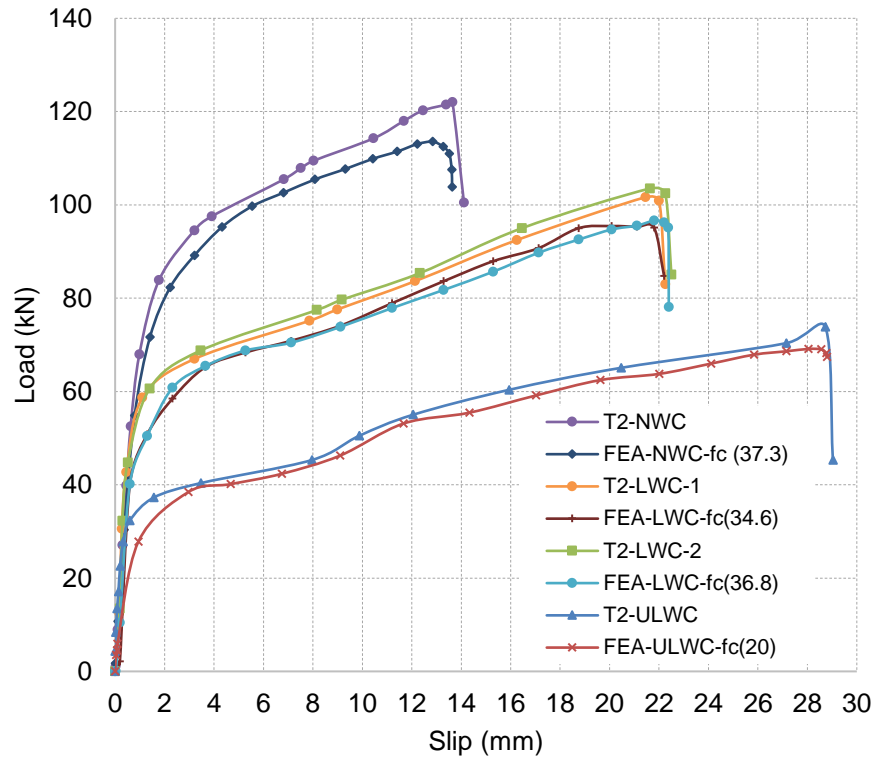
Figure 6-22: Comparison of load-slip curves between FEA models and push-out test specimens with WWSS with dowels

(a)

(b)
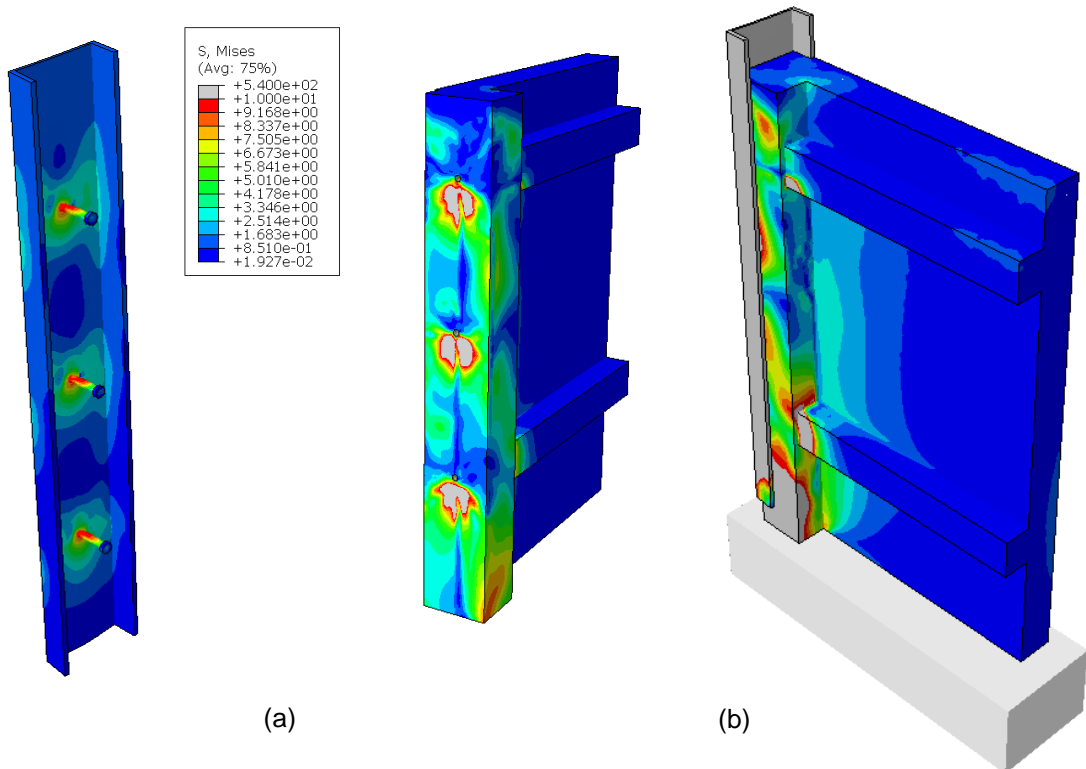
Figure 6-23: Stress contour plots of (a) steel beam: (b) concrete slab of FEA model with WWSS and NWC-fc-38.52MPa
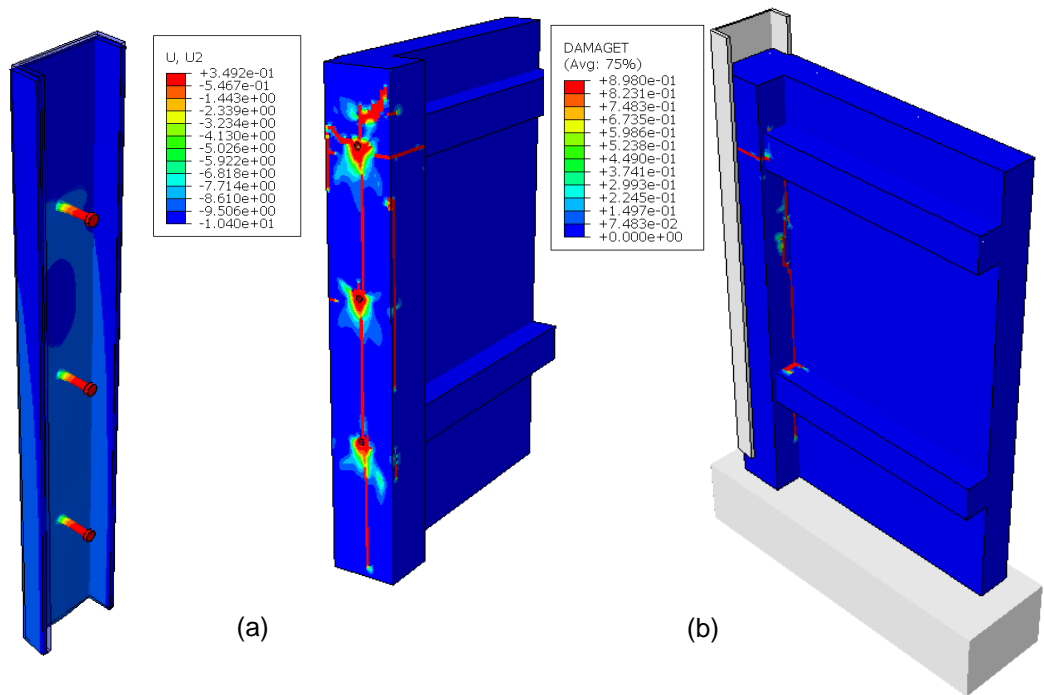
Figure 6-24: Contour plots of: (a) vertical displacement (slips); (b) cracks of FEA model with WWSS and NWC-fc-38.52MPa
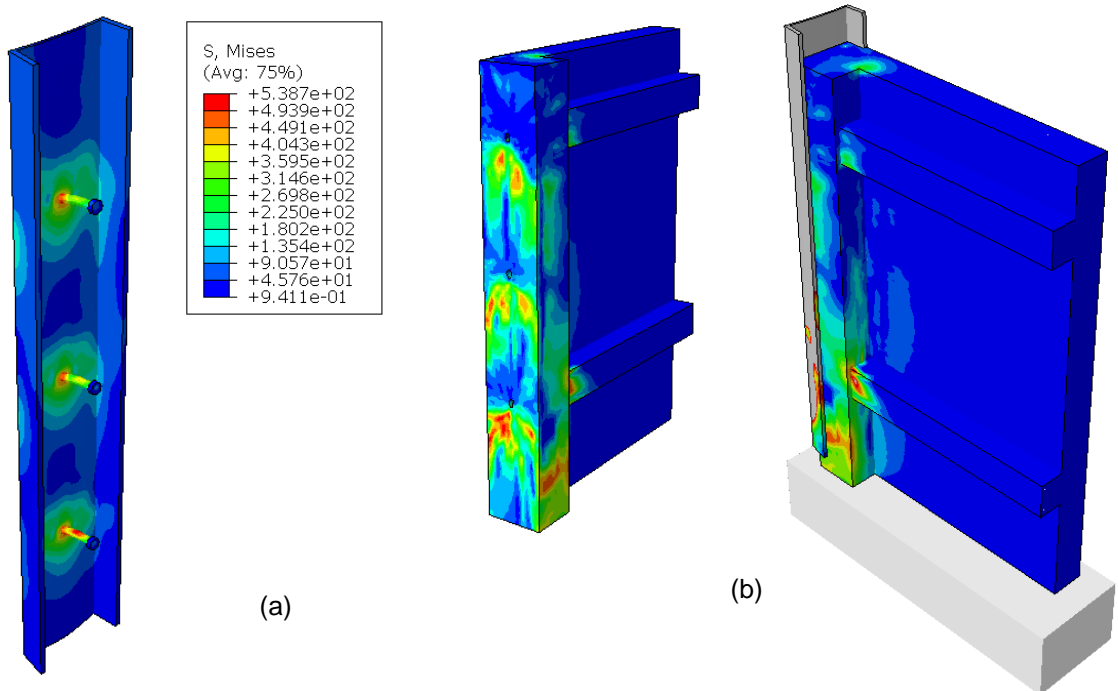
Figure 6-25: Stress contour plots of (a) steel beam: (b) concrete slab of FEA model with WWSS and LWC-fc-32.20MPa
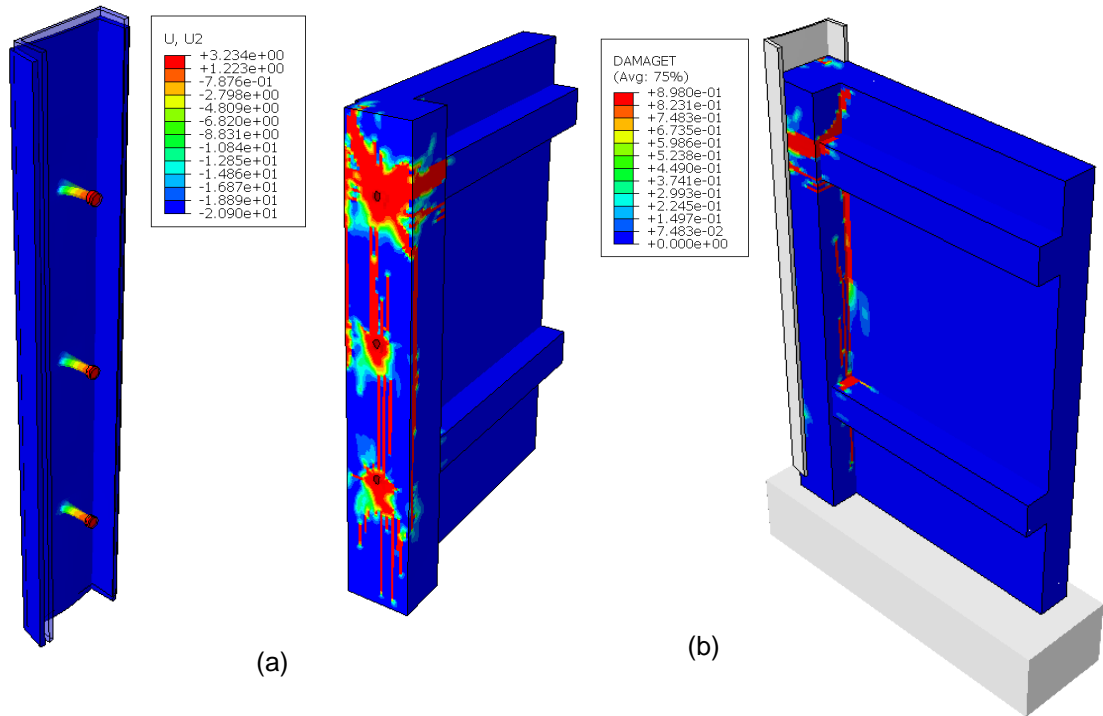
Figure 6-26: Contour plots of: (a) vertical displacement (slips); (b) cracks
of FEA model with WWSS and LWC-fc-32.20MPa
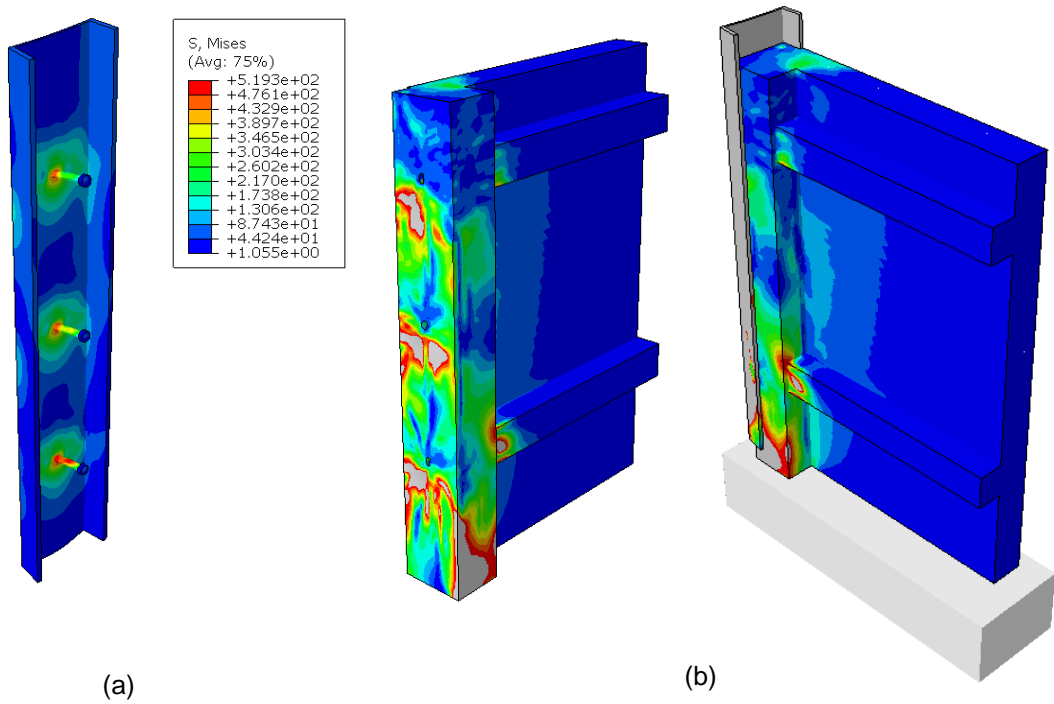
Figure 6-27: Stress plots of (a) steel beam; (b) concrete slab
of FEA model with WWSS and ULWC-fc-20MPa
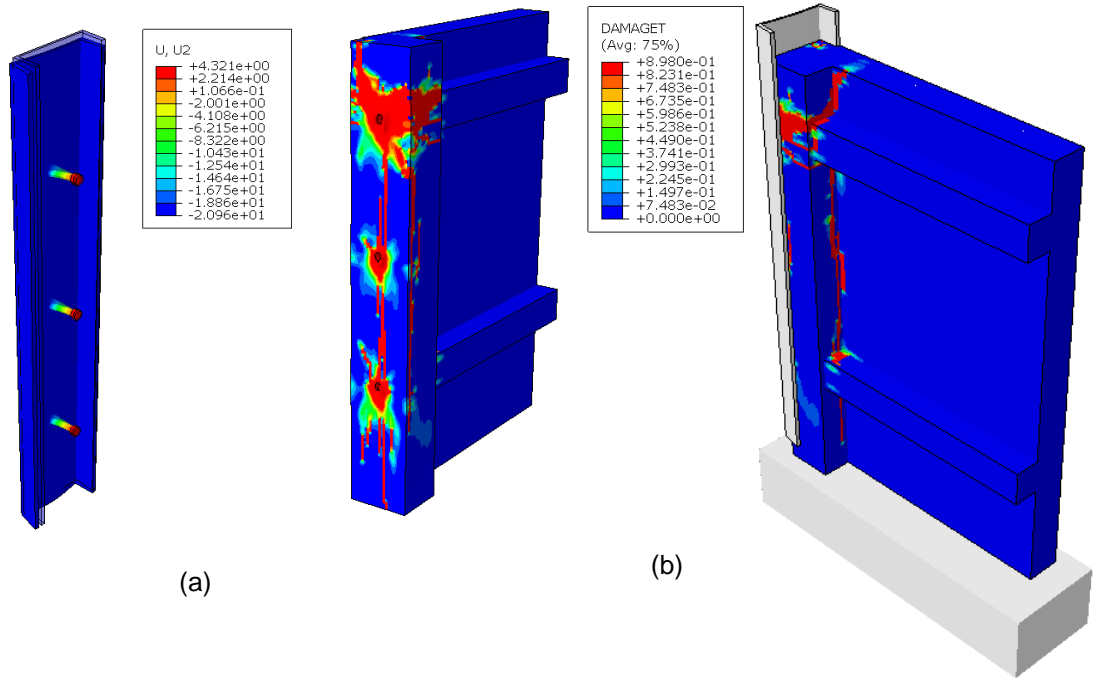
Figure 6-28: Contour plots of: (a) vertical displacement (slips); (b) cracks of FEA model with WWSS and ULWC-fc-20MPa
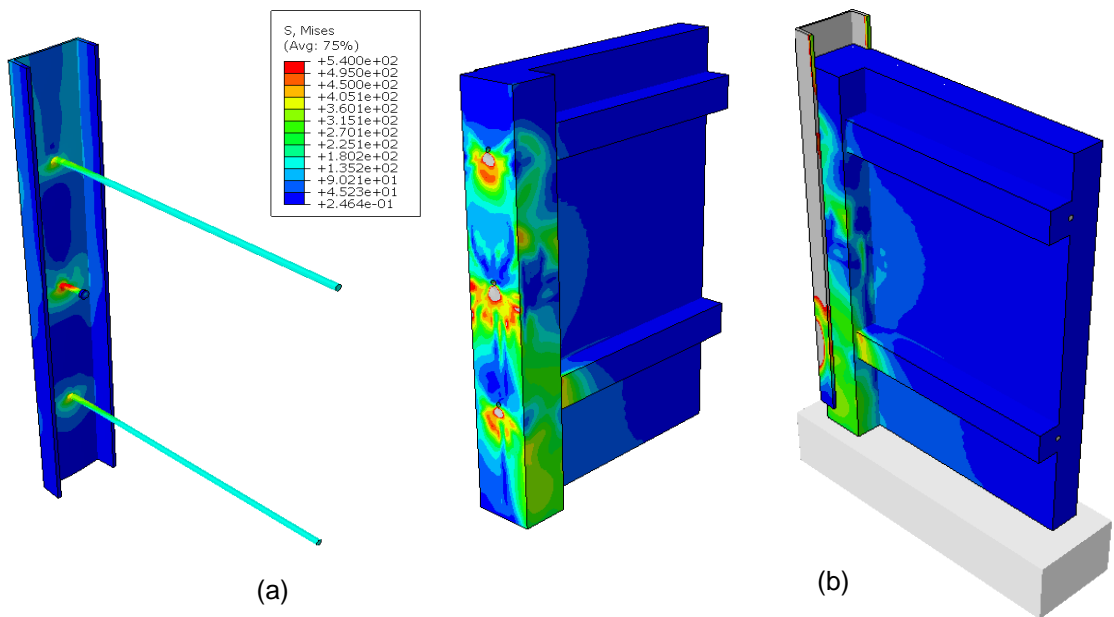
Figure 6-29: Stress contour plots of (a) steel beam; (b) concrete slab of FEA model with WWSS with dowels and NWC-fc-37.3MPa
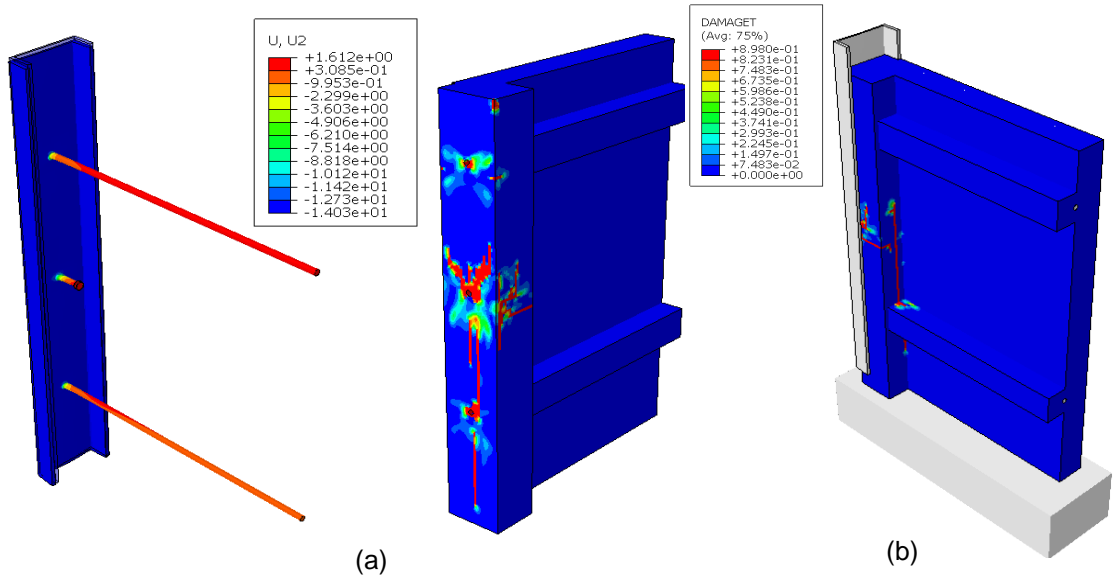
Figure 6-30: Contour plots of: (a) vertical displacement (slips); (b) cracks
of FEA model with WWSS with dowels and NWC-fc-37.3MPa
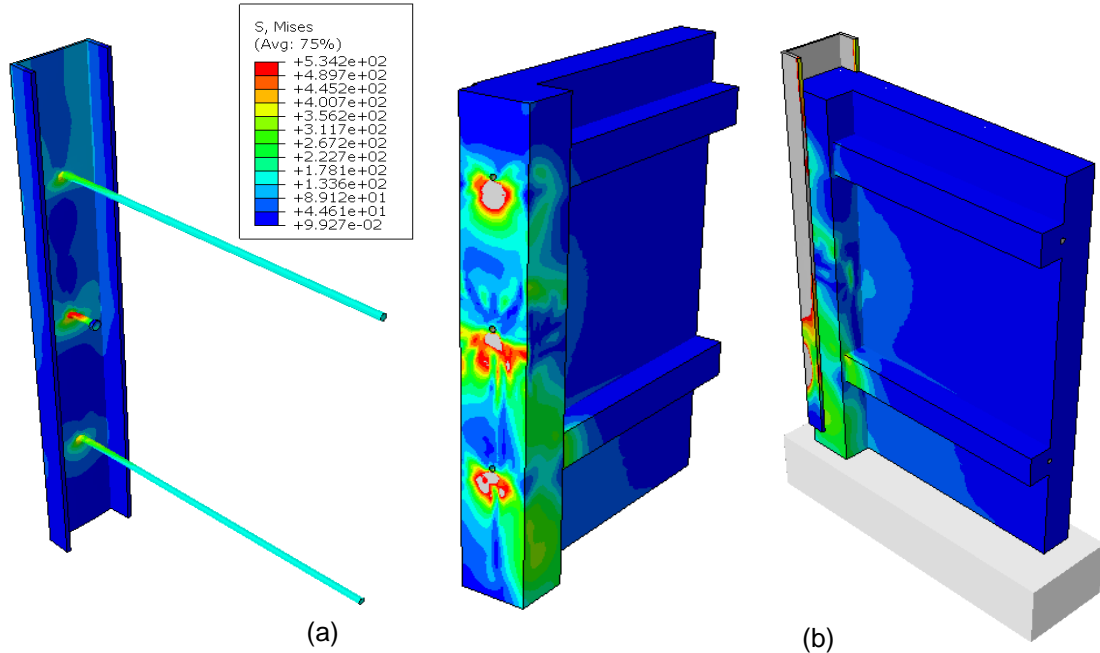
Figure 6-31: Stress contour plots of (a) steel beam; (b) concrete slab of
FEA model with WWSS with dowels and LWC-fc-36.8MPa
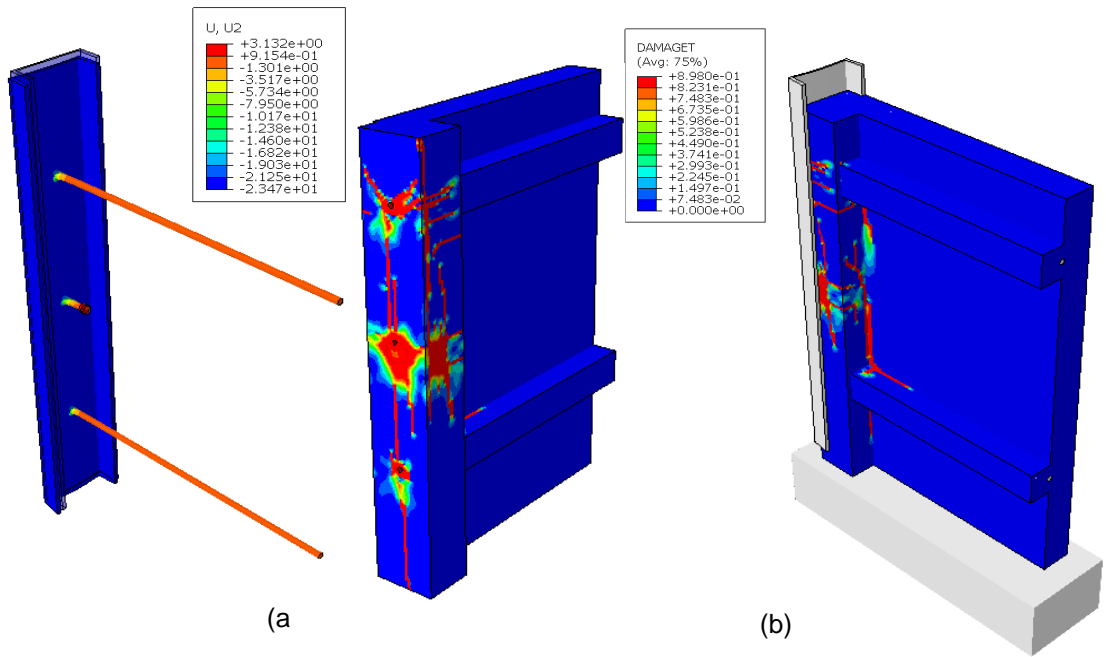
Figure 6-32: Contour plots of: (a) vertical displacement (slips); (b) cracks of FEA model with WWSS with dowels and LWC-fc-36.8MPa
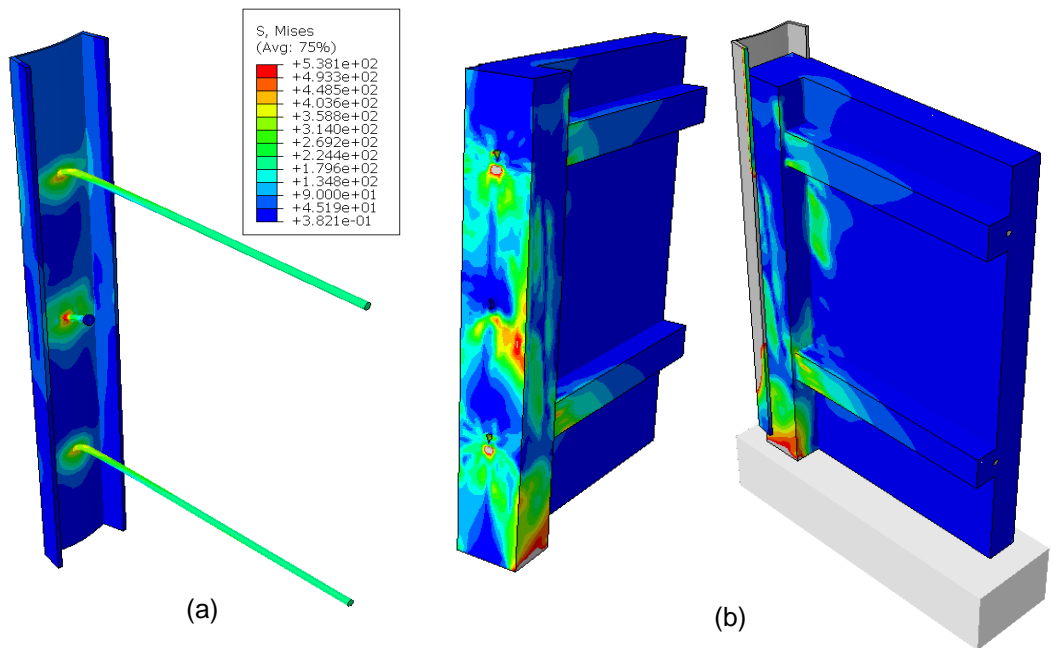
Figure 6-33: Stress contour plots of (a) steel beam; (b) concrete slab of FEA model with WWSS with dowels and ULWC-fc-20MPa
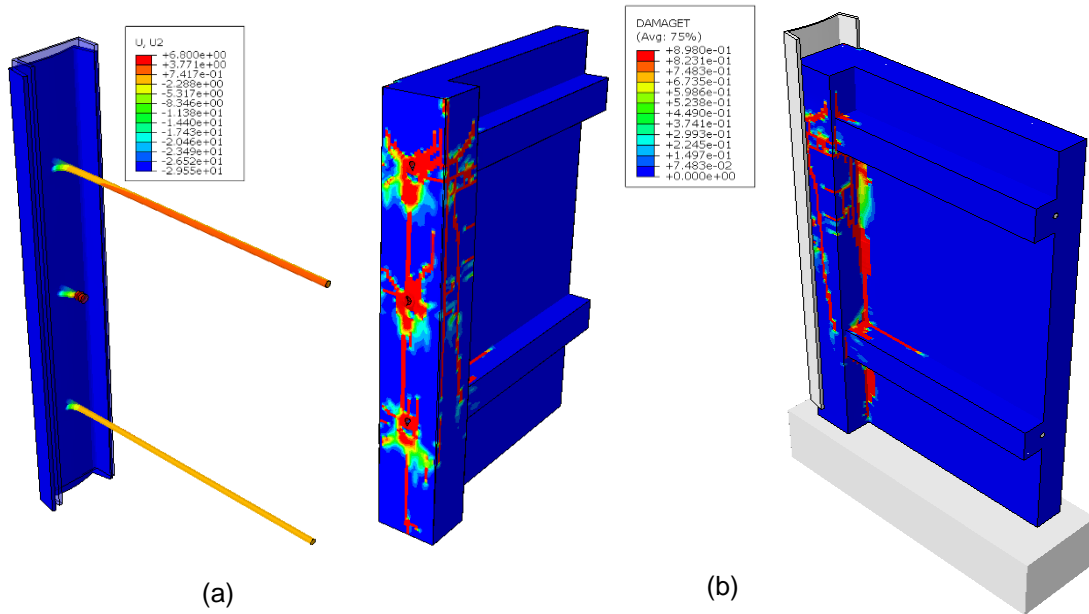
Figure 6-34: Contour plots of: (a) vertical displacement (slips); (b) cracks
of FEA model with WWSS with dowels and ULWC-fc-20MPa
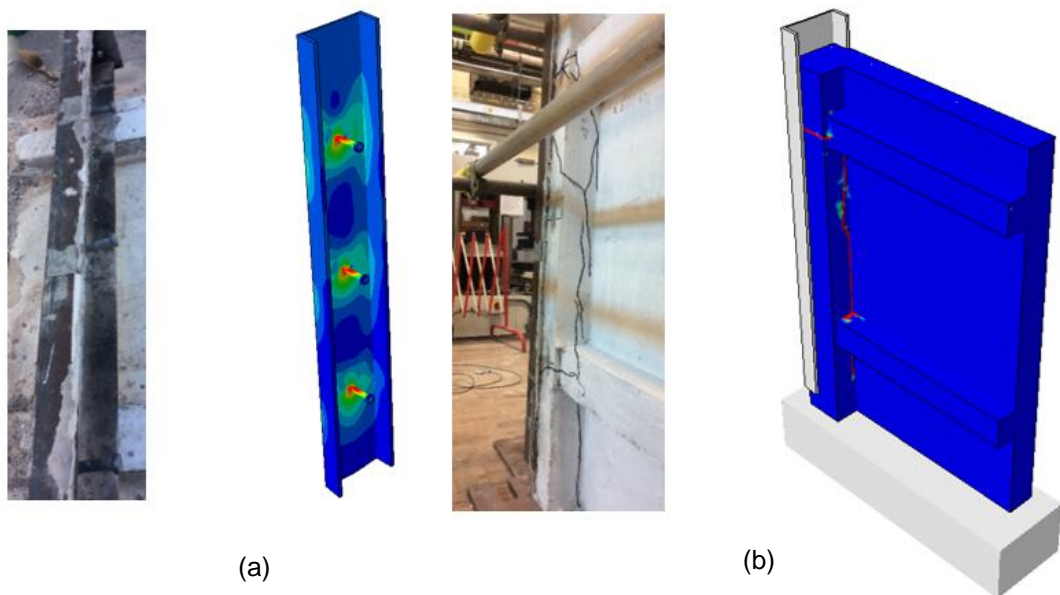
Figure 6-35: Comparison between the FEA model and T1-NWC specimen with
WWSS (a): shear stud connectors' failure, (b) concrete slab failure

(a)

(b)
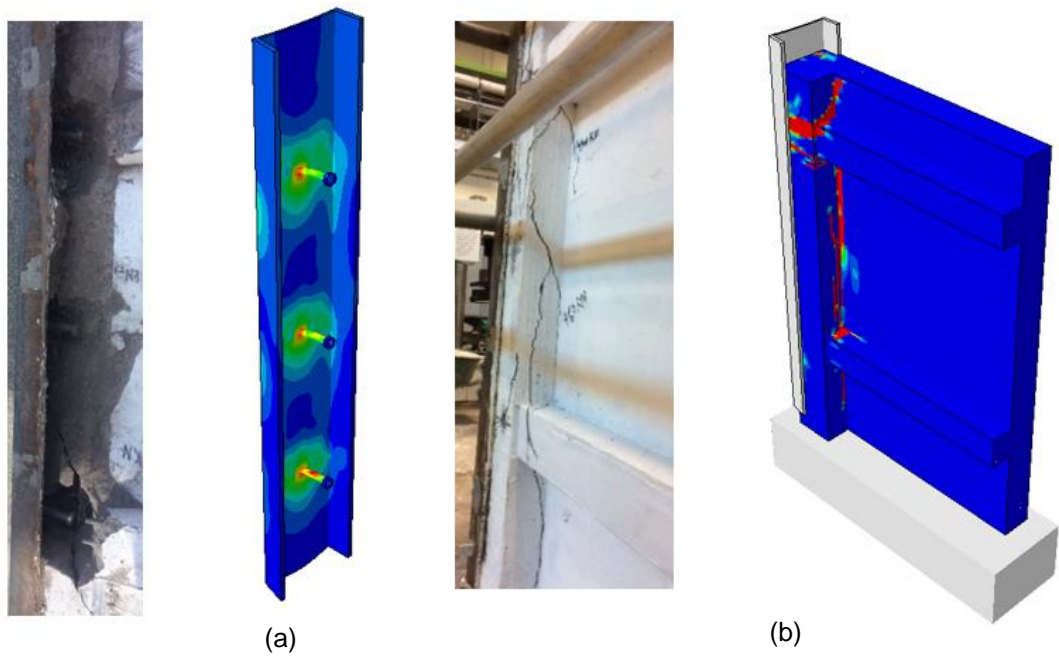
Figure 6-36: Comparison between the FEA model and T1-LWC specimen with WWSS(a): shear stud connectors' failure, (b) concrete slab failure

(a)

(b)
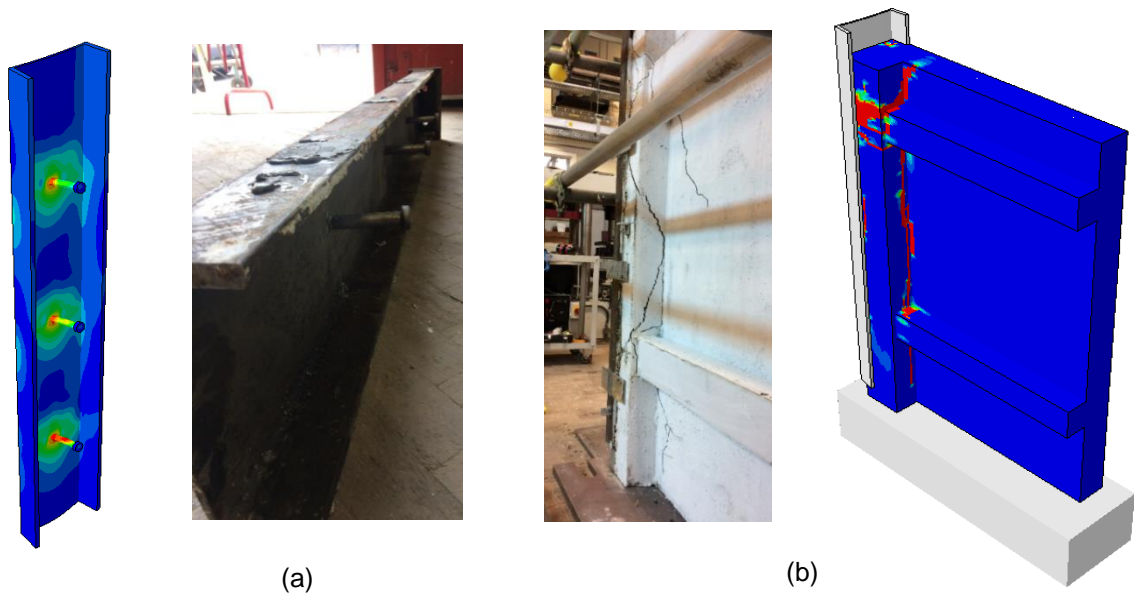
Figure 6-37: Comparison between the FEA model and T1-ULWC specimen with WWSS (a): shear stud connectors' failure, (b) concrete slab failure
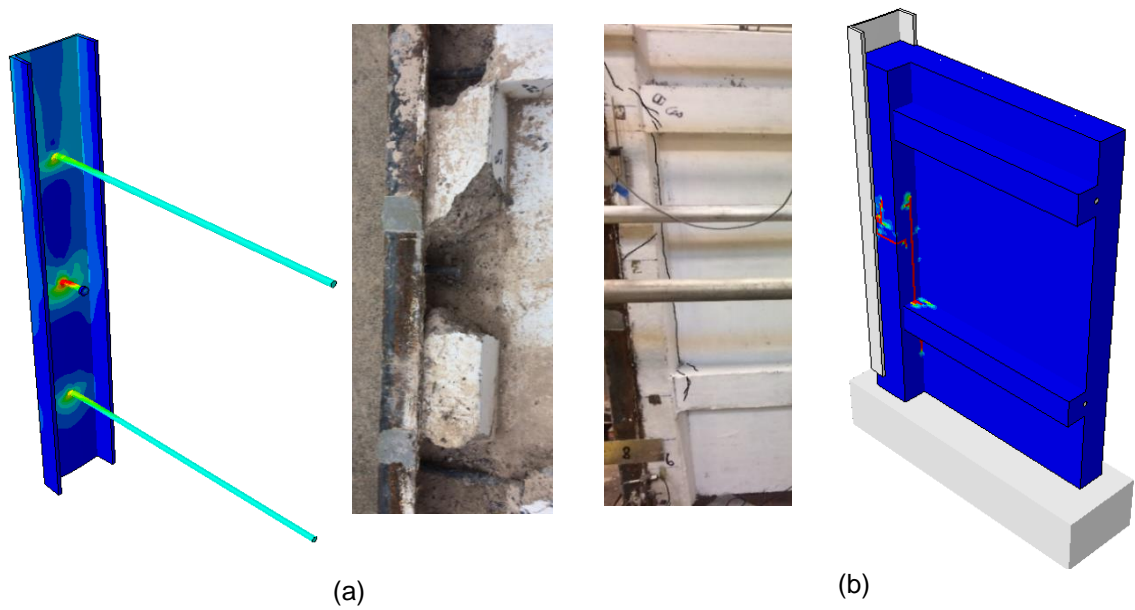
Figure 6-38: Comparison between the FEA model and T2-NWC specimen with WWSS with dowels (a): shear stud connectors' failure, (b) concrete slab failure
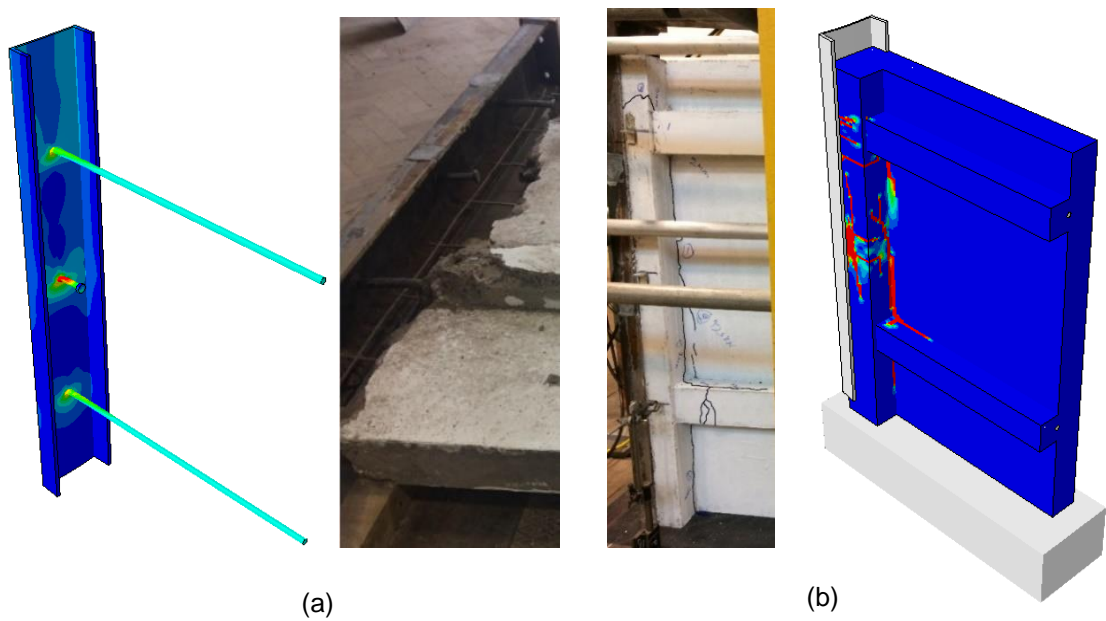
Figure 6-39: Comparison between the FEA model and T2-LWC specimen with WWSS with dowels (a): shear stud connectors' failure, (b) concrete slab failure
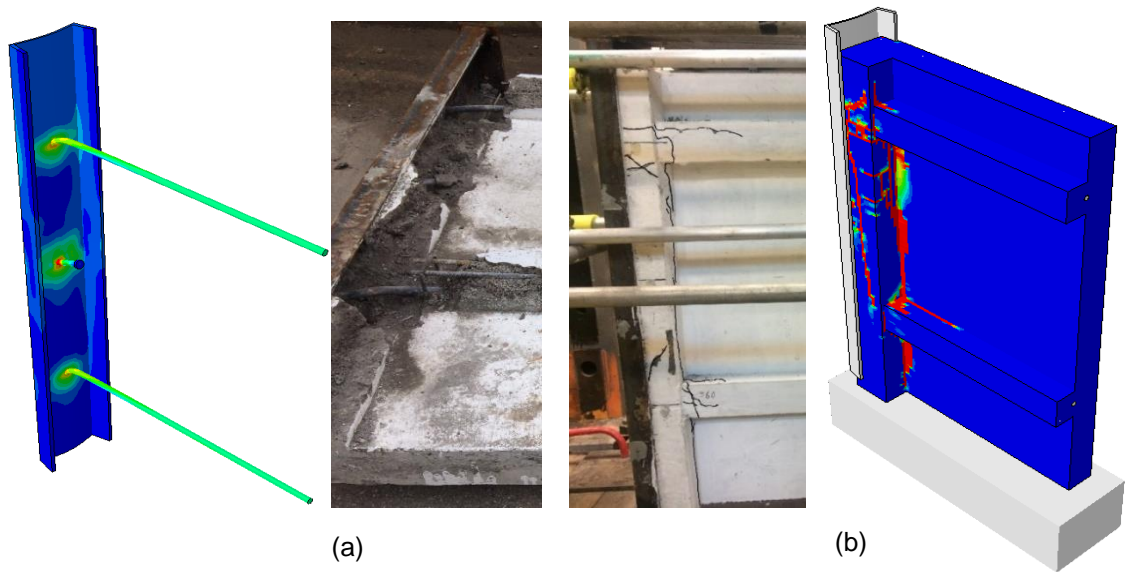
Figure 6-40: Comparison between the FEA model and T2-ULWC specimen with WWSS with dowels (a): shear stud connectors' failure, (b) concrete slab failure

6.11 Parametric study

The elaborated FEA model of the push-out test is used to carry out a parametric study. The variable parameters investigated in the FEA parametric study were the strengths for different types of concrete (NWC, LWC and ULWC) and the diameter of the shear connection systems (WWSS, WWSS with dowels). The concrete strength for all types of concrete varied between 20N/mm^2 to 35N/mm^2 and the connection system diameter varied between 16mm, 19mm, 20mm and 22mm, and the height of the shear studs between 75mm and 100mm.

The FEA models for the push-out test with WWSS with diameters of 16mm and 22mm, heights of 75mm and 100mm and WWSS with dowels with diameters of 16mm and 22mm were developed. These FEA models contained the same types of elements, boundary conditions and contact model with that of the calibrated FEA model, with 19mm diameter for the WWSS and 20mm with WWSS with dowels.

The results of the FE parametric study are summarised in Tables 6-3 & 6-4. The load-slip curves of the FE models with WWSS dimensions of 16×75, 19×100 and 22×100mm and with 16mm, 20mm and 22mm dowels diameters are illustrated in Figures A-1-A-6 in Appendix A. These load-slip curves demonstrated that the FE models with the same diameter had different slip stiffness, where the failure loads and slips varied with the concrete strengths. The slip results were also

compared for the FE models with different shear connection systems' dimensions at concrete strengths of 20, 30 and 35N/mm^2, as shown in Figures A-7-A-12 in Appendix A. It has been shown that the slip stiffness of the shear connection systems is influenced by the diameters of the shear connection system, since the slip stiffness of the FE models increased with the increase of the diameter of the shear connection system. The FEA of the shear connection systems also demonstrated how the failure loads were dependent on the diameter of the shear connection system. For the shear connection system with the same concrete strengths, the failure loads increased with an increase in the shear connection systems' diameters.

Table 6-3: Results of the failure loads and slips of the FEA parametric study of web-welded shear stud connection system (WWSS)

Shear Connection Type	Concrete Type	Concrete Strength		E_c (MPa)	Failure Load (kN) of the FEA Model			Ultimate Slip (mm) of the FEA Model		
		f_c (MPa)	f_t (MPa)		16×75mm	19×100mm	22×100mm	16×75mm	19×100mm	22×100mm
WWSS	NWC	20	2.12	28608	71.85	84.15	93.47	15.47	8.15	20.95
WWSS	NWC	25	2.45	29962	75.45	87.4	97.45	14.58	8.78	18.69
WWSS	NWC	30	2.56	31187	78.25	90.58	101.85	13.45	9.27	17.24
WWSS	NWC	35	2.78	32308	81.65	93.85	105.42	12.45	10.45	16.78
WWSS	NWC	38.52	2.88	33047	82.36	96.78	108.23	11.21	9.27	15.85
WWSS	LWC	20	1.45	17183	61.68	68.65	78.69	19.47	17.86	21.95
WWSS	LWC	25	1.52	17996	64.65	72.85	82.12	18.36	18.47	19.62
WWSS	LWC	30	1.83	18731	67.85	75.85	85.45	17.45	19.14	17.48
WWSS	LWC	32.32	1.61	31719	69.65	78.75	88.74	15.14	17.90	16.80
WWSS	LWC	35	2.11	19405	71.47	80.24	90.34	14.75	16.85	15.47
WWSS	ULWC	20	1.36	9989	47.65	55.74	68.23	13.96	20.15	11.96
WWSS	ULWC	25	1.42	10461	50.48	58.96	71.85	15.28	19.78	13.14
WWSS	ULWC	30	1.70	10889	53.94	61.78	74.65	16.37	17.86	15.78
WWSS	ULWC	35	1.98	11281	56.98	63.45	77.58	19.55	15.96	17.95

Table 6-4: Results of the failure loads and slips of the FEA parametric study of web-welded shear stud with dowels(WWSS with dowels)

Shear Connection Type	Concrete Type	Concrete Strength		Ec (MPa)	Failure Load (kN) of the FEA Model			Ultimate Slip (mm) of the FEA Model		
		fc (MPa)	ft (MPa)		d 16mm	d 20mm	d 22mm	d 16mm	d 20mm	d 22mm
WWSS with dowels	NWC	20	2.12	28608	84.95	100.12	114.26	13.78	14.52	22.45
WWSS with dowels	NWC	25	2.45	29962	87.56	103.87	118.78	12.45	13.45	20.45
WWSS with dowels	NWC	30	2.88	31187	93.74	106.98	121.85	11.65	12.26	18.96
WWSS with dowels	NWC	35	3.2	32308	96.45	110.72	125.85	10.98	11.44	16.87
WWSS with dowels	NWC	37.3	3.34	31937	97.63	113.54	127.66	10.04	12.84	15.64
WWSS with dowels	LWC	20	1.45	17183	68.86	84.32	98.78	24.95	25.78	31.45
WWSS with dowels	LWC	25	1.52	17996	72.95	87.69	102.47	22.78	24.56	28.95
WWSS with dowels	LWC	30	1.83	18731	76.12	90.85	105.96	19.78	23.45	27.95
WWSS with dowels	LWC	35	2.11	19405	79.78	93.12	108.23	18.85	22.65	26.78
WWSS with dowels	LWC	36.8	2.12	19635	82.78	96.62	110.45	17.42	21.79	25.78
WWSS with dowels	ULWC	20	1.38	9989	55.84	69.12	83.73	24.16	28.04	28.98
WWSS with dowels	ULWC	25	1.42	10461	58.96	74.01	86.18	23.17	25.78	25.12
WWSS with dowels	ULWC	30	1.70	10889	61.98	79.12	89.47	21.35	24.56	22.78
WWSS with dowels	ULWC	35	1.98	11281	64.45	85.78	92.78	19.95	23.65	20.17

6.12 Summary

The FEM can be classified into four different steps, which include the geometry and material modelling, boundary and constraint conditions, output analysis and post-processing of the results. This chapter emphasises the importance of providing accurate material properties and choosing the right element and mesh types for all different components of the prefabricated ultra shallow flooring system. In addition, the boundary and constraints conditions of the FEM provide the same external environments as the experimental push-out test series. The contact interactions between each component are explained in detail in this chapter to allow for the modelling of the interaction between each component during analysis.

The proposed 3-D finite element model has been validated with the experimental results, as described in **Chapter 5**. It has been proven to be able to accurately and reliably simulate the overall behaviour of the prefabricated ultra shallow flooring system subjected to longitudinal shear slip. A parametric study is undertaken to investigate the behaviour of the prefabricated ultra shallow flooring system with increases and decreases in the concrete strength and shear connection systems' diameters and heights. The chosen concrete strengths were $20N/mm^2$, $25N/mm^2$, $30N/mm^2$ and $35N/mm^2$. Three different dimensions of WWSS were used for the parametric study (16×75mm, 19×100mm and 22×100mm) with three different diameters of the steel dowels (16, 20mm and 22mm). The prefabricated ultra shallow flooring system has demonstrated an increase in the shear resistance of the shear connection systems, with an increase in concrete strength for the different types of concrete. Additionally, the shear resistance of the shear connection systems increases with an increase in the WWSS diameter, along with height and dowel diameters, due to the increase of the shear interaction area, as well as the concrete bearing area.

Chapter 7 : Analytical study of the shear connection systems

7.1 Introduction

The push-out tests provided comprehensive information on the behaviour and shear resisting capacity of the shear connection systems used for the prefabricated ultra shallow flooring system. The results of the push-out tests are analysed to conclude a calculation method for the shear resistance of the shear connection systems. The calculation method has verified the FEA results. The load-slip model for the shear connection systems is provided in this chapter, based on regression analysis of the load–slip curves obtained from the push-out tests. This chapter also presented the proposed design methodology of the bending capacity of the prefabricated ultra shallow flooring system.

7.2 Shear strength of the web-welded shear studs (WWSS) and WWSS with dowels

7.2.1 Existing design formula for headed shear stud connectors

For the headed shear stud connectors, design codes are available to determine their shear resistance (P_{Rd}). In Eurocode 4 (EN1994-1-1, 2004), the shear strength of the headed shear studs is given as:

$$P_{Rd} = \min\left(\frac{\frac{0.8f_u\pi d^2}{4}}{\gamma_v}, \frac{0.29\alpha d^2\sqrt{f_{ck}E_c}}{\gamma_v}\right) \tag{7.1}$$

Where f_u is the specified ultimate strength of the stud ($\leq$ 500MPa), d is the diameter of the stud, γ_v is the partial factor (1.25), f_{ck} is the concrete cylinder compressive strength, E_{cm} is the secant modulus of concrete, $\alpha = 0.2(h_s/d +1)$ for $3 \leq h_s/d \leq 4$ or $\alpha = 1.0$ for $h_s/d \geq 4$, h_s is the overall height of the stud.

In Annex C of Eurocode 4 (EN1994-2, 2005), the shear strength of the horizontal lying shear stud connector, which causes a splitting in the direction of slab thickness, is specified by:

$$P_{Rd,L} = \frac{1.4k_v(f_{ck}d a_r^{`})^{0.4}(a/s)^{0.3}}{\gamma_v} \tag{7.2}$$

Where:

$a_r^{`}$ is the effective edge distance; = a_r - cv-$\varnothing_s$/2 $\geq$ 50mm;

k_v = 1 for shear connection in an edge position,

   = 1.14 for shear connection in a middle position;

y_v is a partial factor (1.25);

f_{ck} is the characteristic cylinder strength of the concrete at the age considered, in N/mm^2;

d is the diameter of the shank of the stud with 19≤ d≤ 25mm;

h is the overall height of the headed stud with h/d ≥ 4;

a is the horizontal spacing of studs with 110 ≤ a ≤ 440mm;

s is the spacing of stirrups with both a/2 ≤ s ≤ a and $s/a_r^`$ ≤ 3;

$Ø_s$ is the diameter of the stirrups with $Ø_s$ ≥8mm;

$Ø_\ell$ is the diameter of the longitudinal reinforcement with $Ø_\ell$ ≥10mm;

C_v is the vertical concrete cover in mm.

In ANSI/AISC 360-10 (2010), the nominal shear strength of the headed shear stud connectors embedded in concrete (used in composite beams with a concrete slab) is specified by:

$$P_s = 0.5A_s\sqrt{f_{ck}\,E_c} \leq 0.75f_u A_s \tag{7.3}$$

In AASHTO (2004), the shear strength of the shear stud connector embedded in the concrete decking may be calculated as:

$$P_s = Ø0.5A_s\sqrt{f_{ck}\,E_c} \leq 0.75\,f_u\,A_s \tag{7.4}$$

Where Ø is the resistance factor for shear connectors (=0.85).

Chinn (1965) proposed a formula for estimating the shear strength of the headed stud shear connectors embedded in LWC. The shear strength of the headed shear stud is given as:

$$P_s = 39.22d^{1.766} \tag{7.5}$$

Where d is the stud diameter.

Ollgaard et al. (1971) developed a formula for the ultimate strength of the stud (P_s), the shear strength of the headed shear studs is as follows:

$$P_s = 1.106A_s f_c^{`0.3} E_c^{0.44} \tag{7.6}$$

To this end, Eqs. 7.1-7.4 were developed for headed shear stud connectors embedded in NWC. The latter two studies have been conducted in order to establish the shear strength of headed shear stud connectors embedded in LWC, however there is no design guide available for the design of the new shear connection systems, as these are a new proposal that shall be developed through this PhD. Therefore, the design of these new shear connection systems with the use of ULWC requires further calibration with test data, as described in the next section.

7.2.2 Proposed formula for web-welded shear studs (WWSS) and WWSS with dowels

An equation is suggested based on the nonlinear regression analysis of the push-out tests results, using the statistic software MINITAB (2017).

The shear strength (P_{sd}) from the WWSS and the one from the WWSS with dowels is treated as an independent variable. The f_{ck}, d, and a_r were considered dependent variables with respect to the shear strength of the connection system. For specimens in group T1 and T2, shear strength is assumed as an exponential function of the above parameters:

$$P_{sd} = 1.873(f_{ck} \, d \, a_r)^{0.835} \leq 0.8f_u A_s \tag{7.7}$$

Where P_{sd} is the shear resistance of shear stud or dowel, f_{ck} is the cylinder compressive strength of concrete, d is the diameter of stud or dowel, and a_r is the distance from first stud or dowel to the top of concrete, f_u is the ultimate tensile strength of the material of the stud or dowel which should not be greater than 500N/mm^2, and A_s is the cross-sectional area of the shear the stud or dowel.

The shear resistances of both connection systems, as predicted by various formulas, are compared with the test results and are shown in Table 7-1.

From the results shown in Table 7-1 and Figure 7-1, the proposed Equation (Eq. 7.7) demonstrates a good fit. Ollgaard et al. (1971) gives the least reliable predictions, which overestimate the test results by about 36%. The formula given in AASHTO (2004) is almost identical to the design formula given by ANSI/AISC 360-10 (2010), except for the value of the reduction factor (ANSI adopted 0.5 instead of Ø0.5), see Eqs. 7.3 & 7.4. Therefore, the AASHTO (2004) offers lower predictions than the ones offered by ANSI/AISC 360-10 (2010). Eurocode 4

(EN 1994-1-1, 2004) (Eq. 7.1) provides the second most conservative predictions compared to Eq.7.6.

It is worth noting that the exiting formulas given in the aforementioned codes are strictly not applicable to the new shear connection systems with the use of LWC and ULWC. Therefore, considering both accuracy and reliability, the proposed formula (Eq. 7.7) offers a reasonable prediction when compared to the mean and COV values of Eq. 7.7 and specifications and researchers, as shown in Figure 7-1. It is recommended for use in the design of the prefabricated ultra shallow flooring system with both shear connection systems.

The significance of Eq. 7.7 can be summarized in updating the Eurocode 4 (EN 1994-1-1, 2004) particularly in the area of using the new shear connection systems with LWC and ULWC. As there is no design guide available within the scope of Eurocode 4 (EN 1994-1-1, 2004) for the design of the new shear connection systems with the use of lightweight concrete.
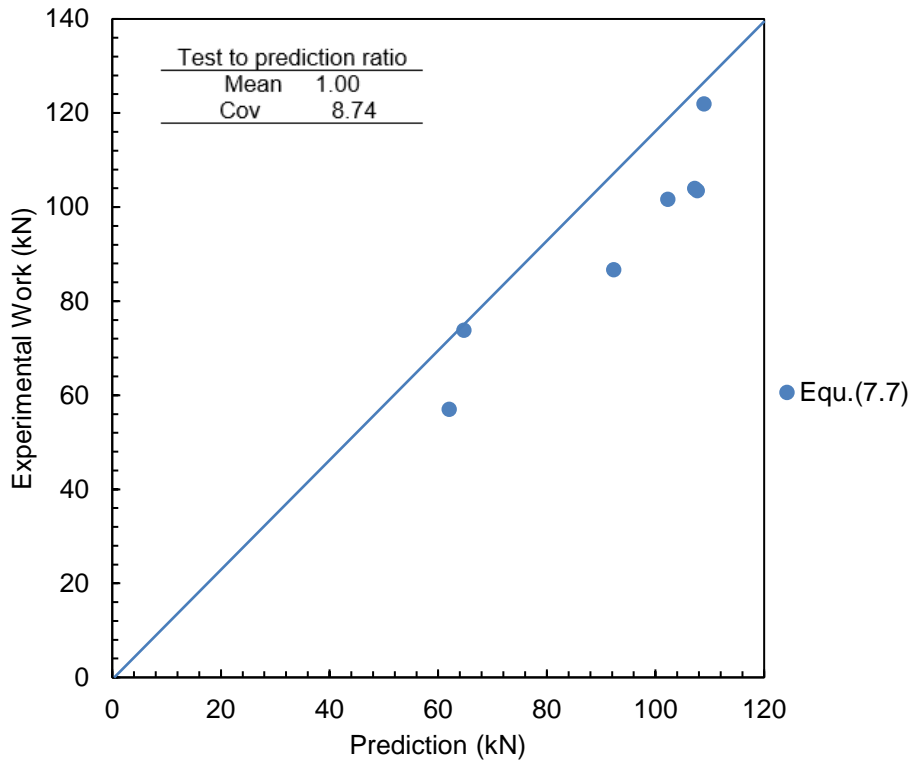
(a) Comparisons between the test results and predictions by Eq. 7.7
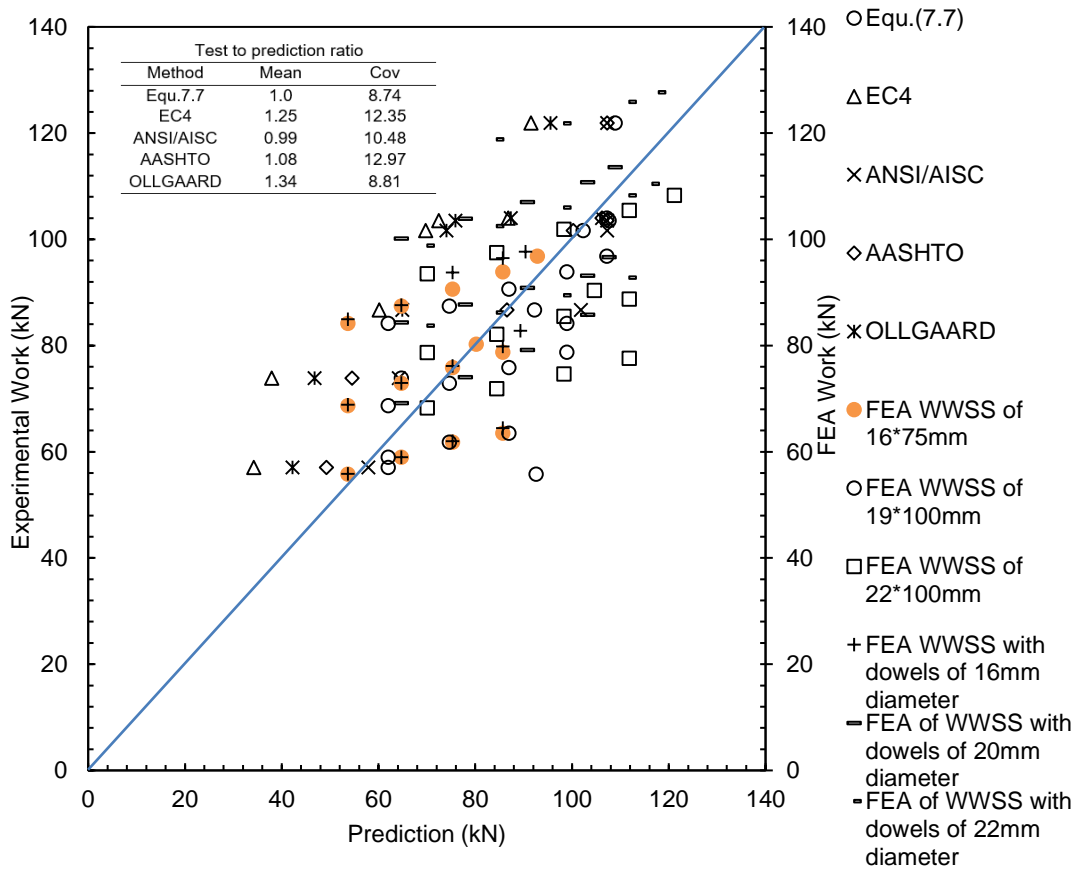
(b) Comparisons between the test, FEA results and predictions by specifications and researchers

Figure 7-1: Comparison between test, FEA results and predictions by Eq. 7.7, specifications and researchers

Table 7-1: Push-out test results and predictions by different equations for testing group T1 and T2

Specimens	P_{test} (kN)	Predictions by different design methods									
		P_{EC4} by Eq. 7.1	P_{test}/P_{EC4}	P_{AN} by Eq.7.3	P_{test}/P_{AN}	P_{AA} by Eq.7.4	P_{test}/P_{AA}	P_{OL} by Eq.7.6	P_{test}/P_{OL}	P_{sd} by Eq.7.7	P_{test}/P_{sd}
T1-NWC-2	103.97	90.72652	1.14	106.26	0.97	106.26	0.97	87.40	1.18	107.21	0.97
T1-LWC	86.70	75.25322	1.15	101.85	0.85	86.57	1.00	64.92	1.33	92.30	0.94
T1-ULWC	57.02	42.83225	1.33	57.97	0.98	49.27	1.15	42.26	1.347	62.01	0.92
T2-NWC	121.90	91.58101	1.33	107.27	1.13	107.27	1.13	95.58	1.27	108.92	1.12
T2-LWC-1	101.65	87.18977	1.16	107.27	0.94	100.30	1.01	74.07	1.37	102.30	0.99
T2-LWC-2	103.51	90.60071	1.14	107.27	0.96	107.27	0.96	75.96	1.36	107.70	0.96
T2-ULWC	73.83	47.45956	1.55	64.23	1.14	54.59	1.35	46.83	1.57	64.73	1.14

7.2.3 Verification of the shear resistance calculation method with the finite element analysis results

The method for calculating the shear resistance of the connection systems (Eq. 7.7) is represented by two terms: the compressive resistance of the concrete, and the tensile resistance of the steel elements, i.e. studs or dowels. The method of combining the compressive resistance of the concrete and tensile resistance of the steel elements to calculate the shear resistance of the shear connection systems is based on the failure mechanism as shown in the push-out tests.

The results of the FEA parametric study were used to further verify the proposed formula (Eq. 7.7) obtained for calculating the shear resistance of the shear connection systems. The FEA parametric study investigated both the shear connection systems with the concrete strengths that varied between $20N/mm^2$ to $35N/mm^2$, dowels diameters of 16mm, 20mm and 22mm and studs of 16×75mm, 19×100mm and 22×100mm. The results of the FEA were compared with the calculated results using Eq. 7.7, which was the method obtained from the regression analysis.

The comparison showed that the calculated shear resistance of the shear connection systems using Eq. 7.7 is (lower or higher) than that obtained in the FEA, as demonstrated in Tables B-1-B-6 in Appendix B. The average ratios for the shear resistance of the calculation to FEA were 0.962, 1.108 and 1.08 for the WWSS with dimensions of 16×75mm, 19×100m and 22×100mm, respectively. In addition, the average ratios for the shear resistance of the calculation to FEA were 0.894, 0.954 and 0.901 for the WWSS with dowels with diameters of 16mm, 20mm and 22mm, respectively.

7.3 Load–slip behaviour of the shear connection systems

To analyse the prefabricated ultra shallow flooring system for load–slip response and ultimate strength, it is necessary to model the load–slip (P–s) behaviour of the shear connection systems. This section proposes a suitable load–slip model for the WWSS, and WWSS with dowels based on a regression analysis of the load–slip curves obtained from tests.

7.3.1 Load-slip models for headed shear stud connectors

Ollgaard et al. (1971) proposed an expression of the load–slip relationship, based on curved fitting with their test data, as follows:

$$\frac{P}{P_u} = \left(1 - e^{-18\delta}\right)^{0.4} \tag{7.8}$$

Where P is the applied shear force, P_u is the shear resistance of the connection, δ is the slip in inch due to applied load P.

However, a modification to the above was made by (Lorenc and Kubica, 2006) on Eq.7.8, based on experimental calibration with test data to arrive at different coefficients:

$$\frac{P}{P_u} = \left(1 - e^{0.55\delta}\right)^{0.3} \tag{7.9}$$

Xue et al. (2008) introduced an expression to predict the load–slip relationship based on 30 push-out tests of headed shear studs and the analysis of other expressions. The expression is as follows:

$$\frac{P}{P_u} = \frac{\delta}{0.5 + 0.97\delta} \tag{7.10}$$

Where δ is the slip in mm.

An and Cederwall (1996) proposed two expressions based on a nonlinear regression analysis of their test results to predict the load–slip behaviour of headed shear stud connectors in NWC and high-performance concrete (HPC) after cyclic loading, as follows:

$$\frac{P}{P_u} = \frac{2.24(\delta - 0.058)}{1 + 0.98(\delta - 0.058)} \quad \text{for NWC,} \tag{7.11a}$$

$$\frac{P}{P_u} = \frac{4.44(\delta - 0.031)}{1 + 4.24(\delta - 0.031)} \quad \text{for HPC,} \tag{7.11b}$$

Where δ is the slip in mm.

Gattesco and Giuriani (1996) proposed an alternative empirical model for the load-slip behaviour, their model being as follows:

$$\frac{P}{P_u} = \alpha\sqrt{1 - e^{-\beta\delta/\alpha}} + \gamma\delta \tag{7.12}$$

Where a, b, and c are empirical parameters and their values are 0.97, 1.3, and 0.0045 mm^{-1}, respectively, obtained by curve fitting with their test data. Eq.712 is a modified model to the models proposed by (Aribert, 1990) and by (Johnson, 1991).

The following section extends the existing models, which are developed for headed shear studs, to predict the load–slip behaviour of the WWSS and WWSS with dowels.

7.3.2 Load-slip models for web-welded shear studs (WWSS) and WWSS with dowels

The experimental non-dimensionalised load (P/P$_u$) and slip (d) curves of the specimens in group T1 and T2 with WWSS and WWSS with dowels embedded in different concrete types, are shown in Figure 7-2. It can be observed that the generalised load–slip curves are very close to each other for specimens with similar concrete types and similar shear connectors. Therefore, it is proposed that the load–slip model should be different for specimens with different concrete types and different shear connection systems.

On the basis of the measured values and the shape of the experimental curves, several scholars (Xue et al., 2008; Ollgaard et al., 1971; Gattesco and Giuriani, 1996) proposed constitutive laws, which were adopted for the theoretical analysis of both proposed systems (WWSS) and (WWSS with dowels).

$$\frac{P}{Pu} = \frac{A\delta}{0.5 + B\delta} \tag{7.13a}$$

$$\frac{P}{Pu} = (1 - e^{A\delta})^{B} \qquad (7.13b)$$

$$\frac{P}{Pu} = A\sqrt{1 - e^{-B\delta/A}} + C\delta \qquad (7.13c)$$

Where A, B and C are the coefficients.

Based on the test results, a nonlinear regression analysis is carried out to obtain the coefficients in Eqs. 7.13a-c. From the regression analysis, different values of A, B, and C are proposed for NWC, LWC, and ULWC and these are summarised in Table 7-2. The comparisons between generalised load–slip curves from Eqs. 7.13a-c and the test results are also shown in Figure 7-2. It is observed that the proposed models for describing load–slip behaviours agree well with the experimental curves, especially for the specimens with LWC. Equation 7.13a is the simplest among the three equations and it is therefore recommended for use in predicting the load–slip response of both shear connection systems using different concrete materials as follows:

For specimens with (WWSS):

$$\frac{P}{Pu} = \frac{4.02\delta}{1 + 4.16\delta} \text{ , for NWC} \qquad (7.14a)$$

$$\frac{P}{Pu} = \frac{0.98\delta}{1 + 0.96\delta} \text{ , for LWC} \qquad (7.14b)$$

$$\frac{P}{Pu} = \frac{1.92\delta}{1 + 1.77\delta} \text{ , for ULWC} \qquad (7.14c)$$

For specimens with WWSS with dowels:

$$\frac{P}{Pu} = \frac{1.81\delta}{1 + 1.95\delta} \text{ , for NWC} \qquad (7.15a)$$

$$\frac{P}{Pu} = \frac{1.09\delta}{1 + 1.25\delta} \text{ , for LWC} \qquad (7.15b)$$

$$\frac{P}{Pu} = \frac{0.23\delta}{1 + 0.21\delta} \text{ , for ULWC} \qquad (7.15c)$$

Table 7-2: Coefficients for proposed design formula

Shear connection type	Concrete type	A	B	C
Eq.7.13a				
WWSS	NWC	4.02	4.16	-
	LWC	0.98	0.96	-
	ULWC	1.92	1.77	-
WWSS with dowels	NWC	1.81	1.95	-
	LWC	1.09	1.25	-
	ULWC	0.23	0.21	-
Eq. 7.13b				
WWSS	NWC	-0.5	0.35	-
	LWC	-0.2	0.35	-
	ULWC	-0.3	0.4	-
WWSS with dowels	NWC	-0.2	0.35	-
	LWC	-0.1	0.35	-
	ULWC	-0.05	0.35	-
Eq. 7.13c				
WWSS	NWC	0.9	0.75	0.0095
	LWC	0.85	0.45	0.0075
	ULWC	0.9	0.5	0.006
WWSS with dowels	NWC	0.85	0.35	0.01
	LWC	0.75	0.3	0.009
	ULWC	0.75	0.35	0.0075
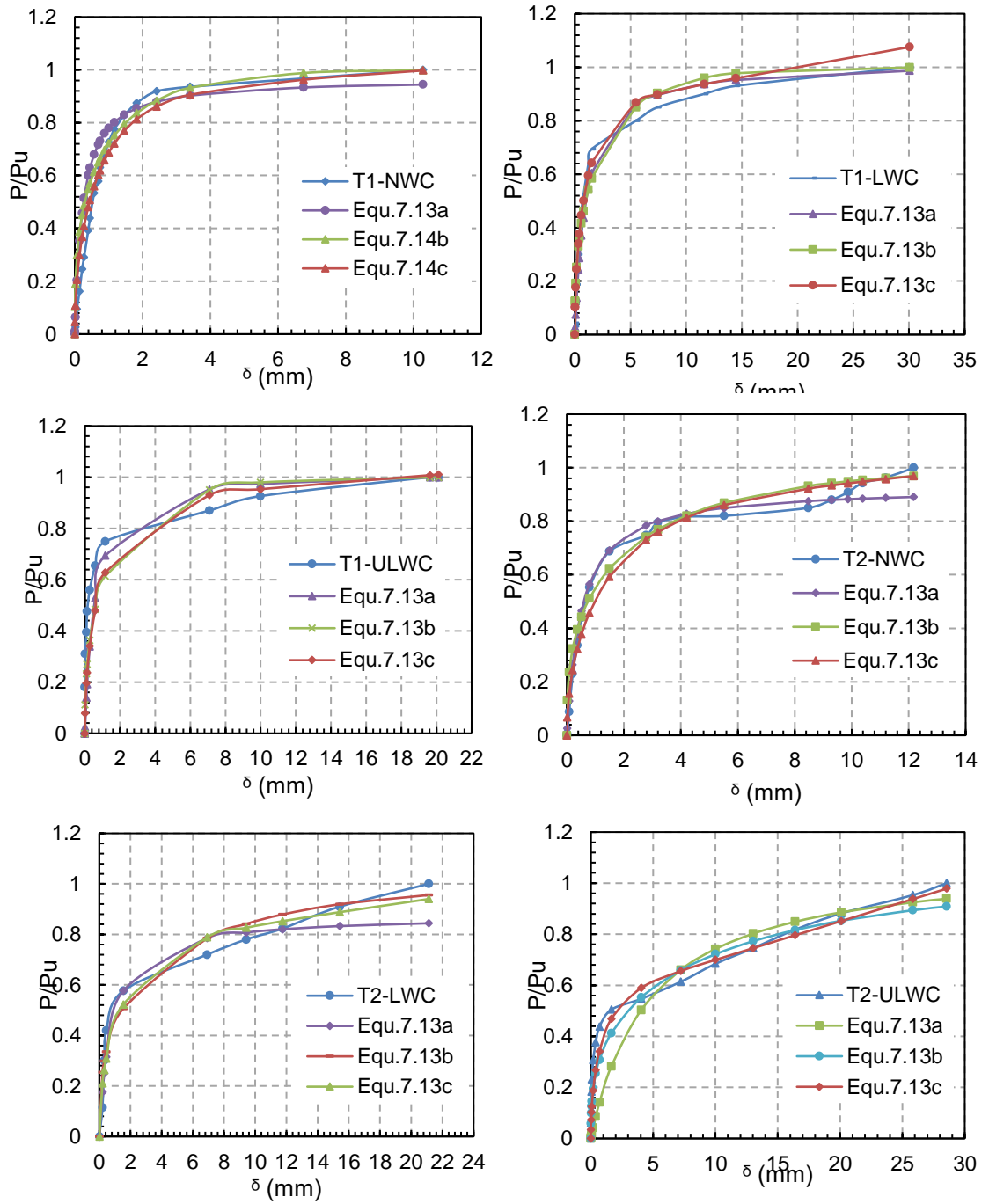
Figure 7-2: Load–slip relationships

7.4 Design moment capacity of the prefabricated ultra shallow flooring system using (BS 5950-3.1,1990) and Eurocode 4 (EN1994-1-1, 2004)

British Standards (BS 5950-3.1, 1990) and Eurocode 4 (EN1994-1-1, 2004) determine the design moment capacity of a composite section by using both stress blocks. This method is based on plastic theory, which assumes that the stresses within the cross section reach a constant value in both tension and compression. The methodology of this method is summarised in the following sections.

A flow chart of the design method for moment resistance of the prefabricated ultra shallow flooring system is illustrated in Chart 7.1.
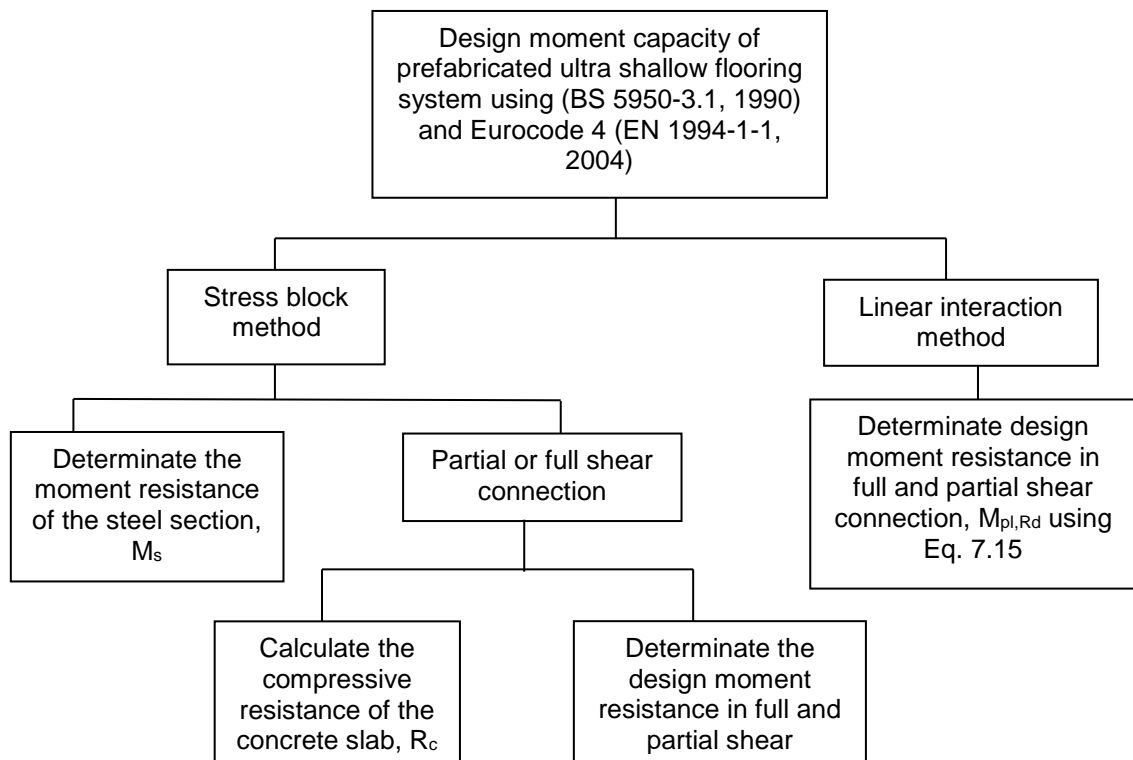
Chart 7.1: Flow chart of the designing steps of prefabricated ultra shallow flooring system in accordance to BS5950 (BS 5950-3.1, 1990) and Eurocode 4 (EN1994-1-1, 2004)

7.4.1 Stress block method

The assumptions specified by the BS (BS 5950-3.1:1990) and Eurocode 4 (EN1994-1-1, 2004) in applying the stress block methods are as follows:

- The structural steel is stressed to a uniform yield stress in both tension and compression.
- The concrete tensile strength is neglected.

- In a full shear connection, the concrete is stressed to a uniform compression over the depth above the plastic neutral axis (P.N.A).

- In partial shear connection, the concrete is stressed to a uniform compression up to the depth where concrete can develop a compressive resistance that equals the longitudinal shear resistance of the shear connectors.

The BS5950 specifies that a yield stress of 355N/mm^2 (MPa) should be used as the steel stress of both tension and compression. The different formulas of the concrete compressive stress, $\sigma_{c,Rd}$, are specified in the (BS 5950-3.1,1990) and Eurocode 4 (EN1994-1-1, 2004), as shown in Table 7-3.

Table 7-3: Concrete compressive stress, $\sigma_{c,Rd}$, specified by
(BS 5950-3.1,1990) and Eurocode 4 (EN1994-1-1, 2004)

(BS 5950-3.1,1990)	$\sigma_{c,Rd}=0.45f_{cu}$	f_{cu} is the concrete characteristic cube strength (N/mm^2)
Eurocode 4 (EN1994-1-1, 2004)	$\sigma_{c,Rd}=0.85f_{cd}$	f_{cd} is the concrete design compressive cylinder strength (N/mm^2)

The stress block diagrams of a typical downstand composite beam are shown in Figure 7-3. The forces within the cross sections are in an equilibrium state. The moment capacity of the cross sections is calculated by taking moments about the plastic neutral axis (P.N.A). The stress block diagrams of the prefabricated ultra shallow flooring system are shown in Figure 7-4. The optimum cross-section with full depth is used to determine the design moment resistance of the ultra shallow flooring system.
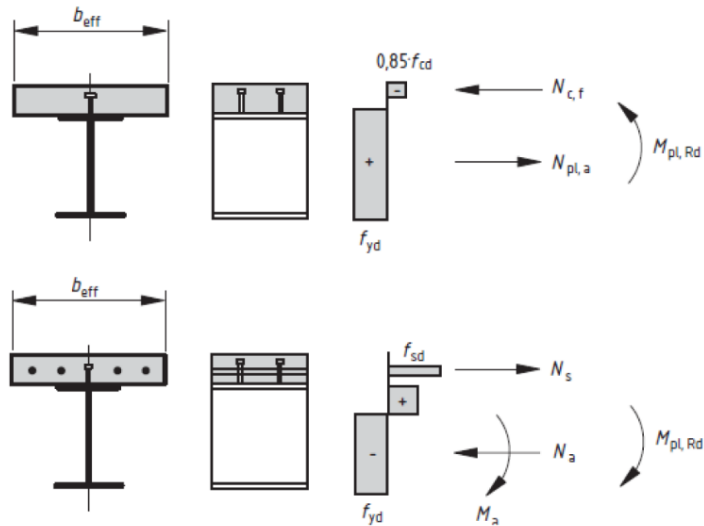
Figure 7-3: Stress block diagrams of downstand composite beam Eurocode 4 (EN1994-1-1, 2004)
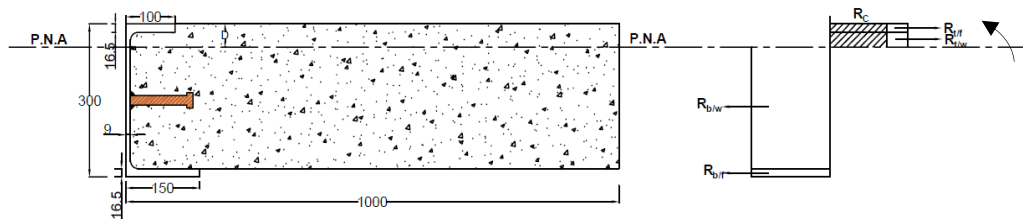
Figure 7-4: Stress block diagram of the optimum cross sections of the prefabricated ultra shallow flooring system in full shear connection

7.4.2 Linear interaction method

The linear interaction method is a simplified relationship between the moment resistance and the degree of shear connection, as expressed in Eq. 7.15. A comparison between the linear interaction and the stress block methods is illustrated in Figure 7-5. It is revealed that the linear interactive method gives conservative results.

$$M_{Rd} = M_{pl,a,Rd} + \eta (M_{pl,Rd} - M_{pl,a,Rd}) \tag{7.15}$$

Where: M_{Rd} is the design moment resistance of the composite section in partial shear connection;

$M_{pl,a,Rd}$ is the plastic moment resistance of the steel section;

η is the degree of shear connection;

$M_{pl,Rd}$ is the design moment resistance of the composite section in full shear connection.
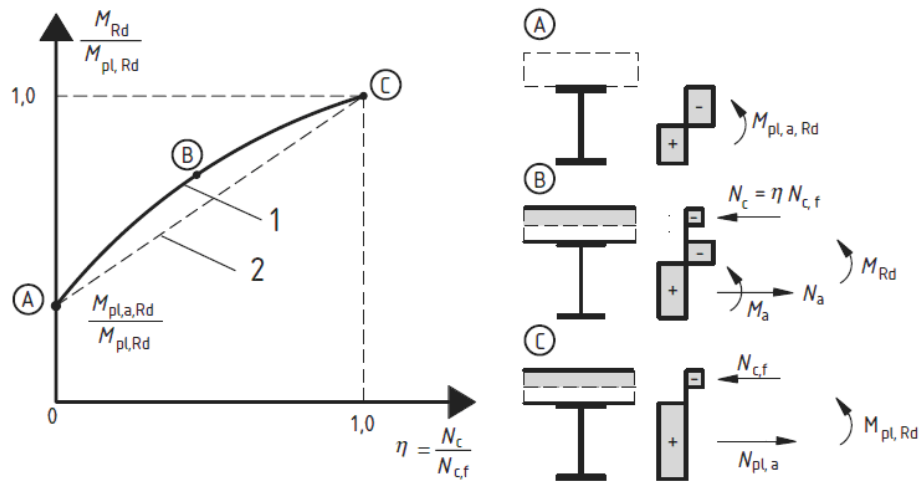
Figure 7-5: Comparisons between the stress block and linear interaction methods Eurocode 4 (EN1994-1-1, 2004)

7.4.3 Design moment capacity

The design moment capacity of the prefabricated ultra shallow flooring system in full and partial shear connections is calculated, in accordance with the (BS 5950-3.1:1990) and Eurocode 4 (EN1994-1-1, 2004). The stress block method is used to calculate the design moment capacities of both the full and partial shear connections. The linear interactive method is used to calculate the design moment capacities of the partial shear connection. A concrete mean compressive cube strength of $30N/mm^2$ is used to calculate the concrete compressive stress, $\sigma_{c,Rd}$. The steel yield stress of $355N/mm^2$ is used for both tension and compression.

7.4.3.1 Moment resistance of the steel section (M_s)

The plastic stress block method is used to determine the moment resistance of the steel section. The stress block diagram is illustrated in Figure 7-6. The tensile stress of $355N/mm^2$ is used for both tension and compression.
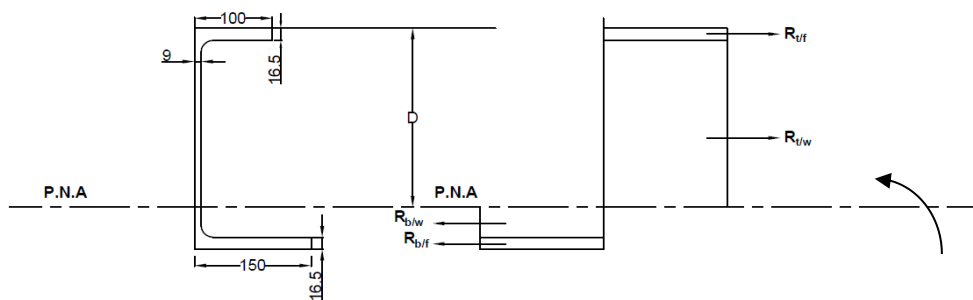
Figure 7-6: Stress block diagram of the steel section

7.4.3.1.1 Determine the depth of plastic neutral axis (P.N.A)

An equilibrium of tension and compression, expressed in Eq. 7.16, is used to determine the depth of P.N.A, D.

$$R_{t/f} + R_{t/w} = R_{b/f} + R_{b/w} \qquad (7.16)$$

Where: $R_{t/f}$ is the resistance of the top flange ($A_{t/f}\,P_y$);

$R_{t/w}$ is the resistance of the top flange ($A_{t/f}\,P_y$);

$R_{b/w}$ is the resistance of the web post of the bottom tee ($A_{b/w}\,P_y$)

$R_{b/f}$ is the resistance of the bottom flange ($A_{b/f}\,P_y$)

By substituting the steel stress and the cross sectional areas of the steel elements into Eq. 7.15, hence D = 195.83mm.

7.4.3.1.2 Determine plastic moment capacity

Taking moments about P.N.A,

$$M_s = R_{t/f}\,D_{t/f} + R_{t/w}\,D_{t/w} + R_{b/w}\,D_{b/w} + R_{b/f}\,D_{b/f} \qquad (7.17)$$

Where: M_s is the plastic moment resistance of the steel section

$D_{t/f}$ is the distance between the $R_{t/f}$ and P.N.A,

$D_{t/w}$ is the distance between the $R_{t/w}$ and P.N.A,

$D_{b/w}$ is the distance between the $R_{b/w}$ and P.N.A,

$D_{b/f}$ is the distance between the $R_{b/f}$ and P.N.A.

By substituting the resistance of the steel elements and their distances to P.N.A into Eq. 7.17, hence, M_s =257.80kNm.

7.4.3.2 Full shear connection

The principle of the full shear connection is that the longitudinal shear resistance of the shear connectors, R_q, is greater than or equal to the full compressive resistance of the concrete slabs, due to the full composite action, R_c, as $R_q \geq R_c$. The assumptions made in applying the full shear connection to the design moment capacity calculation of the prefabricated ultra shallow flooring system are:

- Concrete tensile strength is neglected.
- Local web post buckling of the steel section is prevented by the partially concrete encasement.

- The structural steel is stressed to a uniform yield stress in both tension and compression.

- The concrete is stressed to a uniform compression over the depth above the P.N.A.

- The shear resisting capacities of the shear connectors are not affected by the position of the P.N.A.

The steps involved in applying the stress block method for determining the design moment capacities of the prefabricated ultra shallow flooring system in full shear connection are:

1. To calculate the compressive resistance of the concrete slabs in full composite action, R_c, by using the equilibrium of the forces within the cross section.
2. To determine the depth of the P.N.A.
3. To calculate the design moment capacity in full shear connection, $M_{pl,Rd}$, by taking moments about the P.N.A.

There are two types of cross sections for the proposed slab specimen: cross sections with WWSS and cross sections with WWSS with dowels. The full compressive resistance, R_c, between both cross sections is the same because the steel section of both cross sections is the same. This leads to the same depths of the P.N.A for both cross sections. Furthermore, the design moment capacities in the full shear connection, $M_{pl,Rd}$, between the both cross sections are the same, as the moment capacities are calculated by taking moment about the P.N.A. The details of the calculation are explained further below.

7.4.3.2.1 Full compressive resistance of the concrete slabs, R_c

The equilibrium of the forces within the cross section, expressed in Eq. 7.18, is used to determine the full compressive resistance of the concrete slabs, R_c.

$$R_{t/f} + R_{t/w} + R_c = R_{b/w} + R_{b/f} \tag{7.18}$$

Where: $R_{t/f}$ is the resistance of the top flange ($A_{t/f}P_y$);

$R_{t/w}$ is the resistance of half of the web post ($A_{t/w}P_y$);

R_c is the full compressive resistance of the concrete slabs due to full composite action;

$R_{b/w}$ is the resistance of half of the web post, $(A_{b/w}P_y)$;

$R_{b/f}$ is the resistance of the bottom flange $(A_{b/f}P_y)$.

By substituting the cross sectional areas of the steel elements and steel stress, $P_y = 355\text{N/mm}^2$, into Eq. 7.18, Hence, $R_c = 439\text{kN}$.

7.4.3.2.2 Depth of the P.N.A

The depth of the P.N.A is calculated using the full compressive resistance of the concrete slabs, R_c, and the concrete compressive stress, $\sigma_{c,Rd}$.

$$R_c = \sigma_{c,Rd} B_e D \tag{7.19}$$

Where: R_c is the full compressive resistance of the concrete slabs due to   full composite action;

          $\sigma_{c,Rd}$ is the concrete compressive stress;

          B_e is the effective width of the concrete slab;

          D is the depth of the P.N.A.

The concrete compressive stress, $\sigma_{c,Rd}$, is converted using the mean compressive cube strength of 30N/mm^2, in accordance with the (BS 5950-3.1:1990) and Eurocode 4 (EN1994-1-1, 2004). Both methods have given the same value of $\sigma_{c,Rd}$, as shown in Table 7-4. This shows that there is consistency between the (BS 5950-3.1:1990) and Eurocode 4 (EN1994-1-1, 2004). The effective width of the prefabricated ultra shallow flooring system is equal to 1m. The full compressive resistance of the concrete slabs, R_c, is 439kN. The results of the depth of the P.N.A are listed in Table 7-4.

Table 7-4: Depths of the P.N.A of the prefabricated ultra shallow flooring system in full shear connection

Method of design	Mean Compressive Cube Strength (N/mm^2)	$\sigma_{c,Rd}$ (N/mm^2)	R_c (kN)	D(mm)
BS5950 ($\sigma_{c,Rd}$=0.45fcu)	30.0	9	439	48.7
Eurocode 4 (EN1994-1-1, 2004) ($\sigma_{c,Rd}$=0.85f$_{cd}$)	30.0	9	439	48.7

7.4.3.2.3 Design moment capacities of full shear connection, $M_{pl,Rd}$

The design moment capacities of the prefabricated ultra shallow flooring system in full shear connection, $M_{pl,Rd}$, are determined by taking moments about the P.N.A. The results are presented in Table 7-5. The design moment capacity,

$M_{pl,Rd}$, which is obtained using BS5950 and Eurocode 4 (EN1994-1-1, 2004) are the same.

Table 7-5: Design moment capacities of the beam specimen in full shear connection

Method of design	Concrete Cube Strength (N/mm^2)	P_y (N/mm^2)	Depth of P.N.A (mm)	$M_{pl,Rd}$ (kNm)
BS5950	30.0	355	48.7	327
Eurocode 4 (EN1994-1-1, 2004)	30.0	355	48.7	327

7.4.3.3 Partial shear connection

The criterion of the partial shear connection is that the longitudinal shear resistance of the shear connections, R_q, is less than the compressive resistance of slabs due to in full composite action, R_c, as $R_q<R_c$. The ratio of the R_q to the R_c is defined as the degree of shear connection, η ($\eta=R_q/R_c$). The limits of the degree of shear connection specified by both BS5950 and Eurocode 4 (EN1994-1-1, 2004) are $0.4 \leq \eta \leq 1.0$.

The concrete compressive resistance developed in a partial shear connection is equal the longitudinal shear resistance of the shear connection, R_q. The stress block diagrams of the prefabricated ultra shallow flooring system cross sections in a partial shear connection are illustrated in Figure 7-7. The optimum cross section with full depth is used to determine the design moment capacities of the prefabricated ultra shallow flooring system in partial shear connection. The steps in applying the stress block method are as follows:

1. To calculate the longitudinal shear resistance of the connectors, R_q, at a degree of shear connection, η, as $\eta= R_q/R_c$, where R_c is the full compressive resistance of the concrete slabs;
 2. To calculate the depth of concrete in compression, d;
 3. To calculate the depth of the P.N.A using the equilibrium of the forces within the cross section;
4. To determine the design moment capacities in a partial shear connection, M_{Rd}, by taking moments about the P.N.A.
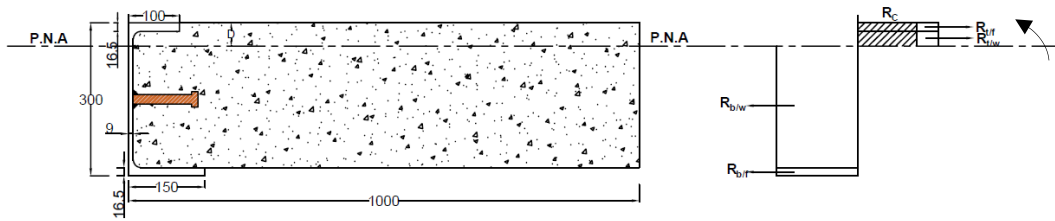
Figure 7-7: Stress block diagrams of the cross sections of the prefabricated ultra shallow flooring system in full shear connection

7.4.3.3.1 Moment resistance of the cross section in degree of shear connection of 0.5

The stress block diagram of the cross section in the degree of shear connection of 0.5 is illustrated below. Figure 7-8 shows the stress block diagram of the cross section in degree of shear connection of 0.5.
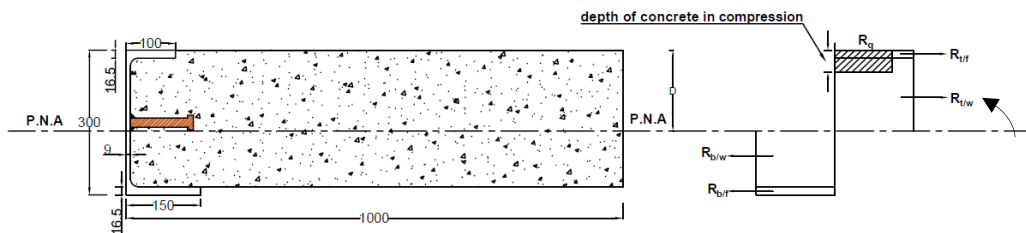
Figure 7-8: Stress block diagrams of the cross sections of the prefabricated ultra shallow flooring system in degree of shear connection of 0.5

7.4.3.3.2 Determine the depth of P.N.A

The longitudinal shear resistance of the shear connections, R_q, is calculated first using the compressive resistance of the concrete slabs, R_c, and the degree of shear connection, η, as $\eta = R_q/R_c$.

The depth of P.N.A, D, is determined using the equilibrium of tension and compression, expressed in Eq. 7.20.

$$R_{t/f} + R_{t/w} + R_q = R_{b/w} + R_{b/f} \qquad (7.20)$$

Where: $R_{t/f}$ is the resistance of the top flange ($A_{t/f}P_y$);

$R_{t/w}$ is the resistance of half of the web post ($A_{t/w}P_y$);

R_q is the longitudinal shear resistance of shear connectors;

$R_{b/w}$ is the resistance of half of the web post, ($A_{b/w}P_y$);

$R_{b/f}$ is the resistance of the bottom flange ($A_{b/f}P_y$).

By substituting the R_q and the cross sectional areas of the steel elements into Eq. 7.20, hence D = 161.5mm.

The depth of concrete in compression, d, is determined using the R_q of 220kN, as the longitudinal shear resistance of the shear connections, R_q, is equal to the compressive resistance of the concrete slabs in partial shear connection. The d of 10.9mm is obtained.

7.4.3.3.3 Determine the depth of P.N.A

Taking moments about P.N.A

$$M = R_{t/f}D_{t/f} + R_{t/w}D_{t/w} + R_qD_q + R_{b/w}D_{b/w} + R_{b/f}D_{b/f} \tag{7.21}$$

Where: M is the moment resistance of the composite section

$D_{t/f}$ is the distance between the $R_{t/f}$ and P.N.A,

$D_{t/w}$ is the distance between the $R_{t/w}$ and P.N.A,

D_q is the distance between the R_q and P.N.A,

$D_{b/w}$ is the distance between the $R_{b/w}$ and P.N.A,

$D_{b/f}$ is the distance between the $R_{b/f}$ and P.N.A.

By substituting the resistance of the steel elements, their distance to P.N.A and the R_q into Eqn. 4.5, hence, M = 262.8kNm.

7.4.3.3.4 Moment resistance of the cross section in degree of shear connection, 0.7

The stress block diagram of the cross section in the degree of shear connection of 0.7 is illustrated below. Figure 7-9 shows The stress block diagram of the cross section in degree of shear connection of 0.7.
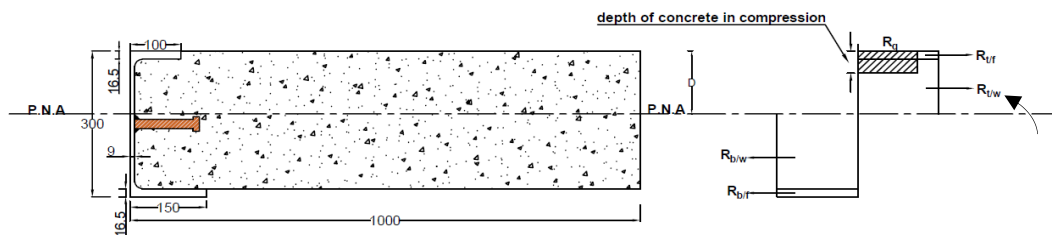
Figure 7-9: Stress block diagrams of the cross sections of the prefabricated ultra shallow flooring system degree of shear connection of 0.7

7.4.3.3.5 Determine the depth of P.N.A

The longitudinal shear resistance of the shear connections, Rq, is calculated first using the compressive resistance of the concrete slabs, Rc, and the degree of shear connection, η, as $\eta = R_q/R_c$.

The depth of P.N.A, D, is determined using the equilibrium of tension and compression expressed in Eq. 7.22.

$$R_{t/f} + R_{t/w} + R_q = R_{b/w} + R_{b/f} \qquad (7.22)$$

Where: $R_{t/f}$ is the resistance of the top flange ($A_{t/f}P_y$);

                       $R_{t/w}$ is the resistance of half of the web post ($A_{t/w}P_y$);

                       R_q is the longitudinal shear resistance of shear connectors;

                       $R_{b/w}$ is the resistance of half of the web post, ($A_{b/w}P_y$);

                       $R_{b/f}$ is the resistance of the bottom flange ($A_{b/f} P_y$).

By substituting the R_q and the cross sectional areas of the steel elements into Eqn. 4.6, hence D =147.8 mm.

The depth of concrete in compression, d, is determined using R_q of 307kN, as the longitudinal shear resistance of the shear connections, R_q, is equal to the compressive resistance of the concrete slabs in a partial shear connection. The d of 15.27mm is obtained.

7.4.3.3.6 Determine the plastic moment capacity

Taking moments about P.N.A

$$M = R_{t/f}D_{t/f} + R_w D_w + R_q D_q + R_{b/w}D_{b/w} + R_{b/f} D_{b/f} \qquad (7.23)$$

Where: M is the moment resistance of the composite section

        $D_{t/f}$ is the distance between the $R_{t/f}$ and P.N.A,

        $D_{t/w}$ is the distance between the $R_{t/w}$ and P.N.A,

        D_q is the distance between the R_q and P.N.A,

        $D_{b/w}$ is the distance between the $R_{b/w}$ and P.N.A,

        $D_{b/f}$ is the distance between the $R_{b/f}$ and P.N.A.

        By substituting the resistance of the steel elements, their distance to P.N.A and the R_q into Eqn. 4.7, hence, M =267.5 kNm.

Table 7-6: Results of the partial shear connection of the prefabricated ultra shallow flooring system

Degree of shear connection, η	Shear resistance of the shear connection, R_q	Depth of concrete in compression, d (mm)	Depth of P.N.A (mm)	Moment resistance, (kNm)
0	--	--	195.8	257.8
0.4	177	8.7	168.4	261.0
0.42	184	9.2	167.0	261.3
0.44	193	9.6	165.6	261.7
0.45	198	9.8	164.9	261.8
0.5	220	10.9	161.5	262.8
0.55	241	12.0	158.0	263.8
0.56	246	12.2	157.4	264.0
0.58	255	12.6	156.0	264.5
0.6	263	13.1	154.6	265.0
0.65	285	14.2	151.2	266.2
0.7	307	15.3	147.8	267.5
0.72	316	15.7	146.4	268.1
0.73	320	15.9	145.7	268.4
0.74	325	16.2	145.0	268.7
0.75	329	16.4	144.3	269.0
0.76	334	16.6	143.6	269.2
0.78	342	17.0	142.2	269.9
0.8	351	17.5	140.9	270.5
0.82	360	17.9	139.5	271.2
0.84	369	18.3	138.1	271.8
0.85	373	18.6	137.4	272.2
0.9	395	19.7	134.0	273.9
0.95	417	20.7	130.6	275.7

7.4.3.4 Linear interaction method

The linear interaction method, as expressed in Eq. 7.15, is a simplified method to determine the design moment capacity in a partial shear connection. The optimum cross section with full depth and the measured material properties of the prefabricated ultra shallow flooring system is used in the linear interaction method. The plastic moment capacity of the steel section, $M_{pl,a,Rd}$, of 257.8kNm is calculated using the stress block method, with the design yield stress of 355N/mm^2 as both tension and compression. The design moment capacity in a full shear connection, $M_{pl,Rd}$, is 327kNm. The results of the linear interaction method are compared with that of the stress block in Figure 7-10. The conservative design moment capacities are obtained by using the linear

interaction method, however, the maximum difference at the region of 0.5-0.6 degrees of shear connection is relatively small (6%).
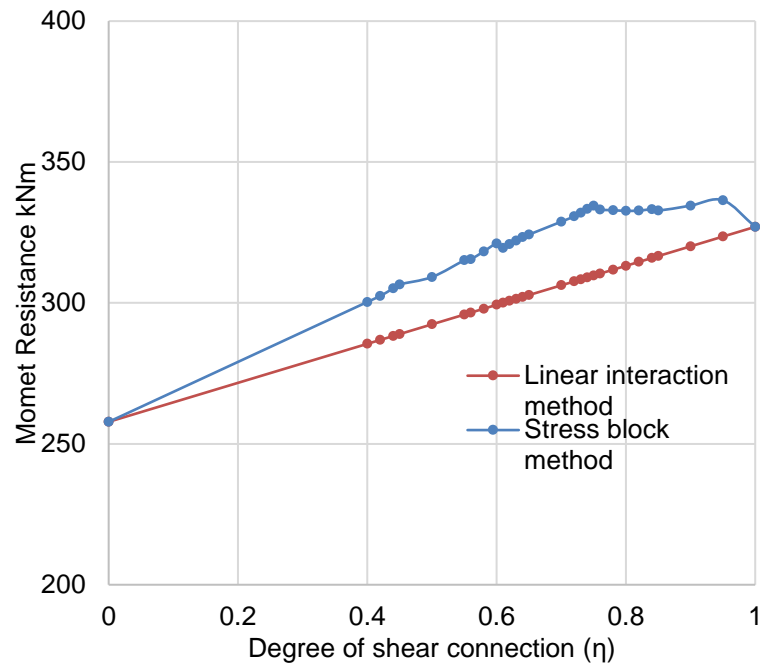
Figure 7-10: Comparison between the stress block method and linear interaction method

7.5 Summary

A proposed design methodology of the bending capacity of the prefabricated ultra shallow flooring system according to (BS 5950-3.1:1990) and Eurocode 4 (EN1994-1-1, 2004) has been presented in this chapter. The conservative design moment capacities are obtained by using the linear interaction method, however, the maximum difference at the region of 0.5-0.6 degrees of shear connection is relatively small (6%).

Specifically, the calculation method for the shear resistance of the shear connection systems has been obtained from the regression analysis of the push-out test results presented in **Chapter 5**. It is represented by two terms: the compressive resistance of the concrete and the tensile resistance of the steel elements. The mathematical formula of the method is expressed in Eq. 7.7. The results of the calculation method compared well with the results of the push-out tests. The ratio for the shear resistance of the calculation to test results is 1.0006.

The FEA parametric study presented in **Chapter 6** further verified the empirical formula obtained for the shear resistance of the shear connection systems, as expressed in Eq. 7.7. The calculated results were very close to the results of the

FEA parametric study, given that the average ratios of the calculated shear resistance to results of the FEA were 0.962, 1.108 and 1.08 for the WWSS with dimensions of 16×75mm, 19×100m and 22×100mm, respectively and 0.894, 0.954 and 0.901 for the WWSS with dowels with diameters of 16mm, 20mm and 22mm, respectively. Overall, the shear resistance of the shear connection systems obtained from the calculation method, Eq. 7.7, were very close to the results of the push-out tests.

Chapter 8 : Conclusions and recommendations

8.1 Summary

The primary objective of this thesis was to study the behaviour of the shear connection systems of a new prefabricated ultra shallow steel-concrete composite flooring system. The research objective was divided into six components, which are summarised below:

1. To carry out a literature review on the topics of the shear connection systems and the existing prefabricated shallow composite flooring systems, with an emphasis on experimental studies, i.e. push-out tests.

2. To examine the Life Cycle Assessment (LCA) and Life Cycle Cost (LCC) of the prefabricated ultra shallow flooring system and compare it with existing similar solutions, such as the hollow core precast slab and the Cofradal slab, which have been used in conjunction with the USFB and the CoSFB.

3. To design and carry out two series of push-out tests. The first series of tests was designed to investigate the web-welded shear stud connection system. The second series of the tests was designed to investigate the horizontally lying dowels together with the web-welded studs shear connection system.

4. To analyse the results of the push-out tests, with aim to develop a design methodology for the shear connection systems.

5. To conduct a comprehensive FEA parametric study in order to identify the effects of the shear capacity of the shear connection systems of the prefabricated ultra shallow flooring system, while varying the mechanical/material and geometrical properties of the prefabricated ultra shallow flooring system's components.

6. To develop a design methodology for the shear capacity of the shear connection systems of the prefabricated ultra shallow flooring system, which will be based on the results of the push-out tests and the FEA parametric study.

These six components have been carried out throughout the thesis. In **Chapter 2**, a detailed literature review on the topic of shear connection systems and the

existing prefabricated shallow composite flooring systems was carried out to provide useful guidelines for the current study.

Chapter 3 provided a background of the ultra shallow flooring system, materials properties and the design of the push-out test series. Analytical Life Cycle Assessment (LCA) and Life Cycle Cost (LCC) studies of the prefabricated ultra shallow flooring system were carried out in **Chapter 4**.

Eight (8) full-scale experimental push-out test series were undertaken in **Chapter 5** to provide the experimental testing required to investigate the behaviour of the novel shear connection systems of the prefabricated ultra shallow flooring system.

Chapter 6 provided the finite element (FE) model of the shear connection systems of the ultra shallow flooring system. A comparison between the FE results and the experimental results validated the 3-D FEM in terms of slip and failure loads. Using the validated model, a parametric study was carried in this chapter with parameters such as different diameters and heights of the shear connection systems, along with different concrete strengths.

In **Chapter 7**, an analytical study of the push-out test results was carried out to develop a design methodology for the shear capacity of the shear connection system. The developed design methodology was further verified using the results of the FEA parametric study. The proposed design methodology for the bending capacity of the prefabricated ultra shallow flooring system was also provided in this chapter. All these chapters carried out all the six objectives of this thesis with detailed and comprehensive execution.

8.2 Concluding remarks

The unique shear transferring mechanism was formed by the web-welded stud shear connection system and horizontally lying dowels together with web-welded stud shear connection system of the prefabricated ultra shallow flooring system. The steel section of the prefabricated ultra shallow flooring system was a short parallel flange C-channel. Three studs/horizontally lying dowels were welded to the web post. The concrete slab of the prefabricated ultra shallow flooring system consisted of a T-ribbed lightweight concrete floor.

One series of push-out tests was carried out to investigate the shear connection systems under direct longitudinal shear force. Analytical LCA and LCC studies of the prefabricated ultra shallow flooring system were carried out to examine the environmental and economic performances of the prefabricated ultra shallow flooring system, in comparison with existing similar solutions, such as hollow core precast slab and Cofradal slab. Analytical studies were performed to establish a design methodology for the shear connection systems and with a view to propose a design methodology for the bending capacity of the prefabricated ultra shallow flooring system. The conclusions from the experimental and analytical studies are presented in three sections, which are detailed below.

Table 8-1: Conclusion sections of the experimental and analytical studies

Section 8.1.1 Analytical LCA and LCC studies	• environmental and economic performance of the prefabricated ultra shallow flooring system;
Section 8.1.2 Experimental study	• Behaviour and failure mechanism of the shear connection systems in push-out tests;
Section 8.1.3 Analytical studies	• Design methodologies for the shear connection systems and prefabricated ultra shallow flooring system.

8.2.1 Conclusions of the analytical LCA and LCC studies

An analytical LCA and LCC for the prefabricated ultra shallow flooring system, the hollow core composite precast flooring and the Cofradal flooring system was carried out to examine the environmental and economic performances of these flooring systems. This study was focused on both semi- and fully-prefabricated methods for flooring systems. The semi prefabrication method was represented by a hollow core composite precast flooring system, with casting in place of the finishing layer, whereas the full prefabrication method was represented by the Cofradal flooring system and the prefabricated ultra shallow flooring system.

Specifically, this study identified a calculation boundary and five energy consumptions and GHG emission sources for both semi and full prefabrication. These included embodied energy and embodied GHG emissions of manufacturing, transportation of building materials, transportation of construction waste, transportation of prefabricated components, and the operation of equipment and construction techniques, demolition and Recycling. In addition, this study also investigated the life cycle cost of these flooring systems, including

both the construction and end-of-life phases. A comparison of these flooring systems that adopt semi and full prefabrication methods was employed to illustrate the differences and characteristics of their energy consumptions, GHG emissions, and cost.

The conclusions of both the LCA and LCC studies are presented in the following points.

- The results indicated that the prefabricated ultra shallow flooring system reduced 28.45% of embodied energy and 43.73% of embodied GHG emissions when compared with the Cofradal260 slab, and 16.32% of embodied energy and 41.60% of embodied GHG emissions when compared with the hollow composite precast slab for the manufacturing phase.

- Regarding onsite construction, the prefabricated ultra shallow flooring system showed a reduction of 37.5% for both embodied energy and embodied GHG emissions when compared with the Cofradal slab, and 53.50% for embodied energy and 53.12% for embodied GHG emissions when compared with the hollow composite precast slab.

- Regarding transportation, the prefabricated ultra shallow flooring system showed a reduction of 15.86% for embodied energy and 15.12% embodied GHG emissions when compared with the Cofradal slab, and 52.28% for embodied energy and 51.9% for embodied GHG emissions when compared with the hollow composite precast slab.

- Regarding Recycling, the prefabricated ultra shallow flooring system had a reduction of 9.25% of embodied energy and 15.56% of embodied GHG emissions when compared with the Cofradal260 slab.

- The reduction percentage in embodied energy and embodied GHG emissions for the prefabricated ultra shallow flooring system in comparison with the hollow composite precast slab was higher than the Cofradal slab for both transportation and onsite construction phases based on this data analysis. This was related to the fact that a hollow composite precast slab is a semi-prefabricated slab with a cast in-situ finishing layer, while the proposed flooring and the Cofradal slabs are fully prefabricated flooring systems, which include the finishing layer; this increases the amount of embodied energy and embodied GHG emissions.

- The reduction percentage in embodied energy and embodied GHG emissions for the prefabricated ultra shallow flooring system in comparison with the Cofradal slab was higher than the hollow composite precast slab for both the manufacture and Recycling phases. The reason for this was based on the use of materials with a high intensity of embodied energy and embodied GHG emissions, such as rock wool insulation material and concrete with high cement content.

- The key approach to enhance embodied energy and embodied GHG emissions reduction in semi prefabrication lies in reducing the amount of offsite casting work, making reasonable and economically efficient proportions of concrete, and selecting off-site factories that are near the projects or material distribution centres. For full prefabrication, the main methods to enhance reductions in embodied energy and embodied GHG emissions reduction were achieved by reducing the amount of used concrete by optimising the design of the reinforced concrete through changing the shape, such as using a ribbed slab in the prefabricated ultra shallow flooring system. They were also achieved by reducing the use of high intensity embodied energy and embodied GHG emissions' materials. For instance, by using lightweight aggregate concrete with lower amounts of cement content and recycled aggregate, as used in the prefabricated ultra shallow flooring system. Reductions can also be achieved by increasing the width of the prefabricated elements, which will reduce the amount of embodied energy and embodied GHG emissions of onsite construction, with an increase in the width of the proposed flooring from 1.2m to 2.0m. These aspects should gain increased recognition by more governments and clients as the competition in the prefabrication market increases.

- The life cycle cost (LCC) of these three flooring systems was also investigated in this study. The outcomes showed that the prefabricated ultra shallow flooring system reduced 13.08% of the construction cost and 41.83% of the end-of-life cost in comparison with the Cofradal260 slab, and, 1.87% of construction cost and 18.95% of end-of-life cost in comparison with the hollow composite precast slab. The reduction percentage of the cost was not too high; this was related to the fact that the life cycle cost study only covers two phases.

- The full prefabrication practice (the prefabricated ultra shallow flooring system) induced lower energy consumptions, lower emissions, and lower costs when compared with the semi and fully prefabrication construction of other currently used systems, which made it a good suggestion for the European building market.

8.2.2 Conclusions of the experimental study

One type of test was carried out to investigate the unique shear transferring mechanism, namely the push-out tests. The push-out tests applied direct longitudinal shear force to the shear connection systems. The load-slip behaviour and shear resisting properties of the shear connection systems were obtained in the push-out tests. The specimens of the push-out tests were designed to represent the actual configurations of the shear connection used for the prefabricated ultra shallow flooring system, and also designed to create the desired loading conditions of the shear connection systems.

The push-out test series investigated the two types of the shear connection systems, i.e. the web-welded shear stud (WWSS) connection system, and the horizontally lying dowels together with the web-welded shear stud (WWSS with dowels) connection system. Comprehensive information was obtained from the push-out tests. The conclusions of both push-out test series are presented in the following section.

8.2.2.1 Push-out tests

The conclusions for the shear connection systems are presented in the areas of behaviour and failure mechanism. The findings of the push-out test series are also summarised below.

<u>Web-welded shear stud shear connection system (WWSS)</u>

- Behaviour: In the push-out test series, the web-welded shear stud connection system showed a ductile failure mode of the entire slab system under direct longitudinal shear force.
- Failure mechanism: The studs were sheared off from one side (either right or left side of the specimen) in the direction of the longitudinal shear force while bending near the root of the stud. However, the studs on the opposite side were bent without being sheared off. This was due to the distribution of stresses over the slab width during the test, which results in stress

concentration on one side of the specimen. The concrete in the vicinity of the studs was crushed in the shear direction. The web-welded shear stud connection demonstrated splitting of the concrete slab in the push-out tests.

<u>Web-welded shear stud with dowels shear connection system (WWSS with dowels)</u>

- Behaviour: The connection system with the horizontal lying steel dowels together with the web-welded shear studs showed a more ductile failure mode of the entire slab system under direct longitudinal shear force in comparison with the system having studs only.

- Failure mechanism: The dowels and studs were sheared off from one side (either right or left side of the specimen) with bending showing near their roots. Nevertheless the dowels and studs on the other side were bent without shearing off. The concrete in the vicinity of the studs was crushed in the shear direction. The steel dowels together with the web-welded studs shear connection system demonstrated the splitting of the concrete slab in the push-out tests.

<u>The findings of both push-out test series are summarised below:</u>

- The horizontally lying steel dowels together with the web-welded shear studs connection system increases the shear resistance and the slip capacity of the shear connection system.

- An interlocking mechanism was found at ultimate loads between the concrete and the horizontally lying dowels together with web-welded shear stud connection system. This mechanism demonstrates the strong tie-resistance of the steel dowels, since very little separation in the transverse direction was observed when compared with the large separation of the specimens with web-welded shear stud connection system.

- The push-out tests showed that the shear resistance of each connection system increased with an increase in the concrete strength.

- The web-welded shear stud connection system showed the ductile failure mode with slip capacities ranging between 2mm and 30mm for different concrete strengths.

- The horizontally lying steel dowels together with the web-welded shear studs connection system showed a more ductile failure mode in comparison with the system having studs only, with slip capacities ranging between 13mm and 29mm for different concrete strengths.

- The push-out tests showed that a larger diameter of dowels (up to 20mm in the present study) increased the shear interaction area, as well as the concrete bearing area, thus enhancing its shear resistance.

- Three types of failure were observed from the push-out tests: (a) shear failure with bending near the roots of the connectors, (b) shear failure of the weld toe of shear studs, and (c) concrete cracking. Brittle weld failure should be avoided by ensuring the quality of welding during the installation of the connectors.

8.2.3 Conclusions of analytical studies

The results of the push-out tests were analysed. The design methodology for the shear connection systems was developed in addition to the proposed design methodology for the bending capacity of the prefabricated ultra shallow flooring system, as listed in the table below. The details of the design methodologies are presented in the next two sections.

Table 8-2:Details of the design methodologies

Design methodologies	
Push-out tests	• Design methodology for shear resistance of the shear connection systems
	• Proposed design methodology for moment resistance of the prefabricated ultra shallow flooring system at the ultimate limit state (ULS)

8.2.3.1 Analytical studies of push-out test results

A mathematical analysis on the results of the push-out tests was carried out, with the aim to develop a design methodology for the shear resistance of the unique shear connection systems. Based on the failure mechanism shown in the push-out tests, a method was proposed first, which is governed by both the tensile strength of the connectors and the concrete bearing strength, in order to calculate the total shear resistance of the shear connection systems. The compressive strength of the concrete significantly influences the ultimate shear strength capacity loads (higher when NWC and lower when ULWC), while changing the

failure mode of the connection. The empirical formula of the method resulted from the mathematical analysis. The calculated shear resistance using the concluded formula compared well with the results of the push-out tests. The ratio for the shear resistance of the calculation to test results was ~1.0006.

The FEA of the shear connection systems was carried out to further verify the formula obtained from the mathematical analysis. Firstly, a calibrated FEA model of the shear connection systems was developed. Then a parametric study was performed by using the calibrated FEA model to investigate the variables of the diameter and the height of the shear connection systems and concrete strength. Finally, the results of the FEA parametric study were compared with the calculated shear resistance using the developed formula.

The calculated results were very close to the results of the FEA parametric study, as the average ratios of the calculated shear resistance to the results of the FEA were 0.962, 1.108 and 1.08 for the WWSS with dimensions of 16×75mm, 19×100m and 22×100mm, respectively, and 0.894, 0.954 and 0.901 for the WWSS with dowels with diameters of 16mm, 20mm and 22mm, respectively. Overall the shear resistance of the shear connection systems obtained from the calculation method, Equ. 7.7, were very close to the results of the push-out tests.

8.2.3.2 The proposed design methodology for moment resistance of the prefabricated ultra shallow flooring system at the ultimate limit state (ULS)

The design methodology for calculating the moment resistance of the prefabricated ultra shallow flooring system was proposed according to (BS 5950-3.1,1990) and Eurocode 4 (EN1994-1-1, 2004), using both stress blocks. This method was based on plastic theory, which assumes that the stresses within the cross section reach a constant value in both tension and compression.

8.3 Recommendations

Recommendations made in this research are discussed in terms of improvements of the shear connection systems and future research topics.

8.3.1 Recommendations for the shear connection systems

The results of the push-out tests provided comprehensive information on the behaviour and shear resisting properties of the shear connection systems.

However, the design details for some of the shear connection systems and concrete types can be improved. The following recommendations are therefore made:

(1) It is recommended that the web-welded shear stud connection system should be used only in a region of low shear, given that low shear resistance of the web-welded shear stud connection system was shown in the push-out tests.

(2) It is recommended that the horizontally lying steel dowels together with the web-welded shear studs connection system should be used in a region of high shear, given that high shear resistance and strong tying resistance of the horizontally lying steel dowels together with the web-welded shear studs connection system was shown in the push-out tests.

(3) It is recommended that the compressive strength of the ultra lightweight concrete should be enhanced by using admixtures or additives, as the compressive strength of the concrete significantly influences the ultimate shear strength capacity loads (higher when NWC and lower when ULWC) while changing the failure mode of the connection system.

8.3.2 Recommendations for future research

(1) The behaviour and shear resistance of the shear connection systems used for the prefabricated ultra shallow flooring system under direct static shear force were extensively investigated in the push-out test series presented in this thesis. Push-out tests with dynamic loading on the shear connection systems are recommended as another future research topic. This will be beneficial in observing the behaviour of the shear connection systems used for the prefabricated ultra shallow flooring system as the prefabricated ultra shallow flooring system might be used in high seismic regions. The findings of the dynamic loading test will provide specific information for design calculation, The findings of the dynamic loading test will provide specific information for design calculation, where the prefabricated ultra shallow flooring system might be subject to repeated loading. These tests will also specify the suitability of using the new shear connection systems in the high seismic regions. The results of the dynamic loading test could also be used to make comparisons with the results of the push-out tests with the static loading performed in this research.

(2) The behaviour and shear resistance of the shear connection systems used for the prefabricated ultra shallow flooring system under static flexural test was not examined in this research. Flexural tests with static loading are recommended as a future research topic. The findings of the static loading flexural test should provide specific information for developing the design methodologies for the prefabricated ultra shallow flooring system at the serviceability limit sate (SLS) and ultimate limit states (ULS).

Bibliography

AASHTO, 2004. LRFD bridge design specifications, 3rd ed. AASHTO, Washington, DC.

AASHTO. LRFD bridge design specifications. 5th ed. Washington (DC): American Association of State Highway and Transportation Officials; 2010.

ABAQUS Documentation, version 6.8.1. Dassault system, USA; 2008.

Ahmed, I.M. and Tsavdaridis, K.D., 2018. Life cycle assessment (LCA) and cost (LCC) studies of lightweight composite flooring systems. Journal of Building Engineering, 20, pp.624-633.

AISC, 1994. Manual of Steel Construction Load and Resistance Factor Design, Second Edition, 1994, Chicago.

Alengaram, U. J., AL Muhit, B. A. & Bin Jumaat, M. Z. 2013. Utilization of oil palm kernel shell as lightweight aggregate in concrete–A review. Construction and Building Materials, 38, 161-172.

Algaard, W., Lyle, J. and Izatt, C., 2005, May. Perforation of composite floors. In 5th European LS-DYNA users conference (pp. 1123-1130).

Almusallam, T.H. and Alsayed, S.H., 1995. Stress-strain relationship of normal, high-strength and lightweight concrete. Magazine of Concrete Research, 47(170).

American Institute of Steel Construction, 1986. Load and Resistance Factor Design Specification for Structural Steel Buildings: September 1, 1986. AISC.

An, L. and Cederwall, K., 1996. Push-out tests on studs in high strength and normal strength concrete. Journal of constructional steel research, 36(1), pp.15-29.

ANSI/AISC 2010. AISC 360-10, specification for structural steel buildings. American National Standards Institute, Chicago.

AreclorMittal Construction Benelux: Arval COFRADAL200® [Online]. Available:http://ds.arcelormittal.com/construction/arval_international Accessed].

Aribert, J. Dimensionnement de poutres mixtes en connection partielle. Mixed structures including new materials, IABSE symposium, Brussels, September, 1990. 215-220.

Asif, M., Muneer, T. and Kelley, R., 2007. Life cycle assessment: A case study of a dwelling home in Scotland. *Building and environment*, *42*(3), pp.1391-1394.

Assefa, G., Glaumann, M., Malmqvist, T., Kindembe, B., Hult, M., Myhr, U. and Eriksson, O., 2007. Environmental assessment of building properties—Where natural and social sciences meet: The case of Eco Effect. *Building and Environment*, *42*(3), pp.1458-1464.

Baran, E., 2015. Effects of cast-in-place concrete topping on flexural response of precast concrete hollow-core slabs. Engineering Structures, 98, 109-117.

Bare, J.C., 2002. TRACI: The tool for the reduction and assessment of chemical and other environmental impacts. Journal of industrial ecology, 6(3-4), pp.49-78.

Bayasi, M. Z. & Zeng, J., 1997. Composite slab construction utilizing carbon fiber reinforced mortar. Structural Journal, 94, 442-446.

Bayasi, Z. & Kaiser, H., 2003. Flexural Behaviour of Composite Concrete Slabs Using Carbon Fibre Laminate Decks. Materials Journal, 100, 274-279.

Beushausen, H.-D., 2001. CONCRETE. REINFORCEMENT-Shear Strength-Unreinforced interfaces: Precast concrete elements and in situ topping. Betonwerk und Fertigteiltechnik, 67, 64-69.

Blengini, G.A., 2009. Life cycle of buildings, demolition and recycling potential: a case study in Turin, Italy. Building and Environment, 44(2), pp.319-330.

Braun, M., Obiala, R. and Odenbreit, C., 2015. Analyses of the loadbearing behaviour of deep-embedded concrete dowels, CoSFB. Steel Construction, 8(3), pp.167-173.

Bribián, I.Z., Capilla, A.V. and Usón, A.A., 2011. Life cycle assessment of building materials: Comparative analysis of energy and environmental impacts and evaluation of the eco-efficiency improvement potential. Building and environment, 46(5), pp.1133-1140.

Brooks, J., Bennett, E. & Owens, P. 1987. Influence of lightweight aggregates on thermal strain capacity on concrete. Magazine of concrete research, 39, 60-72.

BS 1881-116:1983 Testing concrete. Method for determination of compressive strength of concrete cubes.

BS 5950-3.1:1990 Structural use of steelwork in building. Design in composite construction. Code of practice for design of simple and continuous composite beams.

BS 882:1992 Specification for aggregate from natural sources for concrete. London: British Standard Institution.

BS EN 13055-1:2002 Lightweight aggregates. Lightweight aggregates for concrete, mortar and grout.

BS EN 197-1:2011 Composition, specifications and conformity criteria for common cements. British Standard Institution.

BS5950-3.1, B. S. 1990. Structural Use of Steel Work in Building, Part 3: Design in Composite Construction, Section 3.1 Code of Practice for Design of Simple and Continuous Composite Beams.

Canadian Standards Association. 1984. Steel structures for buildings-limit states design. CAN3-S16.1-M84. Rexdale, Ont.

Cheeseman, C., Makinde, A. & Bethanis, S. 2005. Properties of lightweight aggregate produced by rapid sintering of incinerator bottom ash. Resources, Conservation and Recycling, 43, 147-162.

Chinn, J., 1965. Pushout tests on lightweight composite slabs. AISC Engineering Journal, 2, 129-134.

Clarke, J. L. 2002. Structural lightweight aggregate concrete, CRC Press.

COFRADAL200®, A. C. B. A. Cofradal [Online]. [Accessed].

Cole, R.J., 1998. Energy and greenhouse gas emissions associated with the construction of alternative structural systems. Building and Environment, 34(3), pp.335-348.

Cornelissen, H.A.W., Hordijk, D.A. and Reinhardt, H.W., 1986. Experimental determination of crack softening characteristics of normalweight and lightweight. Heron, 31, p.45.

Davies, C., "Small-Scale Push-out Tests on Welded Stud Shear Connectors", Concrete, Sep 1967, pp. 311-316.

Davies, C., "Steel-Concrete Composite Beams for Buildings", George Godwin, 1975.

Defra, 2008. Economics and Statistics. Notes on Scenarios of Environmental Impacts Associated with Construction and Occupation of Homes.Availableonline:⟨http://www.statistics.defra.gov.uk/esg/reports/housing/appendh.pdf⟩ (Accessed on 15 December 2008).

Doel, A. 2007. Lightweight aggregates for use in concrete. Concrete, 41, 36-37.

Dong, Y. H., Jaillon, L., Chu, P., Poon, C. S. & MATERIALS, B. 2015. Comparing carbon emissions of precast and cast-in-situ construction methods–A case study of high-rise private building. 99, 39-53.

Dowell, R. K. & Smith, J. W., 2006. Structural tests of precast, prestressed concrete deck panels for California freeway bridges. PCI journal, 51, 76.

El Zareef, M. and Schlaich, M., 2008. Bond behaviour between GFR bars and infra-lightweight concrete. *Tailor Made Concrete Structures*, pp.721-727.

Ellobody, E., Young, B. and Lam, D., 2006. Behaviour of normal and high strength concrete-filled compact steel tube circular stub columns. Journal of Constructional Steel Research, 62(7), pp.706-715.

EN 1992-1-1 2004. Eurocode 2: Design of concrete structures: Part 1-1: General rules and rules for buildings. London: British Standards Institution.

EN 1994-1-1: Eurocode 4: Design of composite steel and concrete structures, part 1-1: general rules and rules for buildings. European Committee for Standardization: 2004.

EN 1994-2: Eurocode 4. Design of composite steel and concrete structures, part 2: general rules and rules for bridges. European Committee for Standardization; 2005.

EN1992-1-1: 2005. Eurocode 2: Design of concrete structures - Part 1-1: General rules and rules for buildings. European Standards, London.

EN1994, E. -2 2005. Design of composite steel and concrete structures–Part 2: General rules and rules for bridges. BSI, London.

EN1994-1-1: 2004. Design of Composite Steel and Concrete Structures, Part 1-1: General Rules and Rules for Buildings. European Standards, London.

Frangi, A., Knobloch, M., Raveglia, E., Fontana, M., Mensinger, M. and Schwindl, K., 2008, July. Composite Slabs with integrated installation floor using cellular

beams. In Proceedings of 6th Engineering International Conference on Composite Construction in Steel and Concrete.

Frischknecht, R., Jungbluth, N., Althaus, H.J., Hischier, R., Doka, G., Bauer, C., Dones, R., Nemecek, T., Hellweg, S., Humbert, S. and Margni, M., 2007. *Implementation of life cycle impact assessment methods. Data v2.0 (2007). Ecoinvent report No. 3* (No. INIS-CH--10091). Ecoinvent Centre.

Gattesco, N. and Giuriani, E., 1996. Experimental study on stud shear connectors subjected to cyclic loading. Journal of Constructional Steel Research, 38(1), pp.1-21.

Girhammar, U. A. & Pajari, M., 2008. Tests and analysis on shear strength of composite slabs of hollow core units and concrete topping. Construction and Building Materials, 22, 1708-1722.

Goble, G.G., "Shear Strength of Thin Flange composite Specimens", AISC Engineering Journal, AISC, V5, n2, 1968, pp. 62-65.

Goedkoop, M. and Oele, M., 2004. Introduction to LCA (Life Cycle Assessment) with SimaPro. *PRé Consultants, Sept.*

Gohnert, M., 2000. Proposed theory to determine the horizontal shear between composite precast and in situ concrete. Cement and Concrete Composites, 22, 469-476.

González, M.J. and Navarro, J.G., 2006. Assessment of the decrease of CO2 emissions in the construction field through the selection of materials: Practical case study of three houses of low environmental impact. *Building and environment*, *41*(7), pp.902-909.

Gorkum, C., 2010. CO_2 emissions and energy consumption during the construction of concrete structures. Delft University of Technology, Holland, pp.4-3.

Hammond, G., Jones, C., Lowrie, E. F. and Tse, P., 2008. Inventory of Carbon & Energy: ICE,, Sustainable Energy Research Team, Department of Mechanical Engineering, University of Bath, Bath.

Hawkins, N. 1973. The strength of stud shear connectors. Institution of Engineers (Australia) Civ Eng Trans.

Hawkins, N. M. & Ghosh, S., 2006. Shear strength of hollow-core slabs. PCI journal, 51.

Hawkins, N. M. & Mitchell, D., 1984. Seismic response of composite shear connections. Journal of Structural Engineering, 110, 2120-2136.

Hechler, O., Braun, M., Obiala, R., Kuhlmann, U., Eggert, F. and Hauf, G., 2013. CoSFB–Composite Slim-Floor Beam–Experimental Test Campaign and Evaluation. *Composite Construction VII, Australia*.

Hicks, S., 1998. Longitudinal shear resistance of steel and concrete composite beams. PhD thesis, University of Cambridge.

Hicks, S., 2003. Current trends in modern floor construction. *New steel construction, 11*(1), pp.32-33.

Hillerborg, A., 1985. The theoretical basis of a method to determine the fracture energy of concrete. *Materials and structures, 18*(4), pp.291-296.

HMRC, HM Revenue & Customs, London, 2011. A General Guide to Landfill Tax, HM Revenue & Customs, London.

Huberman, N. and Pearlmutter, D., 2008. A life-cycle energy analysis of building materials in the Negev desert. Energy and Buildings, 40(5), pp.837-848.

Humphreys, K.K., 1995. *Basic cost engineering*. CRC Press.

Huo, B. 2012. Experimental and analytical study of the shear transfer in composite shallow cellular floor beams. City University London.

Islam, H., Jollands, M. and Setunge, S., 2015. Life cycle assessment and life cycle cost implication of residential buildings—A review. *Renewable and Sustainable Energy Reviews, 42*, pp.129-140.

ISO 6892-1: 2009 Metallic materials – tensile testing – Part 1: Method of test at room temperature.

ISO 6892-1:2009 Metallic materials – tensile testing – Part 1: Method of test at room temperature.

ISO, 2006a. Environmental management. Life cycle assessment. Requirements and guidelines Managements environmental, Anal. Cycle. .

ISO, E., 2006b. 14040: 2006. Environmental management-Life cycle assessment-Principles and framework. European Committee for Standardization.

ISO, T., 2012. 14049: 2012 Environmental management—Life cycle assessment—Illustrative examples on how to apply ISO 14044 to goal and scope definition and inventory analysis. International Organization for Standardization (ISO): Geneva.

ISO15686-5, 2008. Buildings and Constructed Assets-Service-Life Planning-Part 5: Life-Cycle Costing. Geneva, Switzerland: International Organization for Standardization.

Jaillon, L., Poon, C. S. & Chiang, Y. H. 2009. Quantifying the waste reduction potential of using prefabrication in building construction in Hong Kong. 29, 309-320.

Jayas, B. & Hosain, M., 1988. Behaviour of headed studs in composite beams: push-out tests. Canadian Journal of Civil Engineering, 15, 240-253.

Johnson, R. & Oehlers, D. Analysis and design for longitudinal shear in composite T-beams. Institution of Civil Engineers, Proceedings, Pt 1, 1981.

Johnson, R.P., Molenstra, N. 1991. Partial shear connection in composite beams for buildings. Proceedings of the Institution of Civil Engineers, 91(4), pp.679-704.

Jung, D. 1998. Study of dynamic explicit analysis in sheet metal forming processes using faster punch velocity and mass scaling scheme. Journal of materials engineering and performance, 7, 479-490.

Kansinally, R. and Tsavdaridis, K.D., 2015, September. Vibration response of USFB composite floors. In *Nordic Steel Construction Conference*. Leeds.

Karlsson, B.I. and Sorensen, E.P. (2006a) *ABAQUS: Analysis user's manual version6.5*, Pawtucket, Rhode Island, Hibbitt Publication.

Karlsson, B.I. and Sorensen, E.P. (2006b) *ABAQUS: Analysis user's manual volumeIV: Element*, Pawtucket, Rhode Island, Hibbitt Publication.

Karlsson, B.I. and Sorensen, E.P. (2006c) *ABAQUS: Analysis user's manual volumeV: Prescribed conditions, constraints and interactions*, Pawtucket, Rhode Island, Hibbitt Publication.

Khasreen, M., Banfill, P.F. and Menzies, G., 2009. Life-cycle assessment and the environmental impact of buildings: a review. *Sustainability*, *1*(3), pp.674-701.

Kim, B., Wright, H. D. & Cairns, R., 2001. The behaviour of through-deck welded shear connectors: an experimental and numerical study. Journal of Constructional Steel Research, 57, 1359-1380.

Kuhlmann, U. & Breuninger, U. 2002. Behaviour of horizontally lying studs with longitudinal shear force. Composite Construction in Steel and Concrete IV.

Kuhlmann, U. & Kürschner, K. 2006. Structural behaviour of horizontally lying shear studs. Composite Construction in Steel and Concrete V.

Langdon, D., 2014. Spon's Civil Engineering and Highway Works Price Book 2014, CRC Press.

Lawson, M., Beguin, P., Obiala, R. and Braun, M., 2015. Slim-floor construction using hollow-core and composite decking systems. *Steel Construction*, *8*(2), pp.85-89.

Lee, J. and Fenves, G.L., 1998. Plastic-damage model for cyclic loading of concrete structures. Journal of engineering mechanics, 124(8), pp.892-900.

Lemaitre, J., 1985. A continuous damage mechanics model for ductile fracture. Journal of engineering materials and technology, 107(1), pp.83-89.

Lloyd, R. & Wright, H., 1990. Shear connection between composite slabs and steel beams. Journal of Constructional Steel Research, 15, 255-285.

Lopez-Mesa, B., Pitarch, A., Tomás, A. and Gallego, T., 2009. Comparison of environmental impacts of building structures with in situ cast floors and with precast concrete floors. Building and Environment, 44(4), pp.699-712.

Lorenc, W. and Kubica, E., 2006. Behavior of composite beams prestressed with external tendons: Experimental study. *Journal of constructional steel research*, *62*(12), pp.1353-1366.

Lubliner, J., Oliver, J., Oller, S. and Oñate, E., 1989. A plastic-damage model for concrete. International Journal of solids and structures, 25(3), pp.299-326.

Malin, N., 2005. Life cycle assessment for whole buildings: seeking the holy grail. *Building Design and Construction*, *5*, pp.6-11.

Mangerig, I. & Zapfe, C., 2003. Concrete Dowels in Composite Construction. Proceedings of the 5th Japanese-German Joint Symposium on Steel and Composite Bridge,. Osaka.

Mateus, R., Neiva, S., Bragança, L., Mendonça, P. and Macieira, M., 2013. Sustainability assessment of an innovative lightweight building technology for partition walls–comparison with conventional technologies. *Building and Environment*, *67*, pp.147-159.

MINITAB Release 18, 2017. Minitab Reference Manual. Minitab, State college, Philadelphia.

Mones, R. M. & Breña r, S. F., 2013. Hollow-core slabs with cast-in-place concrete toppings: A study of interfacial shear strength. PCI journal, 58.

Mullett, D.L. and Lawson, R.M., 1993. *Slim floor construction using deep decking*. UK: Steel Construction Institute.

Mullett, D.L., 1992. Slim Floor Design and Construction, Publication 110, The Steel Construction Institute.

Neville A.M. & Brooke J.J. 2005. Properties of concrete, 4thEdition, Pearson.

Nguyen, H.T. and Kim, S.E., 2009. Finite element modelling of push-out tests for large stud shear connectors. *Journal of Constructional Steel Research*, *65*(10-11), pp.1909-1920.

Nguyen, M.Q., Elder, D.J., Bayandor, J., Thomson, R.S. and Scott, M.L., 2005. A review of explicit finite element software for composite impact analysis. Journal of Composite Materials, 39(4), pp.375-386.

NRMCA 2003. Concrete in Practice, CIP 36 Structural Lightweight Concrete. Silver Spring, Maryland USA.

Ollgaad, J., Slutter, R. & Fisher, J. 1971. Shear strength of stud connectors in lightweight and normal-weight concrete. AISC Engineering Journal, 55-64.

Pelisser, F., Zavarise, N., Longo, T. A. & Bernardin, A. M. 2011. Concrete made with recycled tire rubber: effect of alkaline activation and silica fume addition. Journal of Cleaner Production, 19, 757-763.

Peltonen, S. & Leskelä, M. V. 2006. Connection Behaviour of a Concrete Dowel in a Circular Web Hole of a Steel Beam. Composite Construction in Steel and Concrete V.

Precast Concrete Flooring, BISON Precast Ltd. 2007

Qureshi, J., Lam, D. and Ye, J., 2010. Finite element modelling of shear connection behaviour in a push test using profiled sheeting. *Advances and Trends in Structural Engineering, Mechanics and Computation*, p.167.

Rackham, J., Hicks, S. & Newman, G. M., 2006. Design of asymmetric slimflor beams with precast concrete slabs, Steel Construction Institute Ascot, UK.

Real, S., Bogas, J. A. & Pontes, J. 2015. Chloride migration in structural lightweight aggregate concrete produced with different binders. Construction and Building Materials, 98, 425-436.

Reza, B., Sadiq, R. and Hewage, K., 2011. Sustainability assessment of flooring systems in the city of Tehran: An AHP-based life cycle analysis. Construction and Building Materials, 25(4), pp.2053-2066..

Scott, N., 1973. Performance of precast prestressed hollow core slab with composite concrete topping-comment. Journal of prestressed concrete institute, 18, 117-117.

Silfwerbrand, J., 2003. Shear bond strength in repaired concrete structures. Materials and Structures, 36, 419-424.

SilverCrest, 2010. Disposal of Construction Waste. R.C. Franco (ed.).

Sjunnesson, J., 2005. Life cycle assessment of concrete.

Slutter, R.G. and Driscoll, G.C., "Flexural Strength of Steel-Concrete Composite Beams", Journal of Structural Engineering, ASCE, V91, n2, 1965, pp. 71-99.

Tassios, T. P. & Vintzēleou, E. N., 1987. Concrete-to-concrete friction. Journal of Structural Engineering, 113, 832-849.

Treasury, H. M. S., 2003. The green book: appraisal and evaluation in central government. London TSO.

Tsavdaridis, K.D., D Mello, C. and Hawes, M., 2009b, September. Experimental study of ultra shallow floor beams (USFB) with perforated steel sections. In *Nordic Steel 09* (pp. 312-319).

Tsavdaridis, K.D., D'Mello, C. and Huo, B.Y., 2009a. Computational study modelling the experimental work conducted on the shear capacity of perforated concrete-steel Ultra Shallow Floor Beams (USFB). In *Proceedings of 16th Hellenic Concrete Conference* (p. 159).

Tsavdaridis, K.D., D'Mello, C. and Huo, B.Y., 2013. Experimental and computational study of the vertical shear behaviour of partially encased perforated steel beams. *Engineering Structures*, *56*, pp.805-822.

Tse, P., 2016. A BERIA Guide: Life cycle costing.

Ueda, T. & Stitmannaithum, B., 1991. Shear strength of precast prestressed hollow slabs with concrete topping. Structural Journal, 88, 402-410.

Valente, I. B. and Cruz, P. J., 2009. Experimental analysis of shear connection between steel and lightweight concrete. Journal of Constructional Steel Research, 65, 1954-1963.

van den Dobbelsteen, A., Arets, M. and Nunes, R., 2007. Sustainable design of supporting structures: Optimal structural spans and component combinations for effective improvement of environmental performance. *Construction Innovation*, *7*(1), pp.54-71.

Vukotic, L., Fenner, R.A. and Symons, K., 2010, September. Assessing embodied energy of building structural elements. In Proceedings of the Institution of Civil Engineers-Engineering Sustainability (Vol. 163, No. 3, pp. 147-158).

Wong, F. and Tang, Y.T., 2012. Comparative embodied carbon analysis of the prefabrication elements compared with in-situ elements in residential building development of Hong Kong. *World Academy of Science*, *62*(1), pp.161-166.

Xu, C., Sugiura, K., Wu, C. and Su, Q., 2012. Parametrical static analysis on group studs with typical push-out tests. *Journal of constructional steel research*, *72*, pp.84-96.

Xue, W., Ding, M., Wang, H. and Luo, Z., 2008. Static behaviour and theoretical model of stud shear connectors. Journal of bridge engineering, 13(6), pp.623-634.

Yan, J.B., Liu, X.M., Liew, J.R., Qian, X. and Zhang, M.H., 2016. Steel–concrete–steel sandwich system in Arctic offshore structure: Materials, experiments, and design. Materials & Design, 91, pp.111-121.

Yang, K.H., Song, J.K. and Song, K.I., 2013. Assessment of CO_2 reduction of alkali-activated concrete. *Journal of Cleaner Production*, *39*, pp.265-272.

Yee, A. A., 2001. Structural and economic benefits of precast/prestressed concrete construction. PCI journal, 46.

Yohanis, Y.G. and Norton, B., 2002. Life-cycle operational and embodied energy for a generic single-storey office building in the UK. *Energy*, *27*(1), pp.77-92.ACI. Building code requirements for structural concrete: ACI318-05. Detroit (MI): American Concrete Institute; 2005.

Appendix A

(a)

(b)

(c)
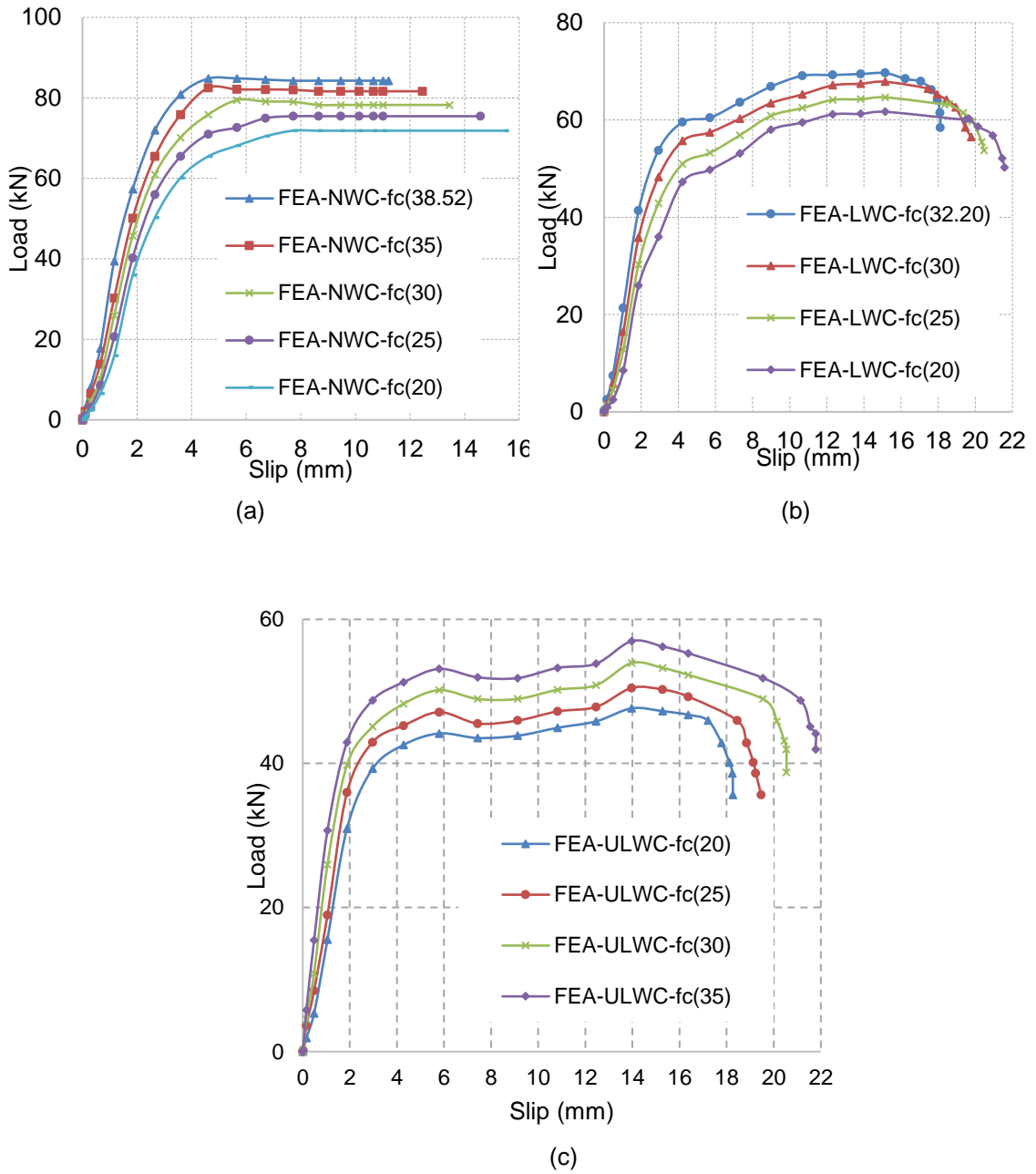
Figure A-1: Load-slip curves of the FEA with WWSS 16×75mm
with different concrete types

(a)

(b)

(c)
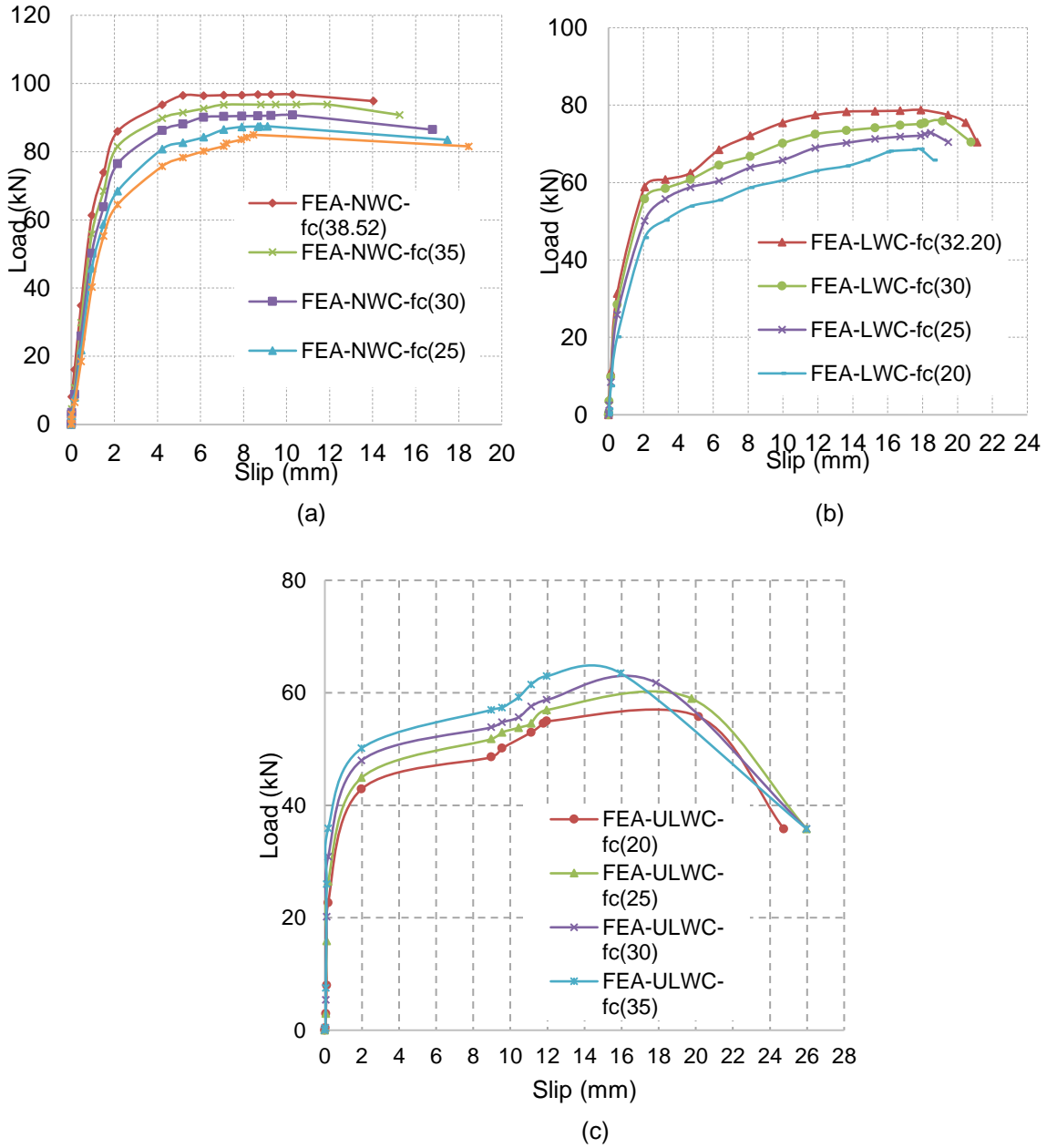
Figure A-2: Load-slip curves of the FEA with WWSS 19×100mm
with different concrete types
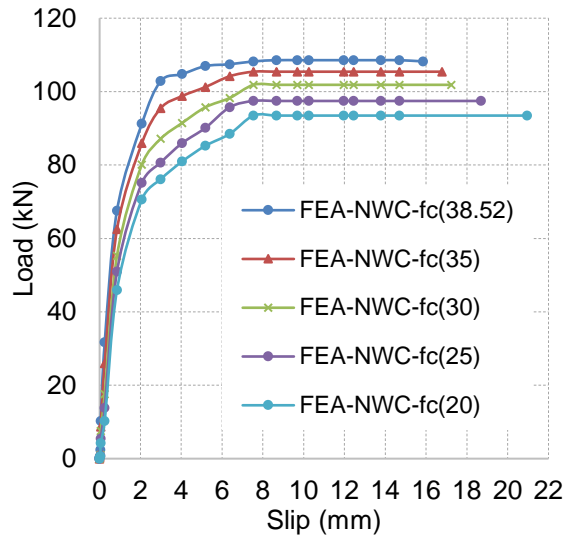
(a)
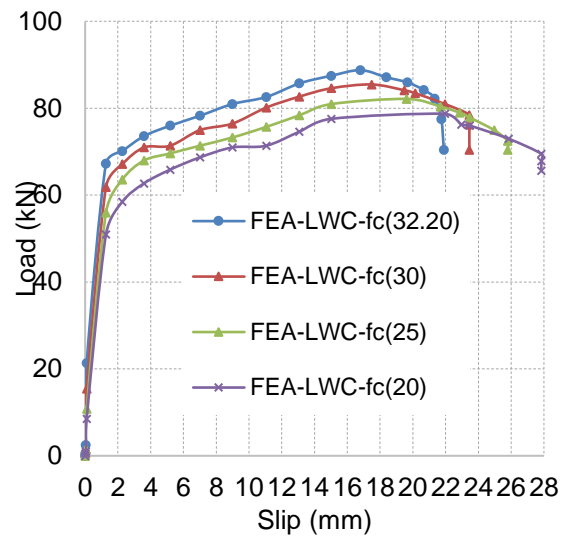
(b)
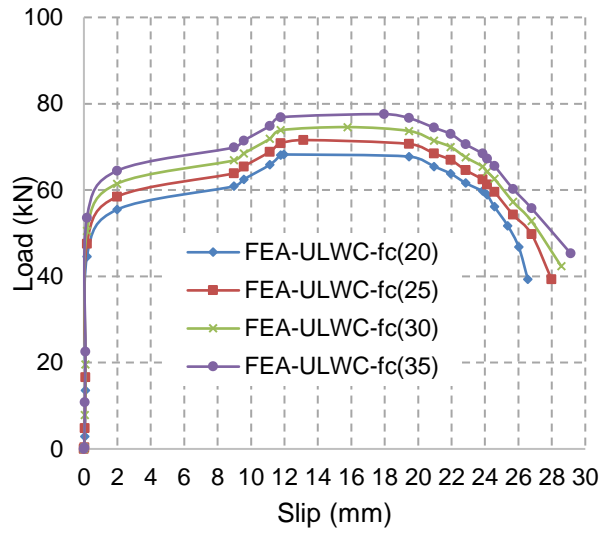
(c)

Figure A-3: Load-slip curves of the FEA with WWSS 22×100mm
with different concrete types

(a)

(b)

(c)
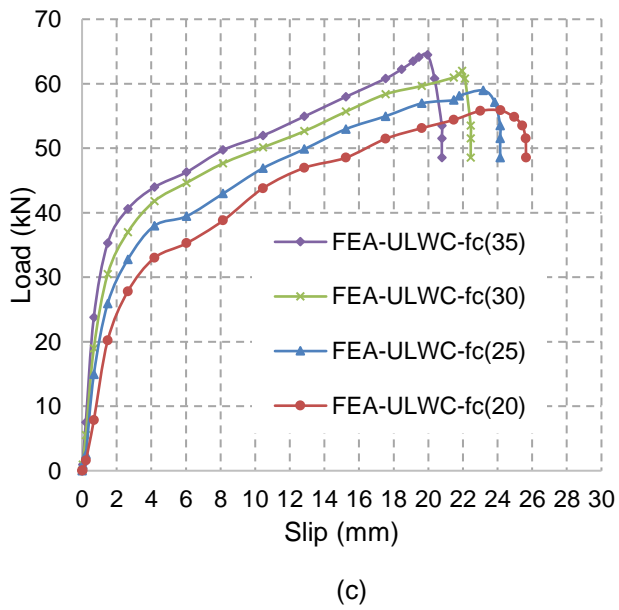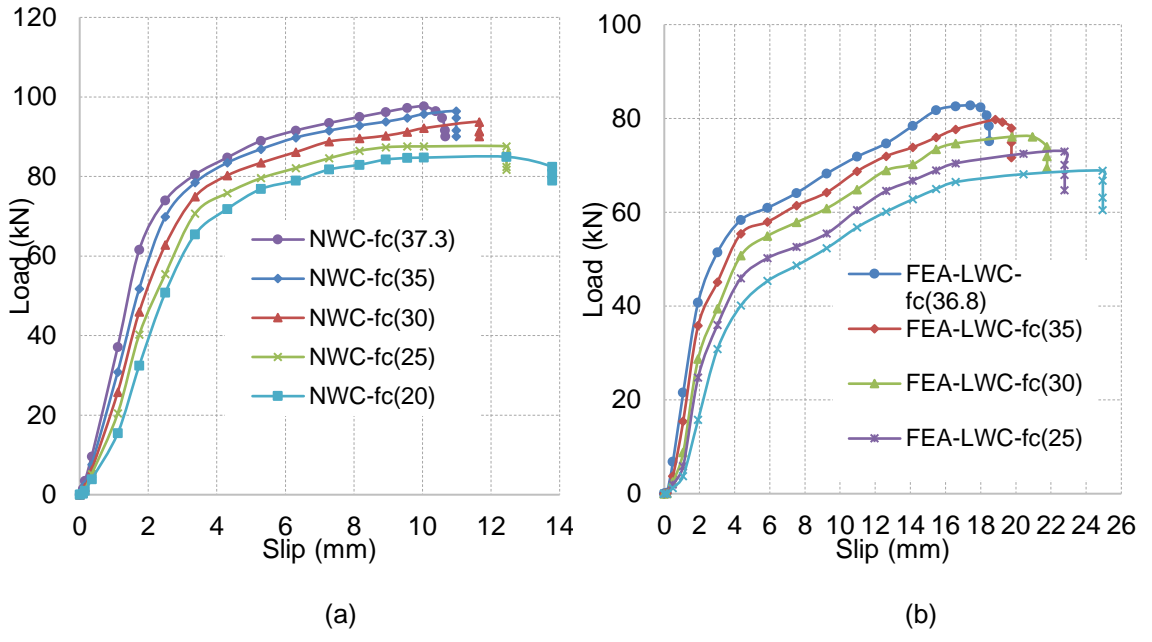
Figure A-4: Load-slip curves of the FEA with WWSS with dowels 16mm diameter with different concrete types
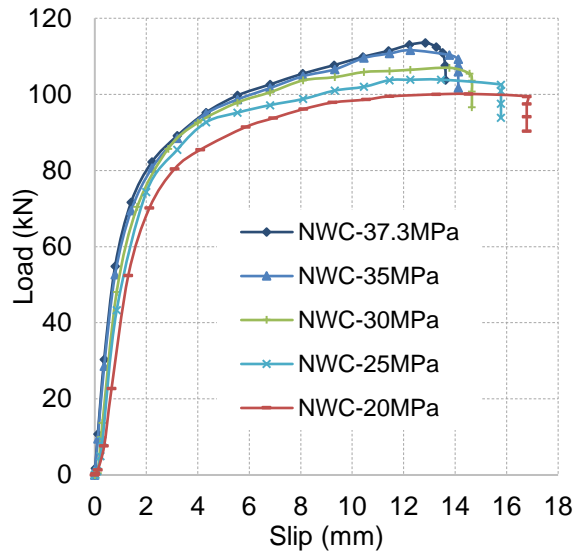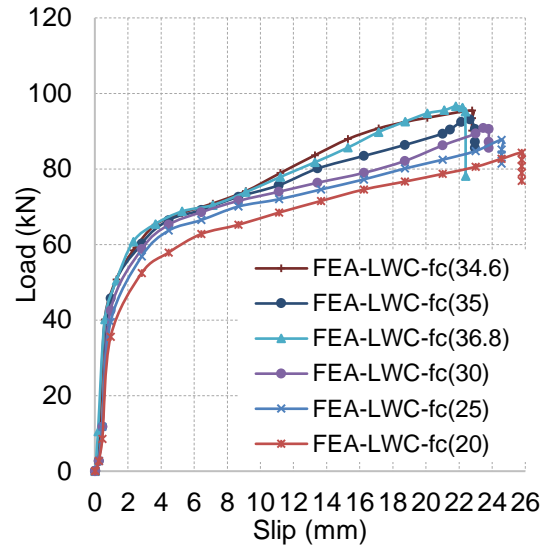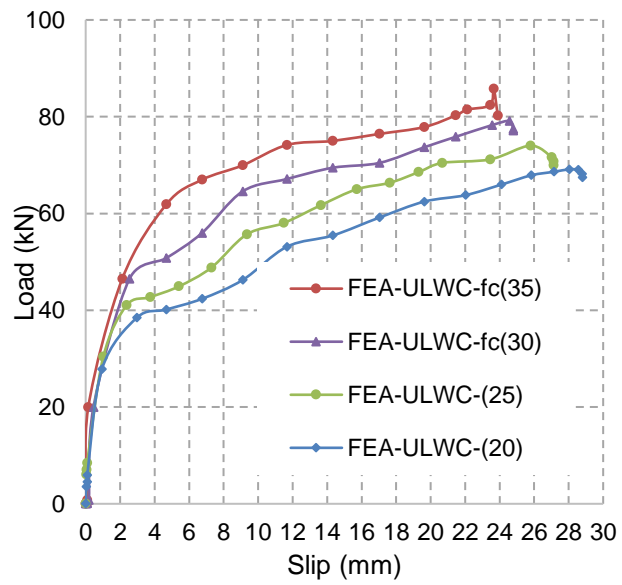
Figure A-5: Load-slip curves of the FEA with WWSS with dowels
20mm diameter with different concrete types
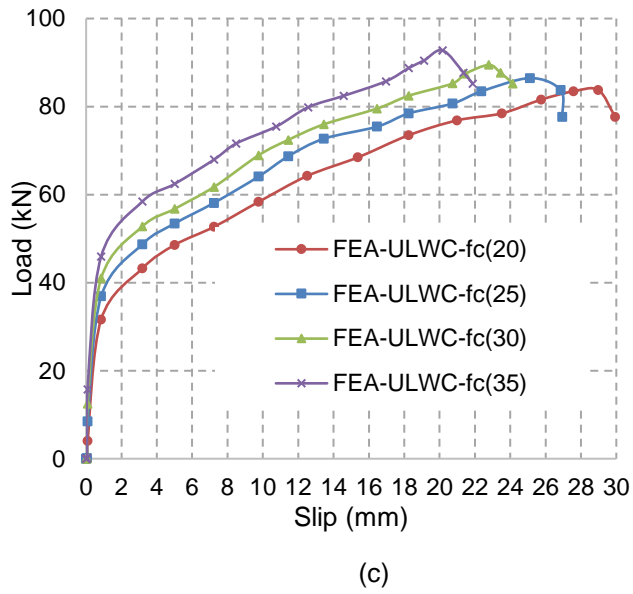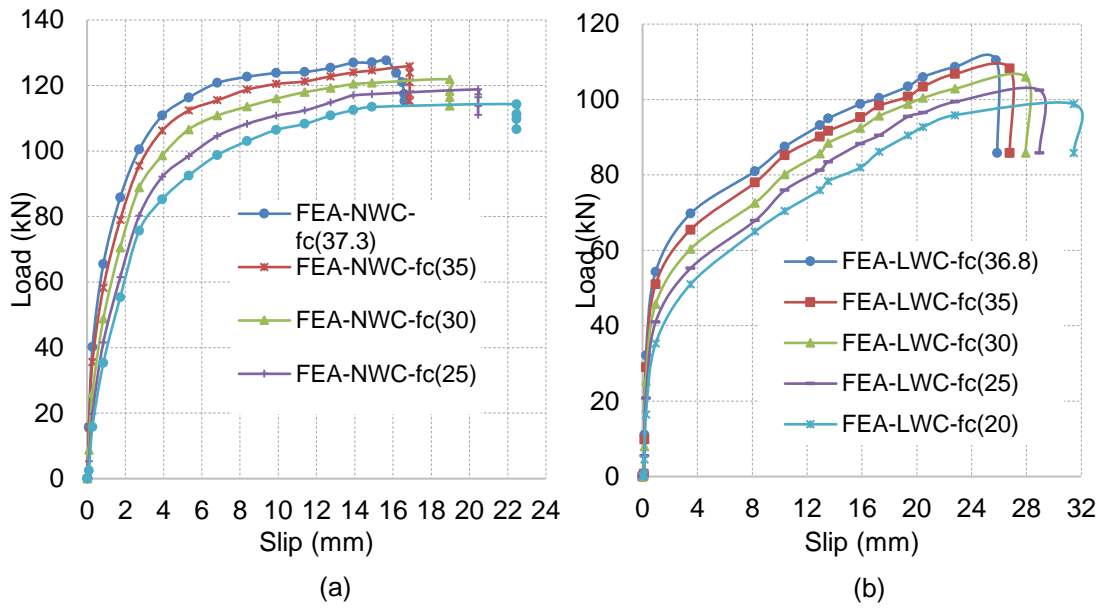
Figure A-6: Load-slip curves of the FEA with WWSS with dowels
22mm diameter with different concrete types
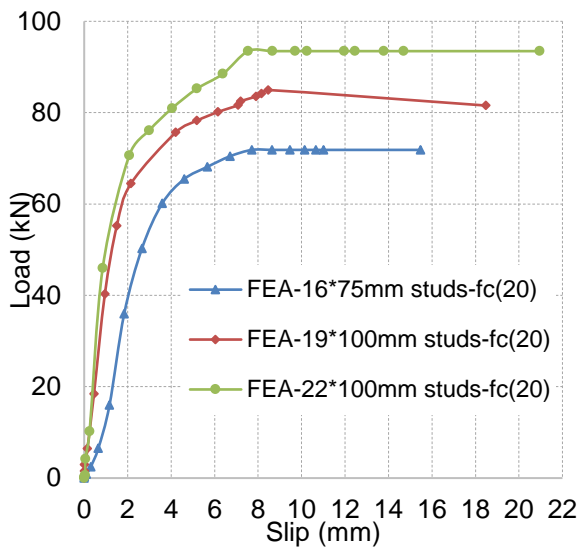
(a): NWC
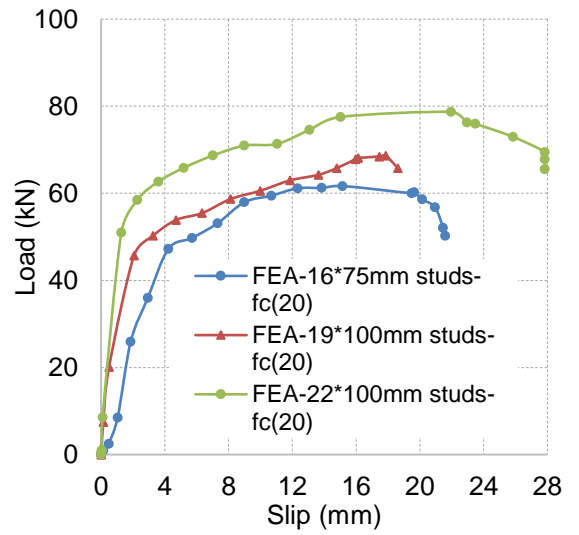
(b): LWC
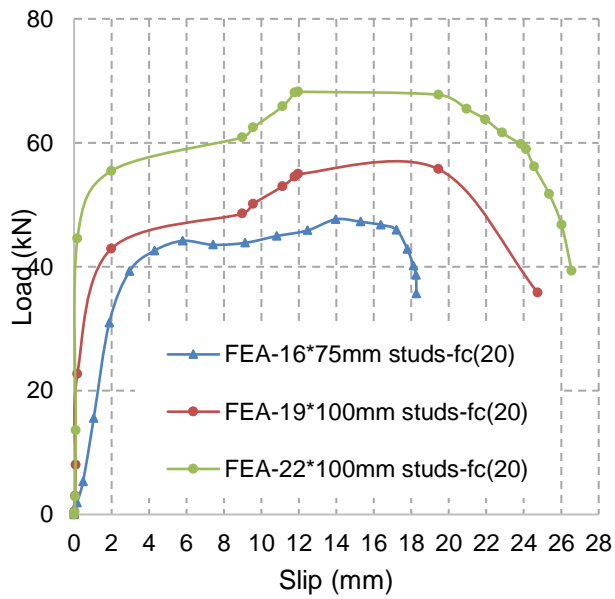
(c): ULWC

Figure A-7: Load-slip curves of the WWSS FEA with concrete strength of 20N/mm^2 with different stud dimensions
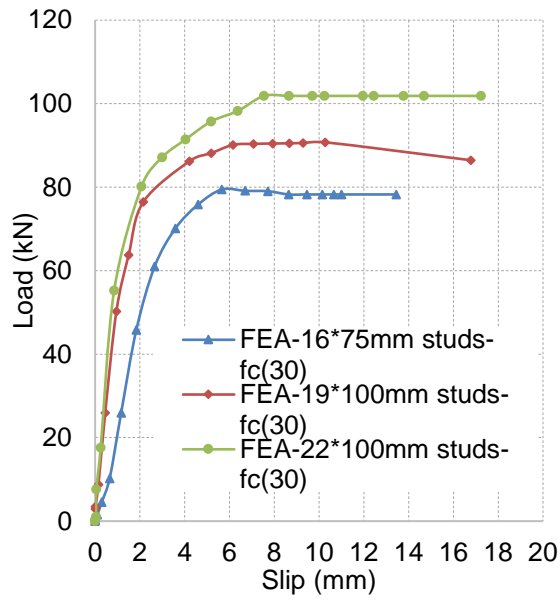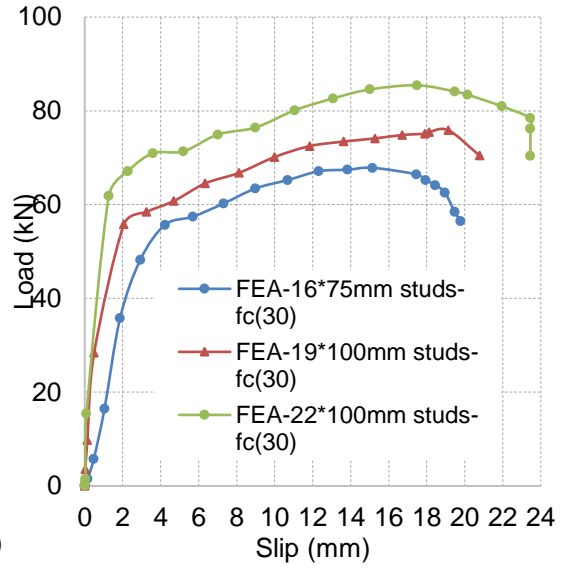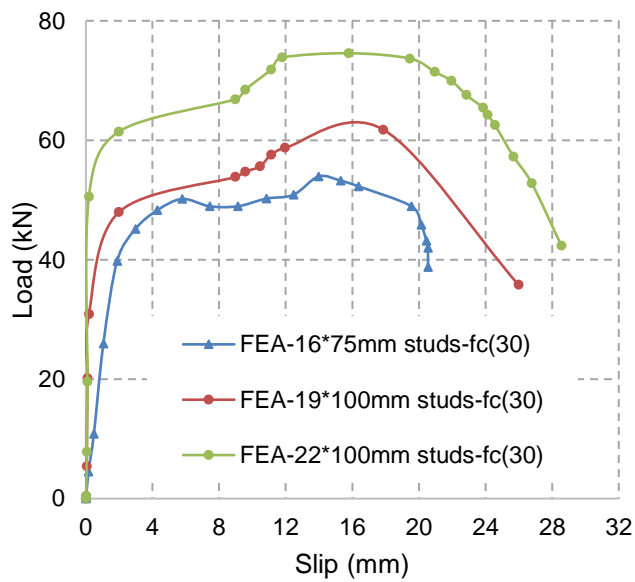
(a): NWC

(b): LWC

(c): ULWC

Figure A-8: Load-slip curves of the WWSS FEA with concrete strength of 30N/mm^2 with different stud dimensions
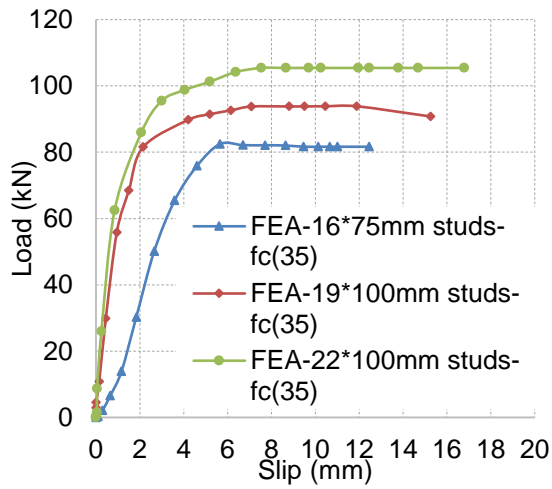
(a): NWC
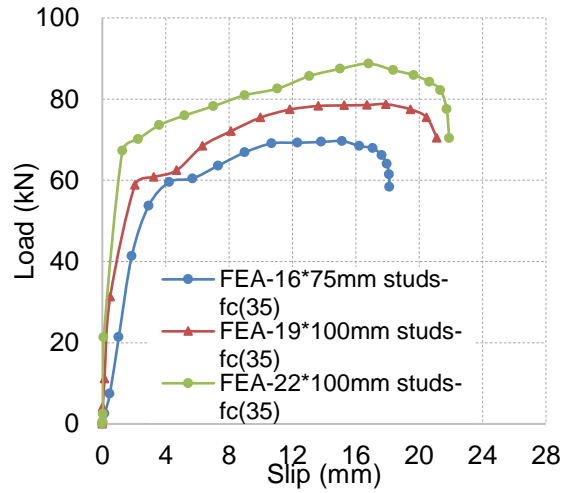
(b): LWC
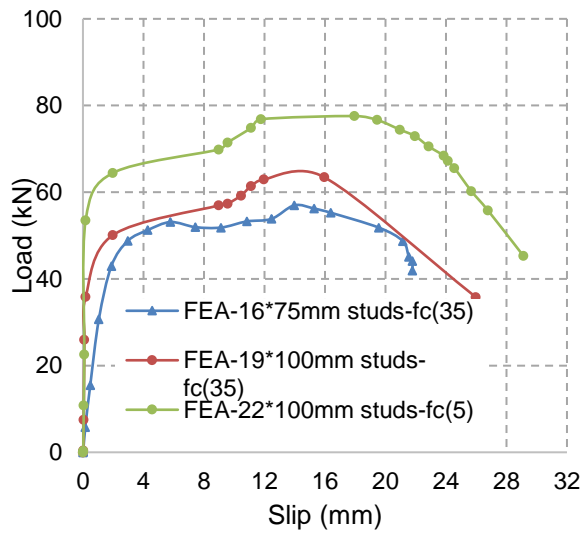
(c): ULWC

Figure A-9: Load-slip curves of the WWSS FEA with concrete strength of 35N/mm^2 with different stud dimensions

(a): NWC

(b): LWC

(c): ULWC
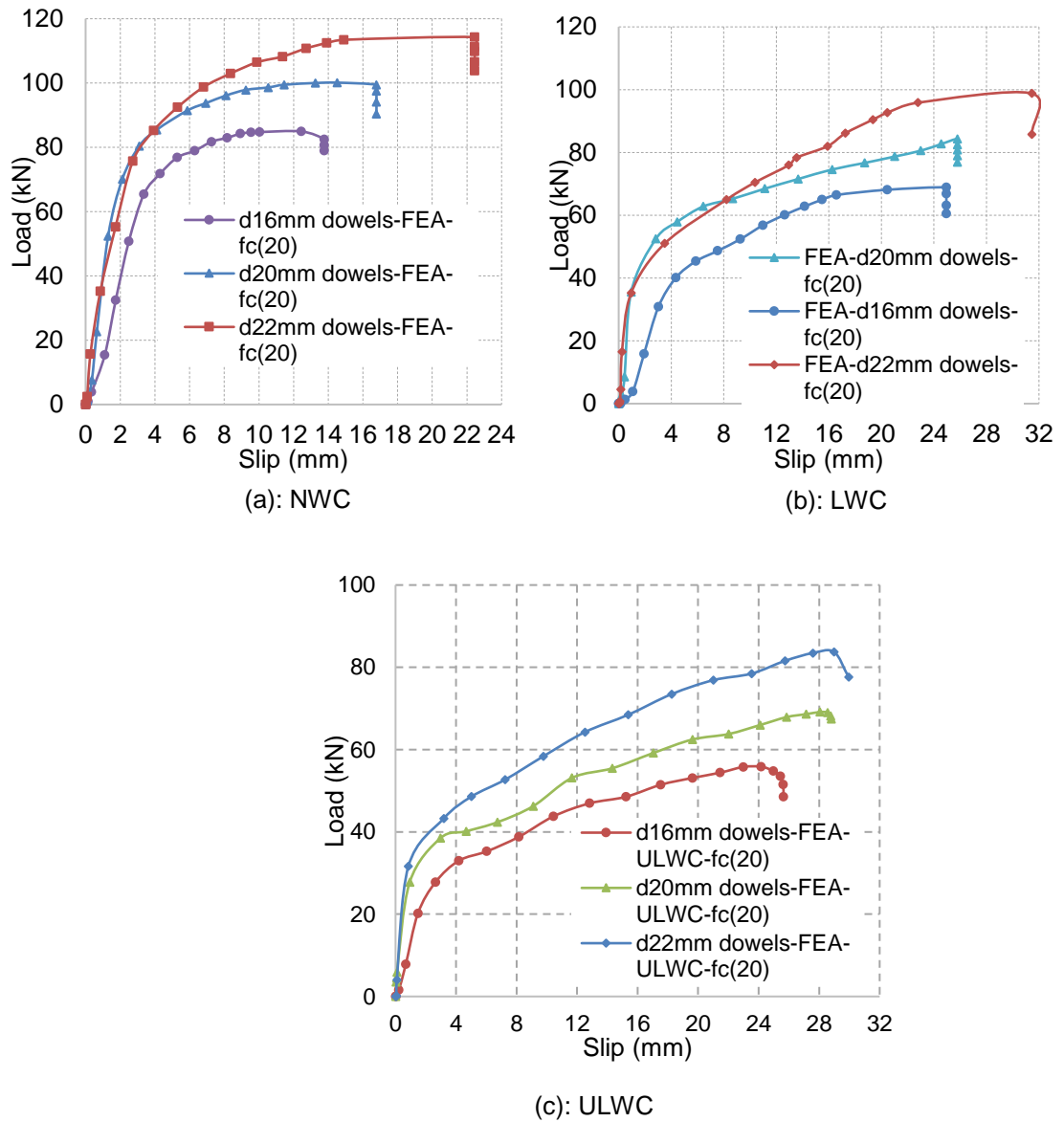
Figure A-10: Load-slip curves of the WWSS with dowels FEA
with concrete strength of 20N/mm^2 with different dowel diameters
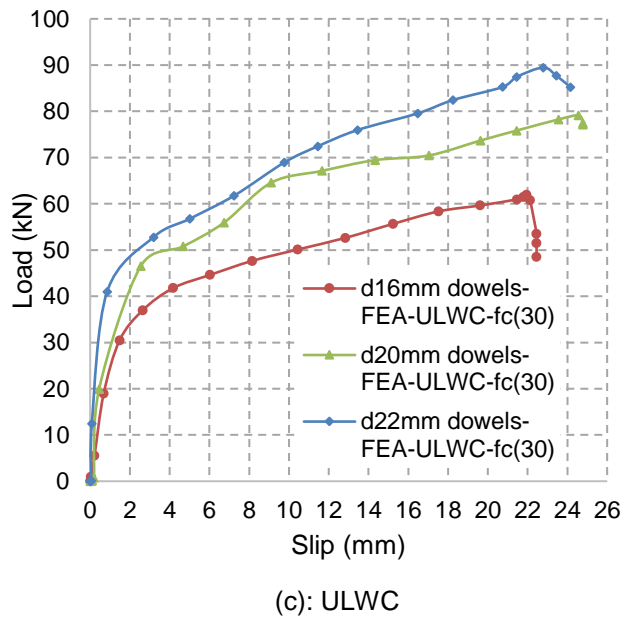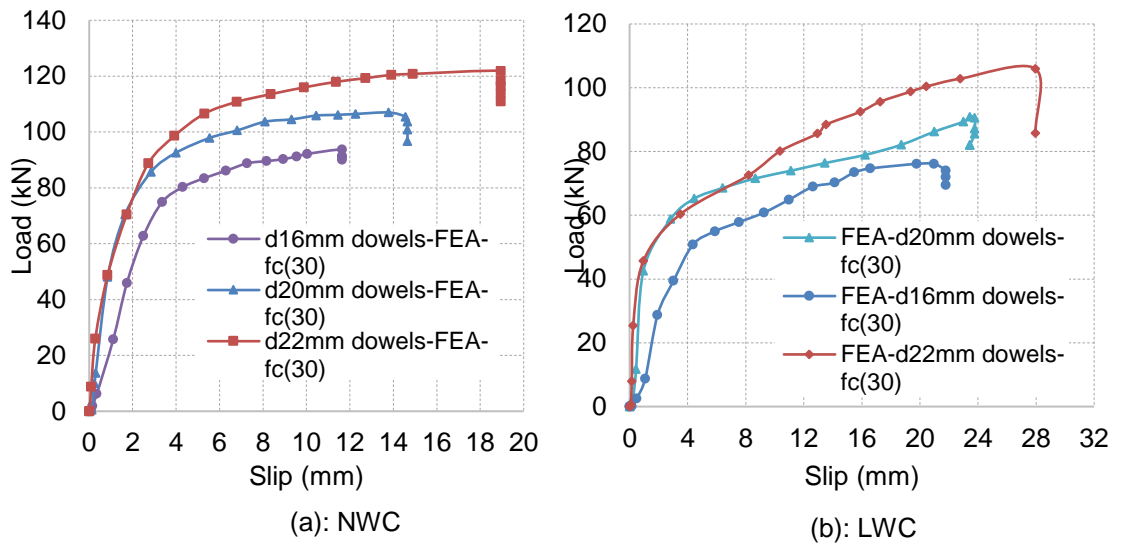
(a): NWC

(b): LWC

(c): ULWC

Figure A-11: Load-slip curves of the WWSS with dowels FEA
with concrete strength of 30N/mm^2 with different dowel diameters
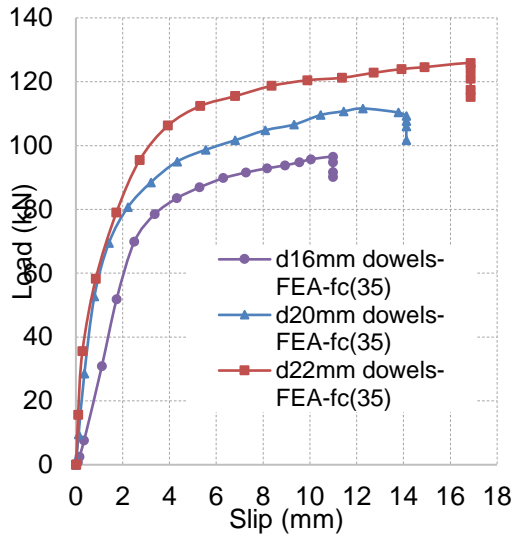
(a): NWC
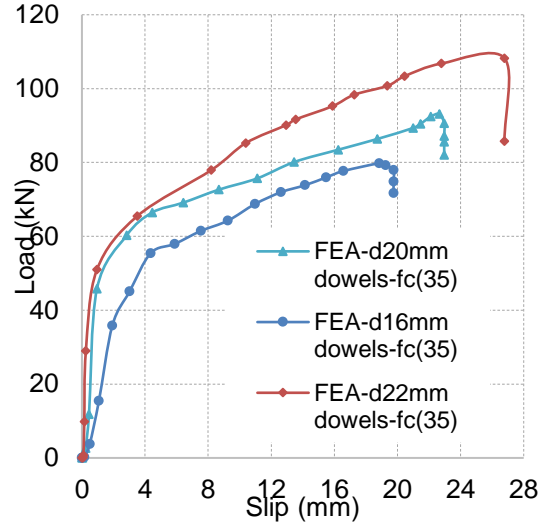
(b): LWC
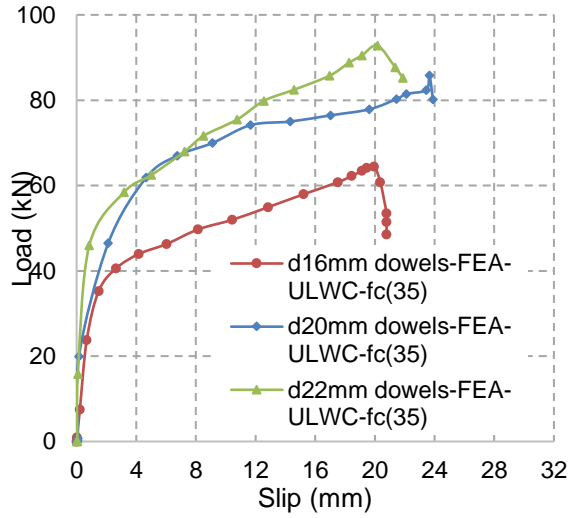
(c): ULWC

Figure A-12: Load-slip curves of the WWSS with dowels FEA
with concrete strength of 35N/mm^2 with different dowel diameters

Appendix B

Table B-1: Comparison between results of calculation and FEA for WWSS of 16×75mm

	Concrete type	f_{ck} (N/mm^2)	d(mm)	a_r(mm)	f_u (N/mm^2)	As(mm^2)	P_{sd}* (kN)	FEA (kN)	Ratio Cal/FEA
WWSS with 16*75mm	NWC	16	16	217.5	510	201.06	53.72	84.15	0.638
	NWC	20	16	217.5	510	201.06	64.73	87.4	0.74
	NWC	24	16	217.5	510	201.06	75.37	90.58	0.832
	NWC	28	16	217.5	510	201.06	85.73	93.85	0.913
	NWC	30.81	16	217.5	510	201.06	92.87	96.78	0.959
	LWC	16	16	217.5	510	201.06	53.72	68.65	0.782
	LWC	20	16	217.5	510	201.06	64.73	72.85	0.888
	LWC	24	16	217.5	510	201.06	75.37	75.85	0.993
	LWC	25.85	16	217.5	510	201.06	85.73	78.75	1.088
	LWC	28	16	217.5	510	201.06	80.21	80.24	0.999
	ULWC	16	16	217.5	510	201.06	53.72	55.74	0.963
	ULWC	20	16	217.5	510	201.06	64.73	58.96	1.097
	ULWC	24	16	217.5	510	201.06	75.37	61.78	1.219
	ULWC	28	16	217.5	510	201.06	85.73	63.45	1.351
* calculated using Eq. 7.7								Average	0.962

Table B-2: Comparison between results of calculation and FEA for WWSS of 19×100mm

	Concrete type	f_{ck} (N/mm^2)	d(mm)	a_r(mm)	f_u (N/mm^2)	As(mm^2)	P_{sd}* (kN)	FEA (kN)	Ratio Cal/FEA
	NWC	16	19	217.5	455.5	283.52	62.01	84.15	0.736
	NWC	20	19	217.5	455.5	283.52	74.71	87.4	0.854
	NWC	24	19	217.5	455.5	283.52	87.00	90.58	0.960
	NWC	28	19	217.5	455.5	283.52	98.95	93.85	1.054
	NWC	30.81	19	217.5	455.5	283.52	107.20	96.78	1.107
	LWC	16	19	217.5	455.5	283.52	62.01	68.65	0.903
WWSS with 19*100mm	LWC	20	19	217.5	455.5	283.52	74.71	72.85	1.025
	LWC	24	19	217.5	455.5	283.52	87.00	75.85	1.147
	LWC	25.85	19	217.5	455.5	283.52	98.95	78.75	1.256
	LWC	28	19	217.5	455.5	283.52	92.59	55.74	1.661
	ULWC	16	19	217.5	455.5	283.52	62.01	58.96	1.051
	ULWC	20	19	217.5	455.5	283.52	74.71	61.78	1.209
	ULWC	24	19	217.5	455.5	283.52	87.00	63.45	1.371
	ULWC	28	19	217.5	455.5	283.52	98.95	84.15	1.175
* calculated using Eq. 7.7								Average	1.108

Table B-3: Comparison between results of calculation and FEA for WWSS of 22×100mm

	Concrete type	f_{ck} (N/mm^2)	d(mm)	a_r(mm)	f_u (N/mm^2)	As(mm^2)	P_{sd}^* (kN)	FEA (kN)	Ratio Cal/FEA
	NWC	16	22	217.5	500	380.12	70.09	93.47	0.749
	NWC	20	22	217.5	500	380.12	84.44	97.45	0.866
	NWC	24	22	217.5	500	380.12	98.33	101.85	0.965
	NWC	28	22	217.5	500	380.12	111.84	105.42	1.06
	NWC	30.81	22	217.5	500	380.12	121.16	108.23	1.119
	LWC	16	22	217.5	500	380.12	70.09	78.69	0.89
WWSS with 22*100mm	LWC	20	22	217.5	500	380.12	84.44	82.12	1.028
	LWC	24	22	217.5	500	380.12	98.33	85.45	1.15
	LWC	25.85	22	217.5	500	380.12	111.84	88.74	1.26
	LWC	28	22	217.5	500	380.12	104.64	90.34	1.158
	ULWC	16	22	217.5	500	380.12	70.09	68.23	1.027
	ULWC	20	22	217.5	500	380.12	84.44	71.85	1.175
	ULWC	24	22	217.5	500	380.12	98.33	74.65	1.317
	ULWC	28	22	217.5	500	380.12	111.84	77.58	1.441
* calculated using Eq. 7.7								Average	1.086

Table B-4: Comparison between results of calculation and FEA for WWSS with dowels of 16mm diameter

	Concrete type	f_{ck} (N/mm^2)	d(mm)	a_r(mm)	f_u (N/mm^2)	As(mm^2)	P_{sd}^* (kN)	FEA (kN)	Ratio Cal/FEA
	NWC	16	16	217.5	400	201.06	53.72	84.95	0.632
	NWC	20	16	217.5	400	201.06	64.73	87.56	0.739
	NWC	24	16	217.5	400	201.06	75.37	93.74	0.804
	NWC	28	16	217.5	400	201.06	85.73	96.45	0.888
	NWC	29.84	16	217.5	400	201.06	90.40	97.63	0.925
	LWC	16	16	217.5	400	201.06	53.72	68.86	0.780
Dowels with 16mm diameter	LWC	20	16	217.5	400	201.06	64.73	72.95	0.887
	LWC	24	16	217.5	400	201.06	75.37	76.12	0.990
	LWC	28	16	217.5	400	201.06	85.73	79.78	1.074
	LWC	29.44	16	217.5	400	201.06	89.39	82.78	1.079
	ULWC	16	16	217.5	400	201.06	53.72	55.84	0.962
	ULWC	20	16	217.5	400	201.06	64.73	58.96	1.097
	ULWC	24	16	217.5	400	201.06	75.37	61.98	1.216
	ULWC	28	16	217.5	400	201.06	85.73	64.45	1.330
* calculated using Eq. 7.7								Average	0.894

Table B-5: Comparison between results of calculation and FEA for WWSS with dowels of 20mm diameter

	Concrete type	f_{ck} (N/mm^2)	d(mm)	a_r(mm)	f_u (N/mm^2)	As(mm^2)	P_{sd}^* (kN)	FEA (kN)	Ratio Cal/FEA
Dowels with 20mm diameter	NWC	16	20	217.5	455.5	314.15	64.73	100.12	0.646
	NWC	20	20	217.5	455.5	314.15	77.98	103.87	0.750
	NWC	24	20	217.5	455.5	314.15	90.81	106.98	0.848
	NWC	28	20	217.5	455.5	314.15	103.28	110.72	0.932
	NWC	29.84	20	217.5	455.5	314.15	108.92	113.54	0.959
	LWC	16	20	217.5	455.5	314.15	64.73	84.32	0.767
	LWC	20	20	217.5	455.5	314.15	77.98	87.69	0.889
	LWC	24	20	217.5	455.5	314.15	90.81	90.85	0.999
	LWC	28	20	217.5	455.5	314.15	103.28	93.12	1.109
	LWC	29.44	20	217.5	455.5	314.15	107.70	96.62	1.114
	ULWC	16	20	217.5	455.5	314.15	64.731	69.12	0.936
	ULWC	20	20	217.5	455.5	314.15	77.989	74.01	1.053
	ULWC	24	20	217.5	455.5	314.15	90.813	79.12	1.147
	ULWC	28	20	217.5	455.5	314.15	103.28	85.78	1.204
* calculated using Eq. 7.7								Average	0.954

Table B-6: Comparison between results of calculation and FEA for WWSS with dowels of 22mm diameter

	Concrete type	f_{ck} (N/mm^2)	d(mm)	a_r(mm)	f_u (N/mm^2)	As(mm^2)	P_{sd}^* (kN)	FEA (kN)	Ratio Cal/FEA
Dowels with 22mm diameter	NWC	16	22	217.5	500	380.13	70.09	114.26	0.6134
	NWC	20	22	217.5	500	380.13	84.44	118.78	0.710
	NWC	24	22	217.5	500	380.13	98.33	121.85	0.806
	NWC	28	22	217.5	500	380.13	111.84	125.85	0.888
	NWC	29.84	22	217.5	500	380.13	117.94	127.66	0.923
	LWC	16	22	217.5	500	380.13	70.09	98.78	0.709
	LWC	20	22	217.5	500	380.13	84.44	102.47	0.824
	LWC	24	22	217.5	500	380.13	98.33	105.96	0.9272
	LWC	28	22	217.5	500	380.13	111.84	108.23	1.033
	LWC	29.44	22	217.5	500	380.13	116.62	110.45	1.055
	ULWC	16	22	217.5	500	380.13	70.09	83.73	0.837
	ULWC	20	22	217.5	500	380.13	84.44	86.18	0.979
	ULWC	24	22	217.5	500	380.13	98.33	89.47	1.099
	ULWC	28	22	217.5	500	380.13	111.84	92.78	1.205
* calculated using Eq. 7.7								Average	0.901